Inversion of probabilistic models of structures using measured transfer functions

THÈSE

présentée par

Maarten Arnst

pour l'obtention du

GRADE DE DOCTEUR
(spécialité mécanique)

soutenue le 23/04/2007.

Composition du jury

Président :	M. Patrick Le Tallec	(École Polytechnique)
Rapporteurs :	M. Roger Ghanem	(University of Southern California, États Unis)
	M. Christian Soize	(Université de Marne-la-Vallée)
	M. Albert Tarantola	(Institut de Physique du Globe de Paris)
Examinateurs :	M. Stéphane Andrieux	(EDF-LaMSID)
	M. Geert Degrande	(K.U. Leuven, Belgique)
Directeurs :	M. Didier Clouteau	(École Centrale Paris)
	M. Marc Bonnet	(École Polytechnique)

Maarten Arnst
Ondes en Milieux Hétérogènes et Aléatoires
Laboratoire de Mécanique des Sols, Structures et Matériaux
École Centrale Paris
Grande Voie des Vignes
F-92295 Châtenay-Malabry
France

Tel: +33 1 41 13 13 59
Fax: +33 1 41 13 14 42
Mail: maarten.arnst@ecp.fr
Web: www.mssmat.ecp.fr/rubrique.php3?id_rubrique=354

Remerciements

Remerciements

ii

Résumé

L'objectif de cette thèse est de développer une méthodologie d'identification expérimentale de modèles probabilistes prédisant le comportement dynamique de structures.

Dans l'introduction générale, nous définissons les différents types de problèmes inverses stochastiques que nous souhaitons étudier, et présentons l'intérêt en ingénierie d'être capable de les résoudre. Nous rappelons sommairement les différentes approches existantes pour construire des modèles probabilistes pour le comportement dynamique de structures, et passons brièvement en revue les méthodes d'inversion déjà connues pour leur identification expérimentale. À partir des caractéristiques et des principales limitations de ces dernières méthodes, nous introduisons les objectifs de cette thèse.

Dans un premier chapitre, nous décrivons les modèles probabilistes et les données expérimentales utilisés. Ces modèles probabilistes, à paramétrage minimal [Soize, 2000, 2001, 2006], ont deux avantages. Le premier est qu'ils possèdent, par construction, les propriétés mathématiques et physiques essentielles de modèles probabilistes de structures. Le deuxième est que leur identification expérimentale peut généralement être formulée comme un problème inverse bien posé, dont la résolution numérique entraîne un coût de calcul raisonnable. Les données utilisées sont des fonctions de transfert expérimentales. Elles sont exprimées dans le domaine fréquentiel, ce qui permet de limiter l'analyse à une bande de fréquences d'intérêt et de caractériser facilement le bruit expérimental.

Ensuite, nous nous focalisons sur l'inversion de modèles probabilistes à paramétrage minimal à partir de fonctions de transfert expérimentales. Nous commençons par montrer que les méthodes classiques d'estimation de la théorie des statistiques mathématiques, telle que la méthode du maximum de vraissemblance, ne sont pas bien adaptées pour aborder ce problème. Nous montrons en particulier que des difficultés numériques, ainsi que des problèmes conceptuels dus au risque d'une mauvaise spécification des modèles, peuvent entraver l'application des méthodes classiques. Ces difficultés nous conduisent à proposer une formulation alternative de l'inversion de modèles probabilistes en minimisant une fonction objectif, mesurant la distance entre les données expérimentales et le modèle probabiliste, par rapport aux paramètres recherchés. Pour la définition de telles distances, nous proposons deux principes de construction: soit la fonction de log-vraissemblance, soit l'entropie relative. Nous montrons comment la restriction de ces distances aux lois marginales d'ordre faible permet de surmonter les difficultés mentionnées plus haut.

Nous distinguons deux types de situations pour l'application des méthodes inverses proposées. Nous considérons d'une part le comportement dynamique d'*une seule structure*. Le problème inverse stochastique a alors pour but d'identifier le modèle probabiliste quantifiant au mieux l'*incertitude sur les prédictions* du comportement dynamique de cette structure, résultant d'incertitudes sur les données et d'erreurs de modélisation. Se concentrant sur le cas où l'utilisation prévue du modèle probabiliste consiste à estimer des régions de confiance, nous développons une méthodologie inverse, basée sur la minimisation d'une distance limitée aux lois marginales d'ordre un. Dans les troisième et quatrième chapitres, cette

Résumé

méthodologie est appliquée à un exemple avec des données simulées, et à un problème en ingénierie civile et environnementale avec des mesures réelles.

Ensuite, nous considérons le comportement dynamique d'une *collection de structures similaires*. Le problème inverse stochastique a alors pour but d'identifier le modèle probabiliste quantifiant au mieux la *variabilité* dans le comportement dynamique de ces structures. En particulier, l'identification de longueurs de corrélation spatiale et de niveaux de dispersion caractérisant la variabilité dans des champs de propriétés mécaniques de structures nous amène à proposer une méthodologie inverse, basée sur les propriétés dispersives d'ondes mécaniques se propageant dans les structures testées. Dans un cinquième chapitre, cette méthodologie est appliquée à un exemple avec des données simulées.

Les annexes concernent d'abord l'extension aux opérateurs de type parabolique du modèle stochastique à paramétrage minimal pour des champs stochastiques définissant des opérateurs aux dérivées partielles stochastiques de type elliptique [Soize, 2006]. Ensuite, nous nous focalisons sur le problème aux valeurs propres généralisées, défini par les matrices aléatoires introduites dans le cadre de l'approche probabiliste non-paramétrique à paramétrage minimal. Dans les troisième et quatrième annexes, de nature bibliographique, nous rappelons quelques méthodes de traitement de mesures vibratoires, puis la méthode inverse d'analyse spectrale des ondes de surface. Enfin, nous présentons des mesures vibratoires réelles, qui seront utilisées dans de futures recherches se focalisant sur le développement de méthodes inverses pour l'identification de champs de propriétés mécaniques de milieux élastiques non-bornés.

Contents

Contents

Contents

List of Notations

The following list of notations gathers the acronyms and symbols that are often used in this dissertation.

Acronyms

a.e.	almost everywhere
a.s.	almost surely
BE	Boundary Element
CLT	Central Limit Theorem
DFT	Discrete Fourier Transform
DOF	Degree Of Freedom
FE	Finite Element
FFT	Fast Fourier Transform
iid	independent and identically-distributed
MCS	Monte Carlo Simulation
ML	Maximum Likelihood
MM	Method of Moments
P	Primary, longitudinal wave
PDF	Probability Density Function
S	Secondary, shear wave
SASW	Spectral Analysis of Surface Waves
SLLN	Strong Law of Large Numbers
TF	Transfer Function
WLLN	Weak Law of Large Numbers

Miscellaneous notations

$\exists$	there exists
$\forall$	for all
$\emptyset$	the empty set
$\mathbb{1}_A(x)$	the indicator function such that $\mathbb{1}_A(x) = 1$ if $x \in A$ and $\mathbb{1}_A(x) = 0$ otherwise
$\Gamma(x)$	the gamma function defined for $x{>}0$ by $\Gamma(x) = \int_0^{+\infty} t^{x-1} \exp(-t)dt$

Euclidean space $\mathbb{R}^m$ and Hermitian space $\mathbb{C}^m$

Let i denote the imaginary unit. Let $\mathbb{N}$, $\mathbb{Z}$, $\mathbb{R}$ and $\mathbb{C}$ respectively denote the set of integers, signed integers, real scalars and complex scalars:

$[a, b]$	$\{x \in \mathbb{R} \mid a \leq x \leq b\}$
$]a, b[$	$\{x \in \mathbb{R} \mid a < x < b\}$
$]a, b]$	$\{x \in \mathbb{R} \mid a < x \leq b\}$
$[a, b[$	$\{x \in \mathbb{R} \mid a \leq x < b\}$
$\mathbb{R}^+, \mathbb{R}^-$	$\mathbb{R}^+ = [0, +\infty[$ and $\mathbb{R}^- =]-\infty, 0]$
$\mathbb{R}_0^+, \mathbb{R}_0^-$	$\mathbb{R}^+ =]0, +\infty[$ and $\mathbb{R}^- =]-\infty, 0[$
$\mathbb{R}^n, \mathbb{C}^n$	The n-th power of $\mathbb{R}$ and $\mathbb{C}$.

Any vector $\boldsymbol{x} = (x_1, \ldots, x_n)$ is identified with the $(n \times 1)$ column matrix of its components.

Let $\boldsymbol{\alpha} = (\alpha_1, \ldots, \alpha_n) \in \mathbb{N}^n$ be a vector of integers:

$|\boldsymbol{\alpha}|$	the modulus of $\boldsymbol{\alpha}$ such that $|\boldsymbol{\alpha}| = \alpha_1 + \ldots + \alpha_n$

Let $z \in \mathbb{C}$ be a complex scalar:

$\Re(z)$	the real part of z
$\Im(z)$	the imaginary part of z
$|z|$	the modulus of z
$\overline{z}$	the complex conjugate of z

Let $\boldsymbol{x}, \boldsymbol{y} \in \mathbb{R}^n$ be two real vectors:

$(\boldsymbol{x}, \boldsymbol{y})$	the Euclidean inner product such that $(\boldsymbol{x}, \boldsymbol{y}) = \sum_{k=1}^n x_k y_k$
$\|\boldsymbol{x}\|$	the Euclidean norm such that $\|\boldsymbol{x}\| = \sqrt{(\boldsymbol{x}, \boldsymbol{x})}$

Let $\boldsymbol{x}, \boldsymbol{y} \in \mathbb{C}^n$ be two complex vectors:

$(\boldsymbol{x}, \overline{\boldsymbol{y}})$	the Hermitian inner product such that $(\boldsymbol{x}, \overline{\boldsymbol{y}}) = \sum_{k=1}^n x_k \overline{y}_k$
$\|\boldsymbol{x}\|$	the Hermitian norm such that $\|\boldsymbol{x}\| = \sqrt{(\boldsymbol{x}, \overline{\boldsymbol{x}})}$

Let the vectors $\{\boldsymbol{i}_k \in \mathbb{R}^n \mid 1 \leq k \leq n\}$ constitute the orthonormal basis for $\mathbb{R}^n$ and $\mathbb{C}^n$ such that $\boldsymbol{i}_k$ is the vector equal to zero, except for the k-th entry, which takes the value 1.

Real and complex matrices

Let $\mathbb{K}$ be $\mathbb{R}$ or $\mathbb{C}$. Let $\mathrm{M}_{m \times n}(\mathbb{K})$ be the space of $(m \times n)$ matrices $\boldsymbol{X}$ whose entries $X_{k\ell}$ are in $\mathbb{K}$. If $m = n$, $\mathrm{M}_{n \times n}(\mathbb{K})$ is denoted simply by $\mathrm{M}_n(\mathbb{K})$. Let $\mathrm{M}_n^S(\mathbb{R})$, $\mathrm{M}_n^{+0}(\mathbb{R})$, $\mathrm{M}_n^+(\mathbb{R})$ and $\mathrm{M}_n^+(\mathbb{C})$ be the subspaces of real symmetric, of real symmetric positive semi-definite, of real symmetric positive definite and of complex Hermitian positive definite square $(n \times n)$ matrices, respectively.

Let $\boldsymbol{X} \in \mathrm{M}_n(\mathbb{K})$ be a real or complex square $(n \times n)$ matrix:

$\det(\boldsymbol{X})$	the determinant of $\boldsymbol{X}$
$\mathrm{tr}(\boldsymbol{X})$	the trace of $\boldsymbol{X}$ such that $\mathrm{tr}(\boldsymbol{X}) = \sum_{k=1}^n X_{kk}$

Let $\boldsymbol{X} \in \mathrm{M}_{m \times n}(\mathbb{K})$ be a real or complex rectangular $(m \times n)$ matrix:

$\boldsymbol{X}^{\mathrm{T}}$	the transpose of $\boldsymbol{X}$
$\boldsymbol{X}^*$	the adjoint of $\boldsymbol{X}$ such that $\boldsymbol{X}^* = \overline{\boldsymbol{X}}^{\mathrm{T}}$
$\|\boldsymbol{X}\|$	the matrix norm of $\boldsymbol{X}$ such that $\|\boldsymbol{X}\| = \sup_{\|\boldsymbol{x}\| \leq 1} \|\boldsymbol{X}\boldsymbol{x}\|$, $\quad \boldsymbol{x} \in \mathbb{K}^n$
$\|\boldsymbol{X}\|_{\mathrm{F}}$	the Frobenius norm of $\boldsymbol{X}$ such that $\|\boldsymbol{X}\|_{\mathrm{F}} = \sqrt{\mathrm{tr}(\boldsymbol{X}\boldsymbol{X}^*)}$

The tensor product of $\boldsymbol{x}, \boldsymbol{y} \in \mathbb{K}^n$ is the matrix $\boldsymbol{x} \otimes \boldsymbol{y} \in \mathrm{M}_n(\mathbb{K})$ such that $\boldsymbol{x} \otimes \boldsymbol{y} = \boldsymbol{x}\boldsymbol{y}^{\mathrm{T}}$.

Differential calculus

Let $\boldsymbol{f}$ be a function of $x \in \mathbb{R}$ or $\boldsymbol{x} \in \mathbb{R}^m$ with values in a Banach space V:

$\boldsymbol{f}' = \frac{d\boldsymbol{f}}{dx}$ the derivative of $\boldsymbol{f} : \mathbb{R} \to V$

$\boldsymbol{f}'' = \frac{d^2\boldsymbol{f}}{dx^2}$ the second derivative of $\boldsymbol{f} : \mathbb{R} \to V$

$\frac{\partial \boldsymbol{f}}{\partial x_k}$ the partial derivative of $\boldsymbol{f} : \mathbb{R}^m \to V$ with respect to the variable x_k

$\boldsymbol{\nabla}_{\boldsymbol{x}} f$ the gradient of $f : \mathbb{R}^m \to \mathbb{R}$ or $\mathbb{C}$ such that $\boldsymbol{\nabla}_{\boldsymbol{x}} f = \sum_{k=1}^{m} \frac{\partial f}{\partial x_k} \boldsymbol{i}_k$

$\mathbf{D}_{\boldsymbol{x}} \boldsymbol{f}$ the gradient of $\boldsymbol{f} : \mathbb{R}^m \to \mathbb{R}^n$ or $\mathbb{C}^n$ such that $\mathbf{D}_{\boldsymbol{x}} \boldsymbol{f} = \sum_{k=1}^{m} \frac{\partial \boldsymbol{f}}{\partial x_k} \otimes \boldsymbol{i}_k$

$\mathrm{div}_{\boldsymbol{x}} \boldsymbol{f}$ the divergence of $\boldsymbol{f} : \mathbb{R}^m \to \mathbb{R}^n$ or $\mathbb{C}^n$ such that:

$$\mathrm{div}_{\boldsymbol{x}} \boldsymbol{f} = \mathrm{tr}\left(\mathbf{D}_{\boldsymbol{x}} \boldsymbol{f}\right) = \sum_{k=1}^{m} \left(\frac{\partial \boldsymbol{f}}{\partial x_k}, \boldsymbol{i}_k \right)$$

$\mathbf{Div}_{\boldsymbol{x}} \boldsymbol{F}$ the divergence of $\boldsymbol{F} : \mathbb{R}^m \to \mathrm{M}_n(\mathbb{R})$ or $\mathrm{M}_n(\mathbb{C})$ such that:

$$\mathbf{Div}_{\boldsymbol{x}} \boldsymbol{F} = \sum_{k=1}^{m} \sum_{\ell=1}^{n} \frac{\partial F_{k\ell}}{\partial x_k} \boldsymbol{i}_\ell$$

Functional spaces[1]

Let K be a compact subset of $\mathbb{R}^m$ and V a Banach space:

$\mathcal{C}^0(K, V)$ the space of continuous functions defined on K with values in V

Let Ω be an open subset of $\mathbb{R}^m$, V a Banach space with norm $\|\cdot\|_V$ and $1 \leq p \leq +\infty$:

$L^p(\Omega, V)$ the space of almost everywhere (a.e.) equivalence classes of measurable functions $\boldsymbol{f} : \Omega \to V$ such that $\int_\Omega \|\boldsymbol{f}\|_V^p \, d\boldsymbol{x} < +\infty$

$L^\infty(\Omega, V)$ the space of a.e. equivalence classes of measurable functions $\boldsymbol{f} : \Omega \to V$ such that $\exists c \in \mathbb{R} : \|\boldsymbol{f}(\boldsymbol{x})\|_V \leq c$ a.e. in Ω

Let Ω be an open subset of $\mathbb{R}^m$, $\mathbb{K}$ be $\mathbb{R}$ or $\mathbb{C}$ and $1 \leq p \leq +\infty$:

$H^p(\Omega, \mathbb{K})$ the Sobolev space of functions $f \in L^2(\Omega, \mathbb{K})$ such that:

$$\forall \boldsymbol{\alpha} \in \mathbb{N}^m \text{ with } |\boldsymbol{\alpha}| \leq p : \left(\frac{\partial}{\partial x_1}\right)^{\alpha_1} \cdots \left(\frac{\partial}{\partial x_m}\right)^{\alpha_m} f \in L^2(\Omega, \mathbb{K})$$

Operators and forms on Hilbert spaces[1]

Let V and W be real Hilbert spaces with norms $\|\cdot\|_V$ and $\|\cdot\|_W$:

$\mathscr{L}(V, W)$ the space of linear continuous (bounded) functions $\boldsymbol{f} : V \to W$ such that:

$\forall \boldsymbol{v} \in V, \lambda \in \mathbb{R} : \boldsymbol{f}(\lambda \boldsymbol{v}) = \lambda \boldsymbol{f}(\boldsymbol{v})$ and $\exists c \in \mathbb{R} : \forall \boldsymbol{v} \in V : \|\boldsymbol{f}(\boldsymbol{v})\|_W \leq c \|\boldsymbol{v}\|_V$

V' the dual space of V, i.e. the space $\mathscr{L}(V, \mathbb{R})$ of linear continuous forms on V

$\langle \cdot, \cdot \rangle_{V', V}$ the duality product between V' and V such that:

$\forall f \in \mathscr{L}(V, \mathbb{R}) : \exists \boldsymbol{f} \in V' : \forall \boldsymbol{v} \in V : f(\boldsymbol{v}) = \langle \boldsymbol{f}, \boldsymbol{v} \rangle_{V', V}$

(denoted simply by $\langle \cdot, \cdot \rangle$ when there is no possible confusion)

$\mathscr{B}(V, W)$ the space of bilinear continuous (bounded) forms $f : V \times W \to \mathbb{R}$ such that:

$\forall \boldsymbol{v} \in V, \boldsymbol{w} \in W, \lambda \in \mathbb{R} : f(\lambda \boldsymbol{v}, \boldsymbol{w}) = f(\boldsymbol{v}, \lambda \boldsymbol{w}) = \lambda f(\boldsymbol{v}, \boldsymbol{w})$

and $\exists c \in \mathbb{R} : \forall \boldsymbol{v} \in V, \boldsymbol{w} \in W : |f(\boldsymbol{v}, \boldsymbol{w})| \leq c \|\boldsymbol{v}\|_V \|\boldsymbol{w}\|_W$

List of Notations

Let V and W be complex Hilbert spaces with norms $||\cdot||_V$ and $||\cdot||_W$:

$\mathscr{L}(V,W)$ the space of antilinear continuous (bounded) functions $\boldsymbol{f} : V \to W$ such that:
$$\forall \boldsymbol{v} \in V, \lambda \in \mathbb{C} : \boldsymbol{f}(\lambda\boldsymbol{v}) = \overline{\lambda}\boldsymbol{f}(\boldsymbol{v}) \text{ and } \exists c \in \mathbb{R} : \forall \boldsymbol{v} \in V : ||\boldsymbol{f}(\boldsymbol{v})||_W \le c\,||\boldsymbol{v}||_V$$

V' the antidual space of V, i.e. the space $\mathscr{L}(V,\mathbb{C})$ of antilinear continuous forms on V

$\langle \cdot, \cdot \rangle_{V',V}$ the antiduality product between V' and V such that:
$$\forall f \in \mathscr{L}(V,\mathbb{C}) : \exists \boldsymbol{f} \in V' : \forall \boldsymbol{v} \in V : f(\boldsymbol{v}) = \langle \boldsymbol{f}, \boldsymbol{v} \rangle_{V',V}$$
(denoted simply by $\langle \cdot, \cdot \rangle$ if there is no possible confusion)

$\mathscr{B}(V,W)$ the space of sesquilinear continuous (bounded) forms $f : V \times W \to \mathbb{C}$ such that:
$$\forall \boldsymbol{v} \in V, \boldsymbol{w} \in W, \lambda \in \mathbb{C} : f(\lambda\boldsymbol{v}, \boldsymbol{w}) = f(\boldsymbol{v}, \overline{\lambda}\boldsymbol{w}) = \lambda f(\boldsymbol{v}, \boldsymbol{w})$$
$$\text{and } \exists c \in \mathbb{R} : \forall \boldsymbol{v} \in V, \boldsymbol{w} \in W : |f(\boldsymbol{v}, \boldsymbol{w})| \le c\,||\boldsymbol{v}||_V\,||\boldsymbol{w}||_W$$

Random variables[2]

Throughout the dissertation, $(\mathcal{A}, \mathcal{F}, P)$ is a probability measure space, where $\mathcal{A}$ is the sample space of outcomes, $\mathcal{F}$ the σ-algebra of events and $P : \mathcal{F} \to [0,1]$ a probability measure. Let $(V, \mathcal{B}_V)$ be a measurable space, where V is a finite- or infinite dimensional space and $\mathcal{B}_V$ is a σ-algebra over V. A random variable $\mathbb{X}$ defined on $(\mathcal{A}, \mathcal{F}, P)$ with values in V is a measurable mapping from $(\mathcal{A}, \mathcal{F})$ into $(V, \mathcal{B}_V)$ such that (definition of a measurable mapping):

$$\forall B \in \mathcal{B}_V : \mathbb{X}^{-1}(B) \in \mathcal{F} \quad , \tag{1}$$

where $\mathbb{X}^{-1}(B)$ denotes the set $\{a \in \mathcal{A} \mid \mathbb{X}(a) \in B\}$. The random variable $\mathbb{X}$ induces a probability measure $P_{\mathbb{X}}$ on $(V, \mathcal{B}_V)$ such that:

$$\forall B \in \mathcal{B}_V : P_{\mathbb{X}}(B) = P\left(\mathbb{X}^{-1}(B)\right). \tag{2}$$

Two random variables $\mathbb{X}, \mathbb{Y} : \mathcal{A} \to V$ are said to be almost surely (a.s.) equal if:

$$P\left(\{a \in \mathcal{A} \mid \mathbb{X}(a) \neq \mathbb{Y}(a)\}\right) = 0. \tag{3}$$

In the dissertation, we make no distinction between a random variable and its a.s. equivalence class wherever this is not required for the clarity of the text.

Let V be, moreover, a Banach space endowed with the norm $||\cdot||_V$ and let $\mathscr{B}(V)$ be the Borel σ-algebra generated by the open sets. The space $L^0(\mathcal{A}, V)$ denotes the space of a.s. equivalence classes of random variables defined on $(\mathcal{A}, \mathcal{F}, P)$ with values in V, i.e. of measurable mappings from $(\mathcal{A}, \mathcal{F})$ into $(V, \mathscr{B}(V))$. The space $L^2(\mathcal{A}, V)$ denotes the subspace of $L^0(\mathcal{A}, V)$ of second-order random variables:

$$L^2(\mathcal{A}, V) = \left\{ \mathbb{X} \in L^0(\mathcal{A}, V) : E\left\{ ||\mathbb{X}||_V^2 \right\} < +\infty \right\} \quad , \tag{4}$$

where the symbol E denotes the integral with respect to the probability measure (the mathematical expectation). For instance, for $\varphi : V \to \mathbb{R}$ a measurable mapping:

$$E\left\{\varphi(\mathbb{X})\right\} = \int_V \varphi(\boldsymbol{x}) P_{\mathbb{X}}(d\boldsymbol{x}). \tag{5}$$

where $P_{\mathbb{X}}$ is the probability measure induced by $\mathbb{X}$ on $(V, \mathscr{B}(V))$.

---

[1] For more details concerning this section, the reader is referred to Brezis [1999], Dautray and Lions [1987], Reed and Simon [1980], Royden [1988].

[2] For more details concerning this section, the reader is referred to Billingsley [1995], Da Prato and Zabczyk [1992], Dudley [2002], Krée and Soize [1986], Ledoux and Talagrand [1991], Lin and Cai [1995], Soize [1993].

d

General introduction

The present chapter serves as a general introduction to the entire dissertation. First, we introduce the problem of the inversion of probabilistic models for the dynamical behaviour of structures (Sec. 1). Subsequently, we describe the state of the art and identify further needs of research (Sec. 2). Finally, we define the objectives of this work and outline the organization of the text (Sec. 3).

1 Problem outline and motivation

Following Keller [1976], two problems are called *inverses* of one another if the formulation of each of them requires full or partial knowledge of the solution of the other. According to this definition, it is clearly arbitrary which of the two problems is called direct and which one is called the inverse problem. In cases where one of the two problems has been studied earlier, and perhaps more extensively, it is generally agreed to call this one the *direct problem*, whereas the other is the *inverse problem*. In this dissertation, we distinguish, moreover, between inverse problems associated either to deterministic, or to probabilistic direct problems. The former are referred to as *classical inverse problems*, whereas the latter are called *stochastic inverse problems*.

In the following, we first recall the main classes of classical inverse problems frequently encountered in computational mechanics and describe their general mathematical formulation (Sec. 1.1). Subsequently, two kinds of stochastic inverse problems are introduced (Sec. 1.2).

1.1 Classical inverse problems in computational mechanics

Let us first introduce the context in which the main types of classical inverse problems are defined (Fig. 1).
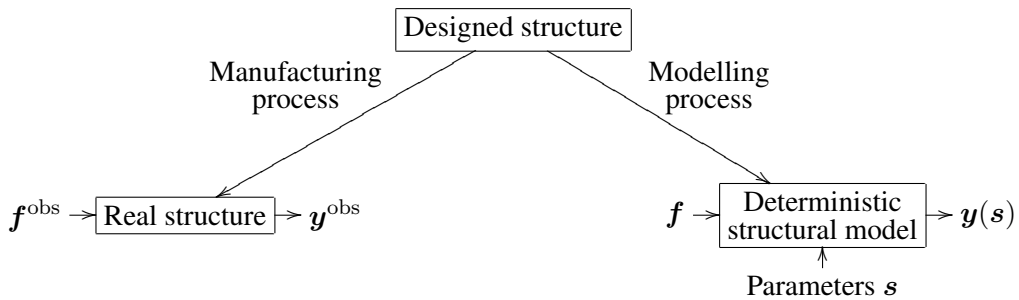
Figure 1: Classical inverse problems: designed structure, real structure and deterministic model.

In computational mechanics, the structure conceived by the designers and analysts is often referred to as the *designed structure*. The design specifies the geometry, the material types and many other features. It may concern a simple structure such as an elastic bar, or a complex structure such as a building.

The structure manufactured according to the design specifications is called here the *real structure*. Usually, the real structure differs from the designed structure in that, for instance, its geometrical parameters and material properties may not coincide with the prescribed design values.

When a *deterministic structural model* is used to predict the dynamical response of the real structure due to a prescribed applied loading f, a deterministic value $y(s)$ is obtained. The model predictions usually depend on a set s of parameters, which typically comprises geometrical parameters, fields of material properties and boundary conditions. A deterministic structural model is most often an imperfect representation of the dynamical behaviour of the real structure for two reasons. First, there may be *parameter uncertainty* in that there may be a lack of knowledge of the geometrical parameters, material properties and boundary conditions of the real structure. In this case, the model parameters are usually referenced from the designed structure and may therefore imperfectly characterize the real structure. Second, *modelling errors* may have been introduced by simplifying approximations made in the modelling process, either stemming from a poor understanding of the dynamical behaviour of the real structure, or being deliberately introduced to reduce the model complexity. Examples of potential modelling errors are linearization, the use of simple constitutive laws, or the use of simplified models for joints.

Three kinds of classical inverse problems are frequently encountered in computational mechanics. The first kind concerns model identification and updating methods [see Bobillot, 2002, Deraemaeker, 2001, Friswell and Mottershead, 1995, Teughels, 2003, and references therein], which aim at improving an initial deterministic structural model, which might be a poor representation of the real structure due to the aforementioned reasons, by tuning its parameters so as to bring the model predictions into agreement with experimental observations. The second class of classical inverse problems gathers model parameter estimation methods [see Andrieux, 2005, Bonnet, 2006, Colton and Kress, 1992, Kirsch, 1996, Tarantola, 2005, and references therein]. Examples are vibration-based structural-health monitoring, gravimetry, acoustic imagery or seismic tomography, where internal heterogeneous characteristics are reconstructed from external measurements. The third kind of classical inverse problems concerns force identification methods [see Bonnet, 2006, and references therein], where, given (perhaps imperfect) knowledge of the experimental dynamical response and the model parameters, the applied forces are sought.

Many classical inverse problems are formulated as the minimization, with respect to the unknown parameters to be identified, of a suitable objective function that quantifies the distance (misfit) between experimental data and corresponding model predictions. For instance, in the aforementioned model updating and model parameter estimation problems, a vibration test is often considered, in which a controlled, or known, force f^{obs} is applied on the real structure and the induced response y^{obs} is measured. Upon using the deterministic structural model to forecast the outcome of the vibration test, obtaining for the force f modelling f^{obs} a predicted response $y(s)$, the optimal value of the unknown parameters s is then identified by:

$$\hat{s} = \arg\min_{s \in S} \left\| y^{\mathrm{obs}} - y(s) \right\| \quad , \tag{6}$$

where the *parameter space S* collects the admissible values of s. The least-squares distance method is frequently used to set up such objective functions, although other metrics have also been considered (see the aforementioned references for examples).

Classical inverse problems are often ill-posed in the sense of Hadamard [1923]. A problem is called *well-posed* if:

1. There exists a solution to the problem (*existence*).

2. The problem admits at most one solution (*uniqueness*).

3. The solution depends continuously on the data (*stability*).

If one of these properties fails to hold, the problem is called *ill-posed*. From the mathematical point of view, the existence or uniqueness of a solution can be enforced by enlarging or shrinking the parameter space. The stability property is the one of primary concern, which is motivated by the fact that, when the inverse problem lacks the stability property, small inevitable measurement errors in the experimental data may be amplified to unacceptable large errors in the solution. Several methods have been proposed in the literature for restoring the uniqueness and the stability:

1. A first class of methods attempts to enforce the stability property by changing the topologies of the parameter and experimental data space.

2. A second class of methods consists in augmenting the objective function with Tikhonov regularization terms [Tikhonov and Arsenin, 1977]. These methods include additional information, often referred to as *a priori* information, in the inverse problem so as to obtain an alternative stable problem whose *regularized solution* lies in the vicinity of the exact solution of the original problem (provided its existence).

3. A third class of methods uses the Bayesian paradigm [Bayes, 1763] to include *a priori* information into the inverse problem so as to obtain an alternative stable problem. First, a Bayesian *prior* Probability Density Function (PDF) is defined representing whatever information on the unknown model parameters is available in advance of making any observations in the current experiment. Then, the information gathered from this experiment using the mathematical-mechanical model is also represented by a PDF. Subsequently, the Bayesian *posterior* PDF, which represents all the information after making the observations, is obtained as the conjunction of these two states of information, or, equivalently, as the intersection of these two PDFs [Tarantola, 2005, 2008]. Finally, as a solution to the inverse problem, one can take, for instance, the model parameters at which the posterior PDF attains its maximum.

1.2 Stochastic inverse problems in computational mechanics

This subsection first describes the contrasting concepts of epistemic and aleatory uncertainty. Subsequently, two kinds of stochastic inverse problems are introduced.

Epistemic and aleatory uncertainty

Two kinds of uncertainties have been debated by scientific philosophers, who have called them epistemic and aleatory uncertainty [see, for instance, O'Hagan, 2004]. *Epistemic uncertainty* refers to a lack of knowledge of some characteristics of a physical system under study. This kind of uncertainty is reducible in that it can be diminished by an increase in knowledge or information. For example, an imperfect knowledge of the field of material properties of a complex structure or a poor understanding of its constitutive behaviour are categorized as epistemic uncertainty.

In contrast, *aleatory uncertainty* refers to an inherent variability in a physical system under study. A key feature is that this kind of uncertainty cannot be reduced by increasing knowledge or information. For

a simple example, consider a steel factory, where, every day, a sample is taken from the daily production and its tensile strength is measured. The variability in the outcome of this experiment due to the variability in the production process can then be viewed as aleatory uncertainty.

The distinction between these two kinds of uncertainty is closely related to the dichotomy between the two principal theories of statistics, namely the *frequentist* and the *Bayesian* theories [Jaynes, 2003, O'Hagan, 2004]. One characterization of the difference between them is that frequentists do not accept that epistemic uncertainty can be described or measured by probabilities, whereas Bayesians use probabilities to *quantify* any kind of uncertainty. For frequentists, a probability represents the long-run *frequency* with which an event occurs if some experiment is repeated an indefinite number of times. For Bayesians, a probability may also represent a state of information or, equivalently, a *degree-of-belief* in the truth of a proposition.

Epistemic uncertainty quantification

We now introduce a first class of stochastic inverse problems, which we gather under the heading "epistemic uncertainty quantification".
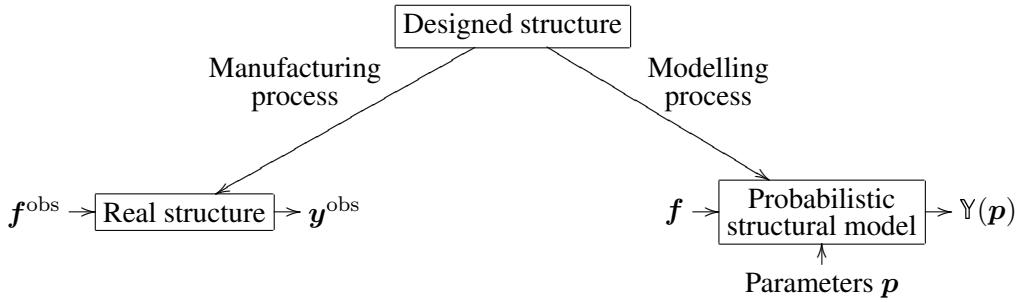
Figure 2: Epistemic uncertainty quantification: designed structure, real structure and probabilistic model.

Similarly to the classical inverse problems, this first kind of stochastic inverse problems is posed in a context in which a *single real structure* is studied (Fig. 2). Since, as discussed above, parameter uncertainty and modelling errors usually arise in the mathematical-mechanical modelling process, any structural model is generally an imperfect representation of the real structure. In other words, given any structural model for the dynamical behaviour of the real structure, one generally remains uncertain about its actual dynamical behaviour. This uncertainty is epistemic in nature in that it represents a lack of knowledge. In order for designers or analysts to be able to use a particular model in a *predictive* manner, it is clearly of key importance to attempt to quantify the epistemic uncertainty in the predictions. This task is closely related to *validation*, which can be defined [AIAA, 1998, Hemez, 2004] as the process of determining the degree to which the model is an accurate representation of the real structure from the perspective of its intended predictive use.

Probabilistic approaches provide a way to account for the uncertainty arising in the modelling process and to quantify its impact on the predictions. When a *probabilistic structural model* is used to predict the dynamical response of the real structure due to a prescribed applied loading $\boldsymbol{f}$, a random variable $\mathbb{Y}(\boldsymbol{p})$ is obtained, rather than a deterministic value, which generally depends on a set $\boldsymbol{p}$ of parameters. The best-known approach for constructing such a probabilistic model is the parametric probabilistic approach [see, for instance, Ghanem and Spanos, 1991, Ibrahim, 1987, Lin and Cai, 1995, Soize, 2006] and involves representing the geometrical parameters, the fields of material properties and the boundary conditions

of a structural model by random quantities (variables, fields, operators). The parameters p then typically control the probability distribution of these random quantities.

The objective of the first kind of stochastic inverse problems is the quantification of the epistemic uncertainty arising in the modelling process. More precisely, a stochastic inverse problem of the first kind is defined as the experimental identification of a probabilistic structural model such that the probability distribution of its random predictions "as adequately as possible" represents the uncertainty in these predictions, which results from parameter uncertainty and modelling errors. This probability distribution should be interpreted from a Bayesian point of view in that it is meant to represent an imperfect knowledge, or, equivalently, a degree-of-belief in the truth of the predictions (since only a single real structure is considered, it can clearly not be interpreted from a frequentist point of view as if it were representing long-run frequencies of occurrence).

Within the general framework of this first class of stochastic inverse problems, we concentrate in this dissertation on the particular case where the intended use of the probabilistic structural model to be identified consists in predicting confidence regions. Specifically, we focus on the inversion of probabilistic structural models such that, upon using the identified model to forecast the dynamical response of the real structure due to a prescribed applied loading, a confidence region (associated to a high probability level) for the predicted random response can be viewed as a region within which the actual dynamical response of the real structure lies. Confidence regions of this kind provide designers and analysts with a characterization of the *predictive accuracy*: if the width of the confidence interval is large, the predictive accuracy is small and vice versa.

Finally, it should be noted that the use of experimental data to quantify epistemic uncertainty, and to validate models, is a controversial subject. To non-Bayesians, the quantification of epistemic uncertainty may seem a *contradictio in terminis*. Furthermore, several authors have argued that experimental data should only be used to *falsify* models and not to validate them [Popper, 1959, Tarantola, 2006].

Box 0.1. Illustrative example: epistemic uncertainty quantification

This box gives an example of a stochastic inverse problem aimed at quantifying epistemic uncertainty.

Figure 3: (left, middle) Real structure and (right) structural model.

In the frame of the European CONVURT project (the CONtrol of Vibrations from Underground Railway Traffic), a deterministic model was built for the transmission of vibrations from the underground-railway tunnel of the RER B line of RATP to the Maison du Mexique building at the Cité Universitaire site in Paris in France (Fig.3) [Arnst, 2003, Chebli et al., 2007, Clouteau et al., 2005, Degrande et al., 2006]. Clearly, parameter uncertainty unavoidably arises, and significant modelling errors may be introduced, when modelling a highly complex coupled dynamical problem of this kind.
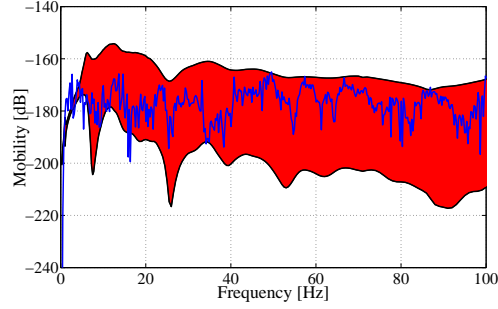
Figure 4: Measured response (blue solid line) and confidence region for the corresponding predicted random response (red patch).

To assess the impact of the parameter uncertainty and modelling errors on the model predictions, *in situ* measurements were performed of the dynamical response in the Maison du Mexique due to excitations applied on the rails in the tunnel [Chatterjee et al., 2003]. Furthermore, a probabilistic model was built associated to the deterministic model [Arnst et al., 2006]. An example of a stochastic inverse problem of the first kind is the experimental identification of this probabilistic model to quantify "as adequately as possible" the uncertainty in the predictions, such that the identified model can be used to predict confidence regions whose size characterizes the predictive accuracy (Fig. 4). This example will be elaborated in detail in Chapter 4.

Aleatory uncertainty quantification

We now introduce a second class of stochastic inverse problems, which we gather under the heading "aleatory uncertainty quantification".
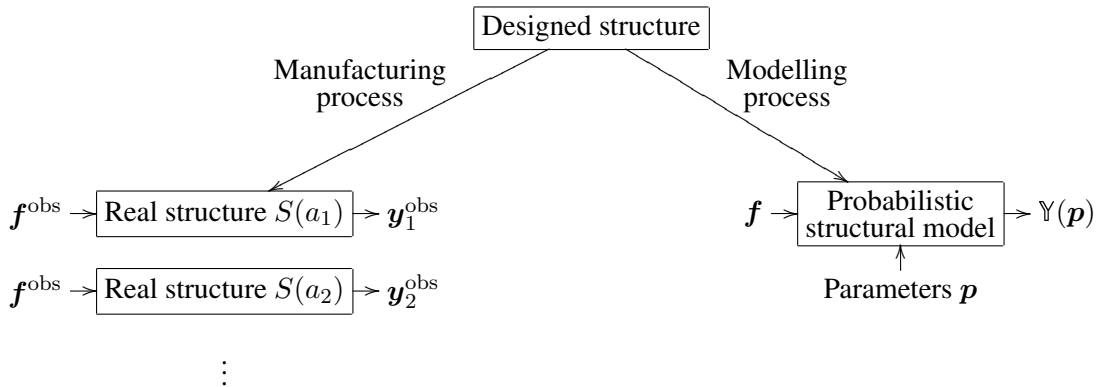
Figure 5: Aleatory uncertainty quantification: designed structure, collection of real structures and probabilistic model.

As opposed to the above-considered classical and stochastic inverse problems, this second kind of stochastic inverse problems is posed in a context in which a *collection of real structures* manufactured

according to the design specifications is studied (Fig. 5).

All manufacturing is subjected to variability, or, equivalently, to aleatory uncertainty. Examples of sources of variability are the manpower, the materials, wear of tools and machines and changes in ambient conditions such as temperature or humidity. Due to the inherent variability in the manufacturing process, the real structures are expected to be similar, but not perfectly identical. Consequently, their dynamical behaviour is expected to exhibit variability.

The objective of the second kind of stochastic inverse problems is the quantification of the aleatory uncertainty arising in the manufacturing process. More precisely, a stochastic inverse problem of the second kind is defined as the experimental identification of a probabilistic structural model which represents "as adequately as possible" the variability in the dynamical behaviour of the real structures. The probability distribution of the random predictions should, this time, be interpreted from a frequentist point of view in that it is meant to represent frequencies of occurrence.

The parameters p may sometimes not only have a mere mathematical meaning as parameters of the probabilistic model to be identified, but may themselves also bear a physical meaning and be of engineering interest. For an example, consider a collection of similar real structures whose fields of material properties are heterogeneous and exhibit variability. Let a probabilistic structural model be built by representing these fields of material properties by random fields parameterized by spatial correlation lengths and dispersion levels. It may then be of engineering interest to recover adequate estimates of these parameters, rather than to obtain an adequate comprehensive probabilistic dynamical model. Within the general framework of the second class of stochastic inverse problems, we concentrate in this dissertation on this particular case, namely on the identification of spatial correlation lengths and dispersion levels that "as adequately as possible" characterize the variability in fields of material properties of structures.

Box 0.2. Illustrative example: aleatory uncertainty quantification (1)

This box gives a first example of a stochastic inverse problem aimed at quantifying aleatory uncertainty. Let us consider a production line manufacturing aircraft engines of a fixed design. The vibratory characteristics of aircraft engines, in particular of bladed-disk assemblies, are well-known to be very sensitive to manufacturing variability [see, for instance, Capiez-Lernout, 2004]. An example of a stochastic inverse problem of the second kind is the experimental identification of a probabilistic model for the dynamical behaviour of the manufactured engines which represents "as adequately as possible" the variability in their vibratory characteristics. The identified model may then be used, for instance, to compare this variability to prescribed performance specifications. When the variability level is too high, the production line may be required to meet more stringent tolerances.

Box 0.3. Illustrative example: aleatory uncertainty quantification (2)

This box gives a second example of a stochastic inverse problem aimed at quantifying aleatory uncertainty. In the frame of our collaboration with the Department of Civil Engineering of KULeuven in Belgium, *in situ* wave propagation measurements were performed along the free surface of the soil at a site in Lincent in Belgium (Fig. 6). In the frame of the French Seismulator ANR-project, a probabilistic model for the dynamical behaviour of this soil was built by representing the fields of mechanical properties by random fields parameterized by spatial correlation lengths and dispersion

levels (Fig. 6). An example of a stochastic inverse problem of the second kind is the identification of the spatial correlation lengths and dispersion levels that "as adequately as possible" characterize the variability in the fields of mechanical soil properties using the experimental data gathered *in situ*. This example will be further elaborated in Chapter 5 and Appendices A and E.
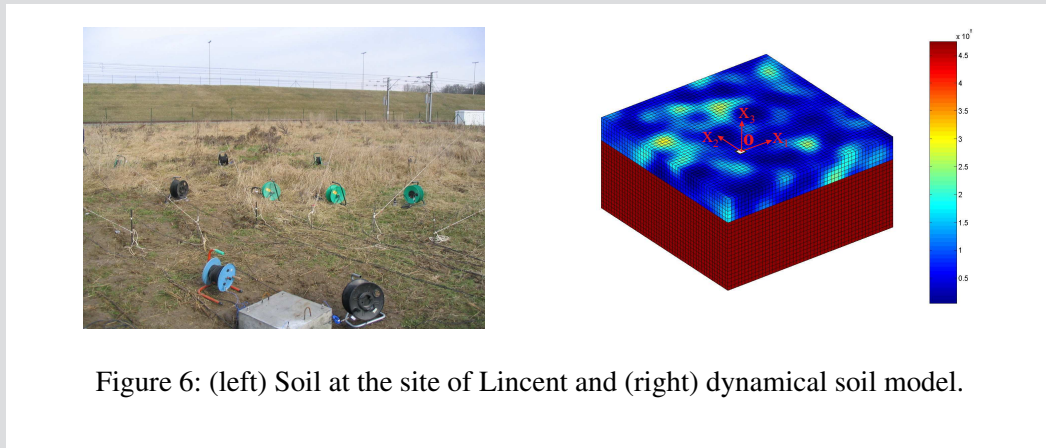
Figure 6: (left) Soil at the site of Lincent and (right) dynamical soil model.

It should be noted that an inverse problem of this kind embeds an implicit ergodicity type hypothesis. Upon viewing the particular soil under study as one realization of a random soil, this hypothesis consists in assuming that the spatial correlation lengths and dispersion levels characterizing the random soil can be recovered from the single available realization.

2 State of the art and further needs

The previous section has demonstrated that the inversion of probabilistic structural models has interesting engineering applications. This has lead to a large amount of research in computational mechanics dedicated to the construction of probabilistic structural models and to current and emerging research devoted to their inversion. In the following, we first briefly describe the state of the art in probabilistic mechanics (Sec. 2.1) and in solving stochastic inverse problems (Sec. 2.2). Subsequently, we indicate where further research is required (Sec. 2.3).

2.1 State of the art in probabilistic mechanics

Probabilistic mechanics is nowadays a rich and well-developed area of research, in which a wide variety of methods for constructing probabilistic structural models has been proposed [see Ibrahim, 1987, Manohar and Ibrahim, 1999, Schueller, 2001, Schueller et al., 1997, for reviews]. A possible way to distinguish between them consists in separating the parametric and the non-parametric methods. *Parametric probabilistic models* accommodate uncertainty by modelling the *local* physical features of a structural model (i.e. its geometrical parameters, fields of material properties and boundary conditions) by random variables or fields [see, for instance, Ghanem and Spanos, 1991, Ibrahim, 1987, Lin and Cai, 1995]. *Non-parametric probabilistic models* incorporate uncertainty by modelling *global* features of a structural model by random variables. An example is the non-parametric approach proposed by Soize [2000, 2001], where reduced matrix models of structures are defined in terms of random matrices.

A central problem in the practical construction of a probabilistic structural model is the choice of the *stochastic model*, that is to say the probability distribution, of the random variables, fields or matrices modelling either the local, or the global features. It is today recognized that this stochastic model should be chosen on the basis of only the *available information*, which typically consists of experimental data (such as measurements of the dynamical response of the real structure(s) under study) and of the essential mathematical or physical properties that the probabilistic model should possess (such as positiveness, symmetry or invertibility, depending on the quantity that is being modelled).

A general approach to the construction of the stochastic model consists in representing the probability distribution of the random variables, fields or matrices in a versatile manner as a function of a large number of parameters. For example, this probability distribution can be represented by a truncated polynomial chaos expansion [see, for instance, Desceliers et al., 2006, Ghanem and Spanos, 1991, Soize and Ghanem, 2004, Wiener, 1938], whereby the coefficients of this expansion make up the large set of parameters of the stochastic model. In this setting, the parameters of the stochastic model, *ergo* of the probabilistic structural model, should be identified from the available information. An inherent difficulty associated to this approach is that the identification of such a large set of parameters may be difficult in practice (ill-posedness, computational cost).

Soize [2000, 2001, 2006] presented an alternative approach whereby the essential mathematical properties are explicitly used to build the probability distribution of the random variables, fields or matrices. That probability distribution is chosen, which maximizes entropy [Jaynes, 1957, 2003, Shannon, 1948] under the constraint that the mathematical properties should be fulfilled. This principle of construction allows obtaining stochastic models parameterized by the mean value of the random variables, fields or matrices, and by a minimal set of essential parameters (such as spatial correlation lengths and dispersion levels). A key advantage is that their experimental identification can generally be formulated as a well-posed inverse problem that is numerically solvable with a reasonable computational effort.

Finally, it should be noted that, even though the above-described probabilistic methods are being developed in collaboration with industrial partners and have already been applied to real engineering case histories, their integration in industrial design and decision processes, insofar as we can judge it, still lacks a lot of maturity and experience and remains a largely open challenge.

2.2 State of the art in stochastic inverse methods

Stochastic inverse problems arise in many scientific disciplines including, apart from computational mechanics, biometry, econometry and sociometry. The theory of mathematical statistics is an interdisciplinary research field within which methods for solving stochastic inverse problems are studied and developed. Its historical development can be traced back to the work of Bernoulli [1778], Gauss [1809] and Bayes [1763] about 2 centuries ago. Today, it is a rich and well-developed research area [see Casella and Berger, 2001, Cramér, 1946, Kullback, 1968, Lehmann and Casella, 1998, O'Hagan and Forster, 2004, Stuart et al., 1999, for standard texts].

The theory of mathematical statistics focuses almost exclusively on stochastic inverse problems aimed at quantifying aleatory uncertainty. The basic model problem that this theory tries to solve has the following setup. Generally, a *random experiment* is considered, i.e. an experiment which can be repeated a large number of times under similar circumstances and whose outcome exhibits variability. For a simple example, consider again a steel factory, where, every day, a sample is taken from the daily production and its tensile strength is measured. A stochastic model for the random experiment is typically assumed to be given, that is to say a probability distribution defined on the possible outcomes depending on a set

of unknown parameters. For example, the steel tensile strength may be modelled by a lognormal random variable with unknown mean value and standard deviation. The problem of interest to the theory of mathematical statistics is then the estimation of these parameters from a data set of observed samples.

The theory of mathematical statistics distinguishes between correctly specified and misspecified stochastic models. A stochastic model is *correctly specified* when it can fit the random experiment perfectly. In this case, the parameters for which the stochastic model perfectly reproduces the *data-generating probability distribution* are called the *"true"* parameters. Conversely, a stochastic model that imperfectly represents the random experiment no matter the value of its parameters is called *misspecified*.

Three stochastic inverse methods, often called the *classical methods of estimation*, are well-established and frequently used, namely the Method of Moments (MM) [Pearson, 1894], the method of Maximum Likelihood (ML) [Fisher, 1912] and the Bayes estimation method [Bayes, 1763]. They were devised specifically for the inversion of correctly specified stochastic models: it can be shown [Cramér, 1946, Strasser, 1981, Wald, 1949] that the parameter estimates obtained using these methods generally converge to the "true" value of the sought parameters when more and more experimental data are acquired.

It is nowadays well-known in the theory of mathematical statistics that considerable difficulties may arise in the practical application of the classical methods of estimation. First, the associated computational cost may be prohibitive. Second, when the stochastic model is misspecified, the estimation method may lead to unsatisfactory parameter estimates or may even simply reject the stochastic model. To overcome these difficulties, alternative methods of estimation were introduced, including the generalized method of moments [Hansen, 1982], M-estimation [Huber, 1967, 1981] and divergence minimization estimation [Basu and Lindsay, 1994, Beran, 1977, Keziou, 2003]. Similarly to the classical inverse problems (Sec. 1.1), these methods formulate stochastic inverse problems as the minimization, with respect to the unknown parameters to be identified, of an objective function that quantifies the distance (misfit) between the experimental data and the stochastic model. These methods identify the stochastic model which represents the random experiment "as adequately as possible" in the sense of the chosen objective function.

In computational mechanics, several authors have applied the classical methods of estimation from the theory of mathematical statistics to the inversion of probabilistic structural models aimed at quantifying aleatory uncertainty [see, for instance, Capiez-Lernout, 2004, Chen et al., 2006, Desceliers et al., 2006, Ghanem and Doostan, 2006, Soize, 2005a, 2006]. In geophysics, Chernov [1968], Iooss [1998], Kravtsov et al. [2005] have applied the MM to the identification of stochastic models for fields of material properties of soils. Desceliers et al. [2006] have reported difficulties related to the computational effort required by the classical methods of estimation. To our best knowledge, difficulties created by misspecification in probabilistic structural models have not yet been described.

The theory of mathematical statistics has directed much less attention towards stochastic inverse problems aimed at quantifying epistemic uncertainty. In computational mechanics, several authors have proposed to apply the classical methods of estimation also to this kind of stochastic inverse problems [see, for instance, Beck and Katafygiotis, 1998, Goodwin et al., 1992, Ljung, 1987, 1993, Reinelt et al., 2002, Soize, 2005b, Yuen and Katafygiotis, 2002]. Measurements performed on the single real structure under study are hereby considered as a single realization of a random experiment.

2.3   Further needs

The previous discussion has shown that considerable effort has already been expended to develop methods for the construction of probabilistic structural models and to elaborate methodologies for their inversion. Based on the aforementioned deficiencies and limitations in the current state of the art, there are

three areas where we believe that further research is desirable:

1. The possibility of, and the potential inversion difficulties created by, misspecification in probabilistic structural models should be addressed. Conjunctionally, the adequacy of the classical estimation methods from the theory of mathematical statistics to formulate and solve the inversion of probabilistic structural models should be further evaluated.

2. Alternative inverse methods should be devised, which require a lower computational effort than the classical methods, and allow to circumvent difficulties created by model misspecification.

3. Practical experience in using and inverting probabilistic structural models in real engineering case histories should be collated. The ways probabilistic methods can be integrated in industrial design and decision processes should be further debated.

3   Objectives and outline of this dissertation

This work aims at contributing in the aforementioned research areas requiring further exploration. We will begin this research with evaluating the adequacy of the classical theory of mathematical statistics to formulate and solve the inversion of probabilistic structural models. It will be shown that computational difficulties, and conceptual problems due to model misspecification, are likely to arise upon applying the classical methods of estimation to the stochastic inverse problems typically encountered in computational mechanics. To overcome these difficulties, we propose, similarly to the more recent methods of estimation (Sec. 2.2), to state the inversion of probabilistic structural models as the minimization, with respect to the unknown parameters to be identified, of an objective function that measures the distance (misfit) between the experimental data and the probabilistic model under study. *The main objective of this work is to investigate how the distance between experimental data and corresponding random predictions of probabilistic structural models can be defined and computed in a suitable manner.*

It should be noted that, similarly to the classical inverse problems (Sec. 1.1), stochastic inverse problems can be mathematically ill-posed. Clearly, the existence property does not pose any problem, upon agreeing that the distance between the experimental data and the probabilistic model should only be minimized and need not vanish. However, the uniqueness and the stability property can be problematic, especially when the probabilistic model under consideration exhibits a large number of parameters to be identified. A large subspace of the parameter space may then solve the optimization problem.

As a framework, we shall work throughout the dissertation with probabilistic structural models with minimal parameterization, and use measured frequency-domain Transfer Functions (TFs) as experimental data. Probabilistic models with minimal parameterization have the advantage that their inversion can generally be expected to result in an optimization problem that admits a unique solution and can be solved numerically with a reasonable computational effort. Measured frequency-domain TFs are often used as experimental data in classical inverse problems. Among their advantages over time-domain TFs are the possibility to select data in a specific frequency range of interest and the relatively easy characterization of the distortion of the data due to experimental noise [Pintelon and Schoukens, 2001]. Compared to modal data, they have the advantage that they can also be used in medium-frequency range problems. It seems to us possible to extend the results obtained in the dissertation to other types of probabilistic structural models and to different kinds of experimental data, but such generalizations are not considered.

The dissertation is organized as follows. The thesis comprises two parts: a theoretical part and a practical one, in which the proposed inverse methods are demonstrated on examples. Part I consists of 2 chapters.

Chapter 1, which is mainly bibliographical, describes the construction of probabilistic structural models with minimal parameterization and defines a generic experimental data set. Chapter 2, which gathers the main contributions of this work, treats the inversion of probabilistic structural models.

Part II consists of 3 chapters. Chapters 3 and 4 demonstrate the inversion of probabilistic models aimed at quantifying epistemic uncertainty on examples featuring respectively simulated and real experimental data. Chapter 5 applies the concepts of Part I to develop a methodology for the experimental identification of spatial correlation lengths and dispersion levels characterizing the variability in heterogeneous fields of material properties of structures using the dispersive characteristics of mechanical waves travelling through specimens. An example featuring simulated data is given.

The dissertation finally includes five appendices. First, Appendix A extends Soize's stochastic model with minimal parameterization for non-Gaussian positive-definite matrix-valued random fields for elliptic stochastic partial differential operators to parabolic stochastic partial differential operators, and demonstrates several mathematical results. Then, Appendix B is devoted to the random matrix eigenvalue problem defined by random reduced matrices of non-parametric probabilistic models. Subsequently, Appendices C and D, which summarize known material, are respectively dedicated to signal processing methods for vibration measurements and to the Spectral Analysis of Surface Waves (SASW) inverse method. Finally, Appendix E presents real experimental data that will be used in future work to further develop inverse methods aimed at identifying spatial correlation lengths and dispersion levels.

Part I

Theory

1

The probabilistic structural models and the experimental data

The main objective of this chapter is to describe the probabilistic structural models and the experimental data that will be used in the next chapter to set up inverse methods. As already announced in the general introduction, we shall work with probabilistic structural models with minimal parameterization, introduced by Soize [2000, 2001, 2006], and use measured frequency-domain Transfer Functions (TFs) as experimental data.

The chapter is organized as follows. First, we recall the construction of probabilistic structural models with minimal parameterization (Sec. 1.1). The main results of the theory are described in a functional framework. Then, we describe the discretization of these probabilistic structural models to obtain alternative problems that can be solved by computers (Sec. 1.2). Basic algorithms are provided allowing practical computations to be performed. Subsequently, we define a generic vibration test and a corresponding experimental data set of measured TFs (Sec. 1.3). Finally, we elaborate on the probabilistic modelling of this vibration test (Sec. 1.4).

The reader unfamiliar with the construction of (probabilistic) mechanical models in a functional framework may want to skip ahead from Section 1.1 to Section 1.2 from time to time to see how the theoretical developments are actually used in practice. On the other hand, the reader already familiar with Soize's construction of probabilistic structural models may want to move quickly through the developments of the first two sections of this chapter, which are mainly bibliographical. We recommend to read either Section 1.1.3 concerning the non-parametric approach, or Section 1.1.4 concerning the parametric approach to get used to our notations.

1.1 Probabilistic structural models

This first section describes the construction of probabilistic structural models with minimal parameterization. Only the main results of the theory will be presented, without giving proofs. The reader interested in the mathematical details and proofs is referred to [Soize, 2000, 2001] for time- and frequency-domain non-parametric models, to [Soize, 2006] for elastostatic parametric models and to appendix A for time-domain parametric models.

In the following, we first outline a basic model problem (Sec. 1.1.1). Subsequently, we give the deterministic equations governing the dynamical behaviour of structures (Sec. 1.1.2). Finally, we describe the

construction of non-parametric and parametric probabilistic structural models with minimal parameterization (Secs. 1.1.3 and 1.1.4).

1.1.1 Model problem
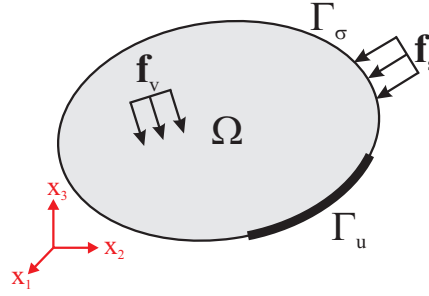
Figure 1.1: The model problem on Ω: notations.

We shall confine ourselves to a classical basic model problem to present the main ideas. The linear vibration of a structure around a reference configuration (without prestress) is considered. Let Ω be the three-dimensional open bounded domain of $\mathbb{R}^3$, occupied by the structure at static equilibrium (Fig. 1.1). Let $\boldsymbol{x} = (x_1, x_2, x_3)$ denote the Cartesian coordinates of any point in Ω. Let Ω have a smooth boundary $\partial\Omega = \Gamma_{\mathrm{u}} \cup \Gamma_\sigma$ such that $\Gamma_{\mathrm{u}} \cap \Gamma_\sigma = \emptyset$ and let $\boldsymbol{n}$ denote the outward unit normal vector. On the part Γ_{u} of the boundary, the structure is fixed.

The dynamical behaviour of the structure is considered in the frequency band of analysis

$$B = [\omega_{\min}, \omega_{\max}], \quad 0 \leq \omega_{\min} < \omega_{\max}. \tag{1.1}$$

With respect to the frequency band B, it is assumed that the constitutive behaviour of the structure can be described accurately by a Kelvin-Voigt material formulation (i.e. a viscoelastic solid material without memory). The structure is subjected (in the frequency band B) to an external body force field in Ω and an external surface force field on Γ_σ.

Structural model for the low- and medium-frequency range

In computational mechanics, the low-, medium- and high-frequency ranges are distinguished [see, for instance, Balmès, 1993, Gibert, 1982, Ohayon and Soize, 1998, Savin, 2002]. At so-called low frequencies, the dynamical response of the structure is primarily constituted of only a few global dynamical eigenmodes (the modal density is low). At intermediate frequencies, the vibration of the structure is characterized by the superposition of some global eigenmodes and clusters of local eigenmodes. Finally, at high frequencies, there is a uniform high modal density.

In the following, it is assumed that B belongs to the low- or medium-frequency range, for which models based on the variational formulation of the dynamical equilibrium of the structure are suitable (specific approaches, such as Statistical Energy Analysis [Lyon, 1975], have been developed for the high frequencies).

1.1.2 Deterministic structural model

This section first gives the deterministic equations governing the frequency-domain dynamical behaviour of the structure. Subsequently, the variational formulation of these equations is presented. Finally, a deterministic reduced matrix model is set up.

Deterministic strong formulation

Let the mass density of the structure be modelled by the deterministic field[3] $x \mapsto \rho(x)$. Let us introduce the space $\mathrm{T}_4^+(\Omega)$ of fourth-rank tensor-valued fields $x \mapsto C(x)$ that verify the usual properties of symmetry and positiveness[4]. Let the elasticity and viscosity tensor fields be modelled by the deterministic fields $x \mapsto C^{\mathrm{e}}(x)$ and $x \mapsto C^{\mathrm{v}}(x)$ in $\mathrm{T}_4^+(\Omega)$. For a fixed $\omega \in B$, let the applied external body and surface force fields be modelled by the respective position-dependent functions $x \mapsto f_{\mathrm{v}}(x; \omega)$ and $x \mapsto f_{\mathrm{s}}(x; \omega)$.

For a fixed $\omega \in B$, the deterministic strong formulation of the studied Boundary Value Problem (BVP) consists in finding the position-dependent response field $x \mapsto u(x; \omega)$ such that:

$$\mathbf{Div}_x \boldsymbol{\sigma}(u) + f_{\mathrm{v}} = -\omega^2 \rho u \qquad \text{in } \Omega \quad , \tag{1.6}$$

$$\boldsymbol{\epsilon}(u) = \frac{1}{2} \left(\mathbf{D}_x u + \mathbf{D}_x u^{\mathrm{T}} \right) \qquad \text{in } \Omega \quad , \tag{1.7}$$

$$\boldsymbol{\sigma}(u) = C^{\mathrm{e}} \left(\boldsymbol{\epsilon}(u) \right) + i\omega C^{\mathrm{v}} \left(\boldsymbol{\epsilon}(u) \right) \qquad \text{in } \Omega \quad , \tag{1.8}$$

with the boundary conditions:

$$u = 0 \qquad \text{on } \Gamma_{\mathrm{u}} \quad , \tag{1.9}$$

$$\boldsymbol{\sigma}(u)(n) = f_{\mathrm{s}} \qquad \text{on } \Gamma_\sigma \quad , \tag{1.10}$$

in which $\boldsymbol{\epsilon}(u)$ and $\boldsymbol{\sigma}(u)$ denote the linearized strain and stress tensor.

Second-rank tensor representation for fourth-rank tensors

For later use, a second-rank tensor representation for fourth-rank tensors is now introduced. Let C be a real $(3 \times 3 \times 3 \times 3)$ fourth-rank tensor that verifies the properties (1.4)-(1.5) of symmetry and positiveness. The tensor C is represented by the symmetric, positive definite real (6×6) second-rank tensor (i.e. ma-

---

[3]From the mathematical point of view, ρ is a strictly positive and essentially bounded function [Dautray and Lions, 1987, ch. 18 sec. 6]:

$$\forall x \in \Omega : \rho(x) > 0 \, , \quad \rho \in L^\infty(\Omega, \mathbb{R}). \tag{1.2}$$

[4]The space $\mathrm{T}_4^+(\Omega)$ collects the fourth-rank tensor fields $x \mapsto C(x)$ fulfilling the following properties of essential boundedness, symmetry and positiveness [Dautray and Lions, 1987, ch. 18 sec. 6]:

$$C_{k\ell mn} \in L^\infty(\Omega, \mathbb{R}) \qquad \qquad \text{for } k, \ell, m, n \in \{1, 2, 3\} \quad , \tag{1.3}$$

$$C_{k\ell mn} = C_{\ell kmn} = C_{k\ell nm} = C_{mnk\ell} \qquad \text{for } k, \ell, m, n \in \{1, 2, 3\} \quad , \tag{1.4}$$

$$\exists c \in \mathbb{R}_0^+ : \forall x \in \Omega : \forall X \in \mathrm{M}_3^{\mathrm{S}}(\mathbb{R}) : \mathrm{tr}\left(C(x)(X)X \right) \geq c \, ||X||_{\mathrm{F}}^2. \tag{1.5}$$

trix) $\widehat{C} \in \mathrm{M}_6^+(\mathbb{R})$ such that:

$$\widehat{C} = \begin{bmatrix} C_{1111} & C_{1122} & C_{1133} & \sqrt{2}C_{1112} & \sqrt{2}C_{1123} & \sqrt{2}C_{1113} \\ C_{1122} & C_{2222} & C_{2233} & \sqrt{2}C_{2212} & \sqrt{2}C_{2223} & \sqrt{2}C_{2213} \\ C_{1133} & C_{2233} & C_{3333} & \sqrt{2}C_{3312} & \sqrt{2}C_{3323} & \sqrt{2}C_{3313} \\ \sqrt{2}C_{1112} & \sqrt{2}C_{2212} & \sqrt{2}C_{3312} & 2C_{1212} & 2C_{1223} & 2C_{1213} \\ \sqrt{2}C_{1123} & \sqrt{2}C_{2223} & \sqrt{2}C_{3323} & 2C_{1223} & 2C_{2323} & 2C_{2313} \\ \sqrt{2}C_{1113} & \sqrt{2}C_{2213} & \sqrt{2}C_{3313} & 2C_{1213} & 2C_{2313} & 2C_{1313} \end{bmatrix}. \tag{1.11}$$

A corresponding first-rank tensor representation for second-rank tensors is introduced. Let $\boldsymbol{X}$ be a symmetric real (3×3) second-rank tensor. This matrix is represented by the real first-order tensor (i.e. vector) $\widehat{\boldsymbol{X}} \in \mathbb{R}^6$ such that:

$$\widehat{\boldsymbol{X}} = \begin{bmatrix} X_{11} & X_{22} & X_{33} & \sqrt{2}X_{12} & \sqrt{2}X_{23} & \sqrt{2}X_{31} \end{bmatrix}^{\mathrm{T}}. \tag{1.12}$$

These representations are such that:

$$\mathrm{tr}\left(\boldsymbol{C}(\boldsymbol{X})\boldsymbol{X}\right) = \left(\widehat{\boldsymbol{C}}\widehat{\boldsymbol{X}}, \widehat{\boldsymbol{X}}\right). \tag{1.13}$$

Deterministic variational formulation

We proceed to elaborate the weak formulation of the BVP. First, let V_0 denote the space of admissible displacements for the problem, which comprises the sufficiently regular[5] deterministic response fields of the structure. For a fixed $\omega \in B$, the deterministic variational formulation of the BVP consists in finding the position-dependent response field $\boldsymbol{u}(\omega) \in V_0$ such that $\forall \boldsymbol{v} \in V_0$:

$$k(\boldsymbol{u}(\omega), \boldsymbol{v}) + i\omega d(\boldsymbol{u}(\omega), \boldsymbol{v}) - \omega^2 m(\boldsymbol{u}(\omega), \boldsymbol{v}) = f(\boldsymbol{v}; \omega). \tag{1.16}$$

The stiffness, damping and mass forms are positive-definite sesquilinear forms[6] defined by:

$$k(\boldsymbol{v}_1, \boldsymbol{v}_2) = \int_\Omega \mathrm{tr}\left(\boldsymbol{C}^{\mathrm{e}}\left(\boldsymbol{\epsilon}(\boldsymbol{v}_1)\right)\boldsymbol{\epsilon}(\overline{\boldsymbol{v}}_2)\right)d\Omega \quad, \tag{1.19}$$

$$d(\boldsymbol{v}_1, \boldsymbol{v}_2) = \int_\Omega \mathrm{tr}\left(\boldsymbol{C}^{\mathrm{v}}\left(\boldsymbol{\epsilon}(\boldsymbol{v}_1)\right)\boldsymbol{\epsilon}(\overline{\boldsymbol{v}}_2)\right)d\Omega \quad, \tag{1.20}$$

$$m(\boldsymbol{v}_1, \boldsymbol{v}_2) = \int_\Omega \rho\left(\boldsymbol{v}_1, \overline{\boldsymbol{v}}_2\right)d\Omega. \tag{1.21}$$

---

[5]The admissible function space is chosen equal to the space

$$V_0 = \left\{\boldsymbol{v} \in \left(H^1(\Omega, \mathbb{C})\right)^3 \mid \boldsymbol{v} = \boldsymbol{0} \text{ on } \Gamma_{\mathrm{u}}\right\}. \tag{1.14}$$

The space V_0 is a Hilbert space for the norm

$$||\boldsymbol{v}||_V^2 = \int_\Omega (\boldsymbol{v}, \overline{\boldsymbol{v}})\,d\Omega + \int_\Omega \mathrm{tr}\left(\mathbf{D}_{\boldsymbol{x}}\boldsymbol{v}\mathbf{D}_{\boldsymbol{x}}\overline{\boldsymbol{v}}\right)d\Omega. \tag{1.15}$$

[6]The stiffness and damping forms are Hermitian, positive definite and continuous on $V_0 \times V_0$. In particular, in view of the Korn inequality [see Duvaut and Lions, 1972, ch. 3], and due to the Dirichlet boundary conditions, there exists a strictly positive constant $\alpha \in \mathbb{R}_0^+$ such that:

$$k(\boldsymbol{v}, \boldsymbol{v}) = \int_\Omega \left(\widehat{\boldsymbol{C}}^{\mathrm{e}}\widehat{\boldsymbol{\epsilon}}(\boldsymbol{v}), \widehat{\boldsymbol{\epsilon}}(\boldsymbol{v})\right)d\Omega \geq \left(\mathrm{ess.}\inf_{\boldsymbol{x} \in \Omega}\left|\left|\widehat{\boldsymbol{C}}^{\mathrm{e}}(\boldsymbol{x})\right|\right|\right)\alpha\,||\boldsymbol{v}||_V^2 \quad, \tag{1.17}$$

$$d(\boldsymbol{v}, \boldsymbol{v}) = \int_\Omega \left(\widehat{\boldsymbol{C}}^{\mathrm{v}}\widehat{\boldsymbol{\epsilon}}(\boldsymbol{v}), \widehat{\boldsymbol{\epsilon}}(\boldsymbol{v})\right)d\Omega \geq \left(\mathrm{ess.}\inf_{\boldsymbol{x} \in \Omega}\left|\left|\widehat{\boldsymbol{C}}^{\mathrm{v}}(\boldsymbol{x})\right|\right|\right)\alpha\,||\boldsymbol{v}||_V^2. \tag{1.18}$$

The mass form is Hermitian, positive definite and continuous on $H \times H$, where $H = \left(L^2(\Omega, \mathbb{C})\right)^3$.

The form representing the external loading is an antilinear form, defined by:

$$f(\boldsymbol{v};\omega) = \int_{\Omega} (\boldsymbol{f}_{\mathrm{v}}(\boldsymbol{x};\omega), \overline{\boldsymbol{v}}(\boldsymbol{x}))\, d\Omega + \int_{\Gamma_{\sigma}} (\boldsymbol{f}_{\mathrm{s}}(\boldsymbol{x};\omega), \overline{\boldsymbol{v}}(\boldsymbol{x}))\, dS. \tag{1.22}$$

For sufficiently regular[7] functions $\boldsymbol{f}_{\mathrm{v}}(\omega)$ and $\boldsymbol{f}_{\mathrm{s}}(\omega)$, it can be shown[8] that the variational formulation (1.16) is well-posed in that the weak solution $\boldsymbol{u}(\omega)$ exists, is unique and depends continuously on the data $\{\boldsymbol{f}_{\mathrm{v}}(\omega), \boldsymbol{f}_{\mathrm{s}}(\omega)\}$.

For later reference, let γ_{P} denote the mapping that, for fixed $\omega \in B$ and given data $\{\boldsymbol{C}^{\mathrm{v}}, \rho, \boldsymbol{f}_{\mathrm{v}}, \boldsymbol{f}_{\mathrm{s}}\}$, maps the tensor field $\boldsymbol{x} \mapsto \boldsymbol{C}^{\mathrm{e}}(\boldsymbol{x})$ onto the unique corresponding weak solution $\boldsymbol{u}(\omega)$ of (1.16):

$$\gamma_{\mathrm{P}}(\omega) : \mathrm{T}_4^+(\Omega) \to V_0 : \boldsymbol{C}^{\mathrm{e}} \mapsto \gamma_{\mathrm{P}}\left(\boldsymbol{C}^{\mathrm{e}};\omega\right) = \boldsymbol{u}(\omega). \tag{1.29}$$

Deterministic reduced matrix model

A deterministic reduced matrix model is now set up. When the frequency band B belongs to the low-frequency range, a reduced model can be built by projecting the variational formulation onto a reduction basis made up of dynamical eigenmodes [see, for instance, Balmès and Leclère, 2006, Le Tallec, 2000, Ohayon and Soize, 1998]. When B belongs to the medium-frequency range, specific reduction bases have to be used. Soize [1998a] has proposed an Energy Operator Approach where an energy operator adapted to B is defined and its dominant eigensubspace is used to build the reduced model. Sarkar and Ghanem [2002] have proposed the Proper Orthogonal Decomposition Method, where spatially dominant coherent structures of the vibration wave field in B are extracted from either numerical or experimental data.

---

[7]For a fixed $\omega \in B$, the position-dependent applied force fields $\boldsymbol{x} \mapsto \boldsymbol{f}_{\mathrm{v}}(\boldsymbol{x};\omega)$ and $\boldsymbol{x} \mapsto \boldsymbol{f}_{\mathrm{s}}(\boldsymbol{x};\omega)$ are taken in the following functional spaces:

$$\boldsymbol{f}_{\mathrm{v}}(\omega) \in \left(L^2(\Omega, \mathbb{C})\right)^3 , \quad \boldsymbol{f}_{\mathrm{s}}(\omega) \in \left(L^2(\Gamma_{\sigma}, \mathbb{C})\right)^3 . \tag{1.23}$$

The antilinear form $f(\cdot;\omega)$ representing the external loading is then continuous (bounded) on V_0:

$$f(\boldsymbol{v};\omega) \leq ||\boldsymbol{f}(\omega)||_{V'}\, ||\boldsymbol{v}||_V \quad , \tag{1.24}$$

where the force vector $\boldsymbol{f}(\omega)$ is such that $\langle \boldsymbol{f}(\omega), \boldsymbol{v}\rangle = f(\boldsymbol{v};\omega)$ and $||\cdot||_{V'}$ is the norm on V' defined by:

$$||\boldsymbol{g}||_{V'} = \sup_{\boldsymbol{v} \in V_0, \boldsymbol{v} \neq 0} \frac{|\langle \boldsymbol{g}, \boldsymbol{v}\rangle|}{||\boldsymbol{v}||_V}. \tag{1.25}$$

[8]For a fixed $\omega \in B$, let the dynamic stiffness form be defined by:

$$s\left(\boldsymbol{v}_1, \boldsymbol{v}_2;\omega\right) = k\left(\boldsymbol{v}_1, \boldsymbol{v}_2\right) + i\omega d\left(\boldsymbol{v}_1, \boldsymbol{v}_2\right) - \omega^2 m\left(\boldsymbol{v}_1, \boldsymbol{v}_2\right). \tag{1.26}$$

It is Hermitian and continuous on $V_0 \times V_0$ (footnote 6). In the static case (when $\omega = 0$), and in the dynamic case (when $\omega \neq 0$), the positive definiteness of the stiffness form k, respectively of the damping form d, ensures the coercivity of $s(\cdot;\omega)$. Since V_0 is a Hilbert space, since $s(\cdot;\omega)$ is Hermitian, coercive and continuous on $V_0 \times V_0$ and since $f(\cdot;\omega)$ is antilinear and continuous on V_0 (footnote 7), the Lax-Milgram theorem [Dautray and Lions, 1987] ensures the well-posedness of the variational formulation (1.16). In particular, the stability property reads in the static case:

$$||\boldsymbol{u}(0)||_V \leq \frac{||\boldsymbol{f}(0)||_{V'}}{\alpha\left(\mathrm{ess.}\inf_{\boldsymbol{x}\in\Omega}\left|\left|\widehat{\boldsymbol{C}}^{\mathrm{e}}(\boldsymbol{x})\right|\right|\right)} \quad , \tag{1.27}$$

and in the dynamic case:

$$||\boldsymbol{u}(\omega)||_V \leq \frac{||\boldsymbol{f}(\omega)||_{V'}}{\omega^2 \alpha\left(\mathrm{ess.}\inf_{\boldsymbol{x}\in\Omega}\left|\left|\widehat{\boldsymbol{C}}^{\mathrm{v}}(\boldsymbol{x})\right|\right|\right)}. \tag{1.28}$$

It is assumed that an appropriate real reduction basis $\{\boldsymbol{\varphi}_\alpha \mid 1 \leq \alpha \leq n_\mathrm{T}\} \subset V_0$ of dimension $n_\mathrm{T} \geq 1$ is given. It is noted that complex reduction bases have also been proposed [see, for instance, Balmès and Leclère, 2006], but are not considered here.

For a fixed $\omega \in B$, the Galerkin projection of the variational formulation onto the reduction basis consists in finding the position-dependent response field

$$\boldsymbol{u}_{n_\mathrm{T}}(\omega) = \sum_{\alpha=1}^{n_\mathrm{T}} q_\alpha(\omega)\boldsymbol{\varphi}_\alpha \in V_0 \quad , \tag{1.30}$$

such that for $1 \leq \beta \leq n_\mathrm{T}$:

$$k\left(\boldsymbol{u}_{n_\mathrm{T}}(\omega), \boldsymbol{\varphi}_\beta\right) + i\omega d\left(\boldsymbol{u}_{n_\mathrm{T}}(\omega), \boldsymbol{\varphi}_\beta\right) - \omega^2 m\left(\boldsymbol{u}_{n_\mathrm{T}}(\omega), \boldsymbol{\varphi}_\beta\right) = f(\boldsymbol{\varphi}_\beta; \omega). \tag{1.31}$$

This expression is equivalent to the following algebraic equation:

$$[\boldsymbol{K} + i\omega\boldsymbol{D} - \omega^2\boldsymbol{M}]\boldsymbol{q}(\omega) = \boldsymbol{g}(\omega). \tag{1.32}$$

Matrices $\boldsymbol{K}$, $\boldsymbol{D}$ and $\boldsymbol{M}$ are the projection of the stiffness, damping and mass forms onto the reduction basis such that:

$$K_{\alpha\beta} = k(\boldsymbol{\varphi}_\alpha, \boldsymbol{\varphi}_\beta) \,, \quad D_{\alpha\beta} = d(\boldsymbol{\varphi}_\alpha, \boldsymbol{\varphi}_\beta) \,, \quad M_{\alpha\beta} = m(\boldsymbol{\varphi}_\alpha, \boldsymbol{\varphi}_\beta) \quad , \tag{1.33}$$

and are symmetric, positive definite real matrices:

$$\boldsymbol{K} \in \mathrm{M}_{n_\mathrm{T}}^+(\mathbb{R}) \,, \quad \boldsymbol{D} \in \mathrm{M}_{n_\mathrm{T}}^+(\mathbb{R}) \,, \quad \boldsymbol{M} \in \mathrm{M}_{n_\mathrm{T}}^+(\mathbb{R}). \tag{1.34}$$

The vector $\boldsymbol{g}(\omega) \in \mathbb{C}^{n_\mathrm{T}}$ of the generalized forces is the projection of the form f onto the reduction basis such that:

$$g_\alpha(\omega) = f(\boldsymbol{\varphi}_\alpha; \omega). \tag{1.35}$$

It can easily be shown that the algebraic equation (1.32) is mathematically well-posed.

For later reference, let γ_NP denote the mapping that, for a fixed $\omega \in B$ and given reduction basis $\{\boldsymbol{\varphi}_\alpha \mid 1 \leq \alpha \leq n_\mathrm{T}\}$ and generalized forces $\boldsymbol{g}$, maps the reduced matrices onto the unique corresponding solution $\boldsymbol{u}_{n_\mathrm{T}}(\omega)$ of (1.30)-(1.32):

$$\gamma_\mathrm{NP}(\omega) : \left(\mathrm{M}_{n_\mathrm{T}}^+(\mathbb{R})\right)^3 \to V_0 : (\boldsymbol{K}, \boldsymbol{D}, \boldsymbol{M}) \mapsto \gamma_\mathrm{NP}(\boldsymbol{K}, \boldsymbol{D}, \boldsymbol{M}; \omega) = \boldsymbol{u}_{n_\mathrm{T}}(\omega). \tag{1.36}$$

1.1.3 Non-parametric probabilistic approach

Following Soize [2000, 2001], non-parametric probabilistic structural models are built by defining reduced matrix models in terms of random matrices. As discussed in the general introduction, a general approach to the construction of the stochastic model of these random matrices consists in representing their probability distribution in a versatile manner as a function of a large number of parameters, for instance by a truncated polynomial chaos expansion [see, for instance, Desceliers et al., 2006, Ghanem and Spanos, 1991, Soize and Ghanem, 2004, Wiener, 1938]. Soize [2000, 2001] has proposed an alternative approach, whereby the stochastic model for the random matrices is deduced using the maximum entropy principle (Box 1.1) from the essential mathematical properties that the probabilistic model should possess. This principle of construction allows obtaining a stochastic model parameterized by a minimal set of essential parameters. In the sequel, we describe the construction of non-parametric probabilistic structural models with minimal parameterization.

Principle of construction

A non-parametric probabilistic model is built by modelling the reduced stiffness, damping and mass matrices in (1.30)-(1.32) by random matrices. The essential mathematical properties required are:

(P1) The random reduced matrices should a.s. be symmetric positive definite matrices.

(P2) The predicted random structural response should be of the second order.

Property **(P1)** ensures that each realization of the probabilistic model is physically acceptable. Property **(P2)** ensures that the well-known theoretical properties and computational tools for second-order random variables are applicable. For example, the mean value of the predicted random response field can be computed numerically by Monte Carlo integration whereby the convergence is controlled by the Central Limit Theorem (CLT) [see, for instance, Robert and Casella, 2005, Rubinstein, 1981]. Another example is the use of **(P2)** by Soize [2001] to demonstrate convergence properties of non-parametric probabilistic models with respect to the dimension of the reduced model.

The construction of the non-parametric probabilistic structural model with minimal parameterization features three steps:

1. First, the maximum entropy principle is applied to construct a class of normalized (i.e. whose mean is the identity matrix) symmetric positive definite real random matrices satisfying a fundamental invertibility property in that the second-order moment of their inverse is bounded (this property will appear in eq. (1.47)).

2. Subsequently, each random reduced matrix is modelled as the product of a normalized random matrix of this kind with the Cholesky factors of a user-defined positive definite matrix. Using the positive-definiteness of the normalized random matrices, the fulfilment of **(P1)** is shown (this property will appear in eq. (1.54)).

3. Finally, a non-parametric probabilistic model is set up, which propagates the uncertainty introduced in the reduced matrices to the predicted dynamical response of the structure. Using the fundamental invertibility property of the normalized random matrices, the fulfilment of **(P2)** is shown (this property will be reflected by eq. (1.56)).

Box 1.1. The maximum entropy principle

This box briefly recalls the maximum entropy principle, introduced by Jaynes [1957, 2003].

Entropy as a measure of uncertainty
Let us first recall the definition of the entropy. Let $\mathbb{X}$ be a random variable with values in $\mathbb{R}$ a.s., which has a PDF $f_{\mathbb{X}}(\boldsymbol{x})$. The Shannon entropy of $\mathbb{X}$ is defined [Shannon, 1948] by:

$$\mathcal{S}\left(f_{\mathbb{X}}\right) = -\int_{\mathbb{R}^n} f_{\mathbb{X}}(\boldsymbol{x}) \log f_{\mathbb{X}}(\boldsymbol{x}) d\boldsymbol{x}. \tag{1.37}$$

The entropy is often interpreted as a measure of uncertainty. For discrete random variables, this interpretation holds in the sense of a set of axioms given by Shannon [1948]. However, as remarked by Shannon [1948], not all axioms hold for continuous random variables, since their entropy depends

on the coordinate system. For a simple example of the interpretation of entropy as a measure of uncertainty, consider a Gaussian random variable $\mathbb{G}$ with values in $\mathbb{R}$ a.s. with mean value m and standard deviation σ. The entropy of $\mathbb{G}$ equals $\log(\sigma\sqrt{2\pi e})$. Intuitively, the uncertainty related to $\mathbb{G}$ is determined by the level of dispersion of the values of $\mathbb{G}$ around the mean value, that is to say by the standard deviation. The entropy is found to increase with the standard deviation, i.e. with the uncertainty.

Maximum entropy principle
The maximum entropy principle was introduced by Jaynes [1957, 2003]. It consists in choosing, out of all probability distributions consistent with a given set of constraints, the one that has maximum entropy.

Illustrative example
As a (classical) illustration, let us apply the maximum entropy principle to determine a probability distribution for a random variable $\mathbb{X}$ under the constraints that (i) $\mathbb{X} \in \mathbb{R}$ a.s., (ii) the mean value of $\mathbb{X}$ equals $E\{\mathbb{X}\} = m_{\mathbb{X}}$ and (iii) the variance of $\mathbb{X}$ equals $E\left\{(\mathbb{X}-m_{\mathbb{X}})^2\right\} = \sigma_{\mathbb{X}}^2$. The PDF $\hat{f}_{\mathbb{X}}$ of $\mathbb{X}$ is then the solution of the following functional optimization problem:

$$\hat{f}_{\mathbb{X}} = \arg\max_{f_{\mathbb{X}}} \mathcal{S}\left(f_{\mathbb{X}}\right) \quad , \tag{1.38}$$

where $x \mapsto f_{\mathbb{X}}(x)$ is a function from $\mathbb{R}$ into $\mathbb{R}^+$, subjected to the equality constraints:

$$\int_{\mathbb{R}} f_{\mathbb{X}}(x)dx = 1 \quad , \tag{1.39}$$

$$\int_{\mathbb{R}} x f_{\mathbb{X}}(x)dx = m_{\mathbb{X}} \quad , \tag{1.40}$$

$$\int_{\mathbb{R}} (x - m_{\mathbb{X}})^2 f_{\mathbb{X}}(x)dx = \sigma_{\mathbb{X}}^2. \tag{1.41}$$

The constrained functional optimization problem (1.38) with (1.39)-(1.39)-(1.40) can easily be solved by the method of the Lagrange multipliers [see, for instance, Ciarlet, 2000, Laporte and Le Tallec, 2002, Udwadia, 1989] to obtain:

$$\hat{p}_{\mathbb{X}}(x|m_{\mathbb{X}}, \sigma_{\mathbb{X}}^2) = \frac{1}{\sqrt{2\pi}\sigma_{\mathbb{X}}} \exp(-\frac{(x - m_{\mathbb{X}})^2}{2\sigma_{\mathbb{X}}^2}). \tag{1.42}$$

The PDF maximizing entropy under the constraints (i), (ii) and (iii) is the Gaussian PDF.

Stochastic model for normalized, symmetric, positive definite real random matrices

The set SG^+ is defined as the set of all normalized, symmetric, positive definite real random matrices $\mathbb{N}(\delta)$, defined on the probability measure space $(\mathcal{A}, \mathcal{F}, P)$, parameterized by a dispersion parameter δ (to be defined shortly), whose probability distribution maximizes entropy under the following constraints:

- $\mathbb{N}(\delta) \in \mathrm{M}_n^+(\mathbb{R})$ a.s.

- $\mathbb{N}(\delta)$ is of the second order and its mean value is the identity matrix $\boldsymbol{I}$:

$$E\{\mathbb{N}(\delta)\} = \boldsymbol{I}. \tag{1.43}$$

- $\mathbb{N}(\delta)$ is such that (Box 1.2):

$$\left| E\left\{ \log\left(\det\left(\mathbb{N}(\delta)\right)\right)\right\}\right| < +\infty. \tag{1.44}$$

The parameter δ controlling the dispersion of $\mathbb{N}(\delta)$ is defined by:

$$\delta^2 = \frac{E\left\{ ||\mathbb{N}(\delta) - \boldsymbol{I}||_{\mathrm{F}}^2\right\}}{E\left\{ ||\boldsymbol{I}||_{\mathrm{F}}^2\right\}} = \frac{E\left\{ ||\mathbb{N}(\delta) - \boldsymbol{I}||_{\mathrm{F}}^2\right\}}{n}. \tag{1.45}$$

If δ satisfies:

$$0 < \delta < \sqrt{\frac{n+1}{n+5}} < 1 \quad , \tag{1.46}$$

the random matrix $\mathbb{N}(\delta)$ possesses the following invertibility property [Soize, 2000, 2001]:

$$E\left\{ ||\mathbb{N}(\delta)^{-1}||_{\mathrm{F}}^2\right\} < +\infty. \tag{1.47}$$

Upon applying (Box 1.1) the method of Lagrange multipliers to solve the constrained optimization problem, the following expression is obtained for the PDF $f_{\mathbb{N}}(\cdot|\delta)$ of a generic random matrix $\mathbb{N}(\delta) \in \mathrm{SG}^+$ as a function of the dimension n and the dispersion level δ:

$$f_{\mathbb{N}}(\boldsymbol{N}|\delta) = \mathbb{1}_{\mathrm{M}_n^+(\mathbb{R})}(\boldsymbol{N}) \times c \times \det(\boldsymbol{N})(n+1)((1-\delta^2)/2\delta^2)\exp\left(-\frac{(n+1)}{2\delta^2}\mathrm{tr}(\boldsymbol{N})\right) \quad , \tag{1.48}$$

in which the normalization constant c is given by:

$$c = \frac{(2\pi)^{-n(n-1)/4}\left(\dfrac{n+1}{2\delta^2}\right)^{n(n+1)(2\delta^2)^{-1}}}{\prod_{k=1}^{n}\Gamma\left(\dfrac{n+1}{2\delta^2} + \dfrac{1-j}{2}\right)}. \tag{1.49}$$

This PDF is defined with respect to the measure (volume element)

$$\tilde{d}\boldsymbol{N} = 2^{n(n-1)/4}\prod_{1\leq k\leq \ell\leq n} dN_{k\ell} \quad , \tag{1.50}$$

where each $dN_{k\ell}$ is the Lebesgue measure on $\mathbb{R}$.

Stochastic model for the random reduced stiffness, damping and mass matrices

The stochastic model for the random reduced matrices is now defined. The mean value of these random matrices must be chosen by the user. Let $\underline{\boldsymbol{K}}(\boldsymbol{p}_0), \underline{\boldsymbol{D}}(\boldsymbol{p}_0), \underline{\boldsymbol{M}}(\boldsymbol{p}_0) \in \mathrm{M}_{n_{\mathrm{T}}}^+(\mathbb{R})$ respectively denote the user-defined mean reduced stiffness, damping and mass matrices. They are parameterized by so-called mean-model parameters $\boldsymbol{p}_0$, that may consist of local features of the model, such as material properties or geometrical parameters, or of global characteristics, such as eigenfrequencies (an example of such mean-model parameters is given in Chapter 3 in part II).

The random reduced stiffness, damping and mass matrices are respectively constructed as:

$$\mathbb{K}(\boldsymbol{p}) = \underline{\boldsymbol{L}}_{\mathrm{K}}(\boldsymbol{p}_0)^{\mathrm{T}}\mathbb{N}_{\mathrm{K}}(\delta_{\mathrm{K}})\underline{\boldsymbol{L}}_{\mathrm{K}}(\boldsymbol{p}_0) \text{ a.s.} \qquad \text{with} \qquad \underline{\boldsymbol{K}}(\boldsymbol{p}_0) = \underline{\boldsymbol{L}}_{\mathrm{K}}(\boldsymbol{p}_0)^{\mathrm{T}}\underline{\boldsymbol{L}}_{\mathrm{K}}(\boldsymbol{p}_0) \quad , \tag{1.51}$$

$$\mathbb{D}(\boldsymbol{p}) = \underline{\boldsymbol{L}}_{\mathrm{D}}(\boldsymbol{p}_0)^{\mathrm{T}}\mathbb{N}_{\mathrm{D}}(\delta_{\mathrm{D}})\underline{\boldsymbol{L}}_{\mathrm{D}}(\boldsymbol{p}_0) \text{ a.s.} \qquad \text{with} \qquad \underline{\boldsymbol{D}}(\boldsymbol{p}_0) = \underline{\boldsymbol{L}}_{\mathrm{D}}(\boldsymbol{p}_0)^{\mathrm{T}}\underline{\boldsymbol{L}}_{\mathrm{D}}(\boldsymbol{p}_0) \quad , \tag{1.52}$$

$$\mathbb{M}(\boldsymbol{p}) = \underline{\boldsymbol{L}}_{\mathrm{M}}(\boldsymbol{p}_0)^{\mathrm{T}}\mathbb{N}_{\mathrm{M}}(\delta_{\mathrm{M}})\underline{\boldsymbol{L}}_{\mathrm{M}}(\boldsymbol{p}_0) \text{ a.s.} \qquad \text{with} \qquad \underline{\boldsymbol{M}}(\boldsymbol{p}_0) = \underline{\boldsymbol{L}}_{\mathrm{M}}(\boldsymbol{p}_0)^{\mathrm{T}}\underline{\boldsymbol{L}}_{\mathrm{M}}(\boldsymbol{p}_0) \quad , \tag{1.53}$$

where the random matrices $\mathbb{N}_K(\delta_K)$, $\mathbb{N}_D(\delta_D)$ and $\mathbb{N}_M(\delta_M)$ are independent random matrices of dimension n_T in the above-defined set SG^+. The matrices $\underline{L}_K(p_0)$, $\underline{L}_D(p_0)$ and $\underline{L}_M(p_0)$ are the Cholesky factors of the corresponding matrices $\underline{K}(p_0)$, $\underline{D}(p_0)$ and $\underline{M}(p_0)$. The set of dispersion parameters p_δ is defined by $p_\delta = \{\delta_K, \delta_D, \delta_M\}$. The parameter set $p = \{p_0, p_\delta\}$ gathers the mean-model and dispersion parameters.

The random matrices $\mathbb{K}(p)$, $\mathbb{D}(p)$ and $\mathbb{M}(p)$ are, by construction, a.s. positive definite matrices:

$$\mathbb{K}(p) \in \mathrm{M}_{n_T}^+(\mathbb{R}) \text{ a.s. }, \quad \mathbb{D}(p) \in \mathrm{M}_{n_T}^+(\mathbb{R}) \text{ a.s. }, \quad \mathbb{M}(p) \in \mathrm{M}_{n_T}^+(\mathbb{R}) \text{ a.s. }, \tag{1.54}$$

ensuring that the above-mentioned property **(P1)** holds.

Non-parametric probabilistic model

We now proceed to define the non-parametric probabilistic model. Let us first introduce the admissible function space $\mathcal{V}_0$ of the problem comprising the second-order random sufficiently regular[9] response fields of the structure. The non-parametric probabilistic model is obtained by modelling the reduced matrices of the reduced matrix model (1.32) by the random matrices $\mathbb{K}(p)$, $\mathbb{D}(p)$ and $\mathbb{M}(p)$. For a fixed $\omega \in B$, it consists in finding the random response field

$$\mathbb{U}(\omega; p) = \sum_{\alpha=1}^{n_T} \mathbb{Q}_\alpha(\omega; p) \varphi_\alpha \in \mathcal{V}_0 \quad , \tag{1.56}$$

such that:

$$[\mathbb{K}(p) + i\omega \mathbb{D}(p) - \omega^2 \mathbb{M}(p)] \mathbb{Q}(\omega; p) = g(\omega) \text{ a.s.} \tag{1.57}$$

When the dispersion parameters $\delta_K, \delta_D, \delta_M$ fulfil inequality (1.46), it can be shown (see also appendix A) that there exists a unique random variable $\mathbb{U}(\omega; p) \in \mathcal{V}_0$ solving (1.57). Since the random response fields in $\mathcal{V}_0$ are of the second order, property **(P2)** holds. Finally, for later use, the random variables obtained by this procedure at all frequencies in B are collected in the stochastic process

$$\{\mathbb{U}(\omega; p) \mid \omega \in B\}. \tag{1.58}$$

In view of the inversion of the probabilistic model in the next chapter, it should be noted that equations (1.56)-(1.57) propagate the uncertainty introduced in the reduced matrices *through the deterministic model* to the dynamical response field. Using the mapping γ_{NP} defined in (1.36), this consideration is highlighted by writing these equations in the following, equivalent, form:

$$\mathbb{U}(\omega; p) = \gamma_{\mathrm{NP}}\big(\mathbb{K}(p), \mathbb{D}(p), \mathbb{M}(p); \omega\big) \text{ a.s.} \tag{1.59}$$

---

[9]The theory of the random variables with values in functional spaces (Box 1.3) is applied to define the admissible function space $\mathcal{V}_0$. It is chosen equal to the stochastic Hilbert space

$$\mathcal{V}_0 = L^2(\mathcal{A}, V_0) = \big\{ \mathbb{V} \in L^0(\mathcal{A}, V_0) \mid E\{\|\mathbb{V}\|_V^2\} < +\infty \big\}. \tag{1.55}$$

Box 1.2. Illustrative example: random spring

This box gives a simple example of the construction of a probabilistic model with minimal parameterization. In particular, the purpose of the constraint (1.44) is highlighted. We consider a single-DOF linear static spring, which is fixed at one end point and loaded by a prescribed force at the other. The stiffness of the spring is assumed to be uncertain.
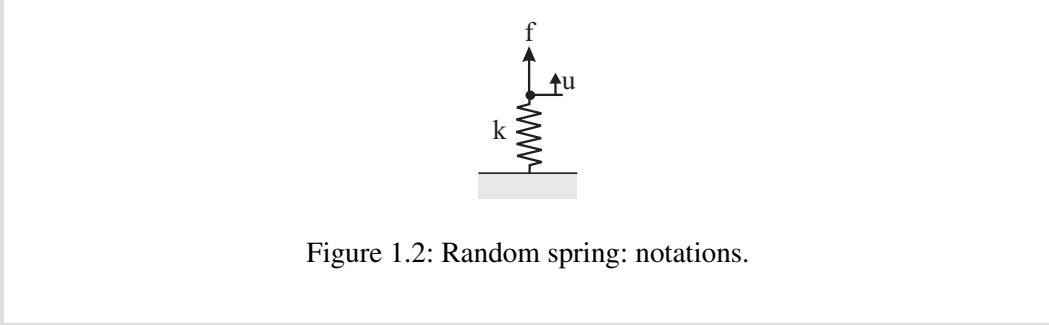
Figure 1.2: Random spring: notations.

The following probabilistic model is considered:

$$\mathbb{K}\mathbb{U} = f \text{ a.s. } ,$$ (1.60)

in which $\mathbb{K}$ is the random spring stiffness, f is the deterministic applied force and $\mathbb{U}$ is the random induced displacement. The essential mathematical properties read here:

(P1) $\mathbb{K} \in \mathbb{R}_0^+$ a.s.

(P2) $E\left\{||\mathbb{U}||^2\right\} < +\infty.$

Let us investigate how the entropy maximization principle (Box 1.1) can be applied to obtain a stochastic model for $\mathbb{K}$ which possesses the properties **(P1)** and **(P2)**.

Application with given support $\mathbb{R}_0^+$ and mean value $E\{\mathbb{K}\}$
Let us apply the maximum entropy principle using the constraints (Box 1.1) that (i) $\mathbb{K} > 0$ a.s. and (ii) the mean value of $\mathbb{K}$ equals $E\{\mathbb{K}\} = \underline{k} \in \mathbb{R}_0^+$. The PDF $\hat{f}_{\mathbb{K}}$ of $\mathbb{K}$ is then the solution of the following functional optimization problem:

$$\hat{f}_{\mathbb{K}} = \arg \max_{f_{\mathbb{K}}} \mathcal{S}\left(f_{\mathbb{K}}\right) \quad ,$$ (1.61)

where $k \mapsto f_{\mathbb{K}}(k)$ is a function from $\mathbb{R}_0^+$ into $\mathbb{R}^+$, subjected to the equality constraints:

$$\int_{\mathbb{R}_0^+} f_{\mathbb{K}}(k)dk = 1 \ , \quad \int_{\mathbb{R}_0^+} k f_{\mathbb{K}}(k)dk = \underline{k}.$$ (1.62)

The constrained functional optimization problem (1.61)-(1.62) is solved by the method of Lagrange multipliers, to obtain:

$$\hat{f}_{\mathbb{K}}(k|\underline{k}) = \mathbb{1}_{\mathbb{R}_0^+}(k)\frac{1}{\underline{k}} \exp(-\frac{k}{\underline{k}}).$$ (1.63)

The PDF maximizing entropy under the constraints (i) and (ii) is the well-known exponential PDF. Upon modelling the spring stiffness by an exponential random variable $\mathbb{K}$ with PDF (1.63), expression (1.60) sets up a probabilistic model for the mechanical behaviour of the spring, which, clearly, possesses the property **(P1)**. However, since

$$\int_{\mathbb{R}_0^+} \frac{1}{k^2} \frac{1}{\underline{k}} \exp\left(-\frac{k}{\underline{k}}\right) dk = +\infty \quad , \tag{1.64}$$

the property **(P2)** does not hold and the stochastic model is therefore inadequate.

Application with given support $\mathbb{R}_0^+$, mean value $E\{\mathbb{K}\}$ and $E\{\log \mathbb{K}\}$

To overcome the incompatibility of the previous probabilistic model with the property **(P2)**, a third constraint is introduced. If the set of constraints consists, moreover, of the knowledge that (iii) the mean value of $\log \mathbb{K}$ equals $E\{\log \mathbb{K}\} = \underline{\nu} \in \mathbb{R}$, then the PDF $\hat{f}_{\mathbb{K}}$ of $\mathbb{K}$ is the solution of the functional optimization problem (1.61), where the function $f_{\mathbb{K}}$ is still subjected to (1.62), but, this time, also to the following third equality constraint:

$$\int_{\mathbb{R}_0^+} \log k \, f_{\mathbb{K}}(k) dk = \underline{\nu}. \tag{1.65}$$

The problem (1.61) with (1.62)-(1.65) is then solved by applying the method of Lagrange multipliers to obtain an analytical expression of $\hat{f}_{\mathbb{K}}$ as a function of $\underline{k}$ and $\underline{\nu}$. Since the parameter $\underline{\nu}$ does not have a simple physical or mathematical meaning, it is replaced by the dispersion parameter δ defined by:

$$\delta = \frac{\sqrt{E\{(\mathbb{K} - \underline{k})^2\}}}{\underline{k}}. \tag{1.66}$$

It is the coefficient of variation and controls the level of dispersion of $\mathbb{K}$ around the mean value $\underline{k}$. The expression of $\hat{f}_{\mathbb{K}}$ as a function of $\underline{k}$ and δ reads:

$$\hat{f}_{\mathbb{K}}(k|\underline{k}, \delta) = \mathbb{1}_{\mathbb{R}_0^+}(k) \frac{1}{\underline{k}} \left(\frac{1}{\delta^2}\right)^{\frac{1}{\delta^2}} \frac{1}{\Gamma(1/\delta^2)} \left(\frac{k}{\underline{k}}\right)^{\frac{1}{\delta^2}-1} \exp\left(-\frac{k}{\delta^2 \underline{k}}\right). \tag{1.67}$$

The PDF maximizing entropy under the constraints (i), (ii) and (iii) is the well-known gamma PDF. Upon modelling the spring stiffness by a gamma random variable $\mathbb{K}$ with PDF (1.67), expression (1.60) defines a probabilistic model for the mechanical behaviour of the spring. Clearly, it possesses the property **(P1)**. Moreover, it can easily be verified that, for $\delta \in [0, 1/\sqrt{2}[$, the property **(P2)** also holds.

Discussion
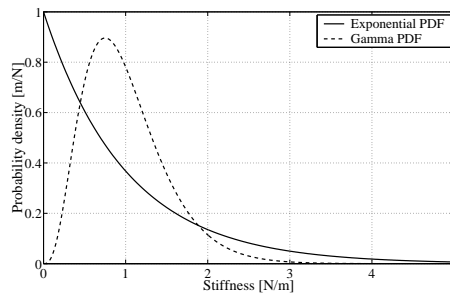
Figure 1.3: Random spring: exponential PDF for $\underline{k} = 1\,\text{N/m}$ and gamma PDF for $\underline{k} = 1\,\text{N/m}$ and $\delta = 0.5$.

Figure 1.3 compares the exponential PDF for $\underline{k} = 1\,\text{N/m}$ with the gamma PDF for $\underline{k} = 1\,\text{N/m}$ and $\delta = 0.5$. The value taken by the exponential PDF is large in the vicinity of the origin. Since small values of the spring stiffness result in large values of the spring displacement, modelling the spring stiffness by an exponential random variable therefore results in a random spring displacement that is not of the second order. The introduction of the constraint $E\{\log \mathbb{K}\} = \underline{\nu}$ has suitably modified the shape of the PDF near the origin, that is to say, the probability associated by the gamma PDF to small spring stiffness is sufficiently low.

1.1.4 Parametric probabilistic approach

Parametric probabilistic models are built by modelling the local physical features of structural models, i.e. their geometrical parameters, fields of material properties and boundary conditions, by random variables or fields. A general approach to the construction of the stochastic model of these random variables or fields consists in representing their probability distribution in a versatile manner as a function of a large number of parameters, for instance by a truncated Karhunen-Loève and/or polynomial chaos expansion [see, for instance, Desceliers et al., 2006, Ghanem and Spanos, 1991, Mercer, 1909, Soize and Ghanem, 2004, Wiener, 1938]. Recently, Soize [2006] has proposed an alternative approach, whereby the stochastic model is defined such that the resulting probabilistic structural model fulfils certain essential mathematical properties and exhibits only a minimal set of parameters. In the following, we describe the construction of parametric probabilistic structural models of the latter kind.

Principle of construction

In the frame of the present model problem, a parametric probabilistic model can be built by modelling the elasticity tensor, the viscosity tensor and the mass density field in the variational formulation (1.16) by random fields. The essential mathematical properties required are:

(P1) The sample paths of the random elasticity and viscosity tensor fields should a.s. fulfil the mathematical properties (1.3)-(1.5) of essential boundedness, symmetry and positiveness, i.e. they should a.s. belong to the space $\text{T}_4^+(\Omega)$ defined in footnote 4. Similarly, the sample paths of the random mass density field should a.s. fulfil the mathematical properties (1.2) of essential boundedness and positiveness.

(P2) The predicted random structural response should be of the second order.

These properties, analogous to those imposed on the stochastic model for the random reduced matrices in Section 1.1.3, respectively ensure that each realization of the probabilistic model is physically acceptable and that the theoretical properties and computational tools for second-order random variables are applicable.

In Section 1.1.2, it was noted that the norm of the weak solution of the deterministic variational formulation (1.16) can be bounded from above using the coercivity constants of the positive definite stiffness and damping forms, which depend themselves on the essential extremum norms of the elasticity and the viscosity tensor field (footnote 8). This result suggests the possibility to control the second-order moment of the random response predicted by the parametric probabilistic model through the stochastic properties of the extrema of the sample paths of the random elasticity and viscosity tensor fields. In order

to obtain probabilistic models fulfilling **(P2)**, an important aspect of Soize's approach to the construction of random field models is therefore the control of the stochastic properties of the extrema of the sample paths.

Unfortunately, the theory of the classical stochastic processes and random fields, which is commonly used in engineering research, is not well-suited to controlling the stochastic properties of extrema of sample paths of random fields. For this reason, Soize has applied the more general, and more powerful, theory of random variables with values in functional spaces, which provides the required tools. Box 1.3 gives a brief summary of these two theories.

As a generic example, we shall detail in the following the construction of a parametric probabilistic model with minimal parameterization by modelling only the elasticity tensor field by a random field. Although they can be modelled by random fields in a similar way, the viscosity tensor and the mass density field will be kept deterministic for the sake of brevity. The construction of this parametric probabilistic model features four steps:

1. First, the theory of the classical stochastic processes is applied to define a class of normalized (i.e. with zero mean and unit variance) Gaussian random fields defined on the probability measure space $(\mathcal{A}, \mathcal{F}, P)$, indexed by the closure $\overline{\Omega} = \Omega \cup \partial\Omega$ of the open domain Ω occupied by the structure and with values in $\mathbb{R}$ a.s. Their autocorrelation function is chosen such that the Dudley lemma [Dudley, 1967] ensures the existence of random fields with continuous sample paths in this class. These sample-continuous random fields are called *stochastic germs*. Each stochastic germ defines (Box 1.3) through its sample paths a random variable defined on $(\mathcal{A}, \mathcal{F}, P)$ with values in the functional space $\mathcal{C}^0(\overline{\Omega}, \mathbb{R})$ a.s., which is recalled to gather all continuous real-valued functions on $\overline{\Omega}$. The measurability properties of random variables of this kind allow studying the stochastic properties of the extrema of the sample paths of the stochastic germs (this property will appear in footnote 12).

2. Then, subsets of stochastic germs are transformed through a continuous non-linear mapping to construct a class of sample-continuous normalized (i.e. whose mean is the identity matrix) symmetric positive definite real matrix-valued random fields. The stochastic properties of the extrema of the sample paths of the stochastic germs and the asymptotic properties of the non-linear transformation mapping are used to demonstrate a fundamental invertibility property (this property will appear in eq. (1.85)).

3. Subsequently, the random elasticity tensor field (in its second-rank tensor representation) is modelled as the product of a normalized random field of this kind with the Cholesky factors of a user-defined positive definite real matrix-valued field. Using the sample continuity and the positive-definiteness of the normalized random fields, the fulfilment of **(P1)** is shown (this property will appear in footnote 13).

4. Finally, a parametric probabilistic model is set up, which propagates the uncertainty introduced in the elasticity tensor field to the predicted dynamical response of the structure. Using the fundamental invertibility property of the normalized random fields, the fulfilment of **(P2)** is shown (this property will appear in eq. (1.87)).

Box 1.3. "Random functions"

This box contains a brief summary of two closely related approaches to work with "random functions". The first approach consists in working with random variables with values in functional, hence

infinite dimensional, spaces. The second is the theory of the classical stochastic processes. The reader is referred to [Da Prato and Zabczyk, 1992, Krée and Soize, 1986, Ledoux and Talagrand, 1991] for more complete accounts.

We will use a basic example to give the main ideas. Let K be a compact subset of $\mathbb{R}$. It will be studied how the notion of a "random function" from K into $\mathbb{R}$ can be formalized.

First approach: random variables with values in functional spaces
In this setting, first, a space X of functions of interest from K into $\mathbb{R}$ is defined (usually, X is of infinite dimension). Examples are the space $X = \mathbb{R}^K$ of all functions from K into $\mathbb{R}$, or the smaller space $\mathcal{C}^0(K, \mathbb{R})$ of continuous functions from K into $\mathbb{R}$. Then, the space X is endowed with a σ-algebra $\mathcal{B}_X$ such that $(X, \mathcal{B}_X)$ is a measurable space. An example of such a σ-algebra is the Borel σ-algebra generated by the open sets induced by, for instance, the uniform-convergence norm on $\mathcal{C}^0(K, \mathbb{R})$. A random variable defined on $(\mathcal{A}, \mathcal{F}, P)$ with values in the functional space X is then a measurable mapping from $(\mathcal{A}, \mathcal{F})$ into $(X, \mathcal{B}_X)$. The probability distribution of the random variable $\mathbb{X}$ is the probability measure $P_{\mathbb{X}}$ induced by $\mathbb{X}$ on $(X, \mathcal{B}_X)$.

Second approach: classical stochastic processes
In this setting, the set K is viewed as a so-called set of indices. This time, the space $\mathbb{R}$ (instead, *a priori*, of a space of functions from K into $\mathbb{R}$) is endowed with a σ-algebra. For the sake of simplicity, let us work here with the Borel σ-algebra $\mathscr{B}(\mathbb{R})$. A classical stochastic process defined on $(\mathcal{A}, \mathcal{F}, P)$, indexed by K and with values in $\mathbb{R}$ a.s. is then a collection $\{\mathbb{Y}(k) \mid k \in K\}$ of random variables indexed by K, or, equivalently, a mapping $\mathbb{Y}(k)$ from K into the space of random variables defined on $(\mathcal{A}, \mathcal{F}, P)$ with values in $\mathbb{R}$ a.s.

The probability distribution of a stochastic process is its so-called system of cylindrical distributions. Let J denote the set of finite nonempty and nonordered subsets of distinct elements of K. For every n-subset $\boldsymbol{j} = \{k_1, \dots, k_n\} \subset K$, a measurable space $(\mathbb{R}^n, (\mathscr{B}(\mathbb{R}))^n)$ is set up, where $\mathbb{R}^n$ and $(\mathscr{B}(\mathbb{R}))^n$ are the Cartesian product and the product σ-algebra of n copies of $\mathbb{R}$ and $\mathscr{B}(\mathbb{R})$, respectively. The cylindrical distribution of the process $\{\mathbb{Y}(k) \mid k \in K\}$ for the index subset $\boldsymbol{j}$ is the probability distribution of the random variable $(\mathbb{Y}(k_1), \dots, \mathbb{Y}(k_n))$, i.e. of the measurable mapping

$$\big(\mathbb{Y}(k_1), \dots, \mathbb{Y}(k_n)\big) : \mathcal{A} \to V^n : a \mapsto \big(\mathbb{Y}(k_1; a), \dots, \mathbb{Y}(k_n; a)\big) \tag{1.68}$$

from $(\mathcal{A}, \mathcal{F})$ into $(\mathbb{R}^n, (\mathscr{B}(\mathbb{R}))^n)$. The system of cylindrical distributions is obtained when $\boldsymbol{j}$ runs through J.

For a given stochastic process $\{\mathbb{Y}(k) \mid k \in K\}$, the mapping

$$\mathbb{Y} : \mathcal{A} \to \mathbb{R}^K : a \mapsto (k \mapsto \mathbb{Y}(k, a)) \tag{1.69}$$

assigns to each $a \in \mathcal{A}$ a sample path, or a trajectory, of $\{\mathbb{Y}(k) \mid k \in K\}$. By the means of the sample paths, the stochastic process $\{\mathbb{Y}(k) \mid k \in K\}$ defines a random variable on $(\mathcal{A}, \mathcal{F}, P)$ with values in the functional space $\mathbb{R}^K$. Indeed, the mapping (1.69) can be made measurable by endowing $\mathbb{R}^K$ with the so-called cylindrical σ-algebra. The probability measure $P_{\mathbb{Y}}$ induced by $\mathbb{Y}$ on $\mathbb{R}^K$, endowed with this σ-algebra, is determined entirely by the system of cylindrical distributions and vice versa [see, for instance, Krée and Soize, 1986, ch. 3 sec. 1 and ch. 10]).

Discussion
The two approaches are closely related. In both approaches, the probability distribution of the "random function" is a probability measure on a functional space. In the first approach, this functional

space can be chosen freely and can be equipped with the most appropriate σ-algebra. In contrast, in the second approach, it is necessarily a product space, such as $\mathbb{R}^K$ in the example, endowed with its cylindrical σ-algebra. The disadvantage of the cylindrical σ-algebra is that it may not be sufficiently fine. For example, the cylindrical σ-algebra on $\mathbb{R}^K$ does not contain the set of "all continuous functions from K into $\mathbb{R}$" [see Billingsley, 1995, ch. 7]. Hence, even the knowledge of the entire system of cylindrical distributions of the stochastic process does not suffice to determine whether or not the sample paths are a.s. continuous. More generally, the countable system of cylindrical distributions of a stochastic process does not always suffice to determine regularity properties of the sample paths. The first approach is therefore more suitable to work with random functions whose realizations verify certain regularity properties.

The main advantage of working with stochastic processes is that certain probabilistic properties of the "random function" can easily be studied by the means of the system of cylindrical distributions. Examples are the mean value of the random function or the correlation between the values taken by the random function at different indices. To facilitate the analysis of random variables with values in functional spaces, so-called projective systems have been introduced, allowing to project such random variables on stochastic processes [see, for instance, Krée and Soize, 1986, ch. 10].

Stochastic model for stochastic germs

This paragraph defines the set $\mathcal{E}_{\mathbb{G}}$ of stochastic germs. Let $\{\mathbb{G}(\boldsymbol{x}; \boldsymbol{p}_{\mathrm{L}}) \mid \boldsymbol{x} \in \mathbb{R}^3\}$ denote a generic Gaussian random field defined on $(\mathcal{A}, \mathcal{F}, P)$, indexed by $\mathbb{R}^3$, with values in $\mathbb{R}$ a.s. and parameterized by the parameter set $\boldsymbol{p}_{\mathrm{L}}$ (to be defined shortly). Since $\{\mathbb{G}(\boldsymbol{x}; \boldsymbol{p}_{\mathrm{L}}) \mid \boldsymbol{x} \in \mathbb{R}^3\}$ is Gaussian, the complete definition of its probability distribution only requires the choice of its mean field and autocorrelation function. For the sake of simplicity, Soize [2006] has taken $\{\mathbb{G}(\boldsymbol{x}; \boldsymbol{p}_{\mathrm{L}}) \mid \boldsymbol{x} \in \mathbb{R}^3\}$ stationary, such that the mean field $m_{\mathbb{G}}(\boldsymbol{x}; \boldsymbol{p}_{\mathrm{L}}) = E\{\mathbb{G}(\boldsymbol{x}; \boldsymbol{p}_{\mathrm{L}})\}$ does not depend on the position and the autocorrelation function $R_{\mathbb{G}}(\boldsymbol{\eta}; \boldsymbol{p}_{\mathrm{L}}) = E\{\mathbb{G}(\boldsymbol{x}; \boldsymbol{p}_{\mathrm{L}})\mathbb{G}(\boldsymbol{x} + \boldsymbol{\eta}; \boldsymbol{p}_{\mathrm{L}})\}$ only depends on the lag distances η_1, η_2 and η_3 along the three spatial directions $\boldsymbol{i}_1$, $\boldsymbol{i}_2$ and $\boldsymbol{i}_3$. Soize [2006] has chosen $m_{\mathbb{G}}$ and $R_{\mathbb{G}}$ such that:

$$m_{\mathbb{G}}(\boldsymbol{x}; \boldsymbol{p}_{\mathrm{L}}) = 0 \quad , \tag{1.70}$$

$$R_{\mathbb{G}}(\boldsymbol{\eta}; \boldsymbol{p}_{\mathrm{L}}) = \rho(\eta_1; L_1)\rho(\eta_2; L_2)\rho(\eta_3; L_3) \quad , \tag{1.71}$$

in which:

$$\rho(\eta; L) = \begin{cases} 1 & \text{if } \eta = 0 \quad , \\ \dfrac{4L^2}{\pi^2\eta^2} \sin^2\left(\dfrac{\pi\eta}{2L}\right) & \text{otherwise.} \end{cases} \tag{1.72}$$

The power spectral density function[10] $S_{\mathbb{G}}$ corresponding to the choice (1.71)-(1.72) reads:

$$S_{\mathbb{G}}(\boldsymbol{k}; \boldsymbol{p}_{\mathrm{L}}) = s(k_1; L_1)s(k_2; L_2)s(k_3; L_3) \quad , \tag{1.75}$$

---

[10]The power spectral density function

$$S_{\mathbb{G}}(\cdot; \boldsymbol{p}_{\mathrm{L}}) : \mathbb{R}^3 \to \mathbb{R} : \boldsymbol{k} = (k_1, k_2, k_3) \mapsto S_{\mathbb{G}}(\boldsymbol{k}; \boldsymbol{p}_{\mathrm{L}}) \tag{1.73}$$

and the autocorrelation function $R_{\mathbb{G}}$ form a Fourier pair such that:

$$\forall \boldsymbol{\eta} \in \mathbb{R}^3 \; : \; R_{\mathbb{G}}(\boldsymbol{\eta}; \boldsymbol{p}_{\mathrm{L}}) = \int_{\mathbb{R}^3} \exp(i\,(\boldsymbol{\eta}, \boldsymbol{k}))S_{\mathbb{G}}(\boldsymbol{k}; \boldsymbol{p}_{\mathrm{L}})d\boldsymbol{k}. \tag{1.74}$$

in which:

$$s(k; L) = \frac{L}{\pi} \Delta \left(\frac{kL}{\pi} \right) \quad , \tag{1.76}$$

where $\Delta : \mathbb{R} \to \mathbb{R}^+$ is the triangle function with compact support $[-1, 1]$ such that:

$$\Delta(0) = 1 \ , \quad \Delta(-\tau) = \Delta(\tau) \ , \quad \Delta(\tau) = 1 - \tau \text{ for } \tau \in [0, 1]. \tag{1.77}$$

The parameter set $\boldsymbol{p}_\mathrm{L} = \{L_1, L_2, L_3\}$ gathers the three so-called spatial correlation lengths. In view of (1.75)-(1.76), they can be interpreted as parameters controlling the wavenumber content of the stochastic germs [see, for instance, Lin and Cai, 1995, Soize, 1993, for details on the spectral analysis of stochastic processes].

The asymptotic behaviour of the autocorrelation function defined by (1.71)-(1.72) for $||\boldsymbol{\eta}|| \to 0$ ensures that there exists a version[11] of $\{\mathbb{G}(\boldsymbol{x}; \boldsymbol{p}_\mathrm{L}) \mid \boldsymbol{x} \in \mathbb{R}^3\}$ that a.s. has continuous sample paths (this can be shown by the Dudley lemma [see, for instance, Soize, 1993, ch. 7 sec. 1]).

Let the set $\overline{\Omega} = \Omega \cup \partial\Omega$ be the closure of Ω. The set $\mathcal{E}_\mathbb{G}$ of stochastic germs is defined as the set comprising all random fields of the generic form

$$\{\mathbb{G}(\boldsymbol{x}; \boldsymbol{p}_\mathrm{L}) \mid \boldsymbol{x} \in \overline{\Omega}\} \quad , \tag{1.78}$$

which are defined on $(\mathcal{A}, \mathcal{F}, P)$, are indexed by $\overline{\Omega}$, have values in $\mathbb{R}$ a.s. and are the restrictions to the bounded domain $\overline{\Omega}$ of the sample-continuous versions of the stationary, Gaussian random fields on $(\mathcal{A}, \mathcal{F}, P)$, indexed by $\mathbb{R}^3$ with values in $\mathbb{R}$ a.s., whose mean field and autocorrelation function are given by (1.70)-(1.72). The measurability properties of the stochastic germs defined in this way allow controlling the stochastic properties of the extrema of their sample paths[12].

Stochastic model for normalized, symmetric, positive definite real matrix-valued random fields

This paragraph defines the set SFG^+ of normalized random fields with values in $\mathrm{M}_6^+(\mathbb{R})$ a.s. It follows from the symmetry and positiveness properties of the matrices in $\mathrm{M}_6^+(\mathbb{R})$ that the matrix-valued random fields in SFG^+ are constituted of 21 mutually dependent real scalar-valued random fields. In the following, the random fields in SFG^+ are constructed as non-linear transformations of subsets of 21 stochastic germs in $\mathcal{E}_\mathbb{G}$.

In [Soize, 2000, 2001, 2006], a deterministic, non-linear continuous mapping

$$\boldsymbol{N}(\cdot; \delta) : \mathbb{R}^{21} \to \mathrm{M}_6^+(\mathbb{R}) : \boldsymbol{g} \mapsto \boldsymbol{N}(\boldsymbol{g}; \delta) \quad , \tag{1.80}$$

---

[11] A system of cylindrical distributions generally does not uniquely define a stochastic process (in the sense of the collection of mappings from the probability space into the space of values). Distinct stochastic processes admitting the same system of cylindrical distributions are called "versions" of each other.

[12] In view of the sample continuity, each stochastic germ defines a random variable on $(\mathcal{A}, \mathcal{F}, P)$ with values in the function space $\mathcal{C}^0(\overline{\Omega}, \mathbb{R})$ a.s. (Box 1.3). It can be shown [see Krée and Soize, 1986, ch. 10 sec. 4]) that this random variable is measurable from $(\mathcal{A}, \mathcal{F})$ into $((\mathcal{C}^0(\overline{\Omega}, \mathbb{R}), \mathscr{B}(\mathcal{C}^0(\overline{\Omega}, \mathbb{R}))))$, where $\mathscr{B}(\mathcal{C}^0(\overline{\Omega}, \mathbb{R}))$ is the Borel σ-algebra generated by the open sets induced by the uniform convergence norm on $\mathcal{C}^0(\overline{\Omega}, \mathbb{R})$. Since sets of the form

$$\{g(\boldsymbol{x}) \in \mathcal{C}^0(\overline{\Omega}, \mathbb{R}) \mid \sup_{\boldsymbol{x} \in \overline{\Omega}} g(\boldsymbol{x}) > u\} \quad , \tag{1.79}$$

where $u \in \mathbb{R}$ is a real scalar, are open metric sets for this norm, they belong to $\mathscr{B}(\mathcal{C}^0(\overline{\Omega}, \mathbb{R}))$. The probability measure induced by the stochastic germs on $(\mathcal{C}^0(\overline{\Omega}, \mathbb{R}), \mathscr{B}(\mathcal{C}^0(\overline{\Omega}, \mathbb{R})))$ therefore allows measuring the probability of the sets of the form (1.79), i.e. of the extrema of the stochastic germs [see, for instance, Ledoux and Talagrand, 1991, Piterbarg, 1996].

was defined, which maps any (21×1) real random vector with mutually independent Gaussian components with zero mean and unit variance onto a (6×6) normalized, symmetric, positive definite real random matrix with dispersion level δ in the set SG$^+$, defined in Section 1.1.3.

The set SFG$^+$ gathers all random fields of the form

$$\{\mathbb{N}(\boldsymbol{x}; \boldsymbol{p}_{\mathrm{L}}; \delta) \mid \boldsymbol{x} \in \overline{\Omega}\} \quad , \tag{1.81}$$

which are defined on $(\mathcal{A}, \mathcal{F}, P)$, indexed by $\overline{\Omega}$, valued in $\mathrm{M}_6^+(\mathbb{R})$ a.s., of the second order, stationary and are the transformation of a subset

$$\left\{\{\mathbb{G}_k(\boldsymbol{x}; \boldsymbol{p}_{\mathrm{L}}) \mid \boldsymbol{x} \in \overline{\Omega}\} \big| 1 \leq k \leq 21\right\} \tag{1.82}$$

of 21 independent stochastic germs in $\mathcal{E}_{\mathbb{G}}$ through the mapping $\boldsymbol{N}(\cdot; \delta)$ such that:

$$\left(\forall \boldsymbol{x} \in \overline{\Omega} \; : \; \mathbb{N}(\boldsymbol{x}; \boldsymbol{p}_{\mathrm{L}}; \delta) = \boldsymbol{N}\Big((\mathbb{G}_1(\boldsymbol{x}; \boldsymbol{p}_{\mathrm{L}}), \dots, \mathbb{G}_{21}(\boldsymbol{x}; \boldsymbol{p}_{\mathrm{L}})); \delta\Big)\right) \text{ a.s.} \tag{1.83}$$

The parameter δ will allow controlling the dispersion level of the fluctuations of the random elasticity tensor field (to be constructed).

It follows from the sample-continuity of the stochastic germs and the continuity of the mapping $\boldsymbol{N}(\cdot; \delta)$ that the random fields in SFG$^+$ are sample-continuous, such that:

$$0 < \sup_{\boldsymbol{x} \in \overline{\Omega}} \left|\left|\mathbb{N}(\boldsymbol{x}; \boldsymbol{p}_{\mathrm{L}}; \delta)^{-1}\right|\right| < +\infty \text{ a.s.} \tag{1.84}$$

Moreover, if the dispersion parameter δ satisfies inequality (1.46), it can be shown that the following fundamental invertibility property is fulfilled:

$$E\left\{\left(\sup_{\boldsymbol{x} \in \overline{\Omega}} \left|\left|\mathbb{N}(\boldsymbol{x}; \boldsymbol{p}_{\mathrm{L}}; \delta)^{-1}\right|\right|\right)^2\right\} < +\infty. \tag{1.85}$$

The proof [see Soize, 2006] is based on the stochastic properties of the extrema of the sample paths of the stochastic germs and the asymptotic properties of the non-linear transformation $\boldsymbol{N}(\cdot; \delta)$ [Abramowitz and Stegun, 1964, Piterbarg, 1996].

Stochastic model for the random elasticity-tensor field

The stochastic model for the random elasticity tensor field is now defined. The mean field must be chosen by the user. Let $(\boldsymbol{x} \mapsto \underline{\boldsymbol{C}}^{\mathrm{e}}(\boldsymbol{x}; \boldsymbol{p}_0)) \in \mathrm{T}_4^+(\Omega)$ denote the user-defined mean field, where $\boldsymbol{p}_0$ collects the parameters of the mean model. The random field $\{\mathbb{C}^{\mathrm{e}}(\boldsymbol{x}; \boldsymbol{p}) \mid \boldsymbol{x} \in \Omega\}$ defined on $(\mathcal{A}, \mathcal{F}, P)$, indexed by Ω with values in the space of fourth-rank tensors is constructed as:

$$\left(\forall \boldsymbol{x} \in \Omega \; : \; \widehat{\mathbb{C}}^{\mathrm{e}}(\boldsymbol{x}; \boldsymbol{p}) = \underline{\boldsymbol{L}_C}(\boldsymbol{x}; \boldsymbol{p}_0)^{\mathrm{T}} \mathbb{N}(\boldsymbol{x}; \boldsymbol{p}_{\mathrm{L}}; \delta) \underline{\boldsymbol{L}_C}(\boldsymbol{x}; \boldsymbol{p}_0)\right) \text{ a.s.} \quad , \tag{1.86}$$

in which $\{\mathbb{N}(\boldsymbol{x}; \boldsymbol{p}_{\mathrm{L}}; \delta) \mid \boldsymbol{x} \in \overline{\Omega}\}$ is a random field in SFG$^+$. The matrix $\underline{\boldsymbol{L}_C}(\boldsymbol{x}; \boldsymbol{p}_0)$ is the Cholesky factor of the matrix $\underline{\widehat{\boldsymbol{C}}}^{\mathrm{e}}(\boldsymbol{x}; \boldsymbol{p}_0)$. The parameter set $\boldsymbol{p} = \{\boldsymbol{p}_0, \boldsymbol{p}_{\mathrm{L}}, \delta\}$ gathers the mean-model parameters, the spatial correlation lengths and the dispersion parameter.

It can be verified[13] that the sample paths of the random field $\{\mathbb{C}^{\mathrm{e}}(\boldsymbol{x}; \boldsymbol{p}) \mid \boldsymbol{x} \in \Omega\}$ a.s. fulfil the usual properties of essential boundedness, symmetry and positiveness, ensuring that property **(P1)** holds.

---

[13] It follows from the sample-continuity of the random fields in SFG$^+$ that the sample paths of $\{\mathbb{C}^{\mathrm{e}}(\boldsymbol{x}; \boldsymbol{p}) \mid \boldsymbol{x} \in \Omega\}$ a.s. verify the property (1.3) of essential boundedness. By construction, the property (1.4) of symmetry is fulfilled. Finally, it can readily be deduced from (1.84) that the sample paths of $\{\mathbb{C}^{\mathrm{e}}(\boldsymbol{x}; \boldsymbol{p}) \mid \boldsymbol{x} \in \Omega\}$ a.s. fulfil the property (1.5) of positiveness.

Parametric probabilistic model

We now proceed to the definition of the parametric probabilistic model with minimal parameterization. We will still work with the admissible function space $\mathcal{V}_0$, defined in footnote 9, of the second-order random sufficiently regular response fields of the structure. The parametric probabilistic model is obtained by modelling the elasticity tensor field of the variational formulation (1.16) by the random field $\{\mathbb{C}^{\mathrm{e}}(\boldsymbol{x};\boldsymbol{p}) \mid \boldsymbol{x} \in \Omega\}$. For a fixed $\omega \in B$, it consists in finding the random response field

$$\mathbb{U}(\omega;\boldsymbol{p}) \in \mathcal{V}_0 \quad , \tag{1.87}$$

such that:

$$\Big(\forall \boldsymbol{v} \in V_0 \ : \ \mathbb{K}\big(\mathbb{U}(\omega;\boldsymbol{p}),\boldsymbol{v}\big) + i\omega d\big(\mathbb{U}(\omega;\boldsymbol{p}),\boldsymbol{v}\big) - \omega^2 m\big(\mathbb{U}(\omega;\boldsymbol{p}),\boldsymbol{v}\big) = f(\omega;\boldsymbol{v})\Big) \text{ a.s.} \tag{1.88}$$

The random stiffness form is defined by:

$$\mathbb{K}\left(\boldsymbol{v}_1,\boldsymbol{v}_2;\boldsymbol{p}\right) = \int_\Omega \mathrm{tr}\big(\mathbb{C}^{\mathrm{e}}(\boldsymbol{p})\left(\boldsymbol{\epsilon}(\boldsymbol{v}_1)\right)\boldsymbol{\epsilon}(\overline{\boldsymbol{v}}_2)\big)d\Omega \text{ a.s.} \tag{1.89}$$

If the dispersion parameter δ fulfils the inequality (1.46), it can be shown (see also appendix A) that there exists a unique random variable $\mathbb{U}(\omega;\boldsymbol{p}) \in \mathcal{V}_0$ solving (1.88). Since the random response fields in $\mathcal{V}_0$ are of the second order, property **(P2)** holds. Finally, for later use, the random variables obtained by this procedure at all frequencies in B are collected in the stochastic process

$$\{\mathbb{U}(\omega;\boldsymbol{p}) \mid \omega \in B\}. \tag{1.90}$$

In view of the inversion of the probabilistic model in the next chapter, it should be noted that equation (1.88) propagates the uncertainty introduced in the elasticity tensor field *through the deterministic model* to the dynamical response field. This consideration is highlighted by writing the equation (1.88) in the following equivalent form[14]:

$$\mathbb{U}(\omega;\boldsymbol{p}) = \gamma_{\mathrm{P}}\big(\mathbb{C}^{\mathrm{e}}(\boldsymbol{p});\omega\big) \text{ a.s.} \quad , \tag{1.91}$$

where the mapping γ_{P} was defined in (1.29).

1.1.5 Time-domain probabilistic structural models

This section presented the construction of non-parametric and parametric probabilistic models for the frequency-domain dynamical behaviour of structures. A similar methodology can be followed to build time-domain probabilistic structural models. The reader is referred to [Soize, 2001] for time-domain non-parametric models and to appendix A for time-domain parametric models.

1.2 Discretization of the probabilistic structural models

In the previous section, the construction of probabilistic structural models with minimal parameterization was presented in a functional framework. Our objective in this section is to describe the discretization of these probabilistic models to obtain alternative problems that can be solved by computers. We

---

[14]The random variable $\mathbb{C}^{\mathrm{e}}(\boldsymbol{p})$ is the random variable defined on $(\mathcal{A},\mathcal{F},P)$ with values in $T_4^+(\Omega)$ a.s. defined by the sample paths of the random field $\{\mathbb{C}^{\mathrm{e}}(\boldsymbol{x};\boldsymbol{p}) \mid \boldsymbol{x} \in \Omega\}$ (see also Box 1.3).

shall provide basic algorithms for performing computations with non-parametric (Sec. 1.2.1) or parametric (Sec. 1.2.2) probabilistic models.

The Finite Element (FE) method will be used for the discretization of the space [see, for instance, Bonnet and Frangi, 2006, Ciarlet, 1978, Hughes, 1987, Oden and Reddy, 1976, Zienkiewicz and Taylor, 2000a,b]. The random dimension will be discretized by MCS, which is the appropriate method considering that the probabilistic models have been built by writing the equilibrium equations of the structure in the almost sure sense with respect to the random coordinate[15]

1.2.1 Non-parametric probabilistic approach

A typical computation with the non-parametric probabilistic model, set up in Section 1.1.3, encompasses two main steps. First, a deterministic reduced matrix model is built for the studied structure. Subsequently, the MCS method is applied to perform calculations with the associated non-parametric probabilistic model. Algorithm 1 details this procedure for the basic case where the reduced model is obtained by projecting a FE model onto a reduction basis of dynamical eigenmodes.

Algorithm 1: computation with the non-parametric probabilistic model

---

- **Step 1: construction of the deterministic reduced matrix model:**
  Step 1a: initialization:
  Choose the level of refinement of the FE model.
  Choose the dimension n_T of the reduction basis.

  Step 1b: construction of the FE model:
  Build a FE model for the studied structure with the chosen level of refinement to obtain a matrix model of the following form:

  $$[\boldsymbol{K}_h + i\omega \boldsymbol{D}_h - \omega^2 \boldsymbol{M}_h]\boldsymbol{u}_h(\omega) = \boldsymbol{f}_h(\omega) \,, \quad \omega \in B \quad , \tag{1.92}$$

  where $\boldsymbol{K}_h, \boldsymbol{D}_h, \boldsymbol{M}_h \in \mathrm{M}_{n_h}^+(\mathbb{R})$ (where n_h is the number of FE DOFs) are the FE stiffness, damping and mass matrices. For a fixed $\omega \in B$, the vectors $\boldsymbol{u}_h(\omega)$ and $\boldsymbol{f}_h(\omega)$ in $\mathbb{C}^{n_h}$ collect the FE DOFs and nodal forces. We note that, formally, $\boldsymbol{K}_h, \boldsymbol{D}_h, \boldsymbol{M}_h$ and $\boldsymbol{f}_h(\omega)$ are obtained by projecting the forms k, d, m and $f(\cdot; \omega)$, defined in the previous section, onto the chosen FE basis.

  Step 1c: calculation of the reduction basis:
  Solve the generalized eigenvalue problem

  $$\boldsymbol{K}_h \boldsymbol{\varphi}_h = \lambda_h \boldsymbol{M}_h \boldsymbol{\varphi}_h \tag{1.93}$$

  to obtain the n_T eigenvectors $\{\boldsymbol{\varphi}_{h,\alpha} \in \mathbb{R}^{n_h} \mid 1 \le \alpha \le n_T\}$ associated to the n_T lowest eigenfrequencies. Gather these eigenvectors in the columns of the rectangular transformation matrix $\boldsymbol{T}_{n_T} \in \mathrm{M}_{n_h \times n_T}(\mathbb{R})$.

---

[15]If the equilibrium equations had been written in the weak sense with respect to the random coordinate, the natural methodology for the discretization of the random dimension would have consisted in the Galerkin projection of the variational formulation onto a suitable approximating stochastic functional space. Ghanem and Spanos [1991] have proposed building this approximating stochastic functional space using the polynomial chaos expansion. Babuška et al. [2005], Deb et al. [2001] have proposed using FE spaces.

Step 1d: construction of the deterministic reduced model:
Project the FE model (1.92) onto the reduction basis to obtain the following reduced matrix model:

$$[\boldsymbol{K} + i\omega\boldsymbol{D} - \omega^2\boldsymbol{M}]\boldsymbol{q}_{n_{\mathrm{T}}}(\omega) = \boldsymbol{T}_{n_{\mathrm{T}}}^{\mathrm{T}}\boldsymbol{f}_{\mathrm{h}}(\omega) , \quad \omega \in B \quad , \tag{1.94}$$

$$\boldsymbol{u}_{\mathrm{h}}(\omega) = \boldsymbol{T}_{n_{\mathrm{T}}}\boldsymbol{q}_{n_{\mathrm{T}}}(\omega). \tag{1.95}$$

The matrices $\boldsymbol{K}, \boldsymbol{D}, \boldsymbol{M} \in \mathrm{M}_{n_{\mathrm{T}}}^{+}(\mathbb{R})$ are the reduced stiffness, damping and mass matrices, respectively, obtained by the projection of the corresponding matrices of the FE model onto the reduction basis. For a fixed $\omega \in B$, $\boldsymbol{q}_{n_{\mathrm{T}}}(\omega)$ is the vector of the generalized coordinates and $\boldsymbol{u}_{\mathrm{h}}(\omega)$ gathers the FE DOFs for the reduced model.

- **Step 2: computation with the non-parametric probabilistic model:**
  Step 2a: initialization:
  Choose a number n_{S} of Monte Carlo samples.
  Choose the mean matrices $\{\underline{\boldsymbol{K}}(\boldsymbol{p}_0), \underline{\boldsymbol{D}}(\boldsymbol{p}_0), \underline{\boldsymbol{M}}(\boldsymbol{p}_0)\}$ and the dispersion levels $\{\delta_{\mathrm{K}}, \delta_{\mathrm{D}}, \delta_{\mathrm{M}}\}$.
  Choose a set $\{\omega_\ell \mid 1 \leq \ell \leq n_{\mathrm{F}}\} \subset B$ of discrete frequencies.

Step 2b: simulation of the samples of the random reduced matrices:
Simulate (see Algorithm 2 of Box 1.4) a set $\big\{\big(\mathbb{K}(a_s; \boldsymbol{p}), \mathbb{D}(a_s; \boldsymbol{p}), \mathbb{M}(a_s; \boldsymbol{p})\big) \mid 1 \leq s \leq n_{\mathrm{S}}\big\}$ of n_{S} independent and identically-distributed (iid) samples of the triple $(\mathbb{K}(\boldsymbol{p}), \mathbb{D}(\boldsymbol{p}), \mathbb{M}(\boldsymbol{p}))$ gathering the random reduced stiffness, damping and mass matrix.

Step 2c: calculation of the samples of the random response:
For each $s \in \{1 \leq s \leq n_{\mathrm{S}}\}$, solve the deterministic problem for $(\mathbb{K}(a_s; \boldsymbol{p}), \mathbb{D}(a_s; \boldsymbol{p}), \mathbb{M}(a_s; \boldsymbol{p}))$.

For the s-th iteration, solve, for each $\ell \in \{1 \leq \ell \leq n_{\mathrm{F}}\}$, the following matrix equation:

$$[\mathbb{K}(a_s; \boldsymbol{p}) + i\omega_\ell\mathbb{D}(a_s; \boldsymbol{p}) - \omega_\ell^2\mathbb{M}(a_s; \boldsymbol{p})]\mathbb{Q}_{n_{\mathrm{T}}}(\omega_\ell; a_s; \boldsymbol{p}) = \boldsymbol{T}_{n_{\mathrm{T}}}^{\mathrm{T}}\boldsymbol{f}_{\mathrm{h}}(\omega_\ell) \quad , \tag{1.96}$$

$$\mathbb{U}_{\mathrm{h}}(\omega_\ell; a_s; \boldsymbol{p}) = \boldsymbol{T}_{n_{\mathrm{T}}}\mathbb{Q}_{n_{\mathrm{T}}}(\omega_\ell; a_s; \boldsymbol{p}). \tag{1.97}$$

Gather the iid samples of the random response obtained by this procedure in the set

$$\{\mathbb{U}_{\mathrm{h}}(\omega_\ell; a_s; \boldsymbol{p}) \mid 1 \leq \ell \leq n_{\mathrm{F}} , \ 1 \leq s \leq n_{\mathrm{S}}\}. \tag{1.98}$$

Step 2d: statistical estimation of quantities of interest:
Apply the theory of mathematical statistics to study the probabilistic properties of the random response field. For instance, the expectation value of the random displacement field at the frequency ω_ℓ can be estimated by the statistical average of the n_{S} iid samples $\{\mathbb{U}_{\mathrm{h}}(\omega_\ell; a_s; \boldsymbol{p}) \mid 1 \leq s \leq n_{\mathrm{S}}\}$ as follows:

$$\hat{\boldsymbol{m}}_{\mathrm{h}, n_{\mathrm{S}}}(\omega_\ell; \boldsymbol{p}) = \frac{1}{n_{\mathrm{S}}}\sum_{s=1}^{n_{\mathrm{S}}}\mathbb{U}_{\mathrm{h}}(\omega_\ell; a_s; \boldsymbol{p}). \tag{1.99}$$

In this algorithm, the discretization of the space and the random dimension introduces a *discretization error* in that the computed result is usually only an approximation of the exact result. However, the non-parametric probabilistic model has been built, and the numerical discretization methods have been chosen, in such a way that this error can be controlled. The error induced by the discretization of the space can be reduced by refining the FE model of the structure [see, for instance, Babuška and Strouboulis, 2001, Demkowicz et al., 2002, Schwab, 1999]. The statistical error, corresponding to the computation of the estimate (1.99) on the basis of only a finite number of samples, can be reduced by increasing this number of samples. The statistical error is controlled by the CLT since, by construction, the random variable $\mathbb{U}_{\mathrm{h}}(\omega_\ell; \boldsymbol{p})$ is of the second order.

Box 1.4. Simulation of the random matrices

This box describes the numerical simulation of the random reduced matrices featured in non-parametric probabilistic models with minimal parameterization.

In [Soize, 2000, 2001, 2006], a deterministic mapping

$$\boldsymbol{N}(\cdot; \delta) : \mathbb{R}^{n(n+1)/2} \rightarrow \mathrm{M}_n^+(\mathbb{R}) : \boldsymbol{g} \mapsto \boldsymbol{N}(\boldsymbol{g}; \delta) \tag{1.100}$$

was introduced, which maps any $(n(n+1)/2 \times 1)$ real random vector with mutually independent Gaussian components with zero mean and unit variance onto a $(n \times n)$ normalized, symmetric, positive definite real random matrix with dispersion level δ in the set SG^+, defined in Section 1.1.3. Soize [2000, 2001, 2006] has given a generic expression for this mapping as a function of the dimension n and the dispersion level δ, which allows the numerical approximation of $\boldsymbol{N}(\cdot; \delta)$. Therefore, the matrix $\boldsymbol{N}(\boldsymbol{g}; \delta)$ was written as:

$$\boldsymbol{N}(\boldsymbol{g}; \delta) = \boldsymbol{L}(\boldsymbol{g}; \delta)^{\mathrm{T}} \boldsymbol{L}(\boldsymbol{g}; \delta) \quad, \tag{1.101}$$

where $\boldsymbol{L}(\boldsymbol{g}; \delta) \in \mathrm{M}_n^+(\mathbb{R})$ is an upper triangular matrix such that:

$$L_{kk'}(\boldsymbol{g}; \delta) = \delta \sqrt{n+1} g_{(k-1)n+k'} \quad \text{for } k < k' \quad, \tag{1.102}$$

$$L_{kk}(\boldsymbol{g}; \delta) = \delta \sqrt{n+1} \sqrt{h\left(g_{(k-1)n+k'}; \frac{n+1}{2\delta^2} + \frac{1-k}{2}\right)}. \tag{1.103}$$

The mapping $h(\cdot; \alpha) : \mathbb{R} \rightarrow \mathbb{R}_0^+ : g \mapsto h(g; \alpha)$ is such that:

$$h(g; \alpha) = F_\gamma^{-1}\left(F_{\mathrm{N}}(g); \alpha\right) \quad, \tag{1.104}$$

where $F_{\mathrm{N}} : \mathbb{R} \rightarrow]0, 1[$ is the cumulative distribution function of a normalized Gaussian random variable:

$$F_{\mathrm{N}}(g) = \int_{-\infty}^g \frac{1}{\sqrt{2\pi}} \exp\left(-\frac{x^2}{2}\right) dx \quad, \tag{1.105}$$

and $F_\gamma(\cdot; \alpha) : \mathbb{R}_0^+ \rightarrow]0, 1[$ is the cumulative distribution function of a gamma random variable:

$$F_\gamma(g; \alpha) = \int_0^g \frac{1}{\Gamma(\alpha)} x^{\alpha-1} \exp(-x) dx. \tag{1.106}$$

The integrals (1.105) and (1.106) cannot be solved analytically and must therefore be approximated numerically [see, for instance, Abramowitz and Stegun, 1964]. Algorithm 2 details the procedure for the numerical simulation of a random reduced matrix using the mapping $\boldsymbol{N}(\cdot; \delta)$.

Algorithm 2: simulation of a random reduced matrix $\mathbb{A}(\boldsymbol{p})$

- **Step 1: initialization:**
  Choose a number n_{S} of Monte Carlo samples.
  Choose the mean matrix $\underline{\boldsymbol{A}}(\boldsymbol{p}_0) \in \mathrm{M}_n^+(\mathbb{R})$ and the dispersion level δ_{A}.

- **Step 2: simulation of the samples of a Gaussian random vector:**
  Simulate a set $\{\mathbb{G}(a_s) \mid 1 \leq s \leq n_{\mathrm{S}}\}$ of n_{S} iid samples of a random vector $\mathbb{G}$ with values in $\mathbb{R}^{n(n+1)/2}$ with mutually independent Gaussian components with zero mean and unit variance. The Box-Muller transformation can, for instance, be used to perform this task [see, for instance, Robert and Casella, 2005].

- **Step 3: calculation of the samples of the random reduced matrix:**
  For each $s \in \{1 \leq s \leq n_{\mathrm{S}}\}$, compute the matrix

$$\mathbb{A}(a_s; \boldsymbol{p}) = \underline{\boldsymbol{L}}_{\mathrm{A}}^{\mathrm{T}}(\boldsymbol{p}_0) \boldsymbol{N}\big(\mathbb{G}(a_s); \delta_{\mathrm{A}}\big) \underline{\boldsymbol{L}}_{\mathrm{A}}(\boldsymbol{p}_0) \quad , \tag{1.107}$$

  where $\underline{\boldsymbol{L}}_{\mathrm{A}}(\boldsymbol{p}_0)$ is the Cholesky factor of $\underline{\boldsymbol{A}}(\boldsymbol{p}_0)$. Gather the iid samples of the random reduced matrices obtained by this procedure in the set

$$\{\mathbb{A}(a_s; \boldsymbol{p}) \mid 1 \leq s \leq n_{\mathrm{S}}\}. \tag{1.108}$$

1.2.2 Parametric probabilistic approach

Algorithm 3 details the main steps in a computation with the parametric probabilistic model, set up in Section 1.1.4.

Algorithm 3: computation with the parametric probabilistic model

---

- **Step 1: initialization:**
  Choose a number n_{S} of Monte Carlo samples.
  Choose the mean field $\boldsymbol{x} \mapsto \underline{\boldsymbol{C}}^{\mathrm{e}}(\boldsymbol{x}; \boldsymbol{p}_0)$, the correlation lengths $\boldsymbol{p}_{\mathrm{L}}$ and the dispersion level δ.
  Choose the level of refinement of the FE model.
  Choose a set $\{\omega_\ell \mid 1 \leq \ell \leq n_{\mathrm{F}}\} \subset B$ of discrete frequencies.

- **Step 2: simulation of the samples of the random elasticity tensor field:**
  Simulate (see Algorithm 4 of Box 1.5) a set $\{\boldsymbol{x} \mapsto \mathbb{C}^{\mathrm{e}}(\boldsymbol{x}; a_s; \boldsymbol{p}) \mid 1 \leq s \leq n_{\mathrm{S}}\}$ of n_{S} iid sample paths of the random elasticity tensor field $\{\mathbb{C}^{\mathrm{e}}(\boldsymbol{x}; \boldsymbol{p}) \mid \boldsymbol{x} \in \Omega\}$.

- **Step 3: calculation of the samples of the random response:**
  For each $s \in \{1 \leq s \leq n_{\mathrm{S}}\}$, solve the deterministic problem associated to the sample path $\boldsymbol{x} \mapsto \mathbb{C}^{\mathrm{e}}(\boldsymbol{x}; a_s; \boldsymbol{p})$.

  Step 3a: construction of a FE model:
  For the s-th iteration, build a FE model with the chosen level of refinement to obtain a matrix model of the following form:

$$[\mathbb{K}_{\mathrm{h}}(a_s; \boldsymbol{p}) + i\omega \boldsymbol{D}_{\mathrm{h}} - \omega^2 \boldsymbol{M}_{\mathrm{h}}] \mathbb{U}_{\mathrm{h}}(\omega; a_s; \boldsymbol{p}) = \boldsymbol{f}_{\mathrm{h}}(\omega) , \quad \omega \in B \quad , \tag{1.109}$$

  where $\mathbb{K}_{\mathrm{h}}(a_s; \boldsymbol{p}) \in \mathrm{M}_{n_{\mathrm{h}}}^+(\mathbb{R})$ (where n_{h} is the number of FE DOFs) is the FE stiffness matrix corresponding to the elasticity tensor field $\boldsymbol{x} \mapsto \mathbb{C}^{\mathrm{e}}(\boldsymbol{x}; a_s; \boldsymbol{p})$. The matrices $\boldsymbol{D}_{\mathrm{h}}, \boldsymbol{M}_{\mathrm{h}} \in \mathrm{M}_{n_{\mathrm{h}}}^+(\mathbb{R})$ are the FE damping and mass matrices. For a fixed $\omega \in B$, the vectors $\mathbb{U}_{\mathrm{h}}(\omega; a_s; \boldsymbol{p})$ and $\boldsymbol{f}_{\mathrm{h}}(\omega)$ in $\mathbb{C}^{n_{\mathrm{h}}}$

collect the FE DOFs and nodal forces. We note that, formally, $\mathbb{K}_\mathrm{h}(a_s; \boldsymbol{p})$, $\boldsymbol{D}_\mathrm{h}$, $\boldsymbol{M}_\mathrm{h}$ and $\boldsymbol{f}_\mathrm{h}(\omega)$ are obtained by projecting the forms $\mathbb{K}(\cdot; a_s; \boldsymbol{p})$, d, m and $f(\cdot; \omega)$, defined in the previous section, onto the chosen FE basis.

Step 3b: calculation of the samples of the random response:
For the s-th iteration, solve, for each $\ell \in \{1 \leq \ell \leq n_\mathrm{F}\}$, the following matrix equation:

$$[\mathbb{K}_\mathrm{h}(a_s; \boldsymbol{p}) + i\omega_\ell \boldsymbol{D}_\mathrm{h} - \omega_\ell^2 \boldsymbol{M}_\mathrm{h}]\mathbb{U}_\mathrm{h}(\omega_\ell; a_s; \boldsymbol{p}) = \boldsymbol{f}_\mathrm{h}(\omega_\ell). \tag{1.110}$$

Gather the iid samples of the random response obtained by this procedure in the set

$$\{\mathbb{U}_\mathrm{h}(\omega_\ell; a_s; \boldsymbol{p}) \mid 1 \leq \ell \leq n_\mathrm{F} \ , \ 1 \leq s \leq n_\mathrm{S}\}. \tag{1.111}$$

- **Step 4: statistical estimation of quantities of interest:** (see Algorithm 1).

In this algorithm, the discretization of the space and the random dimension introduces a discretization error. As it was also the case for the non-parametric probabilistic model, this error can be reduced by refining the FE model and by increasing the number of Monte Carlo samples.

Box 1.5. Simulation of the random elasticity tensor field

This box describes the numerical simulation of the random elasticity tensor field of parametric probabilistic models with minimal parameterization. A practical methodology is given based on the simulation of the underlying Gaussian stochastic germs by the spectral representation method [see, for instance, Poirion and Soize, 1989, Puig, 2003, Shinozuka and Jan, 1972]. We refer the reader to [Puig, 2003] for a review of the various other approaches that were proposed in the literature for the simulation of random fields.

Let us first detail the simulation of a stochastic germ $\{\mathbb{G}(\boldsymbol{x}; \boldsymbol{p}_\mathrm{L}) \mid \boldsymbol{x} \in \overline{\Omega}\}$ in the set $\mathcal{E}_\mathbb{G}$. The spectral representation method is based on the approximation of the continuous power spectral density function $S_\mathbb{G}(\cdot; \boldsymbol{p}_\mathrm{L})$, defined in (1.75)-(1.76), by a discrete power spectrum. More specifically, the stochastic germ $\{\mathbb{G}(\boldsymbol{x}; \boldsymbol{p}_\mathrm{L}) \mid \boldsymbol{x} \in \overline{\Omega}\}$ is approximated by an alternative random field $\{\mathbb{G}^{(n)}(\boldsymbol{x}; \boldsymbol{p}_\mathrm{L}) \mid \boldsymbol{x} \in \overline{\Omega}\}$ defined as the superposition of n^3 cosine functions, each with a random amplitude and a random phase shift:

$$\left\{\mathbb{G}^{(n)}(\boldsymbol{x}; \boldsymbol{p}_\mathrm{L}) = \sqrt{2\frac{\pi}{L_1}\frac{\pi}{L_2}\frac{\pi}{L_3}} \sum_{\boldsymbol{\alpha} \in A_n} \sqrt{S_\mathbb{G}(\boldsymbol{k}_{\boldsymbol{\alpha}}; \boldsymbol{p}_\mathrm{L})} \mathbb{X}_{\boldsymbol{\alpha}} \cos\big((\boldsymbol{k}_{\boldsymbol{\alpha}}, \boldsymbol{x}) + \mathbb{Y}_{\boldsymbol{\alpha}}\big) \Big| \boldsymbol{x} \in \overline{\Omega}\right\} \quad , \tag{1.112}$$

where:

$$A_n = \{\boldsymbol{\alpha} = (\alpha_1, \alpha_2, \alpha_3) \mid 1 \leq \alpha_\ell \leq n \text{ for } \ell \in \{1, 2, 3\}\} \quad , \tag{1.113}$$

$$\boldsymbol{k}_{\boldsymbol{\alpha}} = (k_{\alpha_1}, k_{\alpha_2}, k_{\alpha_3}) \text{ such that } k_{\alpha\ell} = \left(-1 + \frac{2\alpha_\ell - 2}{2n}\right)\frac{\pi}{L_\ell} \text{ for } \ell \in \{1, 2, 3\}. \tag{1.114}$$

The expressions (1.113)-(1.114) discretize the support $[\frac{-\pi}{L_1}, \frac{\pi}{L_1}] \times [\frac{-\pi}{L_2}, \frac{\pi}{L_2}] \times [\frac{-\pi}{L_3}, \frac{\pi}{L_3}]$ of $S_\mathbb{G}(\cdot; \boldsymbol{p}_\mathrm{L})$ using n^3 points. The random amplitudes are such that, for all $\boldsymbol{\alpha} \in A_n$, $\mathbb{X}_{\boldsymbol{\alpha}} = \sqrt{-\log \mathbb{Z}_{\boldsymbol{\alpha}}}$, where

the set $\{\mathbb{Z}_{\boldsymbol{\alpha}} \mid \boldsymbol{\alpha} \in A_n\}$ collects n^3 independent uniform random variables with values in $[0, 1]$. The set $\{\mathbb{Y}_{\boldsymbol{\alpha}} \mid \boldsymbol{\alpha} \in A_n\}$ of random phases gathers n^3 independent uniform random variables with values in $[0, 2\pi]$, which are independent of the random amplitudes $\{\mathbb{X}_{\boldsymbol{\alpha}} \mid \boldsymbol{\alpha} \in A_n\}$. It can be shown [Poirion and Soize, 1989] that $\{\mathbb{G}^{(n)}(\boldsymbol{x}; \boldsymbol{p}_{\mathrm{L}}) \mid \boldsymbol{x} \in \overline{\Omega}\}$ converges in distribution to $\{\mathbb{G}(\boldsymbol{x}; \boldsymbol{p}_{\mathrm{L}}) \mid \boldsymbol{x} \in \overline{\Omega}\}$ as n tends to infinity.

Algorithm 4 details the procedure for the numerical simulation of the random elasticity tensor field using the spectral representation method and the mapping $\boldsymbol{N}(\cdot; \delta)$, defined in Section 1.2.1.

Algorithm 4: simulation of the random elasticity tensor field

---

- **Step 1: initialization:**
  Choose a number n_{S} of Monte Carlo samples.
  Choose the mean field $\underline{\boldsymbol{C}}^{\mathrm{e}}(\boldsymbol{p}_0)$, the correlation lengths $\boldsymbol{p}_{\mathrm{L}}$ and the dispersion level δ.
  Choose the parameter n governing the discretization of the support of $S_{\mathbb{G}}(\cdot; \boldsymbol{p}_{\mathrm{L}})$.

- **Step 2: simulation of the samples of the random amplitudes and phases:**
  First, simulate a set

$$\{\mathbb{X}_{\boldsymbol{\alpha},k}(a_s) \mid \boldsymbol{\alpha} \in A_n , \ 1 \le k \le 21 , \ 1 \le s \le n_{\mathrm{S}}\} \tag{1.115}$$

  of $n_{\mathrm{S}} \times 21 \times n^3$ iid samples of a real random variable $\mathbb{X} = \sqrt{-\log \mathbb{Z}}$, where $\mathbb{Z}$ is a uniform random variable with values in $[0, 1]$. Then, simulate a set

$$\{\mathbb{Y}_{\boldsymbol{\alpha},k}(a_s) \mid \boldsymbol{\alpha} \in A_n , \ 1 \le k \le 21 , \ 1 \le s \le n_{\mathrm{S}}\} \tag{1.116}$$

  of $n_{\mathrm{S}} \times 21 \times n^3$ iid samples of a uniform random variable $\mathbb{Y}$ with values in $[0, 2\pi]$, which is independent of $\mathbb{X}$.

- **Step 3: construction of the samples of the 21-subsets of stochastic germs:**
  For each $s \in \{1 \le s \le n_{\mathrm{S}}\}$ and $k \in \{1 \le k \le 21\}$, build the sample path

$$\boldsymbol{x} \mapsto \mathbb{G}_k^{(n)}(\boldsymbol{x}; a_s; \boldsymbol{p}_{\mathrm{L}}) = \sqrt{2\frac{\pi}{L_1}\frac{\pi}{L_2}\frac{\pi}{L_3}} \sum_{\boldsymbol{\alpha} \in A_n} \sqrt{S_{\mathbb{G}}(\boldsymbol{k}_{\boldsymbol{\alpha}}; \boldsymbol{p}_{\mathrm{L}})} \mathbb{X}_{\boldsymbol{\alpha},k}(a_s) \cos\left((\boldsymbol{k}_{\boldsymbol{\alpha}}, \boldsymbol{x}) + \mathbb{Y}_{\boldsymbol{\alpha},k}(a_s)\right).$$
$$\tag{1.117}$$

- **Step 4: construction of the samples of the random elasticity tensor field:**
  For each $s \in \{1 \le s \le n_{\mathrm{S}}\}$, build the sample path

$$\boldsymbol{x} \mapsto \hat{\mathbb{C}}^{\mathrm{e}(n)}(\boldsymbol{x}; a_s; \boldsymbol{p}) = \underline{L}_{\boldsymbol{C}}(\boldsymbol{x}; \boldsymbol{p}_0)^{\mathrm{T}} \boldsymbol{N}\left(\mathbb{G}_1^{(n)}(\boldsymbol{x}; a_s; \boldsymbol{p}_{\mathrm{L}}), \ldots, \mathbb{G}_{21}^{(n)}(\boldsymbol{x}; a_s; \boldsymbol{p}_{\mathrm{L}}); \delta\right) \underline{L}_{\boldsymbol{C}}(\boldsymbol{x}; \boldsymbol{p}_0) \quad,$$
$$\tag{1.118}$$

  where the matrix $\underline{L}_{\boldsymbol{C}}(\boldsymbol{x}; \boldsymbol{p}_0)$ is the Cholesky factor of $\hat{\underline{\boldsymbol{C}}}^{\mathrm{e}}(\boldsymbol{x}; \boldsymbol{p}_0)$. Gather the iid samples obtained by this procedure in the set

$$\{\boldsymbol{x} \mapsto \mathbb{C}^{\mathrm{e}(n)}(\boldsymbol{x}; a_s; \boldsymbol{p}) \mid 1 \le s \le n_{\mathrm{S}}\}. \tag{1.119}$$

1.3 Vibration test and experimental data

In the previous two sections, the probabilistic mathematical-mechanical modelling of structures was presented. This section now turns to the experimental characterization of the dynamical behaviour of structures. In the following, we define a generic vibration test, along with a corresponding experimental data set of observed TFs, which will be used in the next chapter to set up inverse methods. We do not elaborate on the practical aspects of vibration tests, but refer the reader to [Heylen et al., 1997, Inman, 1994, McConnell, 1995, Pintelon and Schoukens, 2001] for details concerning this topic.
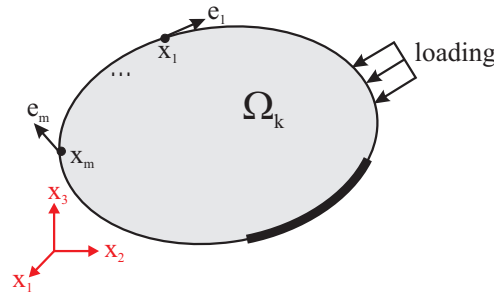

Figure 1.4: The generic instrumentation of the k-th tested structure: notations.

It is noted that we will define the generic vibration test from the point of view of a stochastic inverse problem aimed at quantifying aleatory uncertainty (see the general introduction), in that the testing of a collection of similar structures is considered. Nevertheless, upon simply setting the number of tested structures to one, a vibration test is obtained that is well-adapted to a stochastic inverse problem aimed at quantifying epistemic uncertainty.

In our generic vibration test, it is assumed that a collection of realizations of a so-called *random structure*, i.e. a collection of similar, but not perfectly identical, structures is considered. Furthermore, the vibration test is assumed to be performed on a subset of n_K realizations of this random structure (i.e. on a subset of n_K samples out of the entire collection under study). Finally, the n_K tested samples are assumed to be instrumented in the same way (Fig. 1.4) by means of n_M transducers to measure the mechanical motion at the positions $\{x_m \mid 1 \leq m \leq n_M\}$ (located on the boundary of the structure) along the directions $\{e_m \mid 1 \leq m \leq n_M\}$. For example, if the collection of all similar aircraft engines manufactured by a production line during its operational life were under study, the vibration test could concern the aircraft engines manufactured by this production line during say one month.

The dynamical behaviour of each tested sample structure is studied by applying a broadband time-limited pressure field on a small portion of its boundary and by measuring the induced mechanical motion in the n_M experimental Degrees Of Freedom (DOFs). Various devices can be used to apply the excitation, e.g. impact hammers, falling-weight devices and electromechanical or electrohydraulic devices. In our generic vibration test, this experiment is repeated n_R times for each tested sample structure. The excitation is hereby assumed to be applied on the same portion of the boundary for each tested structure and each consecutive repetition. In other words, only the time history, and not the spatial distribution, of the applied loading is allowed to change from one tested structure or repetition to the next. For instance, for an excitation generated by an impact hammer, the strike area is assumed to remain unchanged, whereas the time duration and the magnitude of the impact are allowed to vary.

The repetition of the experiment ($n_R > 1$) is particularly useful in view of the experimental noise which may disturb the measurement of the applied force and the induced mechanical response. The noise may

concern the mechanical motion of the structure due to parasite excitations, electrical noise in the transducers and the wires and discretization errors. Under some assumptions, the repetition of the experiment allows recovering, from the noisy measurement data, those data which would be obtained if the vibration test were not disturbed by noise (App. C). Moreover, it allows estimating the coherence function to quantify the level of distortion of the experimental data due to noise (App. C).

Experimental data

The raw measurement data consist of a time-dependent applied force and of time-dependent responses measured in n_{M} experimental DOFs for n_{R} repetitions of the experiment for n_{K} structures. Accordingly, let $f_{kr}^{\mathrm{obs}}(t)$ and $y_{krm}^{\mathrm{obs}}(t)$ denote the measured applied force and response at the m-th sensor, respectively, for the r-th repetition and the k-th tested structure. These data are sampled in the time domain and, subsequently, transformed into the frequency domain by means of the Discrete Fourier Transform (DFT) to obtain:

$$\{f_{kr}^{\mathrm{obs}}(\omega_\ell) \mid 1 \le \ell \le n_{\mathrm{F}} \,,\, 1 \le k \le n_{\mathrm{K}} \,,\, 1 \le r \le n_{\mathrm{R}}\} \quad, \tag{1.120}$$

$$\{y_{krm}^{\mathrm{obs}}(\omega_\ell) \mid 1 \le \ell \le n_{\mathrm{F}} \,,\, 1 \le k \le n_{\mathrm{K}} \,,\, 1 \le r \le n_{\mathrm{R}} \,,\, 1 \le m \le n_{\mathrm{M}}\} \quad, \tag{1.121}$$

where $\{\omega_\ell \mid 1 \le \ell \le n_{\mathrm{F}}\}$ is the set of n_{F} discrete frequencies. The value taken by the observed Transfer Function (TF) for the m-th sensor, the r-th repetition and the k-th structure at the frequency ω_ℓ is defined as the frequency-domain ratio of the measured response and applied force:

$$g_{krm}^{\mathrm{obs}}(\omega_\ell) = \frac{y_{krm}^{\mathrm{obs}}(\omega_\ell)}{f_{kr}^{\mathrm{obs}}(\omega_\ell)}. \tag{1.122}$$

For the k-th structure, these values are gathered in the data set

$$\boldsymbol{D}_k = \{\boldsymbol{g}_{k1}^{\mathrm{obs}}(\omega_\ell), \ldots, \boldsymbol{g}_{kn_{\mathrm{R}}}^{\mathrm{obs}}(\omega_\ell) \mid 1 \le \ell \le n_{\mathrm{F}}\} \quad, \tag{1.123}$$

where the values taken by the n_{M} observed TFs for the r-th repetition and the k-th structure at the frequency ω_ℓ are gathered in the vector $\boldsymbol{g}_{kr}^{\mathrm{obs}}(\omega_\ell) \in \mathbb{C}^{n_{\mathrm{M}}}$. Finally, all experimental results thus obtained are gathered in the data set

$$\boldsymbol{D} = \{\boldsymbol{D}_k \mid 1 \le k \le n_{\mathrm{K}}\}. \tag{1.124}$$

Experimental data: the noise-free idealization

When the vibration test is not disturbed by noise, the experiment is carried out only once for each tested structure ($n_{\mathrm{R}} = 1$). For the k-th tested structure, a data set

$$\boldsymbol{D}_k^0 = \{\boldsymbol{h}_k^0(\omega_\ell) \mid 1 \le \ell \le n_{\mathrm{F}}\} \tag{1.125}$$

is then obtained collecting the values taken by the noise-free TFs of this structure at the n_{F} discrete frequencies. The m-th component $h_{km}^0(\omega_\ell)$ is the frequency-domain ratio of the undisturbed response in the m-th transducer and the applied force at the discrete frequency ω_ℓ. All experimental results are then gathered in the data set

$$\boldsymbol{D}^0 = \{\boldsymbol{D}_k^0 \mid 1 \le k \le n_{\mathrm{K}}\}. \tag{1.126}$$

1.4 Stochastic modelling of the vibration test

After having presented the probabilistic modelling of the dynamical behaviour of structures and defined a generic vibration test, our main goal is now to describe the probabilistic modelling of this vibration test. Before addressing this issue, a representation of the observed TF values as realizations of random variables will be introduced, which will be useful in Chapter 2, for instance to analyze the asymptotic behaviour of inverse methods as more and more data are acquired.

1.4.1 The vibration test as a random experiment

A representation of the observed TF values as realizations of random variables is now introduced. We first expound on the case where the vibration test is not disturbed by experimental noise, and subsequently deal with the case where it is distorted by noise.

Undisturbed vibration test

Let us consider a general problem where the generic vibration test (Sec. 1.3) is carried out under noise-free conditions on a collection of similar, but not perfectly identical, samples of a random structure. The observed TFs obtained for these sample structures are expected to be similar, but not perfectly identical. We make the fundamental modelling assumption that the differences or fluctuations in the observed TFs can be described in a stochastic framework. More precisely, it is assumed that these fluctuations show a statistical regularity in the particular sense that the observed TF values can adequately be regarded as iid realizations of a certain (possibly unknown) data-generating stochastic process.

More specifically, let the observed TF values be collected in a generic data set $\boldsymbol{D}^0$ of the form (1.125)-(1.126). We then introduce a random data set

$$\mathbb{D}^0 = \{\mathbb{D}_k^0 \mid 1 \leq k \leq n_{\mathrm{K}}\} \quad , \tag{1.127}$$

which gathers n_{K} independent copies, of the generic form $\mathbb{D}_k^0 = \{\mathbb{H}_k^0(\omega_\ell) \mid 1 \leq \ell \leq n_{\mathrm{F}}\}$, of a data-generating stochastic process

$$\tilde{\mathbb{D}}^0 = \left\{\tilde{\mathbb{H}}^0(\omega_\ell) \mid 1 \leq \ell \leq n_{\mathrm{F}}\right\} \quad , \tag{1.128}$$

which is assumed to perfectly represent the fluctuations in the observed TFs (and whose existence is postulated). The actually observed data set $\boldsymbol{D}^0$ is then viewed as a particular realization of $\mathbb{D}^0$, or, equivalently, as a collection of n_{K} iid realizations of $\tilde{\mathbb{D}}^0$.

The stochastic process (1.128) is assumed to admit a system of cylindrical PDFs (Box 1.3). The n-th order cylindrical PDF is denoted by

$$\xi^{(n)}\left(\cdot\middle|\omega_{\ell_1}, \ldots, \omega_{\ell_n}\right) : \mathbb{C}^{n_{\mathrm{M}} \times n} \to \mathbb{R}^+ \tag{1.129}$$

and is defined as the joint PDF of the n random variables $\{\tilde{\mathbb{H}}^0(\omega_{\ell_1}), \ldots, \tilde{\mathbb{H}}^0(\omega_{\ell_n})\}$. Under the aforementioned modelling assumption, the n_{F}-th order cylindrical PDF $\xi^{(n_{\mathrm{F}})}$ is the data-generating PDF: it perfectly represents the joint probability distribution of the values taken by the observed TFs of the random structure at all discrete frequencies.

Disturbed vibration test

Let us now consider a similar general problem where the generic vibration test is carried out on a collection of sample structures, this time, under noisy conditions. As outlined in Section 1.3, the vibration measurement is then repeated several times for each tested structure. For a fixed sample structure, the observed TFs thus obtained are expected to show fluctuations due to experimental noise. We make the fundamental modelling assumption that these fluctuations can be described in a stochastic framework, and, in particular, that the observed TF values can adequately be viewed as iid realizations of a certain (possibly unknown) data-generating stochastic process. Moreover, the experimental noise is assumed to be independent among, and allowed to have different characteristics for, distinct tested structures.

More specifically, let the observed TF values be gathered in a generic data set $\boldsymbol{D}$ of the form (1.123)-(1.124). We then introduce a random data set

$$\mathbb{D} = \{\mathbb{D}_k \mid 1 \leq k \leq n_{\mathrm{K}}\} \quad , \tag{1.130}$$

which gathers n_{K} independent, but not necessarily identically-distributed (reflecting the fact that the noise may have different characteristics for distinct tested structures), random subsets of data of the form

$$\mathbb{D}_k = \{\mathbb{G}_{k1}(\omega_\ell), \dots, \mathbb{G}_{kn_{\mathrm{R}}}(\omega_\ell) \mid 1 \leq \ell \leq n_{\mathrm{F}}\}. \tag{1.131}$$

For each tested structure (indexed by k), the stochastic process $\mathbb{D}_k$ is assumed to gather n_{R} independent copies, having the generic form $\{\mathbb{G}_{kr}(\omega_\ell) \mid 1 \leq \ell \leq n_{\mathrm{F}}\}$, of a data-generating stochastic process

$$\tilde{\mathbb{D}}_k = \{\tilde{\mathbb{G}}_k(\omega_\ell) \mid 1 \leq \ell \leq n_{\mathrm{F}}\} \quad , \tag{1.132}$$

which is assumed to perfectly represent the variability in the observed TFs for the k-th tested structure due to the experimental noise (and whose existence is postulated). The actually observed data set $\boldsymbol{D}$ is viewed as a particular realization of $\mathbb{D}$. For each tested structure, the data subset $\boldsymbol{D}_k$ is viewed as a particular realization of $\mathbb{D}_k$, or, equivalently, as a collection of n_{R} iid realizations of $\tilde{\mathbb{D}}_k$.

For each tested structure, the stochastic process (1.132) is assumed to admit a system of cylindrical PDFs. The n-th order cylindrical PDF is denoted by

$$\psi_k^{(n)}(\cdot|\omega_{\ell_1}, \dots, \omega_{\ell_n}) : \mathbb{C}^{n_{\mathrm{M}} \times n} \to \mathbb{R}^+ \tag{1.133}$$

and is defined as the joint PDF of the n random variables $\{\tilde{\mathbb{G}}_k(\omega_{\ell_1}), \dots, \tilde{\mathbb{G}}_k(\omega_{\ell_n})\}$. Under the above-made modelling assumptions, the n_{F}-th order cylindrical PDF $\psi_k^{(n_{\mathrm{F}})}$ is the data-generating PDF for the k-th tested structure: it perfectly represents the joint probability distribution of the values taken by the observed TFs for this structure at all discrete frequencies. The n-th order cylindrical PDF of the stochastic process (1.131) is denoted by

$$\psi_k^{(n,n_{\mathrm{R}})}(\cdot|\omega_{\ell_1}, \dots, \omega_{\ell_n}) : \mathbb{C}^{n_{\mathrm{M}} \times n_{\mathrm{R}} \times n} \to \mathbb{R}^+ \tag{1.134}$$

and is defined as the joint PDF of the n random variables

$$\{\mathbb{G}_{k1}(\omega_{\ell_1}), \dots, \mathbb{G}_{kn_{\mathrm{R}}}(\omega_{\ell_1}), \dots, \mathbb{G}_{k1}(\omega_{\ell_n}), \dots, \mathbb{G}_{kn_{\mathrm{R}}}(\omega_{\ell_n})\}. \tag{1.135}$$

Clearly, the first-order cylindrical PDF $\psi_k^{(1,n_{\mathrm{R}})}$ is such that:

$$\psi_k^{(1,n_{\mathrm{R}})}(\boldsymbol{g}_1, \dots, \boldsymbol{g}_{n_{\mathrm{R}}}|\omega_\ell) = \prod_{r=1}^{n_{\mathrm{R}}} \psi_k^{(1)}(\boldsymbol{g}_r|\omega_\ell). \tag{1.136}$$

More generally, the n-order cylindrical PDF $\psi_k^{(n,n_{\mathrm{R}})}$ is such that:

$$\psi_k^{(n,n_{\mathrm{R}})}(\boldsymbol{g}_{11}, \dots, \boldsymbol{g}_{1n_{\mathrm{R}}}, \dots, \boldsymbol{g}_{n1}, \dots, \boldsymbol{g}_{nn_{\mathrm{R}}}|\omega_{\ell_1}, \dots, \omega_{\ell_n}) = \prod_{r=1}^{n_{\mathrm{R}}} \psi_k^{(n)}(\boldsymbol{g}_{1r}, \dots, \boldsymbol{g}_{1r}|\omega_{\ell_1}, \dots, \omega_{\ell_n}). \tag{1.137}$$

1.4.2 Probabilistic mathematical-mechanical modelling

We now describe the probabilistic mathematical-mechanical modelling of the generic vibration test. Again, we first expound on the case where the vibration test is not disturbed by experimental noise, and then address the case where it is distorted by noise.

Undisturbed vibration test

The outcome of a vibration test carried out under noise-free conditions is modelled as follows. First, the experimental excitation is modelled by a position- and frequency-dependent surface force field $(\boldsymbol{x};\omega) \mapsto \boldsymbol{f}_{\mathrm{s}}(\boldsymbol{x};\omega)$. Subsequently, either a non-parametric or a parametric probabilistic structural model is set up and used to forecast the induced dynamical response field to obtain a stochastic process $\{\mathbb{U}(\omega;\boldsymbol{p}) \mid \omega \in B\}$, parameterized by $\boldsymbol{p}$ (corresponding to either equation (1.58), or (1.90)). Finally, a stochastic process

$$\{\mathbb{H}(\omega_\ell;\boldsymbol{p}) \mid 1 \le \ell \le n_{\mathrm{F}}\} \tag{1.138}$$

is defined, where, for each frequency ω_ℓ, the random variable $\mathbb{H}(\omega_\ell;\boldsymbol{p})$ with values in $\mathbb{C}^{n_{\mathrm{M}}}$ a.s. is the ratio at that frequency of the predicted random response in the n_{M} transducers and the magnitude of the applied force[16]:

$$\mathbb{H}_m(\omega_\ell;\boldsymbol{p}) = \frac{(\mathbb{U}(\boldsymbol{x}_m;\omega_\ell;\boldsymbol{p}), \boldsymbol{e}_m)}{\int_{\Gamma_\sigma} (\boldsymbol{f}_{\mathrm{s}}(\boldsymbol{x};\omega_\ell), \boldsymbol{n})\, dS} \text{ a.s.} \quad \text{for } 1 \le m \le n_{\mathrm{M}}. \tag{1.139}$$

The stochastic process (1.138) is assumed to admit a system of cylindrical PDFs. The n-th order cylindrical PDF, conditioned on $\boldsymbol{p}$, is denoted by

$$\theta^{(n)}\left(\cdot\middle|\omega_{\ell_1},\ldots,\omega_{\ell_n};\boldsymbol{p}\right) : \mathbb{C}^{n_{\mathrm{M}} \times n} \to \mathbb{R}^+ \tag{1.140}$$

and is defined as the joint PDF of the n random variables $\{\mathbb{H}(\omega_{\ell_1};\boldsymbol{p}),\ldots,\mathbb{H}(\omega_{\ell_n};\boldsymbol{p})\}$.

Disturbed vibration test

The outcome of a noisy vibration test is modelled as follows. First, similarly to the previous subsection, a probabilistic structural model is used to model the vibration test to obtain a stochastic process $\{\mathbb{H}(\omega_\ell;\boldsymbol{p}) \mid 1 \le \ell \le n_{\mathrm{F}}\}$ with n-th order cylindrical PDF $\theta^{(n)}(\cdot|\cdot;\boldsymbol{p})$.

Subsequently, a probabilistic model for the experimental noise is built. For each tested sample structure (indexed by k) and for each discrete frequency ω_ℓ, the random variable $\tilde{\mathbb{G}}_k(\omega_\ell)$, introduced in (1.132) and representing the variability of the observed TFs for the k-th structure at the frequency ω_ℓ due to the noise, is written in the following form:

$$\tilde{\mathbb{G}}_k(\omega_\ell) = \boldsymbol{h}_k^0(\omega_\ell) + \tilde{\mathbb{E}}_k(\omega_\ell) \text{ a.s.} \quad , \tag{1.141}$$

where the random variable $\tilde{\mathbb{E}}_k(\omega_\ell)$, with values in $\mathbb{C}^{n_{\mathrm{M}}}$ a.s., represents the fluctuations of the observed TF values around the noise-free TF value $\boldsymbol{h}_k^0(\omega_\ell)$ due to the noise. To obtain a simple probabilistic model

---

[16]It should be noted that the equation (1.139) is ill-defined from the mathematical point of view. Indeed, for a fixed ω, the random displacement field $\mathbb{U}(\omega;\boldsymbol{p})$ has values in a functional space of the form $\{\boldsymbol{v} \in \left(H^1(\Omega,\mathbb{C})\right)^3 | \boldsymbol{v} = \boldsymbol{0} \text{ on } \Gamma_{\mathrm{u}}\}$ and is therefore only "almost everywhere" defined. This difficulty can easily be circumvented by applying the trace theorem [see, for instance, Duvaut and Lions, 1972, ch. 1 sec. 4] to map the displacement field $\mathbb{U}(\omega;\boldsymbol{p})$ defined in Ω to a corresponding field defined on the boundary $\partial\Omega$, and, subsequently, by averaging over a small portion of this boundary around the considered position.

that can easily be identified from the experimental data, we model the random variables $\{\tilde{\mathbb{E}}_k(\omega_\ell) \mid 1 \leq \ell \leq n_{\mathrm{F}}\}$ as circular complex Gaussian random variables (Box 1.6) that are independent among the frequencies. The mean value of $\tilde{\mathbb{E}}_k(\omega_\ell)$ is set to zero and its covariance matrix is identified from the experimental data set as:

$$\widehat{\boldsymbol{C}}_k(\omega_\ell) = \frac{1}{n_{\mathrm{R}}} \sum_{r=1}^{n_{\mathrm{R}}} \left(\boldsymbol{y}_{kr}^{\mathrm{obs}}(\omega_\ell) - \hat{\boldsymbol{h}}_k(\omega_\ell) f_{kr}^{\mathrm{obs}}(\omega_\ell)\right) \otimes \overline{\left(\boldsymbol{y}_{kr}^{\mathrm{obs}}(\omega_\ell) - \hat{\boldsymbol{h}}_k(\omega_\ell) f_{kr}^{\mathrm{obs}}(\omega_\ell)\right)} \quad , \tag{1.142}$$

where $\hat{\boldsymbol{h}}_k(\omega_\ell)$ is the so-called $H1$-estimate of the TF value, defined by (App. C):

$$\hat{\boldsymbol{h}}_k(\omega_\ell) = \frac{\frac{1}{n_{\mathrm{R}}} \sum_{r=1}^{n_{\mathrm{R}}} \boldsymbol{y}_{kr}^{\mathrm{obs}}(\omega_\ell) \overline{f}_{kr}^{\mathrm{obs}}(\omega_\ell)}{\frac{1}{n_{\mathrm{R}}} \sum_{r=1}^{n_{\mathrm{R}}} \left|f_{kr}^{\mathrm{obs}}(\omega_\ell)\right|^2}. \tag{1.143}$$

The random variable $\tilde{\mathbb{E}}_k(\omega_\ell)$ admits the following PDF (Box 1.6):

$$N^{\mathrm{c}}\left(\,\cdot\,|\boldsymbol{0}, \widehat{\boldsymbol{C}}_k(\omega_\ell)\right) : \mathbb{C}^{n_{\mathrm{M}}} \to \mathbb{R}^+. \tag{1.144}$$

Finally, for each tested structure, a stochastic process

$$\left\{\mathbb{H}(\omega_\ell; \boldsymbol{p}) + \mathbb{E}_{k1}(\omega_\ell), \ldots, \mathbb{H}(\omega_\ell; \boldsymbol{p}) + \mathbb{E}_{kn_{\mathrm{R}}}(\omega_\ell) \mid 1 \leq \ell \leq n_{\mathrm{F}}\right\} \quad , \tag{1.145}$$

is defined, where, for each frequency ω_ℓ, the random variables $\{\mathbb{E}_{kr}(\omega_\ell) \mid 1 \leq r \leq n_{\mathrm{R}}\}$ are n_{R} independent copies of $\tilde{\mathbb{E}}_k(\omega_\ell)$. The stochastic process (1.145) is assumed to admit a system of cylindrical PDFs. The n-th order cylindrical PDF, conditioned on $\boldsymbol{p}$, is denoted by

$$\varphi_k^{(n, n_{\mathrm{R}})}\left(\cdot | \omega_{\ell_1}, \ldots, \omega_{\ell_n}; \boldsymbol{p}\right) : \mathbb{C}^{n_{\mathrm{M}} \times n_{\mathrm{R}} \times n} \to \mathbb{R}^+ \tag{1.146}$$

and is defined as the joint PDF of the $n \times n_{\mathrm{R}}$ random variables

$$\{\mathbb{H}(\omega_{\ell_1}; \boldsymbol{p}) + \mathbb{E}_{k1}(\omega_{\ell_1}), \ldots, \mathbb{H}(\omega_{\ell_1}; \boldsymbol{p}) + \mathbb{E}_{kn_{\mathrm{R}}}(\omega_{\ell_1}), \ldots, \mathbb{H}(\omega_{\ell_n}; \boldsymbol{p}) + \mathbb{E}_{k1}(\omega_{\ell_n}), \ldots, \mathbb{H}(\omega_{\ell_n}; \boldsymbol{p}) + \mathbb{E}_{kn_{\mathrm{R}}}(\omega_{\ell_n})\}. \tag{1.147}$$

Clearly, the first-order cylindrical PDF has the following convolution expression:

$$\varphi_k^{(1, n_{\mathrm{R}})}\left(\boldsymbol{g}_1, \ldots, \boldsymbol{g}_{n_{\mathrm{R}}} | \omega_\ell; \boldsymbol{p}\right) = \int_{\mathbb{C}^{n_{\mathrm{M}}}} \theta^{(1)}\left(\boldsymbol{h} | \omega_\ell; \boldsymbol{p}\right) \prod_{r=1}^{n_{\mathrm{R}}} \rho_k^{(1)}\left(\boldsymbol{g}_r | \omega_\ell; \boldsymbol{h}\right) d\boldsymbol{h} \quad , \tag{1.148}$$

where the PDF $\rho_k^{(1)} : \mathbb{C}^{n_{\mathrm{M}}} \to \mathbb{R}^+$ is defined by:

$$\rho_k^{(1)}\left(\boldsymbol{g} | \omega_\ell; \boldsymbol{h}\right) = N^{\mathrm{c}}\left(\boldsymbol{g} - \boldsymbol{h} | \boldsymbol{0}, \widehat{\boldsymbol{C}}_k(\omega_\ell)\right). \tag{1.149}$$

More generally, the n-th order cylindrical PDF reads:

$$\varphi_k^{(n, n_{\mathrm{R}})}\left(\boldsymbol{g}_{11}, \ldots, \boldsymbol{g}_{1n_{\mathrm{R}}}, \ldots, \boldsymbol{g}_{n1}, \ldots, \boldsymbol{g}_{nn_{\mathrm{R}}} | \omega_{\ell_1}, \ldots, \omega_{\ell_n}; \boldsymbol{p}\right) \tag{1.150}$$

$$= \int_{\mathbb{C}^{n_{\mathrm{M}} \times n}} \theta^{(n)}\left(\boldsymbol{h}_1, \ldots, \boldsymbol{h}_n | \omega_{\ell_1}, \ldots, \omega_{\ell_n}; \boldsymbol{p}\right) \prod_{r=1}^{n_{\mathrm{R}}} \left(\rho_k^{(1)}\left(\boldsymbol{g}_{1r} | \omega_{\ell_1}; \boldsymbol{h}_1\right) \ldots \rho_k^{(1)}\left(\boldsymbol{g}_{nr} | \omega_{\ell_n}; \boldsymbol{h}_n\right)\right) d\boldsymbol{h}_1 \ldots d\boldsymbol{h}_n.$$

Box 1.6. Circular complex Gaussian random variables

This box recalls the notion of circularity for complex Gaussian random variables. We refer the reader to [Picinbono, 1993, Pintelon and Schoukens, 2001] for more details concerning this topic.

Let us first recall that a real random variable $\mathbb{X}$ with values in $\mathbb{R}^n$ a.s. is Gaussian if it admits a PDF of the following form:

$$N(\boldsymbol{x}|\boldsymbol{\mu}, \boldsymbol{C}) = \frac{1}{\sqrt{(2\pi)^n \det(\boldsymbol{C})}} \exp\left(-\frac{1}{2}\left(\boldsymbol{C}^{-1}(\boldsymbol{x}-\boldsymbol{\mu}), \boldsymbol{x}-\boldsymbol{\mu}\right)\right) \quad, \tag{1.151}$$

where $\boldsymbol{\mu} \in \mathbb{R}^n$ and $\boldsymbol{C} \in \mathrm{M}_n^+(\mathbb{R})$ denote the mean value and the covariance matrix defined by:

$$\boldsymbol{\mu} = E\{\mathbb{X}\} \quad, \tag{1.152}$$
$$\boldsymbol{C} = E\{(\mathbb{X}-\boldsymbol{\mu}) \otimes (\mathbb{X}-\boldsymbol{\mu})\}. \tag{1.153}$$

A complex random variable $\mathbb{X}$ with values in $\mathbb{C}^n$ a.s. is said to be Gaussian if its real and imaginary part are jointly real Gaussian random variables, that is to say if the real random variable $[\Re(\mathbb{X}); \Im(\mathbb{X})]$ with values in $\mathbb{R}^{2n}$ a.s. is Gaussian.

Let $\boldsymbol{\mu}_{\mathrm{R}} = \Re(\boldsymbol{\mu})$ and $\boldsymbol{\mu}_{\mathrm{I}} = \Im(\boldsymbol{\mu})$ denote the real and the imaginary part of the mean value $\boldsymbol{\mu} = E\{\mathbb{X}\}$. Furthermore, let the four covariance matrices C_{RR}, C_{RI}, C_{IR} and C_{II} be given by:

$$\boldsymbol{C}_{\mathrm{RR}} = E\{(\mathbb{X}_{\mathrm{R}} - \boldsymbol{\mu}_{\mathrm{R}}) \otimes (\mathbb{X}_{\mathrm{R}} - \boldsymbol{\mu}_{\mathrm{R}})\}, \quad \boldsymbol{C}_{\mathrm{RI}} = E\{(\mathbb{X}_{\mathrm{R}} - \boldsymbol{\mu}_{\mathrm{R}}) \otimes (\mathbb{X}_{\mathrm{I}} - \boldsymbol{\mu}_{\mathrm{I}})\} \quad, \tag{1.154}$$
$$\boldsymbol{C}_{\mathrm{IR}} = E\{(\mathbb{X}_{\mathrm{I}} - \boldsymbol{\mu}_{\mathrm{I}}) \otimes (\mathbb{X}_{\mathrm{R}} - \boldsymbol{\mu}_{\mathrm{R}})\}, \quad \boldsymbol{C}_{\mathrm{II}} = E\{(\mathbb{X}_{\mathrm{I}} - \boldsymbol{\mu}_{\mathrm{I}}) \otimes (\mathbb{X}_{\mathrm{I}} - \boldsymbol{\mu}_{\mathrm{I}})\} \quad, \tag{1.155}$$

where $\mathbb{X}_{\mathrm{R}} = \Re(\mathbb{X})$ and $\mathbb{X}_{\mathrm{I}} = \Im(\mathbb{X})$. These four real covariance matrices are entirely defined if the following two complex covariance matrices $\boldsymbol{C}_0, \boldsymbol{C}_1 \in \mathrm{M}_n^+(\mathbb{C})$ are known:

$$\boldsymbol{C}_0 = E\{(\mathbb{X}-\boldsymbol{\mu}) \otimes (\overline{\mathbb{X}-\boldsymbol{\mu}})\} = (\boldsymbol{C}_{\mathrm{RR}} + \boldsymbol{C}_{\mathrm{II}}) + i(\boldsymbol{C}_{\mathrm{IR}} - \boldsymbol{C}_{\mathrm{RI}}) \quad, \tag{1.156}$$
$$\boldsymbol{C}_1 = E\{(\mathbb{X}-\boldsymbol{\mu}) \otimes (\mathbb{X}-\boldsymbol{\mu})\} = (\boldsymbol{C}_{\mathrm{RR}} - \boldsymbol{C}_{\mathrm{II}}) + i(\boldsymbol{C}_{\mathrm{IR}} + \boldsymbol{C}_{\mathrm{RI}}). \tag{1.157}$$

Indeed:

$$\boldsymbol{C}_{\mathrm{RR}} = \frac{1}{2}\Re(\boldsymbol{C}_0 + \boldsymbol{C}_1) \quad, \qquad\qquad \boldsymbol{C}_{\mathrm{II}} = \frac{1}{2}\Re(\boldsymbol{C}_0 - \boldsymbol{C}_1) \quad, \tag{1.158}$$

$$\boldsymbol{C}_{\mathrm{IR}} = \frac{1}{2}\Im(\boldsymbol{C}_0 + \boldsymbol{C}_1) \quad, \qquad\qquad \boldsymbol{C}_{\mathrm{RI}} = \frac{1}{2}\Im(-\boldsymbol{C}_0 + \boldsymbol{C}_1). \tag{1.159}$$

The complex Gaussian random variable $\mathbb{X}$ is said to be circular if the covariance matrix C_1 vanishes. Clearly, $\boldsymbol{C}_1 = \boldsymbol{0}$ if and only if the real and the imaginary part of $\mathbb{X}$ have the same covariance matrix, i.e. $C_{\mathrm{RR}} = C_{\mathrm{II}}$, and their cross-covariance matrix is skew-symmetric, i.e. $C_{\mathrm{IR}} = C_{\mathrm{RI}}^{\mathrm{T}} = -C_{\mathrm{RI}}$. The latter condition implies that the diagonal of C_{RI} vanishes: the real and imaginary part of each component $\mathbb{X}_k$ of $\mathbb{X}$ are necessarily uncorrelated (hence, independent), but the real part of $\mathbb{X}_k$ and the imaginary part of $\mathbb{X}_\ell$ with $k \neq \ell$ may be correlated. If the complex Gaussian random variable $\mathbb{X}$ is circular, then it admits the following PDF [Pintelon and Schoukens, 2001, ch. 14 sec. 1]:

$$N^c(\boldsymbol{x}|\boldsymbol{\mu}, \boldsymbol{C}_0) = \frac{1}{\pi^n \det(\boldsymbol{C}_0)} \exp\left(-\left(\boldsymbol{C}_0^{-1}(\boldsymbol{x}-\boldsymbol{\mu}_{\mathbb{X}}), \overline{(\boldsymbol{x})-\boldsymbol{\mu}_{\mathbb{X}}}\right)\right). \tag{1.160}$$

1.4.3   Numerical simulation

The numerical simulation of the stochastic process $\{\mathbb{H}(\omega_\ell; \boldsymbol{p}) \mid 1 \leq \ell \leq n_{\mathrm{F}}\}$, defined by (1.139), can be performed on the basis of the following algorithm.

Algorithm 5: simulation of the stochastic process $\{\mathbb{H}(\omega_\ell; \boldsymbol{p}) \mid 1 \leq \ell \leq n_{\mathrm{F}}\}$

- **Step 1: initialization:**
  Get information on the experimental setup (loading, sensors, discrete frequencies).
  Get the probabilistic structural model, built as outlined in Section 1.1.

- **Step 2: computation with the probabilistic model:**
  Apply the FE and MCS methods to discretize the probabilistic model (see Algorithms 1 and 3 of Section 1.2). Use the discretized model to forecast the outcome of the vibration test as follows:

  Step 2a: calculation of samples of the predicted random response:
  Model and, subsequently, discretize the experimental loading to obtain the frequency-dependent nodal-forces vector $\boldsymbol{f}_{\mathrm{h}}(\omega)$. For these nodal forces, calculate the set

  $$\{\mathbb{U}_{\mathrm{h}}(\omega_\ell; a_s; \boldsymbol{p}) \mid 1 \leq \ell \leq n_{\mathrm{F}} ,\ 1 \leq s \leq n_{\mathrm{S}}\} \tag{1.161}$$

  of iid samples of the predicted random FE DOFs.

  Step 2b: calculation of samples of the predicted random TFs:
  Decompose the nodal-forces vector into a product $\boldsymbol{f}_{\mathrm{h}}(\omega) = \boldsymbol{b}_{\mathrm{h}} f(\omega)$ where the *input shape vector* $\boldsymbol{b}_{\mathrm{h}}$ is frequency-independent and characterizes the spatial distribution of the experimental loading and the scalar $f(\omega)$ is the frequency-dependent magnitude of this loading.

  Similarly, build the sensor *output shape matrix* $\boldsymbol{C}_{\mathrm{h}}$ relating the predicted response $\boldsymbol{y}_{\mathrm{h}}(\omega)$ in the sensors to the FE DOFs $\boldsymbol{u}_{\mathrm{h}}(\omega)$ such that $\boldsymbol{y}_{\mathrm{h}}(\omega) = \boldsymbol{C}_{\mathrm{h}} \boldsymbol{u}_{\mathrm{h}}(\omega)$.

  For each $s \in \{1 \leq s \leq n_{\mathrm{S}}\}$ and $\ell \in \{1 \leq \ell \leq n_{\mathrm{F}}\}$, calculate

  $$\mathbb{H}_{\mathrm{h}}(\omega_\ell; a_s; \boldsymbol{p}) = \frac{\boldsymbol{C}_{\mathrm{h}} \mathbb{U}_{\mathrm{h}}(\omega_\ell; a_s; \boldsymbol{p})}{f(\omega_\ell)}. \tag{1.162}$$

  Gather the iid samples of the predicted random TFs obtained by this procedure in the set

  $$\{\mathbb{H}_{\mathrm{h}}(\omega_\ell; a_s; \boldsymbol{p}) \mid 1 \leq \ell \leq n_{\mathrm{F}} ,\ 1 \leq s \leq n_{\mathrm{S}}\}. \tag{1.163}$$

1.5   Summary and conclusion

In the first two sections of this chapter, the construction of probabilistic models with minimal parameterization for the frequency-domain dynamical behaviour of structures was presented. While verifying the essential mathematical properties of probabilistic structural models, their main advantage is that they are parameterized only by a small set of essential parameters. In the parametric approach, they comprise mean-model parameters, dispersion parameters and correlation lengths, while, in the non-parametric approach, there are only mean-model and dispersion parameters. In the last two sections of this chapter, a

generic vibration test was defined, along with a corresponding experimental data set of observed TFs, and its probabilistic modelling was described. The development of inverse methods for the identification of probabilistic structural models with minimal parameterization from experimental data sets of observed TFs is the subject of the next chapter.

2

The stochastic inverse problem

In the previous chapter, the construction of probabilistic structural models with minimal parameterization was described and a generic experimental data set of observed Transfer Functions (TFs) was defined. The inversion of these probabilistic models using experimental data of this kind is the subject of this chapter.

As announced in the general introduction, we will begin this chapter with pointing out the difficulties in the application of the classical theory of mathematical statistics to the inversion of probabilistic structural models. To circumvent these difficulties, we will propose to formulate this inversion alternatively as the minimization, with respect to the unknown parameters to be identified, of an objective function that measures the distance between the experimental data and the probabilistic structural model. Our main objective in this chapter is to study how this distance can be defined and computed suitably.

The chapter is organized as follows. First, we review the main concepts and important results of the theory of mathematical statistics, which are relevant to this dissertation (Sec. 2.1). Subsequently, we examine the difficulties that may arise in the application of the classical methods of estimation (Sec. 2.2), and propose two versatile methods for defining and computing the distance between an experimental data set of observed TF values and corresponding random TFs predicted by a probabilistic structural model (Sec. 2.3). The asymptotic properties of the proposed distances are discussed (Sec. 2.4), and basic algorithms for their practical computation are proposed (Sec. 2.5). Finally, we define a practical methodology for the inversion of probabilistic structural models (Secs. 2.6 and 2.7).

The reader already familiar with the theory of mathematical statistics may want to move quickly through the first section of this chapter, which is entirely bibliographical. We recommend to read either Section 2.1.3, which contains a theoretical account of the problem of the misspecification of stochastic models, or Box 2.2 that provides a simple illustration of this issue.

2.1 Mathematical statistics

This section reviews existing concepts and results of the theory of mathematical statistics, namely the classical methods of estimation (Sec. 2.1.1), the relative entropy (Sec. 2.1.2) and the evaluation of the adequacy of estimation rules (Sec. 2.1.3). For a more complete account of the theory of mathematical statistics, we refer the reader, for instance, to [Casella and Berger, 2001, Cramér, 1946, Dudley, 2005, Lehmann and Casella, 1998, O'Hagan and Forster, 2004, Stuart et al., 1999] for general texts, to [Kapur and Kesavan, 1992, Kullback, 1968] for the theory of information and its relationship with mathematical statistics, to [Ferguson, 1996, Le Cam, 1986] for large-sample theory, to [Dudley, 2002, Williams, 1991]

for the theory of conditional expectation and conditional probability and to [Mosegaard and Tarantola, 2002, Tarantola, 2005, 2008] for the notion of the intersection of probabilities.

2.1.1 Classical methods of estimation

The classical methods of estimation, namely the Method of Moments (MM), the method of Maximum Likelihood (ML) and the Bayesian method, are summarized in this section.

General considerations

The basic model problem that the theory of mathematical statistics tries to solve has the following setup. Usually, a *random experiment* is considered, i.e. an experiment which can be repeated a large number of times under similar circumstances and whose outcome exhibits variability. Furthermore, a stochastic model for this random experiment is typically assumed to be given, i.e. a probability distribution defined on the possible outcomes depending on a set of unknown parameters. The problem of interest to the theory of mathematical statistics is then the estimation of these parameters from a data set of observed samples.

Let us work in the following with a random experiment whose possible outcomes are real numbers. Let the random variable $\tilde{\mathbb{X}}$ with values in $\mathbb{R}$ a.s. perfectly represent the outcome. Let $\tilde{\mathbb{X}}$ admit a (possibly unknown) Probability Density Function (PDF) $g(x)$ defined on $\mathbb{R}$, which is called the *data-generating PDF*. Let the set $\{f(x|\boldsymbol{p}) \mid \boldsymbol{p} \in P\}$ be a collection of candidate PDFs with common support $S \subset \mathbb{R}$, parameterized by $\boldsymbol{p} \in P$, where P is an open subset of $\mathbb{R}^m$. Let $\boldsymbol{x} = (x_1, \ldots, x_n)$ denote a data set of n outcomes of the random experiment, that is to say of n independent and identically-distributed (iid) realizations of $\tilde{\mathbb{X}}$. In this setting, we call an *estimation rule* any mapping

$$\hat{\boldsymbol{p}}_n : \mathbb{R}^n \to P : \boldsymbol{x} \mapsto \hat{\boldsymbol{p}}_n(\boldsymbol{x}) \tag{2.1}$$

giving an *estimate* $\hat{\boldsymbol{p}}_n(\boldsymbol{x})$ of the unknown parameters as a function of the data set $\boldsymbol{x}$ of samples. In the following, we recall several classical methods for the construction of such estimation rules. We note that all methods can be readily extended to vector-valued observations and also to observations taking values in functional spaces [see, for instance, Basawa and Prakasa Rao, 1980, for a survey of estimation methods for stochastic processes].

Method of Moments

The MM, first introduced by Pearson [1894], consists in equating a convenient number of the sample moments to the corresponding moments of the distribution, which are functions of the unknown parameters. Usually, as many moments as there are parameters to be estimated are considered, such that the system of moment equations to be solved reads:

$$\frac{1}{n} \sum_{k=1}^{n} x_k = \int_S x f(x|\boldsymbol{p}) dx \quad , \tag{2.2}$$

$$\cdots$$

$$\frac{1}{n} \sum_{k=1}^{n} x_k^m = \int_S x^m f(x|\boldsymbol{p}) dx. \tag{2.3}$$

The MM consists in identifying, as an estimate of the unknown parameters, a parameter point $\hat{\boldsymbol{p}}_n^{\text{MM}}(\boldsymbol{x}) \in P$ which solves the system (2.2)-(2.3).

Maximum Likelihood estimation

The ML method was first introduced by Fisher [1912]. The *likelihood* of the parameters $\boldsymbol{p}$ given the samples $\boldsymbol{x}$ is defined by:

$$L_n(\boldsymbol{p}; \boldsymbol{x}) = \prod_{k=1}^{n} f(x_k | \boldsymbol{p}). \tag{2.4}$$

The ML method consists in choosing a parameter point so as to maximize $L_n(\boldsymbol{p}; \boldsymbol{x})$:

$$\hat{\boldsymbol{p}}_n^{\text{ML}}(\boldsymbol{x}) = \arg \max_{\boldsymbol{p} \in P} L_n(\boldsymbol{p}; \boldsymbol{x}). \tag{2.5}$$

In other words, a parameter point such that the observed samples are most likely is chosen.

Bayes estimation

In the Bayesian approach, first introduced by Bayes [1763], PDFs are used to represent the available information on the unknown parameters. First, a *prior PDF* $\pi(\boldsymbol{p})$ is chosen representing whatever information on the unknown $\boldsymbol{p}$ is available in advance of making any observations in the current experiment. Then, the *posterior PDF* $\pi_{\boldsymbol{x},n}(\boldsymbol{p})$, representing all information available after observing $\boldsymbol{x}$, is built as follows:

$$\pi_{\boldsymbol{x},n}(\boldsymbol{p}) = \frac{\pi(\boldsymbol{p}) L_n(\boldsymbol{p}; \boldsymbol{x})}{\int_P \pi(\boldsymbol{p}) L_n(\boldsymbol{p}; \boldsymbol{x}) d\boldsymbol{p}} \quad, \tag{2.6}$$

where $L_n(\boldsymbol{p}; \boldsymbol{x})$ still denotes the likelihood of $\boldsymbol{p}$, defined in (2.4). Finally, the *Bayes estimate with respect to the square-error loss function* of the unknown parameters is defined as the posterior mean value:

$$\hat{\boldsymbol{p}}_n^{\text{Bayes}}(\boldsymbol{x}) = \int_P \boldsymbol{p} \pi_{\boldsymbol{x},n}(\boldsymbol{p}) d\boldsymbol{p}. \tag{2.7}$$

2.1.2 Relative entropy

The concept of relative entropy is now recalled. For the sake of simplicity, we restrict ourselves to complex-valued, finite-dimensional, random variables. We refer the reader to [Kullback, 1968] for the generalization to random variables with values in more general spaces.

Definition. Let f_1 and f_2 be two PDFs with supports $T \subset \mathbb{C}^n$ and $S \subset \mathbb{C}^n$, respectively, where $T \subset S$. The *relative entropy* from f_1 to f_2 is then defined by:

$$\mathcal{I}(f_1 || f_2) = \int_T f_1(\boldsymbol{x}) \log \frac{f_1(\boldsymbol{x})}{f_2(\boldsymbol{x})} d\boldsymbol{x}. \tag{2.8}$$

The relative entropy can be interpreted as a distance-like measure of the separation between the PDFs f_1 and f_2. However, since it does not in general satisfy the symmetry property and the triangle inequality, it is not a true metric distance. It should be noted that there exist many other functionals which allow measuring the separation between PDFs. The relative entropy belongs to the more general class of so-called f-divergences, which was introduced by Csiszár [1967] and also includes the χ^2-divergence, the Hellinger divergence and the L^1-distance.

Box 2.1. Properties of the relative entropy

This box lists the main properties of the relative entropy. We refer the reader to [Kullback, 1968] for the proofs corresponding to these properties.

Theorem (convexity). *Let f_1 and f_2 be two PDFs with common support $S \subset \mathbb{C}^n$. Then:*

$$\mathcal{I}(f_1||f_2) \geq 0 \quad , \tag{2.9}$$

$$\mathcal{I}(f_1||f_2) = 0 \text{ if and only if } f_1(\boldsymbol{x}) = f_2(\boldsymbol{x}) \text{ a.e.} \tag{2.10}$$

Theorem (invariance). *Let the real scalar random variables $\mathbb{X}_1$ and $\mathbb{X}_2$ admit the PDFs f_1 and f_2 with common support $S \subset \mathbb{C}^n$. Let g_1 and g_2 be the PDFs of the images $\mathbb{Y}_1 = \varphi(\mathbb{X}_1)$ a.s. and $\mathbb{Y}_2 = \varphi(\mathbb{X}_2)$ a.s. of these random variables through a measurable mapping $\varphi : \mathbb{C}^n \to \mathbb{C}^m$. We then have:*

$$\mathcal{I}(f_1||f_2) \geq \mathcal{I}(g_1||g_2) \quad , \tag{2.11}$$

$$\mathcal{I}(f_1||f_2) = \mathcal{I}(g_1||g_2) \text{ if and only if } \frac{f_1(\boldsymbol{x})}{f_2(\boldsymbol{x})} = \frac{g_1(\varphi(\boldsymbol{x}))}{g_2(\varphi(\boldsymbol{x}))} \text{ a.e.} \tag{2.12}$$

Definition (Fisher information). Let $\{f(\boldsymbol{x}|\boldsymbol{p}) \mid \boldsymbol{p} \in P\}$ be a collection of PDFs with common support $S \subset \mathbb{C}^n$ and parameterized by $\boldsymbol{p} \in P$, where P is an open subset of $\mathbb{R}^m$. If the gradient $\boldsymbol{\nabla_p} \log f(\boldsymbol{x}|\boldsymbol{p})$ exists a.e. for all $\boldsymbol{p} \in P$, then the *Fisher information matrix $\boldsymbol{I}(\boldsymbol{p})$* is defined by:

$$\boldsymbol{I}(\boldsymbol{p}) = \int_S f(\boldsymbol{x}|\boldsymbol{p}) \boldsymbol{\nabla_p} \log f(\boldsymbol{x}|\boldsymbol{p}) \otimes \boldsymbol{\nabla_p} \log f(\boldsymbol{x}|\boldsymbol{p}) d\boldsymbol{x}. \tag{2.13}$$

Theorem. *Let $\{f(\boldsymbol{x}|\boldsymbol{p}) \mid \boldsymbol{p} \in P\}$ be a collection of PDFs with common support $S \subset \mathbb{C}^n$ and parameterized by $\boldsymbol{p} \in P$, where P is an open subset of $\mathbb{R}^m$. Under regularity conditions [Kullback, 1968, ch. 2 sec. 6], the Fisher information matrix is then the Hessian of the relative entropy, and is such that:*

$$\mathcal{I}\big(f(\cdot|\boldsymbol{p})\big||f(\cdot|\boldsymbol{p}+\delta\boldsymbol{p})\big) = \frac{1}{2}\left(\boldsymbol{I}(\boldsymbol{p})\delta\boldsymbol{p}, \delta\boldsymbol{p}\right) + O\left(||\delta\boldsymbol{p}||^3\right) \text{ if } ||\delta\boldsymbol{p}|| \to 0. \tag{2.14}$$

The Fisher information $\boldsymbol{I}(\boldsymbol{p})$ is a measure of the sensitivity of the PDF $f(\boldsymbol{x}|\boldsymbol{p})$ with respect to perturbations of $\boldsymbol{p}$. Expression (2.14) means that the PDF $f(\boldsymbol{x}|\boldsymbol{p})$ changes more rapidly (in the sense of the relative entropy) as a function of a small perturbation $\delta\boldsymbol{p}$ of the parameters $\boldsymbol{p}$ when $\boldsymbol{I}(\boldsymbol{p})$ is larger, that is to say when its eigenvalues are larger. Conversely, when the problem of the identification of $\boldsymbol{p}$ from a data set of iid samples with PDF $f(\boldsymbol{x}|\boldsymbol{p})$ is considered, this inverse problem is better-conditioned when $\boldsymbol{I}(\boldsymbol{p})$ is larger.

2.1.3 Evaluation of the performance of estimation rules

In estimation problems, the application of distinct estimation rules on the same data set of observed samples usually leads to distinct estimates of the unknown parameters to be identified. In practice, a fundamental problem is therefore the choice of the "most adequate" estimation rule leading to the "most adequate" estimate of the unknown parameters. Our goal in this section is to describe how the adequacy of estimation rules can be evaluated.

General considerations

Let us consider again the generic estimation problem outlined in Section 2.1.1. A first difficulty to the evaluation of the adequacy of an estimation rule $\hat{\boldsymbol{p}}_n$, giving an estimate $\hat{\boldsymbol{p}}_n(\boldsymbol{x})$ of the unknown parameters as a function of a data set $\boldsymbol{x} = (x_1, \ldots, x_n)$, is that every estimate is a function of the data set of outcomes of the random experiment. If a new data set of n samples were collected, it is likely that different values would be obtained such that a different estimate of the unknown parameters would be proposed. Consequently, it may not be legitimate to judge the adequacy of an estimation rule by evaluating the adequacy of an individual estimate for a specific data set. This difficulty is remedied in the theory of mathematical statistics by introducing a random data set, chosen here equal to the random variable $\mathbb{X} = (\mathbb{X}_1, \ldots, \mathbb{X}_n)$ gathering n independent copies of the random variable $\tilde{\mathbb{X}}$ that is assumed to perfectly represent the outcome of the random experiment. The performance of the estimation rule $\hat{\boldsymbol{p}}_n$ is then evaluated based upon the stochastic properties of the *estimator* $\hat{\boldsymbol{p}}_n(\mathbb{X})$, obtained upon applying $\hat{\boldsymbol{p}}_n$ to $\mathbb{X}$. Many approaches have been proposed in the literature for the study of these properties. A possible way to distinguish between them consists in separating, on the one hand, the approaches dealing with the finite-sample properties (typically bias/variance) when the size n of the data set is a fixed number, and, on the other hand, the approaches concerning the asymptotic properties (typically consistency/asymptotic variance) as the size n of the data set tends to infinity.

A more fundamental difficulty to the evaluation of the adequacy of estimation rules is the potential problem of misspecification. A stochastic model is *correctly specified* when it can fit the random experiment perfectly, i.e. when there exist *"true"* parameters $\boldsymbol{p}^{\text{true}}$ such that the candidate PDF $f(x|\boldsymbol{p}^{\text{true}})$ perfectly reproduces the data-generating PDF $g(x)$. Conversely, a stochastic model that imperfectly represents the random experiment for any choice of its parameters is called *misspecified*. In that case, the data-generating PDF $g(x)$ does not belong to the collection $\{f(x|\boldsymbol{p}) \mid \boldsymbol{p} \in P\}$ of candidate PDFs.

The asymptotic properties of the estimators obtained by applying the MM, the ML method and the Baysian estimation method to the estimation problem under study are now examined with emphasis on the fundamentally different factors determining the adequacy of estimation rules according to whether the stochastic model is correctly specified, or misspecified.

Estimation under the correct models assumption

Let us first consider the case where the stochastic model is correctly specified. Let us assume, moreover, that the model is *identifiable* in that the "true" value $\boldsymbol{p}^{\text{true}}$ is unique. It then turns out [Cramér, 1946, Strasser, 1981, Wald, 1949] that, under regularity conditions, any sequence of estimators obtained by applying any classical method of estimation is *consistent* in that it converges a.s. to the "true" value as the size n of the data set tends to infinity:

$$\lim_{n \to +\infty} \hat{\boldsymbol{p}}_n^{\text{MM}}(\mathbb{X}) = \boldsymbol{p}^{\text{true}} \text{ a.s. }, \quad \lim_{n \to +\infty} \hat{\boldsymbol{p}}_n^{\text{ML}}(\mathbb{X}) = \boldsymbol{p}^{\text{true}} \text{ a.s. }, \quad \lim_{n \to +\infty} \hat{\boldsymbol{p}}_n^{\text{Bayes}}(\mathbb{X}) = \boldsymbol{p}^{\text{true}} \text{ a.s.} \tag{2.15}$$

In other words, the "true" value $\boldsymbol{p}^{\text{true}}$ can be recovered from experimental data by applying any of these estimation rules on a sufficiently large data set. However, the size of the data set required to achieve estimates of a given accuracy depends on the method. When seeking the most adequate estimation method for a correctly specified model, the key issue is *efficiency*, i.e. to find the consistent estimation rule achieving estimates of a given accuracy with the least possible observations. It can be shown [Bahadur, 1964, Cramér, 1946, Fisher, 1922] that, for a correctly specified model, the ML method is generally the best possible estimation method from the efficiency point of view.

Estimation under misspecified models with compatible support

Let us now consider the case where the stochastic model is misspecified. Let us assume, here, moreover, that the support T of the data-generating PDF $g(x)$ is included in the support S of the candidate PDFs in $\{f(x|\boldsymbol{p}) \mid \boldsymbol{p} \in P\}$. It then turns out that, under some regularity conditions, any sequence of estimators obtained by applying any classical method of estimation still converges a.s. to a deterministic parameter point. In the literature, this asymptotic value is sometimes called the "*pseudo-true*" value. It is very important to note that this "pseudo-true" value generally depends on the estimation method: distinct estimation rules lead to distinct sequences of estimators that converge to distinct asymptotic estimates of the sought parameters when applied on the same sequence of data sets. Hence, when seeking the most adequate estimation method for a misspecified model, the key issue is not efficiency, but rather to find the estimation rule leading to a sequence of estimators that converges to the "most adequate" "pseudo-true" value. Since the adequacy of the "pseudo-true" value cannot be judged based upon its distance to some "true" value, the adequacy of an estimation method for a misspecified model can only be measured when what is meant by the "most adequate" "pseudo-true" value was explicitly defined beforehand.

Let us now focus on characterizing the "pseudo-true" value for sequences of MM, ML and Bayes estimators. As the size n of the data set tends to infinity, it follows from the Strong Law of Large Numbers (SLLN) that the system of moment equations (2.2)-(2.3) converges to the system:

$$E\left\{\tilde{\mathbb{X}}\right\} = \int_S x f(x|\boldsymbol{p}) dx \quad , \tag{2.16}$$

$$\cdots$$

$$E\left\{\tilde{\mathbb{X}}^m\right\} = \int_S x^m f(x|\boldsymbol{p}) dx. \tag{2.17}$$

A parameter point $\boldsymbol{p}_\infty^{\text{MM}}$ solving this system of equations is a "pseudo-true" value of the sought parameters for the MM.

The maximization of the likelihood function in (2.5) is replaced by the maximization of the *loglikelihood function*, rescaled by the factor $1/n$:

$$\hat{\boldsymbol{p}}_n^{\text{ML}}(\boldsymbol{x}) = \arg\max_{\boldsymbol{p}\in P} \frac{1}{n} \log L_n(\boldsymbol{p};\boldsymbol{x}) = \arg\max_{\boldsymbol{p}\in P} \frac{1}{n} \sum_{k=1}^n \log f(\boldsymbol{x}_k|\boldsymbol{p}). \tag{2.18}$$

Clearly, $(1/n)\log L_n(\boldsymbol{p};\boldsymbol{x})$ attains its maximum at the same parameter value as $L_n(\boldsymbol{p};\boldsymbol{x})$. As the size n of the data set tends to infinity, it follows from the SLLN that:

$$\lim_{n\to+\infty} \frac{1}{n} \sum_{k=1}^n \log f(\mathbb{X}_k|\boldsymbol{p}) = E\left\{\log f(\tilde{\mathbb{X}}|\boldsymbol{p})\right\} = -\mathcal{S}(g) - \mathcal{I}\big(g\big|\big|f(\cdot|\boldsymbol{p})\big) \text{ a.s.} \quad , \tag{2.19}$$

where $\mathcal{S}(\cdot)$ is the Shannon entropy (1.37). If the asymptotic deterministic function attains a global maximum at

$$\boldsymbol{p}_\infty^{\text{ML}} = \arg\max_{\boldsymbol{p}\in P} E\left\{\log f(\tilde{\mathbb{X}}|\boldsymbol{p})\right\} = \arg\min_{\boldsymbol{p}\in P} \mathcal{I}\big(g\big|\big|f(\cdot|\boldsymbol{p})\big) \quad , \tag{2.20}$$

then $\boldsymbol{p}_\infty^{\text{ML}}$ is a "pseudo-true" value for the ML method, which minimizes the distance (in the sense of the relative entropy) between the data-generating PDF and the modelled PDF. Under regularity conditions, it can be shown [Huber, 1967] that, if the "pseudo-true" value exists and is unique, any sequence of ML estimators converges a.s. to $\boldsymbol{p}_\infty^{\text{ML}}$.

It can be shown that the distribution of Bayes estimators tends to become independent of the prior distribution as the size n of the data set tends to infinity (hence, it tends to become entirely dependent on the likelihood function). Under regularity conditions, it can be demonstrated [Berk, 1966, 1970, Bunke and Milhaud, 1998] that, if the "pseudo-true" value $\boldsymbol{p}_\infty^{\mathrm{ML}}$ exists and is unique, any sequence of Bayes estimators also converges a.s. to $\boldsymbol{p}_\infty^{\mathrm{ML}}$.

Estimation under misspecified models with incompatible support

In this paragraph, we keep on studying the case where the stochastic model is misspecified. However, it is assumed, this time, that the support T of the data-generating PDF $g(x)$ is not (entirely) included in the support S of the candidate PDFs in $\{f(x|\boldsymbol{p}) \mid \boldsymbol{p} \in P\}$. Under the stated assumptions, an observed data set may then sometimes contain samples belonging to the set $T \backslash S$. According to the mathematical model, such observations shouldn't occur except with a vanishing probability, no matter the parameter value $\boldsymbol{p}$. When the data set contains such samples, it may lead to a non-solvable system of moment equations (2.2)-(2.3). Moreover, it follows from (2.4) that the ML estimate then does not exist since the likelihood function vanishes at all parameter values. Similarly, it follows from (2.6) that the Bayesian posterior PDF cannot be defined since it would be equal to the fraction 0/0 at all parameter values. By definition, the stochastic model is rejected in such a situation.

Box 2.2. Illustrative example: lognormal stochastic model

This box provides an illustration of the misspecification of models in estimation problems. Let us consider a random experiment whose outcomes are real numbers. Let a collection $\{f_{\mathrm{LN}}(x|\mu,\sigma) \mid \mu, \sigma \in \mathbb{R}_0^+\}$ of lognormal candidate PDFs be available such that:

$$f_{\mathrm{LN}}(x|\mu,\sigma) = \frac{\mathbb{1}_{\mathbb{R}_0^+}(x)}{xb\sqrt{2\pi}} \exp\left(-\frac{(\log x - a)^2}{2b^2}\right) \quad, \tag{2.21}$$

where a and b are related to the mean value μ and the standard deviation σ as follows:

$$a = \log\left(\frac{\mu^2}{\sqrt{\sigma^2 + \mu^2}}\right) \quad, \quad b = \sqrt{\log\left(\left(\frac{\sigma}{\mu}\right)^2 + 1\right)}. \tag{2.22}$$

For the definition of the Bayes estimators in the following, let the prior PDF be equal to the improper (i.e. non-normalizable) uniform PDF $\pi(\mu,\sigma) = \mathbb{1}_{\mathbb{R}_0^+}(\mu)\mathbb{1}_{\mathbb{R}_0^+}(\sigma)$.

Estimation under the correct models assumption
For an example of an estimation problem where the correct models assumption is fulfilled, let the observations be iid samples of a lognormal PDF $f_{\mathrm{LN}}(x|\mu^{\mathrm{true}}, \sigma^{\mathrm{true}})$, where the "true" value of the parameters is chosen equal to $(\mu^{\mathrm{true}}, \sigma^{\mathrm{true}}) = (1, \ 0.5)$. Let the following synthetically generated data set be given:

$$\boldsymbol{x} = \{0.72 \,, \ 0.40 \,, \ 0.94 \,, \ 1.02 \,, \ 0.52 \,, \ 1.56 \,, \ 1.56 \,, \ 0.87 \,, \ 1.04 \,, \ 0.97\}. \tag{2.23}$$

Figure 2.1 shows the likelihood function and the posterior PDF for these observations. The MM, the ML and the Bayes estimate are:

$$(\hat{\mu}, \hat{\sigma})_{10}^{\mathrm{MM}}(\boldsymbol{x}) = (0.96, \ 0.36) \,, \quad (\hat{\mu}, \hat{\sigma})_{10}^{\mathrm{ML}}(\boldsymbol{x}) = (0.97, \ 0.41) \,, \quad (\hat{\mu}, \hat{\sigma})_{10}^{\mathrm{Bayes}}(\boldsymbol{x}) = (1.13, \ 0.72).$$

The asymptotic results given in Section 2.1.3 state that these estimates all converge to the "true" value $(\mu^{\text{true}}, \sigma^{\text{true}}) = (1, 0.5)$ when the size n of the data set tends to infinity. The quickest convergence is achieved with the ML method.
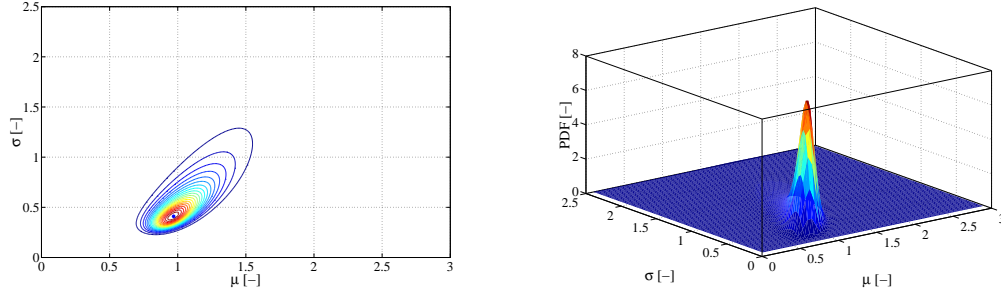

Figure 2.1: Lognormal stochastic model: (left) contours of the likelihood function $L_{10}(\mu, \sigma; \boldsymbol{x})$ and (right) posterior PDF $\pi_{\boldsymbol{x},10}(\mu, \sigma)$.

Estimation under misspecified models with compatible support

For an example of an estimation problem under misspecified models with compatible support, let the observations be iid samples of a gamma PDF with mean value m and standard deviation s:

$$f_\gamma(x|m, s) = \mathbb{1}_{\mathbb{R}_0^+}(x) \frac{\left(\dfrac{m}{s^2}\right)^{(m^2/s^2)}}{\Gamma\left(m^2/s^2\right)} \exp\left(-\frac{m}{s^2}x\right). \tag{2.24}$$

The parameters m and s are chosen equal to $m = 1$ and $s = 0.5$. Clearly, the support $\mathbb{R}_0^+$ of this gamma PDF is included in, and therefore compatible with, the support $\mathbb{R}_0^+$ of the lognormal candidate PDFs. Let the following synthetically generated data set be given:

$$\boldsymbol{x} = \{0.32, 0.49, 0.93, 0.72, 1.80, 1.26, 0.67, 1.42, 1.45, 0.65\}. \tag{2.25}$$

Figure 2.2 shows the likelihood function and the posterior PDF for these observations. The MM, the ML and the Bayes estimate are:

$$(\hat{\mu}, \hat{\sigma})_{10}^{\text{MM}}(\boldsymbol{x}) = (0.97, 0.46), \quad (\hat{\mu}, \hat{\sigma})_{10}^{\text{ML}}(\boldsymbol{x}) = (0.98, 0.54), \quad (\hat{\mu}, \hat{\sigma})_{10}^{\text{Bayes}}(\boldsymbol{x}) = (1.21, 1.01).$$

The asymptotic results given in Section 2.1.3 state that the MM estimate converges to the population mean and standard deviation $(\mu, \sigma)_\infty^{\text{MM}} = (1, 0.5)$ when the size n of the data set tends to infinity. In contrast, the ML estimate and the Bayes estimate converge to the parameter point $(\mu, \sigma)_\infty^{\text{ML}}$ where the relative entropy from the chosen gamma PDF to the lognormal PDF $f_{\text{LN}}(x|\mu, \sigma)$ attains a global minimum as a function of μ and σ. Figure 2.3 illustrates that $(\mu, \sigma)_\infty^{\text{ML}} = (1.01, 0.58)$.
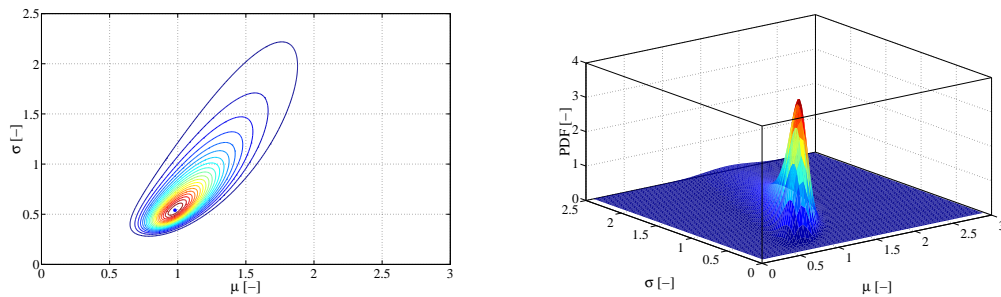

Figure 2.2: Lognormal stochastic model: (left) contours of the likelihood function $L_{10}(\mu, \sigma; \boldsymbol{x})$ and (right) posterior PDF $\pi_{\boldsymbol{x},10}(\mu, \sigma)$.
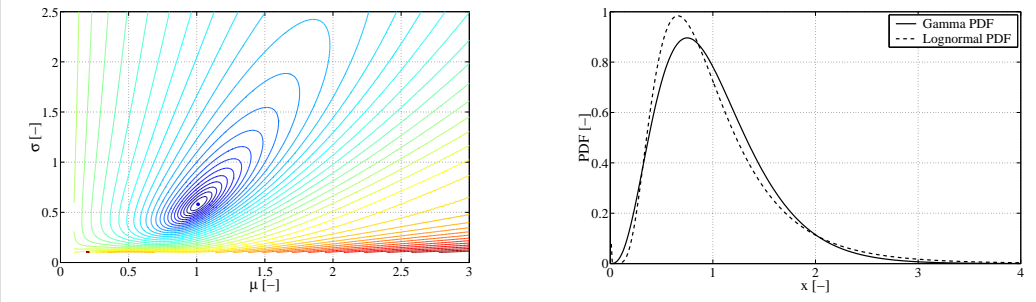
Figure 2.3: Lognormal stochastic model: (left) relative entropy $\mathcal{I}\big(f_\gamma\big|\big|f_{\text{LN}}(\,\cdot\,|\mu,\sigma)\big)$ as a function of μ and σ and (right) comparison of the data-generating gamma PDF f_γ with the lognormal PDF $f_{\text{LN}}\big(\,\cdot\,|(\mu,\sigma)^{\text{ML}}_\infty\big)$ with $(\mu,\sigma)^{\text{ML}}_\infty = (1.01,\ 0.58)$.

Estimation under misspecified models with incompatible support

For an example of an estimation problem under misspecified models with incompatible support, let the observations be iid samples of a Gaussian PDF with zero mean and unit standard deviation. Clearly, the support $\mathbb{R}$ of this Gaussian PDF is not entirely included in, and therefore incompatible with, the support $\mathbb{R}_0^+$ of the lognormal candidate PDFs. Let the following synthetically generated data set be given:

$$\boldsymbol{x} = \{0.19\,,\ -0.73\,,\ 0.59\,,\ -2.18\,,\ 0.14\,,\ -0.11\,,\ -1.07\,,\ -0.06\,,\ 0.10\,,\ 0.83\}. \tag{2.26}$$

The MM estimate does not exist for these observations since their statistical average is negatively valued. Moreover, neither the ML estimate, neither the Bayes estimate exist since the likelihood function vanishes at all parameter values. By definition, the stochastic model is rejected.

2.2 Difficulties in applying the classical estimation methods

In the previous section, the classical methods of estimation were introduced and the evaluation of the adequacy of estimation methods was discussed. This section now narrows the focus from the inversion of general stochastic models within the framework of the theory of mathematical statistics to the inversion of probabilistic structural models. Our main objective in this section is to evaluate the adequacy of the classical methods of estimation to tackle the inversion of probabilistic structural models from experimental data sets of observed TF values.

Problem setting

Let us consider the following general situation. Let the generic vibration test (Sec. 1.3) be carried out under noise-free conditions on a collection of samples of a random structure to obtain an experimental data set $\boldsymbol{D}^0$ of observed TF values of the form (1.125)-(1.126). Moreover, let a probabilistic model for the dynamical behaviour of the studied random structure (Sec. 1.1) be given, which exhibits a set of parameters $\boldsymbol{p}$. Let this model be used (Sec. 1.4) to model the vibration test to obtain a stochastic process $\{\mathbb{H}(\omega_\ell;\boldsymbol{p}) \mid 1 \leq \ell \leq n_{\text{F}}\}$, modelling the noise-free TFs of the considered random structure, with n-th order cylindrical PDF $\theta^{(n)}(\cdot|\cdot;\boldsymbol{p})$.

Considering that $\theta^{(n_{\mathrm{F}})}(\cdot|\cdot;\boldsymbol{p})$ is a parameterized candidate PDF for the observed TFs, the experimental identification of $\boldsymbol{p}$ is a problem that pertains to the classical framework of the theory of mathematical statistics reviewed in Section 2.1. It is therefore appealing to apply one of the classical methods of estimation. The ML method is particularly attractive, especially in view of its consistency and asymptotic efficiency properties under the correct models assumption (Sec. 2.1.3). The ML estimate reads:

$$\hat{\boldsymbol{p}}_{n_{\mathrm{K}}}^{\mathrm{ML}}(\boldsymbol{D}^0) = \arg\max_{\boldsymbol{p}} L_{n_{\mathrm{K}}}\left(\boldsymbol{p};\boldsymbol{D}^0\right) = \arg\max_{\boldsymbol{p}} \prod_{k=1}^{n_{\mathrm{K}}} \theta^{(n_{\mathrm{F}})}(\boldsymbol{D}_k^0|\omega_1,\ldots,\omega_{n_{\mathrm{F}}};\boldsymbol{p}). \qquad (2.27)$$

Unfortunately, considerable difficulties may arise in this application of the ML method, as explained next. The results described in the following can readily be extrapolated to the MM and the Bayes estimation method.

Potentially prohibitive computational cost

The first difficulty comes from a numerical issue. In Section 1.2, the Monte Carlo simulation method was suggested to perform computations with the probabilistic structural models. Accordingly, the following two-step procedure could be proposed for the numerical approximation of the likelihood $L_{n_{\mathrm{K}}}\left(\boldsymbol{p};\boldsymbol{D}^0\right)$ of a fixed value $\boldsymbol{p}$ of the parameters:

- **Step 1:** Generate a set of iid samples of the stochastic process $\{\mathbb{H}(\omega_\ell;\boldsymbol{p}) \mid 1 \le \ell \le n_{\mathrm{F}}\}$.

- **Step 2:** Compute $L_{n_{\mathrm{K}}}\left(\boldsymbol{p};\boldsymbol{D}^0\right)$ by estimating the value taken by the PDF $\theta^{(n_{\mathrm{F}})}(\cdot|\cdot;\boldsymbol{p})$ at each data subset $\boldsymbol{D}_k^0$ from these samples using a numerical density estimation method.

However, it is well known that the computational effort required to numerically approximate a PDF grows rapidly with the dimension of the sample space. Since this dimension is here equal to $2 \times n_{\mathrm{M}} \times n_{\mathrm{F}}$, the numerical solution of (2.27) is impractical when either n_{M}, or n_{F} is large. This, unfortunately, occurs frequently in vibration tests.

Potential misspecification of the probabilistic model

The second difficulty stems from the fact that the probabilistic structural model may be misspecified. To analyze the potential problem of misspecification, we use the representation of the observed TF values as realizations of random variables, which was introduced in Section 1.4. The experimental data set is thus considered as a collection of n_{K} iid realizations of a data-generating stochastic process $\tilde{\mathbb{D}}^0$ with n_{F}-th order cylindrical PDF $\xi^{(n_{\mathrm{F}})}$. When working with probabilistic models with minimal parameterization, only few parameters are usually available to adjust the shape of the modelled PDF $\theta^{(n_{\mathrm{F}})}(\cdot|\cdot;\boldsymbol{p})$. Considering that the data-generating PDF $\xi^{(n_{\mathrm{F}})}$ is, *a priori*, a completely arbitrary PDF, we must therefore conclude that, for a probabilistic model with minimal parameterization, there will usually not exist any "true" value $\boldsymbol{p}^{\mathrm{true}}$ such that $\xi^{(n_{\mathrm{F}})} = \theta^{(n_{\mathrm{F}})}(\cdot|\cdot;\boldsymbol{p}^{\mathrm{true}})$, or, equivalently, such that the probabilistic model perfectly reproduces the data-generating PDF. When the probabilistic model is misspecified, the consistency and asymptotic efficiency properties of the ML method are no longer defined.

Potential incompatibility of the probabilistic model with the experimental data

The third difficulty stems from the fact that the probabilistic structural model may be not only misspecified, but also incompatible with the experimental data: observed TFs that do not belong to the support of

the PDF $\theta^{(n_\mathrm{F})}(\cdot\,|\cdot\,;\boldsymbol{p})$, irrespective of the parameter value $\boldsymbol{p}$, may occur.

Let us investigate the nature of the support of the PDF $\theta^{(n_\mathrm{F})}(\cdot\,|\cdot\,;\boldsymbol{p})$ in more detail. The discussion is particularized to non-parametric probabilistic models (the reasoning can readily be extended to parametric ones). Let a deterministic reduced matrix model be built for the structure under study and used to forecast the outcome of the vibration test to obtain, rather abstractly considered, a mapping

$$\gamma : \left(\mathrm{M}_{n_\mathrm{T}}^+(\mathbb{R})\right)^3 \to \mathbb{C}^{n_\mathrm{M} \times n_\mathrm{F}} \tag{2.28}$$
$$: (\boldsymbol{K}, \boldsymbol{D}, \boldsymbol{M}) \mapsto \gamma(\boldsymbol{K}, \boldsymbol{D}, \boldsymbol{M}) = \{\boldsymbol{h}(\omega_\ell; \boldsymbol{K}, \boldsymbol{D}, \boldsymbol{M}) \mid 1 \le \ell \le n_\mathrm{F}\} \quad,$$

which relates any set $(\boldsymbol{K}, \boldsymbol{D}, \boldsymbol{M})$ of reduced matrices to a corresponding set of forecasted TF values, such that, for each frequency ω_ℓ, the TF value $\boldsymbol{h}(\omega_\ell; \boldsymbol{K}, \boldsymbol{D}, \boldsymbol{M})$ is the ratio at that frequency of the response in the n_M transducers predicted for the reduced matrices $(\boldsymbol{K}, \boldsymbol{D}, \boldsymbol{M})$ and the magnitude of the applied force.

As outlined in Section 1.1, a non-parametric probabilistic model is obtained on the basis of this deterministic model by modelling the reduced matrices by random matrices $\mathbb{K}(\boldsymbol{p})$, $\mathbb{D}(\boldsymbol{p})$ and $\mathbb{M}(\boldsymbol{p})$ and then transporting the uncertainty introduced in the reduced matrices to the predictions. The stochastic process $\{\mathbb{H}(\omega_\ell; \boldsymbol{p}) \mid 1 \le \ell \le n_\mathrm{F}\}$, modelling the noise-free TFs of the considered random structure, is thus obtained as:

$$\{\mathbb{H}(\omega_\ell; \boldsymbol{p}) \mid 1 \le \ell \le n_\mathrm{F}\} = \gamma\big(\mathbb{K}(\boldsymbol{p}), \mathbb{D}(\boldsymbol{p}), \mathbb{M}(\boldsymbol{p})\big) \text{ a.s.} \tag{2.29}$$

Equation (2.29) means that each realization of the stochastic process $\{\mathbb{H}(\omega_\ell; \boldsymbol{p}) \mid 1 \le \ell \le n_\mathrm{F}\}$ is the image through the mapping γ of a corresponding realization of the triple of random reduced matrices. For a non-parametric probabilistic model with minimal parameterization, the support of the probability distribution of the triple of random matrices is the entire space $(\mathrm{M}_{n_\mathrm{T}}^+(\mathbb{R}))^3$ of admissible triples of reduced matrices. For a probabilistic model of this kind, realizations of $\{\mathbb{H}(\omega_\ell; \boldsymbol{p}) \mid 1 \le \ell \le n_\mathrm{F}\}$ which are not representable in terms of a triple of admissible reduced matrices do not occur except with probability zero, and the support of the probability distribution of $\{\mathbb{H}(\omega_\ell; \boldsymbol{p}) \mid 1 \le \ell \le n_\mathrm{F}\}$, i.e. of the PDF $\theta^{(n_\mathrm{F})}(\cdot\,|\cdot\,;\boldsymbol{p})$, is consequently the image through the deterministic model of the space of admissible values of the reduced matrices:

$$\operatorname{supp} \theta^{(n_\mathrm{F})}(\cdot\,|\cdot\,;\boldsymbol{p}) = \gamma\left(\left(\mathrm{M}_{n_\mathrm{T}}^+(\mathbb{R})\right)^3\right). \tag{2.30}$$

For this reason, the support of $\theta^{(n_\mathrm{F})}(\cdot\,|\cdot\,;\boldsymbol{p})$ is usually only a subset of $\mathbb{C}^{n_\mathrm{M} \times n_\mathrm{F}}$. Considering that the observed TFs are *a priori*, arbitrary elements of $\mathbb{C}^{n_\mathrm{M} \times n_\mathrm{F}}$, we must conclude that the situation sketched in figure 2.4 may arise in that there may be observed TFs which are not compatible with the probabilistic model, i.e. which do not belong to the support of $\theta^{(n_\mathrm{F})}(\cdot\,|\cdot\,;\boldsymbol{p})$. In such a situation, the likelihood function defined in (2.27) vanishes at all parameter values $\boldsymbol{p}$ and, by definition, the ML method rejects the probabilistic model.

We refer the reader to Box 2.4 for a simple example of a probabilistic structural model that is incompatible with experimental data.

Potential difficulties due to experimental noise

The previous discussion concerned a vibration test carried out under noise-free conditions. Additional difficulties caused by distortions of the observed TFs due to experimental noise were not considered, but are to be expected. These will be addressed in Sections 2.3.2 and 2.4.2.
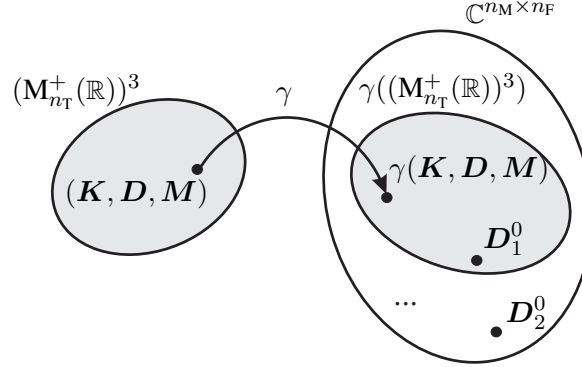
Figure 2.4: Representation of a case where a non-parametric probabilistic model is incompatible with experimental data.

2.3 Proposed distances

The difficulties that may arise in the application of the classical methods of estimation (and in particular of the ML method) to the inversion of probabilistic structural models strongly motivate the development of alternative inverse methods. As discussed in the general introduction, we propose to formulate the inversion as the minimization, with respect to the sought parameters, of an objective function that measures the distance between the experimental data and the considered probabilistic model. Our main objective in this section is to present two versatile methods for measuring the distance between observed TFs and corresponding predicted random TFs. The *core idea* of our methodology (which will be motivated in the sequel) is to account only for the low-order cylindrical PDFs of the predicted random TFs when measuring their distance to the observed TFs. Vibration tests conducted under idealized noise-free, and then noisy, conditions are successively considered in Sections 2.3.1 and 2.3.2.

2.3.1 Undisturbed vibration test

Let us consider again the general situation, where the generic vibration test (Sec. 1.3) is carried out under noise-free conditions to obtain an experimental data set $\boldsymbol{D}^0$ of the form (1.125)-(1.126), and a probabilistic structural model is used (Sec. 1.4) to model the vibration test to obtain a stochastic process $\{\mathbb{H}(\omega_\ell; \boldsymbol{p}) \mid 1 \leq \ell \leq n_{\mathrm{F}}\}$ with n-th order cylindrical PDF $\theta^{(n)}(\cdot|\cdot; \boldsymbol{p})$. Two methods for measuring the distance between the observed TFs and the predicted random TFs, based upon either the loglikelihood function or the relative entropy are now presented.

Distance based upon the loglikelihood function

The distance $\mathcal{L}^{(1)}$, accounting only for the first-order cylindrical PDF, is defined as the average over the frequencies of the sign-reversed loglikelihood function:

$$\mathcal{L}^{(1)}_{n_{\mathrm{F}}, n_{\mathrm{K}}}\left(\boldsymbol{p}; \boldsymbol{D}^0\right) = -\frac{1}{n_{\mathrm{F}}} \sum_{\ell=1}^{n_{\mathrm{F}}} \frac{1}{n_{\mathrm{K}}} \sum_{k=1}^{n_{\mathrm{K}}} \log \theta^{(1)}\left(\boldsymbol{h}_k^0(\omega_\ell)|\omega_\ell; \boldsymbol{p}\right). \tag{2.31}$$

The distance $\mathcal{L}^{(1)}$ is generalized as follows in order to account for higher-order cylindrical PDFs. Let $B_{n_{\mathrm{F}}}^n$ denote the set of all distinct unordered subsets $\{\omega_{\ell_1}, \ldots, \omega_{\ell_n}\}$ of n distinct elements of $\{\omega_\ell \mid 1 \leq \ell \leq$

n_F}. These subsets are the so-called *combinations* of size n from {$\omega_\ell \mid 1 \leq \ell \leq n_F$}. The number of elements of $B_{n_F}^n$ is the binomial coefficient

$$C_{n_F}^n = \frac{n_F!}{n!(n_F - n)!} \quad , \tag{2.32}$$

where $n!$ is the factorial of n. The distance $\mathcal{L}^{(n)}$, accounting for the n-th order cylindrical PDF, is defined as the average of the sign-reversed loglikelihood function over the n-subsets of discrete frequencies in $B_{n_F}^n$:

$$\mathcal{L}_{n_F, n_K}^{(n)} \left(\boldsymbol{p}; \boldsymbol{D}^0 \right) = -\frac{1}{C_{n_F}^n} \sum_{\{\omega_{\ell_1}, \dots, \omega_{\ell_n}\} \in B_{n_F}^n} \frac{1}{n_K} \sum_{k=1}^{n_K} \log \theta^{(n)} \left(\boldsymbol{h}_k^0(\omega_{\ell_1}), \dots, \boldsymbol{h}_k^0(\omega_{\ell_n}) \big| \omega_{\ell_1}, \dots, \omega_{\ell_n}; \boldsymbol{p} \right). \tag{2.33}$$

The factors $1/C_{n_F}^n$ and $1/n_K$ allow $\mathcal{L}^{(n)}$ to remain bounded for arbitrary large n_F and n_K. The unknown parameters can be estimated from the data on the basis of $\mathcal{L}^{(n)}$ by

$$\hat{\boldsymbol{p}}_{n_F, n_K}^{\mathcal{L}, n}(\boldsymbol{D}^0) = \arg \min_{\boldsymbol{p}} \mathcal{L}_{n_F, n_K}^{(n)} \left(\boldsymbol{p}; \boldsymbol{D}^0 \right). \tag{2.34}$$

Finally, it should be noted that, upon choosing n equal to n_F, the expression (2.33) reads

$$\mathcal{L}_{n_F, n_K}^{(n_F)} \left(\boldsymbol{p}; \boldsymbol{D}^0 \right) = -\sum_{k=1}^{n_K} \log \theta^{(n_F)}(\boldsymbol{D}_k^0 | \omega_1, \dots, \omega_{n_F}; \boldsymbol{p}) \quad , \tag{2.35}$$

highlighting that the inverse method (2.34) coincides for $n = n_F$ with the ML method (2.27).

Distance based upon the relative entropy

To introduce the distance based upon the relative entropy, we use the representation of the observed TF values as realizations of random variables (Sec. 1.4). The experimental data set $\boldsymbol{D}^0$ is thus considered as a collection of n_K iid realizations of a data-generating stochastic process $\tilde{\mathbb{D}}^0$ with n-th order cylindrical PDF $\xi^{(n)}$. Let a numerical density estimation method be used to obtain an estimate $\hat{\xi}_{n_K}^{(n)}(\cdot | \cdot; \boldsymbol{D}^0)$ of the data-generating PDF $\xi^{(n)}$ from $\boldsymbol{D}^0$. The distance $\mathcal{D}^{(1)}$ is then defined as the average over the frequencies of the relative entropy between the approximated data-generating first-order cylindrical PDF $\hat{\xi}_{n_K}^{(1)}(\cdot | \cdot; \boldsymbol{D}^0)$ and the modelled PDF $\theta^{(1)}(\cdot | \cdot; \boldsymbol{p})$:

$$\mathcal{D}_{n_F, n_K}^{(1)} \left(\boldsymbol{p}; \boldsymbol{D}^0 \right) = \frac{1}{n_F} \sum_{\ell=1}^{n_F} \mathcal{I} \left(\hat{\xi}_{n_K}^{(1)}(\cdot | \omega_\ell; \boldsymbol{D}^0) \big|\big| \theta^{(1)}(\cdot | \omega_\ell; \boldsymbol{p}) \right). \tag{2.36}$$

More generally, the distance $\mathcal{D}^{(n)}$ is defined as the average over the n-subsets of frequencies in $B_{n_F}^n$ of the relative entropy between the n-th order cylindrical PDFs $\hat{\xi}_{n_K}^{(n)}(\cdot | \cdot; \boldsymbol{D}^0)$ and $\theta^{(n)}(\cdot | \cdot; \boldsymbol{p})$:

$$\mathcal{D}_{n_F, n_K}^{(n)} \left(\boldsymbol{p}; \boldsymbol{D}^0 \right) = \frac{1}{C_{n_F}^n} \sum_{\{\omega_{\ell_1}, \dots, \omega_{\ell_n}\} \in B_{n_F}^n} \mathcal{I} \left(\hat{\xi}_{n_K}^{(n)}(\cdot | \omega_{\ell_1}, \dots, \omega_{\ell_n}; \boldsymbol{D}^0) \big|\big| \theta^{(n)}(\cdot | \omega_{\ell_1}, \dots, \omega_{\ell_n}; \boldsymbol{p}) \right). \tag{2.37}$$

The factor $1/C_{n_F}^n$ allows $\mathcal{D}^{(n)}$ to remain bounded for arbitrary large n_F. The unknown parameters are estimated from the experimental data on the basis of $\mathcal{D}^{(n)}$ by

$$\hat{\boldsymbol{p}}_{n_F, n_K}^{\mathcal{D}, n}(\boldsymbol{D}^0) = \arg \min_{\boldsymbol{p}} \mathcal{D}_{n_F, n_K}^{(n)} \left(\boldsymbol{p}; \boldsymbol{D}^0 \right). \tag{2.38}$$

2.3.2 Disturbed vibration test

Let us now consider the general situation, where the generic vibration test (Sec. 1.3) is carried out, this time, under noisy conditions to obtain an experimental data set $\boldsymbol{D}$ of the form (1.124)-(1.123). The possible distortions of the observed TFs caused by experimental noise present specific difficulties to the inversion of the probabilistic structural model. In particular, it may not be appropriate to simply apply the inverse methods introduced in Section 2.3.1 to the noisy observed TFs (1.124)-(1.123) since the probabilistic model may then be fitted to the experimental noise, rather than to the dynamical characteristics of the tested structures. Two approaches to circumvent these difficulties are now proposed. Insight on the similarities and differences between these two approaches will be gained from the discussion of Sections 2.4.2 and 2.6.3.

(Approach 1) Noise modelling

This approach consists in modelling not only the dynamical behaviour of the considered structure, but also the experimental noise when forecasting the outcome of the vibration test. Let a probabilistic structural model (Sec. 1.1) be given and let a probabilistic model for the experimental noise be built as outlined in Section 1.4. Let these models be jointly used (Sec. 1.4) to forecast the outcome of the noisy vibration test to obtain, for each tested sample structure (indexed by k), a stochastic process

$$\left\{ \mathbb{H}(\omega_\ell; \boldsymbol{p}) + \mathbb{E}_{k1}(\omega_\ell), \ldots, \mathbb{H}(\omega_\ell; \boldsymbol{p}) + \mathbb{E}_{kn_\mathrm{R}}(\omega_\ell) \mid 1 \le \ell \le n_\mathrm{F} \right\} \quad , \tag{2.39}$$

with n-th order cylindrical PDF $\varphi_k^{(n,n_\mathrm{R})}(\cdot|\cdot; \boldsymbol{p})$. The first approach to deal with the experimental noise then consists in formulating the inversion of the probabilistic structural model as the minimization of an objective function that measures the distance between the observed TFs (1.124)-(1.123) and the corresponding predicted random TFs (2.39). As in Section 2.3.1, two methods for measuring this distance, based upon either the loglikelihood function or the relative entropy are now presented.

Distance based upon the loglikelihood function

The distance $\mathcal{L}^{(1)}$, accounting only for the first-order cylindrical PDF, is defined as the average over the frequencies of the sign-reversed loglikelihood function (using equation (1.148)):

$$\mathcal{L}_{n_\mathrm{F}, n_\mathrm{K}, n_\mathrm{R}}^{(1)}(\boldsymbol{p}; \boldsymbol{D}) = -\frac{1}{n_\mathrm{F}} \sum_{\ell=1}^{n_\mathrm{F}} \frac{1}{n_\mathrm{K}} \sum_{k=1}^{n_\mathrm{K}} \log \varphi_k^{(1,n_\mathrm{R})}\left(\boldsymbol{g}_{k1}^{\mathrm{obs}}(\omega_\ell), \ldots, \boldsymbol{g}_{kn_\mathrm{R}}^{\mathrm{obs}}(\omega_\ell) \big| \omega_\ell; \boldsymbol{p} \right) \tag{2.40}$$

$$= -\frac{1}{n_\mathrm{F}} \sum_{\ell=1}^{n_\mathrm{F}} \frac{1}{n_\mathrm{K}} \sum_{k=1}^{n_\mathrm{K}} \log \int_{\mathbb{C}^{n_\mathrm{M}}} \theta^{(1)}\left(\boldsymbol{h} \big| \omega_\ell; \boldsymbol{p} \right) \prod_{r=1}^{n_\mathrm{R}} \rho_k^{(1)}(\boldsymbol{g}_{kr}^{\mathrm{obs}}(\omega_\ell) \big| \omega_\ell; \boldsymbol{h}) d\boldsymbol{h}.$$

More generally, the distance $\mathcal{L}^{(n)}$, accounting for the n-th order cylindrical PDF, is defined by:

$$\mathcal{L}_{n_\mathrm{F}, n_\mathrm{K}, n_\mathrm{R}}^{(n)}(\boldsymbol{p}; \boldsymbol{D}) = -\frac{1}{C_{n_\mathrm{F}}^n} \sum_{\{\omega_{\ell_1}, \ldots, \omega_{\ell_n}\} \in B_{n_\mathrm{F}}^n} \frac{1}{n_\mathrm{K}} \sum_{k=1}^{n_\mathrm{K}} \log \varphi_k^{(n,n_\mathrm{R})}\left(\boldsymbol{D}_k(\omega_{\ell_1}, \ldots, \omega_{\ell_n}) \big| \omega_{\ell_1}, \ldots, \omega_{\ell_n}; \boldsymbol{p} \right), \tag{2.41}$$

where $\boldsymbol{D}_k(\omega_{\ell_1}, \ldots, \omega_{\ell_n}) = \left\{ \boldsymbol{g}_{k1}^{\mathrm{obs}}(\omega_{\ell_1}), \ldots, \boldsymbol{g}_{kn_\mathrm{R}}^{\mathrm{obs}}(\omega_{\ell_1}), \ldots, \boldsymbol{g}_{k1}^{\mathrm{obs}}(\omega_{\ell_n}), \ldots, \boldsymbol{g}_{kn_\mathrm{R}}^{\mathrm{obs}}(\omega_{\ell_n}) \right\}$ and with $B_{n_\mathrm{F}}^n$ and $C_{n_\mathrm{F}}^n$ defined as in Section 2.3.1.

On the basis of $\mathcal{L}^{(n)}$, the unknown parameters are estimated from the data by

$$\hat{\boldsymbol{p}}_{n_\mathrm{F}, n_\mathrm{K}, n_\mathrm{R}}^{\mathcal{L}, n}(\boldsymbol{D}) = \arg\min_{\boldsymbol{p}} \mathcal{L}_{n_\mathrm{F}, n_\mathrm{K}, n_\mathrm{R}}^{(n)}(\boldsymbol{p}; \boldsymbol{D}). \tag{2.42}$$

Distance based upon the relative entropy

To introduce the distance based upon the relative entropy, we use the representation of the observed TF values as realizations of random variables, which was defined in Section 1.4. For each tested structure (indexed by k), the data subset $\boldsymbol{D}_k$ is thus considered as a particular realization of a stochastic process $\mathbb{D}_k$ with n-th order cylindrical PDF $\psi_k^{(n,n_{\mathrm{R}})}$, or, equivalently, as a collection of n_{R} iid realizations of a stochastic process $\tilde{\mathbb{D}}_k$ with n-th order cylindrical PDF $\psi_k^{(n)}$. Let a numerical density estimation method be used to generically obtain an estimate $\hat{\psi}_{k,n_{\mathrm{R}}}^{(n)}(\cdot|\cdot; \boldsymbol{D}_k)$ of the PDF $\psi_k^{(n)}$ from the data subset $\boldsymbol{D}_k$. A generic estimate $\hat{\psi}_{k,n_{\mathrm{R}}}^{(n,n_{\mathrm{R}})}(\cdot|\cdot; \boldsymbol{D}_k)$ of the PDF $\psi_k^{(n,n_{\mathrm{R}})}$ is then defined by:

$$\hat{\psi}_{k,n_{\mathrm{R}}}^{(n,n_{\mathrm{R}})}\left(\boldsymbol{g}_{11},\ldots,\boldsymbol{g}_{1n_{\mathrm{R}}},\ldots,\boldsymbol{g}_{n1},\ldots,\boldsymbol{g}_{nn_{\mathrm{R}}}|\omega_{\ell_1},\ldots,\omega_{\ell_n};\boldsymbol{D}_k\right) = \prod_{r=1}^{n_{\mathrm{R}}} \hat{\psi}_{k,n_{\mathrm{R}}}^{(n)}\left(\boldsymbol{g}_{1r},\ldots,\boldsymbol{g}_{nr}|\omega_{\ell_1},\ldots,\omega_{\ell_n};\boldsymbol{D}_k\right).$$
(2.43)

The distance $\mathcal{J}^{(1)}$ is then defined as the average over the frequencies of the relative entropy between the approximated data-generating first-order cylindrical PDF $\psi_k^{(1,n_{\mathrm{R}})}$ and the modelled PDF $\varphi_k^{(1,n_{\mathrm{R}})}(\cdot|\cdot; \boldsymbol{p})$:

$$\mathcal{J}_{n_{\mathrm{F}},n_{\mathrm{K}},n_{\mathrm{R}}}^{(1)}(\boldsymbol{p};\boldsymbol{D}) = \frac{1}{n_{\mathrm{F}}}\sum_{\ell=1}^{n_{\mathrm{F}}}\frac{1}{n_{\mathrm{K}}}\sum_{k=1}^{n_{\mathrm{K}}}\mathcal{I}\left(\hat{\psi}_{k,n_{\mathrm{R}}}^{(1,n_{\mathrm{R}})}(\cdot|\omega_\ell;\boldsymbol{D}_k)\big|\big|\varphi_k^{(1,n_{\mathrm{R}})}(\cdot|\omega_\ell;\boldsymbol{p})\right).$$
(2.44)

More generally, the distance $\mathcal{J}^{(n)}$ is defined as the average over the n-subsets of frequencies in $B_{n_{\mathrm{F}}}^n$ of the relative entropy between the n-th order cylindrical PDFs $\psi_k^{(1,n_{\mathrm{R}})}$ and $\varphi_k^{(1,n_{\mathrm{R}})}(\cdot|\cdot; \boldsymbol{p})$:

$$\mathcal{J}_{n_{\mathrm{F}},n_{\mathrm{K}},n_{\mathrm{R}}}^{(n)}(\boldsymbol{p};\boldsymbol{D}) = \frac{1}{C_{n_{\mathrm{F}}}^n}\sum_{\{\omega_{\ell_1},\ldots,\omega_{\ell_n}\}\in B_{n_{\mathrm{F}}}^n}\frac{1}{n_{\mathrm{K}}}\sum_{k=1}^{n_{\mathrm{K}}}\mathcal{I}\left(\hat{\psi}_{k,n_{\mathrm{R}}}^{(n,n_{\mathrm{R}})}(\cdot|\omega_{\ell_1},\ldots,\omega_{\ell_n};\boldsymbol{D}_k)\big|\big|\varphi_k^{(n,n_{\mathrm{R}})}(\cdot|\omega_{\ell_1},\ldots,\omega_{\ell_n};\boldsymbol{p})\right),$$
(2.45)

On the basis of $\mathcal{J}^{(n)}$, the unknown parameters are estimated from the data by

$$\hat{\boldsymbol{p}}_{n_{\mathrm{F}},n_{\mathrm{K}},n_{\mathrm{R}}}^{\mathcal{J},n}(\boldsymbol{D}) = \arg\min_{\boldsymbol{p}}\mathcal{J}_{n_{\mathrm{F}},n_{\mathrm{K}},n_{\mathrm{R}}}^{(n)}(\boldsymbol{p};\boldsymbol{D}).$$
(2.46)

(Approach 2) Noise filtering

An alternative strategy consists in estimating, from the noisy observed TFs, the noise-free observed TFs which would have been obtained under undisturbed measurement conditions, and then applying the methods developed in Section 2.3.1 for the case of noise-free data. The noise-free TFs can, for instance, be estimated using the H1-estimation method (see Appendix C).

2.3.3 Bibliographical comments

It should be noted that the concept of building estimation rules using only low-order cylindrical distributions is not new. Within the framework of the theory of mathematical statistics, considerable research effort has already been devoted to developing estimation methods of this kind [see, for instance, Besag, 1974, 1975, Cox and Reid, 2004, Lindsay, 1998, Nott and Ryden, 1999]. In the literature, such restrictions to low-order cylindrical distributions are mostly defended on the grounds of computational tractability. Moreover, we point out that the inverse methods (2.34), (2.42) and (2.46) fit into the very general frameworks of M-estimation [Huber, 1967, 1981] and of the generalized method of moments [Hansen, 1982], which were mentioned in the general introduction.

2.4   Asymptotic properties

We now proceed to study the asymptotic (as $n_F \to +\infty$, $n_R \to +\infty$ and $n_K \to +\infty$) properties of the distances proposed in Section 2.3. The asymptotic behaviour will be analyzed under idealized conditions, that is to say under regularity conditions imposed jointly on the experimental data and the probabilistic models. Since the properties of real experimental data are usually unknown beforehand, it is in practice mostly impossible to prove the fulfilment of the regularity conditions. Nevertheless, the study of the asymptotic properties is interesting since it may be helpful, for instance, to formulate guidelines for the choice of n_F, n_R and n_K in practice, to understand the source of divergence problems, and to devise methodologies for filtering the data (e.g. outlier removal) to enforce convergence properties.

In the following, we confine ourselves, for the sake of the simplicity of the notations, to studying the asymptotic behaviour of the distances accounting only for first-order cylindrical PDFs. The results can readily be generalized to the distances accounting for higher-order cylindrical PDFs. We first elaborate on the case where the vibration test is not disturbed by experimental noise (Sec. 2.4.1), and then deal with the case where it is distorted by noise (Sec. 2.4.2).

2.4.1   Undisturbed vibration test

The asymptotic (as $n_F \to +\infty$ and $n_K \to +\infty$) properties of the distances introduced in Section 2.3.1 for vibration tests carried out under noise-free conditions are here investigated.

Limit as the number n_F of frequencies tends to infinity

Let us assume that the discrete frequencies $\{\omega_\ell \mid 1 \le \ell \le n_F\}$ uniformly sample the frequency band B as $n_F \to +\infty$. Under the regularity condition that the integrand is a continuous function of the frequency, the distances $\mathcal{L}^{(1)}$ and $\mathcal{D}^{(1)}$ then tend towards the following integrals over B:

$$\lim_{n_F \to +\infty} \mathcal{L}_{n_F, n_K}^{(1)} \left(\boldsymbol{p}; \boldsymbol{D}^0 \right) = -\frac{1}{n_K} \sum_{k=1}^{n_K} \frac{1}{|B|} \int_B \log \theta^{(1)} \left(\boldsymbol{h}_k^0(\omega) \big| \omega; \boldsymbol{p} \right) d\omega \quad , \tag{2.47}$$

$$\lim_{n_F \to +\infty} \mathcal{D}_{n_F, n_K}^{(1)} \left(\boldsymbol{p}; \boldsymbol{D}^0 \right) = \frac{1}{|B|} \int_B \mathcal{I} \left(\hat{\xi}_{n_K}^{(1)}(\cdot|\omega; \boldsymbol{D}^0) \big\| \theta^{(1)}(\cdot|\omega; \boldsymbol{p}) \right) d\omega \quad , \tag{2.48}$$

where $|B|$ is the length of the frequency interval B.

Limit as the number n_K of realizations of the random structure tends to infinity

To analyze the large-sample ($n_K \to +\infty$) properties, we use the representation of the observed TF values as realizations of random variables, defined in Section 1.4. The experimental data set $\boldsymbol{D}^0$ is thus considered as a particular realization of a random data set $\mathbb{D}^0$, or, equivalently, as a collection of n_K iid realizations of a data-generating stochastic process $\tilde{\mathbb{D}}^0$ with first-order cylindrical PDF $\xi^{(1)}$. The analysis of the asymptotic ($n_K \to +\infty$) properties of the distances $\mathcal{L}^{(1)}$ and $\mathcal{D}^{(1)}$ then amounts to the study of the

following stochastic limits:

$$\lim_{n_{\mathrm{K}}\to+\infty} \mathcal{L}^{(1)}_{n_{\mathrm{F}},n_{\mathrm{K}}}\left(\boldsymbol{p};\mathbb{D}^0\right) = \lim_{n_{\mathrm{K}}\to+\infty} -\frac{1}{n_{\mathrm{F}}}\sum_{\ell=1}^{n_{\mathrm{F}}}\frac{1}{n_{\mathrm{K}}}\sum_{k=1}^{n_{\mathrm{K}}}\log\theta^{(1)}\left(\mathbb{H}^0_k(\omega_\ell)\big|\omega_\ell;\boldsymbol{p}\right)\quad, \tag{2.49}$$

$$\lim_{n_{\mathrm{K}}\to+\infty} \mathcal{D}^{(1)}_{n_{\mathrm{F}},n_{\mathrm{K}}}\left(\boldsymbol{p};\mathbb{D}^0\right) = \lim_{n_{\mathrm{K}}\to+\infty} \frac{1}{n_{\mathrm{F}}}\sum_{\ell=1}^{n_{\mathrm{F}}}\mathcal{I}\left(\hat{\xi}^{(1)}_{n_{\mathrm{K}}}(\cdot|\omega_\ell;\mathbb{D}^0)\big|\big|\theta^{(1)}(\cdot|\omega_\ell;\boldsymbol{p})\right). \tag{2.50}$$

Let us first analyze the large-sample properties of the distance $\mathcal{L}^{(1)}$. Under the regularity condition that the right-hand side in the following equation is well-defined and remains bounded, it follows from the SLLN that (see also Section 2.1.3):

$$\lim_{n_{\mathrm{K}}\to+\infty} \mathcal{L}^{(1)}_{n_{\mathrm{F}},n_{\mathrm{K}}}\left(\boldsymbol{p};\mathbb{D}^0\right) = \frac{1}{n_{\mathrm{F}}}\sum_{\ell=1}^{n_{\mathrm{F}}}\mathcal{S}\left(\xi^{(1)}(\cdot|\omega_\ell)\right) + \frac{1}{n_{\mathrm{F}}}\sum_{\ell=1}^{n_{\mathrm{F}}}\mathcal{I}\left(\xi^{(1)}(\cdot|\omega_\ell)\big|\big|\theta^{(1)}(\cdot|\omega_\ell;\boldsymbol{p})\right)\ \text{a.s.}\quad, \tag{2.51}$$

where $\mathcal{S}\left(\cdot\right)$ denotes the Shannon entropy (1.37).

Let us now consider the large-sample properties of the inverse method based on distance $\mathcal{L}^{(1)}$. If the average over the frequencies of the distance (in the sense of the relative entropy) between the data-generating PDF $\xi^{(1)}$ and the modelled PDF $\theta^{(1)}(\cdot|\cdot;\boldsymbol{p})$ has a global minimum at

$$\boldsymbol{p}^{\mathcal{L},1}_{n_{\mathrm{F}},\infty} = \arg\min_{\boldsymbol{p}\in P}\frac{1}{n_{\mathrm{F}}}\sum_{\ell=1}^{n_{\mathrm{F}}}\mathcal{I}\left(\xi^{(1)}(\cdot|\omega_\ell)\big|\big|\theta^{(1)}(\cdot|\omega_\ell;\boldsymbol{p})\right)\quad, \tag{2.52}$$

then $\boldsymbol{p}^{\mathcal{L},1}_{n_{\mathrm{F}},\infty}$ is a "pseudo-true" value (Sec. 2.1.3) for this inverse method. Under regularity conditions, it can be shown [Huber, 1967] that, if this "pseudo-true" value exists and is unique, any sequence $\{\hat{\boldsymbol{p}}^{\mathcal{L},1}_{n_{\mathrm{F}},n_{\mathrm{K}}}(\mathbb{D}^0)\mid n_{\mathrm{K}}\in\mathbb{N}\}$ of estimators a.s. converges (as $n_{\mathrm{K}}\to+\infty$) to $\boldsymbol{p}^{\mathcal{L},1}_{n_{\mathrm{F}},\infty}$.

It should be noted that, when the probabilistic structural model is correctly specified and, moreover, identifiable (Sec. 2.1.3), that is to say when there exists a unique "true" value $\boldsymbol{p}^{\mathrm{true}}$, it follows from the convexity of the relative entropy (Box 2.1) that, provided its existence, the "pseudo-true" value $\boldsymbol{p}^{\mathcal{L},1}_{n_{\mathrm{F}},\infty}$ coincides with this "true" value $\boldsymbol{p}^{\mathrm{true}}$. Under the aforementioned list of regularity properties, the inverse method based on $\mathcal{L}^{(1)}$ is then consistent (Sec. 2.1.3) in that any sequence $\{\hat{\boldsymbol{p}}^{\mathcal{L},1}_{n_{\mathrm{F}}n_{\mathrm{K}}}(\mathbb{D}^0)\mid n_{\mathrm{K}}\in\mathbb{N}\}$ of estimators a.s. converges (as $n_{\mathrm{K}}\to+\infty$) to $\boldsymbol{p}^{\mathrm{true}}$.

It seems difficult to establish comparable properties for the distance $\mathcal{D}^{(1)}$. Indeed, even when the employed numerical density estimation method has desirable asymptotic properties ensuring that the estimator $\hat{\xi}^{(1)}_{n_{\mathrm{K}}}(\cdot|\cdot;\mathbb{D}^0)$ converges in some sense to $\xi^{(1)}$, it seems difficult to exploit such properties since the limit and the integral may not simply be interchanged in the right-hand side of the following expression:

$$\lim_{n_{\mathrm{K}}\to+\infty} \mathcal{D}^{(1)}_{n_{\mathrm{F}},n_{\mathrm{K}}}\left(\boldsymbol{p};\mathbb{D}^0\right) = \frac{1}{n_{\mathrm{F}}}\sum_{\ell=1}^{n_{\mathrm{F}}}\lim_{n_{\mathrm{K}}\to+\infty}\int_{\mathbb{C}^{n_{\mathrm{M}}}}\hat{\xi}^{(1)}_{n_{\mathrm{K}}}(\boldsymbol{h}|\omega_\ell;\mathbb{D}^0)\log\frac{\hat{\xi}^{(1)}_{n_{\mathrm{K}}}(\boldsymbol{h}|\omega_\ell;\mathbb{D}^0)}{\theta^{(1)}(\boldsymbol{h}|\omega_\ell;\boldsymbol{p})}d\boldsymbol{h}. \tag{2.53}$$

In the literature, interchanges of limits and integrals are often justified by the Lebesgue dominated convergence theorem [see, for instance, Dudley, 2002, ch. 4 sec. 3]. However, the application of this theorem requires the uniform boundedness of the sequence of integrals. Due to the logarithm in expression (2.53), this requirement is expected to be generally unfulfilled. The asymptotic (as $n_{\mathrm{K}}\to+\infty$) properties of $\mathcal{D}^{(1)}$ remain to us an open problem.

2.4.2 Disturbed vibration test

The asymptotic properties (as $n_{\mathrm{F}}\to+\infty$, $n_{\mathrm{R}}\to+\infty$ and $n_{\mathrm{K}}\to+\infty$) of the distances introduced in Section 2.3.2 for vibration tests carried out under noisy conditions are now considered. To analyze these

asymptotic properties, we use the representation of the observed TF values as realizations of random variables, which was defined in Section 1.4. The experimental data set $\boldsymbol{D}$ is thus viewed as a particular realization of a random data set $\mathbb{D}$. For each tested structure (indexed by k), the data subset $\boldsymbol{D}_k$ is viewed as a particular realization of a stochastic process $\mathbb{D}_k$ with first-order cylindrical PDF $\psi_k^{(1,n_{\rm R})}$, or, equivalently, as a collection of $n_{\rm R}$ iid realizations of a stochastic process $\tilde{\mathbb{D}}_k$ with first-order cylindrical PDF $\psi_k^{(1)}$.

Limit as the number $n_{\rm F}$ of frequencies tends to infinity

The analysis of the asymptotic (as $n_{\rm F} \to +\infty$) properties of the distances $\mathcal{L}^{(1)}$ and $\mathcal{J}^{(1)}$ amounts to the study of the following stochastic limits:

$$\lim_{n_{\rm F} \to +\infty} \mathcal{L}^{(1)}_{n_{\rm F}, n_{\rm K}, n_{\rm R}}(\boldsymbol{p}; \mathbb{D}) = \lim_{n_{\rm F} \to +\infty} -\frac{1}{n_{\rm F}} \sum_{\ell=1}^{n_{\rm F}} \frac{1}{n_{\rm K}} \sum_{k=1}^{n_{\rm K}} \log \varphi_k^{(1,n_{\rm R})} \left(\mathbb{G}_{k1}(\omega_\ell), \ldots, \mathbb{G}_{kn_{\rm R}}(\omega_\ell) \big| \omega_\ell; \boldsymbol{p} \right) \quad , \quad (2.54)$$

$$\lim_{n_{\rm F} \to +\infty} \mathcal{J}^{(1)}_{n_{\rm F}, n_{\rm K}, n_{\rm R}}(\boldsymbol{p}; \mathbb{D}) = \lim_{n_{\rm F} \to +\infty} \frac{1}{n_{\rm F}} \sum_{\ell=1}^{n_{\rm F}} \frac{1}{n_{\rm K}} \sum_{k=1}^{n_{\rm K}} \mathcal{I} \left(\hat{\psi}_{k,n_{\rm R}}^{(1,n_{\rm R})}(\cdot | \omega_\ell; \mathbb{D}_k) \big| \big| \varphi_k^{(1,n_{\rm R})}(\cdot | \omega_\ell; \boldsymbol{p}) \right). \quad (2.55)$$

It seems difficult to establish convergence properties since, even though they have the form of limits of random partial sums, these stochastic limits cannot be analyzed based upon the classical laws of large numbers (for random partial sums made up of independent, or of iid terms) due to the potential dependence of the constituting terms among the frequencies. The asymptotic (as $n_{\rm F} \to +\infty$) properties of $\mathcal{L}^{(1)}$ and $\mathcal{J}^{(1)}$ remain to us an open problem.

Limit as the number $n_{\rm R}$ of repetitions tends to infinity

The analysis of the large-sample ($n_{\rm R} \to +\infty$) properties of the distance $\mathcal{L}^{(1)}$ amounts to the study of the following stochastic limit (with reference to equation (1.148)):

$$\lim_{n_{\rm R} \to +\infty} \mathcal{L}^{(1)}_{n_{\rm F}, n_{\rm K}, n_{\rm R}}(\boldsymbol{p}; \mathbb{D}) = \lim_{n_{\rm R} \to +\infty} -\frac{1}{n_{\rm F}} \sum_{\ell=1}^{n_{\rm F}} \frac{1}{n_{\rm K}} \sum_{k=1}^{n_{\rm K}} \log \int_{\mathbb{C}^{n_{\rm M}}} \theta^{(1)} \left(\boldsymbol{h} \big| \omega_\ell; \boldsymbol{p} \right) \prod_{r=1}^{n_{\rm R}} \rho_k^{(1)} \left(\mathbb{G}_{kr}(\omega_\ell) \big| \omega_\ell; \boldsymbol{h} \right) d\boldsymbol{h}.$$

$$(2.56)$$

For each tested structure (indexed by k) and frequency ω_ℓ, the Bayesian posterior PDF $\pi_{k,n_{\rm R}}^{(1)}(\cdot | \omega_\ell; \mathbb{D}_k)$: $\mathbb{C}^{n_{\rm M}} \to \mathbb{R}^+$ (Sec. 2.1.1) is defined by:

$$\pi_{k,n_{\rm R}}^{(1)}(\boldsymbol{h} | \omega_\ell; \mathbb{D}_k) = c_{k,n_{\rm R}}(\omega_\ell) \pi^{(1)}(\boldsymbol{h}) \prod_{r=1}^{n_{\rm R}} \rho_k^{(1)} \left(\mathbb{G}_{kr}(\omega_\ell) \big| \omega_\ell; \boldsymbol{h} \right) \quad , \quad (2.57)$$

where $c_{k,n_{\rm R}}(\omega_\ell)$ is the normalization constant and $\pi^{(1)} : \mathbb{C}^{n_{\rm M}} \to \mathbb{R}^+$ is a Bayesian prior PDF, chosen equal to the improper (i.e. non-normalizable) uniform PDF $\pi^{(1)}(\boldsymbol{h}) = \mathbb{1}_{\mathbb{C}^{n_{\rm M}}}(\boldsymbol{h})$. If the distance (in the sense of the relative entropy) at the frequency ω_ℓ between the data-generating PDF $\psi_k^{(1)}$ and the modelled PDF $\rho_k^{(1)}(\cdot | \cdot; \boldsymbol{h})$ attains a unique global minimum at

$$\boldsymbol{h}_{k,\infty}^{\rm ML}(\omega_\ell) = \arg \min_{\boldsymbol{h} \in \mathbb{C}^{n_{\rm M}}} \mathcal{I} \left(\psi_k^{(1)}(\cdot | \omega_\ell) \big| \big| \rho_k^{(1)}(\cdot | \omega_\ell; \boldsymbol{h}) \right) \quad , \quad (2.58)$$

it can be shown [see, for instance, Bunke and Milhaud, 1998] that, under a list of regularity conditions, the Bayesian posterior PDF concentrates (as $n_{\rm R} \to +\infty$) on this mimimum, i.e.:

$$\lim_{n_{\rm R} \to +\infty} \pi_{k,n_{\rm R}}^{(1)}(\boldsymbol{h} | \omega_\ell; \mathbb{D}_k) = \delta \left(\boldsymbol{h} - \boldsymbol{h}_{k,\infty}^{\rm ML}(\omega_\ell) \right) \text{ (weakly) a.s.} \quad , \quad (2.59)$$

where δ is the Dirac distribution. Hence, under the regularity condition that the PDF $\theta^{(1)}$ is continuous and remains bounded, it follows from (2.57) and (2.59) that:

$$\lim_{n_R \to +\infty} \mathcal{L}^{(1)}_{n_F,n_K,n_R}(\boldsymbol{p}; \mathbb{D}) = \mathcal{L}^{(1)}_{n_F,n_K,\infty} - \frac{1}{n_F} \sum_{\ell=1}^{n_F} \frac{1}{n_K} \sum_{k=1}^{n_K} \log \theta^{(1)} \left(\boldsymbol{h}^{\mathrm{ML}}_{k,\infty}(\omega_\ell) \big| \omega_\ell; \boldsymbol{p} \right) \text{ a.s. } , \qquad (2.60)$$

where $\mathcal{L}^{(1)}_{n_F,n_K,\infty}$ is a parameter-independent (possibly infinite) constant. This result means that the distance, in the sense of the objective function $\mathcal{L}^{(1)}$ defined in (2.40), between the noisy experimental data set and the probabilistic model converges (as $n_R \to +\infty$) to the distance, in the sense of the objective function $\mathcal{L}^{(1)}$ defined in (2.31), between the estimate of the corresponding noise-free data set defined by (2.58) and the probabilistic model (up to a constant). This result constitutes a point of similarity between the two approaches for dealing with the experimental noise, which were introduced in Section 2.3.2. In particular, the inverse method involving the minimization of the distance $\mathcal{L}^{(1)}$ defined in (2.40), which was categorized under the heading "noise modelling", is asymptotically also an inverse method of "noise filtering" type. Finally, it should be noted that, when the probabilistic model for the experimental noise correctly represents the fluctuations of the observed TFs around the noise-free TFs due to the noise, it follows from the convexity of the relative entropy (Box 2.1) that, provided its existence, the value $\boldsymbol{h}^{\mathrm{ML}}_{k,\infty}(\omega_\ell)$ coincides with the noise-free TF value $\boldsymbol{h}^0_k(\omega_\ell)$. However, this property is most often false when the probabilistic model for the experimental noise is incorrect.

As in Section 2.4, it seems difficult to establish comparable properties for the distance $\mathcal{J}^{(1)}$, since the limit and the integrals related to the relative entropies may not be interchangeable. The large-sample ($n_R \to +\infty$) properties of $\mathcal{J}^{(1)}$ therefore remain to us an open problem.

Limit as the number n_K of realizations of the random structure tends to infinity

The analysis of the large-sample ($n_K \to +\infty$) properties of the distances $\mathcal{L}^{(1)}$ and $\mathcal{J}^{(1)}$ amounts to the study of the following stochastic limits:

$$\lim_{n_K \to +\infty} \mathcal{L}^{(1)}_{n_F,n_K,n_R}(\boldsymbol{p}; \mathbb{D}) = \lim_{n_K \to +\infty} -\frac{1}{n_F} \sum_{\ell=1}^{n_F} \frac{1}{n_K} \sum_{k=1}^{n_K} \log \varphi_k^{(1,n_R)} \left(\mathbb{G}_{k1}(\omega_\ell), \ldots, \mathbb{G}_{kn_R}(\omega_\ell) \big| \omega_\ell; \boldsymbol{p} \right) , \qquad (2.61)$$

$$\lim_{n_K \to +\infty} \mathcal{J}^{(1)}_{n_F,n_K,n_R}(\boldsymbol{p}; \mathbb{D}) = \lim_{n_K \to +\infty} \frac{1}{n_F} \sum_{\ell=1}^{n_F} \frac{1}{n_K} \sum_{k=1}^{n_K} \mathcal{I} \left(\hat{\psi}^{(1,n_R)}_{k,n_R}(\cdot|\omega_\ell; \mathbb{D}_k) \big\| \varphi_k^{(1,n_R)}(\cdot|\omega_\ell; \boldsymbol{p}) \right). \qquad (2.62)$$

Unlike the limits (2.54)-(2.55), these limits can be analyzed based upon the classical laws of large numbers in view of the hypothesis (Sec. 1.4) of mutual independence among the observed TFs for distinct tested structures. Under the regularity condition that the constituting terms of the random partial sums in (2.61)-(2.62) are of the second order and, moreover, that the expectation values in the following expressions exist, it follows from the SLLN that:

$$\lim_{n_K \to +\infty} \left(\mathcal{L}^{(1)}_{n_F,n_K,n_R}(\boldsymbol{p}; \mathbb{D}) - E\left\{ \mathcal{L}^{(1)}_{n_F,n_K,n_R}(\boldsymbol{p}; \mathbb{D}) \right\} \right) = 0 \text{ a.s. } , \qquad (2.63)$$

$$\lim_{n_K \to +\infty} \left(\mathcal{J}^{(1)}_{n_F,n_K,n_R}(\boldsymbol{p}; \mathbb{D}) - E\left\{ \mathcal{J}^{(1)}_{n_F,n_K,n_R}(\boldsymbol{p}; \mathbb{D}) \right\} \right) = 0 \text{ a.s. } \qquad (2.64)$$

2.5 Numerical approximation

Basic algorithms for the practical computation of the distances defined in Section 2.3 are now proposed. For the sake of notational simplicity, only the distances accounting for first-order cylindrical PDFs are

considered. The algorithms can readily be generalized to the distances accounting for higher-order cylindrical PDFs. We first elaborate on the case where the vibration test is not disturbed by experimental noise (Sec. 2.5.1), and then deal with the case where it is distorted by noise (Sec. 2.5.2).

2.5.1 Undisturbed vibration test

Algorithms 6 and 7 detail the computation of the distances introduced in Section 2.3.1.

Algorithm 6: computation of the distance $\mathcal{L}^{(1)}$

- **Step 1: initialization:**
  Get the experimental data set $\boldsymbol{D}^0$, having the form (1.125)-(1.126).
  Get the probabilistic structural model, built as outlined in Section 1.1.

- **Step 2: computation with the probabilistic model:**
  Follow algorithm 5 (Sec. 1.4) to obtain the following set of iid samples of the random TFs predicted by the probabilistic model:

$$\{\mathbb{H}_{\mathrm{h}}(\omega_\ell; a_s; \boldsymbol{p}) \mid 1 \le \ell \le n_{\mathrm{F}} \, , \, 1 \le s \le n_{\mathrm{S}}\}. \tag{2.65}$$

- **Step 3: numerical approximation of the distance:**
  For each $k \in \{1 \le k \le n_{\mathrm{K}}\}$ and $\ell \in \{1 \le \ell \le n_{\mathrm{F}}\}$, apply a density estimation method (Sec. 2.5.3) to obtain, from the samples $\{\mathbb{H}_{\mathrm{h}}(\omega_\ell; a_s; \boldsymbol{p}) \mid 1 \le s \le n_{\mathrm{S}}\}$, an estimate

$$\hat{\theta}^{(1)} \left(\boldsymbol{h}_k^0(\omega_\ell) \middle| \omega_\ell; \boldsymbol{p} \right) \tag{2.66}$$

  of the value taken by the PDF $\theta^{(1)}(\cdot | \omega_\ell; \boldsymbol{p})$ at the observed TF value $\boldsymbol{h}_k^0(\omega_\ell)$.

  Calculate the distance as follows:

$$\mathcal{L}_{n_{\mathrm{F}}, n_{\mathrm{K}}}^{(1)} \left(\boldsymbol{p}; \boldsymbol{D}^0 \right) \simeq -\frac{1}{n_{\mathrm{F}}} \sum_{\ell=1}^{n_{\mathrm{F}}} \frac{1}{n_{\mathrm{K}}} \sum_{k=1}^{n_{\mathrm{K}}} \log \hat{\theta}^{(1)} \left(\boldsymbol{h}_k^0(\omega_\ell) \middle| \omega_\ell; \boldsymbol{p} \right). \tag{2.67}$$

Algorithm 7: computation of the distance $\mathcal{D}^{(1)}$

- **Step 1: initialization:**
  Choose a number n_{J} of Monte Carlo samples.
  Get the experimental data set $\boldsymbol{D}^0$, having the form (1.125)-(1.126).
  Get the probabilistic structural model, built as outlined in Section 1.1.

- **Step 2: computation with the probabilistic model:**
  Follow algorithm 5 (Sec. 1.4) to obtain the following set of iid samples of the random TFs predicted by the probabilistic model:

$$\{\mathbb{H}_{\mathrm{h}}(\omega_\ell; a_s; \boldsymbol{p}) \mid 1 \le \ell \le n_{\mathrm{F}} \, , \, 1 \le s \le n_{\mathrm{S}}\}. \tag{2.68}$$

- **Step 3: numerical approximation of the distance:**
  Step 3a: simulation of samples from $\hat{\xi}^{(1)}$:

For each $\ell \in \{1 \leq \ell \leq n_\text{F}\}$, apply a density estimation method (Sec. 2.5.3) to obtain, from the samples $\{\boldsymbol{h}_k^0(\omega_\ell) \mid 1 \leq k \leq n_\text{K}\}$, an estimate $\hat{\xi}^{(1)}(\cdot|\omega_\ell)$ of the PDF of the noise-free TF values at the frequency ω_ℓ. Subsequently, simulate (Sec. 2.5.3) a set $\{\hat{\mathbb{H}}^0(\omega_\ell; a_j) \mid 1 \leq j \leq n_\text{J}\}$ of n_J iid samples of a random variable $\hat{\mathbb{H}}^0(\omega_\ell)$ admitting this PDF $\hat{\xi}^{(1)}(\cdot|\omega_\ell)$.

Gather the iid samples obtained by this procedure in the set

$$\{\hat{\mathbb{H}}^0(\omega_\ell; a_j) \mid 1 \leq \ell \leq n_\text{F} \,,\ 1 \leq j \leq n_\text{J}\}. \tag{2.69}$$

Step 3b: calculation of the distance:
For each $j \in \{1 \leq j \leq n_\text{J}\}$ and $\ell \in \{1 \leq \ell \leq n_\text{F}\}$, apply a density estimation method to obtain, from the samples $\{\mathbb{H}_\text{h}(\omega_\ell; a_s; \boldsymbol{p}) \mid 1 \leq s \leq n_\text{S}\}$, an estimate

$$\hat{\theta}^{(1)}\left(\hat{\mathbb{H}}^0(\omega_\ell; a_j)\big|\omega_\ell; \boldsymbol{p}\right) \tag{2.70}$$

of the value taken by the PDF $\theta^{(1)}(\cdot|\omega_\ell; \boldsymbol{p})$ at $\hat{\mathbb{H}}^0(\omega_\ell; a_j)$.

Calculate the distance by Monte Carlo integration as follows:

$$\mathcal{D}_{n_\text{F}, n_\text{K}}^{(1)}\left(\boldsymbol{p}; \boldsymbol{D}^0\right) \simeq \frac{1}{n_\text{F}} \sum_{\ell=1}^{n_\text{F}} \frac{1}{n_\text{J}} \sum_{j=1}^{n_\text{J}} \log \frac{\hat{\xi}^{(1)}\left(\hat{\mathbb{H}}^0(\omega_\ell; a_j)\big|\omega_\ell\right)}{\hat{\theta}^{(1)}\left(\hat{\mathbb{H}}^0(\omega_\ell; a_j)\big|\omega_\ell; \boldsymbol{p}\right)}. \tag{2.71}$$

2.5.2 Disturbed vibration test

Algorithms 8 and 9 detail the computation of the distances introduced in Section 2.3.2.

Algorithm 8: computation of the distance $\mathcal{L}^{(1)}$

- **Step 1: initialization:**
  Get the experimental data set $\boldsymbol{D}$, having the form (1.124)-(1.123).
  Get the probabilistic structural model, built as outlined in Section 1.1.

- **Step 2: construction of the probabilistic model for the experimental noise:**
  Build the probabilistic model for the experimental noise as outlined in Section 1.4:

  Step 2a: identification of the probabilistic model for the experimental noise:
  For each $\ell \in \{1 \leq \ell \leq n_\text{F}\}$ and $k \in \{1 \leq k \leq n_\text{K}\}$, use expressions (1.142)-(1.143) to estimate the covariance matrix $\widehat{\boldsymbol{C}}_k(\omega_\ell)$.

  Gather the covariance matrices obtained by this procedure in the set

  $$\{\widehat{\boldsymbol{C}}_k(\omega_\ell) \mid 1 \leq \ell \leq n_\text{F} \,,\ 1 \leq k \leq n_\text{K}\}. \tag{2.72}$$

  Step 2b: construction of the first-order cylindrical PDFs:
  For each $\ell \in \{1 \leq \ell \leq n_\text{F}\}$ and $k \in \{1 \leq k \leq n_\text{K}\}$, use equations (1.149) and (1.160) to obtain the following analytical expression for the PDF $\rho_k^{(1)}(\cdot|\omega_\ell; \cdot)$:

  $$\rho_k^{(1)}(\boldsymbol{g}|\omega_\ell; \boldsymbol{h}) = \frac{1}{\pi^n \det(\widehat{\boldsymbol{C}}_k(\omega_\ell))} \exp\left(-\left(\widehat{\boldsymbol{C}}_k(\omega_\ell)^{-1}(\boldsymbol{g} - \boldsymbol{h}), \overline{(\boldsymbol{g} - \boldsymbol{h})}\right)\right). \tag{2.73}$$

- **Step 3: computation with the probabilistic structural model:**
Follow algorithm 5 (Sec. 1.4) to obtain the following set of iid samples of the random TFs predicted by the probabilistic structural model:

$$\{\mathbb{H}_h(\omega_\ell; a_s; \boldsymbol{p}) \mid 1 \leq \ell \leq n_F \,, \; 1 \leq s \leq n_S\}. \tag{2.74}$$

- **Step 4: numerical approximation of the distance:**
Using (2.73), calculate the distance by Monte Carlo integration as follows:

$$\mathcal{L}_{n_F, n_K, n_R}^{(1)}(\boldsymbol{p}; \boldsymbol{D}) \simeq -\frac{1}{n_F} \sum_{\ell=1}^{n_F} \frac{1}{n_K} \sum_{k=1}^{n_K} \log \frac{1}{n_S} \sum_{s=1}^{n_S} \prod_{r=1}^{n_R} \rho_k^{(1)}\big(\boldsymbol{g}_{kr}^{\mathrm{obs}}(\omega_\ell) \big| \omega_\ell; \mathbb{H}_h(\omega_\ell; a_s; \boldsymbol{p})\big). \tag{2.75}$$

Algorithm 9: computation of the distance $\mathcal{J}^{(1)}$

- **Step 1: initialization:**
Choose a number n_J of Monte Carlo samples.
Get the experimental data set $\boldsymbol{D}$, having the form (1.124)-(1.123).
Get the probabilistic structural model, built as outlined in Section 1.1.

- **Step 2: construction of the probabilistic model for the experimental noise:**
Follow step 2 of algorithm 8 to obtain the following set of covariance matrices:

$$\{\widehat{\boldsymbol{C}}_k(\omega_\ell) \mid 1 \leq \ell \leq n_F \,, \; 1 \leq k \leq n_K\}. \tag{2.76}$$

- **Step 3: computation with the probabilistic structural model:**
Follow algorithm 5 (Sec. 1.4) to obtain the following set of iid samples of the random TFs predicted by the probabilistic structural model:

$$\{\mathbb{H}_h(\omega_\ell; a_s; \boldsymbol{p}) \mid 1 \leq \ell \leq n_F \,, \; 1 \leq s \leq n_S\}. \tag{2.77}$$

- **Step 4: numerical approximation of the distance:**
Step 4a: simulation of samples from $\hat{\psi}_k^{(1)}$:
For each $\ell \in \{1 \leq \ell \leq n_F\}$ and $k \in \{1 \leq k \leq n_K\}$, apply a density estimation method (Sec. 2.5.3) to obtain, from the samples $\{\boldsymbol{g}_{k1}^{\mathrm{obs}}(\omega_\ell), \ldots, \boldsymbol{g}_{kn_R}^{\mathrm{obs}}(\omega_\ell)\}$, an estimate $\hat{\psi}_k^{(1)}(\cdot|\omega_\ell)$ of the PDF of the noisy TF values for the k-th structure at the frequency ω_ℓ. Subsequently, simulate (Sec. 2.5.3) a set $\{\hat{\mathbb{G}}_k(\omega_\ell; a_{rj}) \mid 1 \leq r \leq n_R \,, \; 1 \leq j \leq n_J\}$ of $n_R \times n_J$ iid samples of a random variable $\hat{\mathbb{G}}_k(\omega_\ell)$ admitting this PDF $\hat{\psi}_k^{(1)}$.

Gather the iid samples obtained by this procedure in the set

$$\{\hat{\mathbb{G}}_k(\omega_\ell; a_{rj}) \mid 1 \leq \ell \leq n_F \,, \; 1 \leq r \leq n_R \,, \; 1 \leq j \leq n_J\}. \tag{2.78}$$

Step 4b: calculation of the distance:
Using (2.73), calculate the distance by Monte Carlo integration as follows:

$$\mathcal{J}_{n_F, n_K, n_R}^{(1)}(\boldsymbol{p}; \boldsymbol{D}) \simeq \frac{1}{n_F} \sum_{\ell=1}^{n_F} \frac{1}{n_K} \sum_{k=1}^{n_K} \frac{1}{n_J} \sum_{j=1}^{n_J} \log \frac{\prod_{r=1}^{n_R} \hat{\psi}_k^{(1)}\big(\hat{\mathbb{G}}_k(\omega_\ell; a_{rj}) \big| \omega_\ell\big)}{\frac{1}{n_S} \sum_{s=1}^{n_S} \prod_{r=1}^{n_R} \rho_k^{(1)}\big(\hat{\mathbb{G}}_k(\omega_\ell; a_{rj}) \big| \omega_\ell; \mathbb{H}_h(\omega_\ell; a_s; \boldsymbol{p})\big)}. \tag{2.79}$$

2.5.3   Bibliography on the numerical methods used in algorithms 6 to 9

For completeness, references in the literature for more details on density estimation methods, random variable simulation methods and global-search optimization methods are provided below.

Density estimation methods

Algorithms 6, 7 and 9 require the estimation of PDFs from sets of samples. We refer the reader to [Scott, 1992] for an overview of the methods that were proposed in the literature for the estimation of densities. We suggest applying the kernel density estimation method [see, for instance, Parzen, 1962, Rosenblatt, 1956, Scott, 1992].

Methods for the simulation of non-uniform random variables

Algorithms 7 and 9 necessitate in the respective step 3a and 4a to simulate samples of a random variable with a given PDF. We refer the reader to [Robert and Casella, 2005] for an overview of the methods that were proposed in the literature for the simulation of non-uniform random variables. In some cases, it may be possible to determine analytically an appropriate transformation, which maps a multivariate random variable with mutually-independent uniform components onto the random variable to be simulated. Samples of the non-uniform random variable can then be obtained by transforming samples of the uniform random variable. When it is difficult to find such a transformation, we suggest applying the Monte Carlo Markov Chain method to obtain the required samples [see, for instance, Gamerman, 1997, Hastings, 1970, Metropolis et al., 1953, Robert and Casella, 2005].

Global-search optimization methods

Let us now consider the optimization problems (2.34), (2.38), (2.42) and (2.46). When only few parameters must be identified (i.e. the dimension of the parameter space is three or less), we suggest solving the optimization problem by an exhaustive grid-search. When the set of parameters is larger, it may be more efficient to apply a numerical optimization algorithm. Considering that the distances to be minimized may have multiple local minima and that it may be difficult to accurately calculate gradients with respect to the parameters, we suggest applying a global-search gradient-free optimization method, such as simulated annealing method based upon the Metropolis-Hastings algorithm [see, for instance, Kirkpatrick et al., 1983, Metropolis et al., 1953, Robert and Casella, 2005], or the genetic optimization method [see, for instance, Fogel, 1995, Goldberg, 1989].

2.6   Epistemic uncertainty quantification

In sections 2.1 and 2.2, the general difficulties that may arise in the application of the classical theory of mathematical statistics to the experimental identification of probabilistic structural models were described. Having in mind the goal of formulating this identification alternatively as the minimization of an objective function that measures the distance between the experimental data and the probabilistic model, we considered in sections 2.3-2.5 the general definition and computation of this distance. With these results available, we are now in a position to address the central concern of this dissertation, namely to propose a practical methodology for the inversion of probabilistic structural models, which allows

circumventing the aforementioned difficulties. This section is devoted to stochastic inverse problems aimed at quantifying epistemic uncertainty, stochastic inverse problems aimed at quantifying aleatory uncertainty being deferred to Section 2.7.

2.6.1 Problem setting

Let us consider a general situation where a *single* real structure is under study. As discussed in the general introduction, parameter uncertainty may arise, and modelling errors may be introduced, when modelling the dynamical behaviour of this real structure.

Let the generic vibration test (Sec. 1.3) be carried out on the structure under study, either under noise-free conditions to obtain an experimental data set of the form (1.125)-(1.126), or under noisy conditions to obtain a data set of the form (1.124)-(1.123). Furthermore, let either a non-parametric, or a parametric probabilistic model for the dynamical behaviour of the structure (Sec. 1.1) be built. Let this model be used (Sec. 1.4) to model the vibration test to obtain a stochastic process $\{\mathbb{H}(\omega_\ell; \boldsymbol{p}) \mid 1 \leq \ell \leq n_\mathrm{F}\}$, with n-th order cylindrical PDF $\theta^{(n)}(\cdot | \cdot ; \boldsymbol{p})$. This section then concerns the experimental identification of the parameters $\boldsymbol{p}$ so as to quantify the (epistemic) uncertainty in the predictions, which results from parameter uncertainty and modelling errors.

With reference to sections 2.1 and 2.2, let us summarize the main difficulties that should be considered when developing methods for solving this stochastic inverse problem:

1. When the solution method necessitates the numerical approximation of high-dimensional PDFs, the associated computational cost may be prohibitive.

2. Since only a single structure is under study, there is no data-generating PDF such that the difficulty of the potential misspecification of the probabilistic model does not apply. Nevertheless, the probabilistic model can be incompatible with the experimental data.

3. Upon formulating the inverse problem as the minimization of an objective function measuring the distance between the probabilistic model and the experimental data, that model will be identified which fits the experimental data best *in the sense of the chosen objective function*. The application of distinct objective functions is generally expected to lead to the identification of distinct probabilistic models. For this reason, there is a need for a criterion to choose the "most adequate" objective function leading to the identification of the "most adequate" probabilistic model.

2.6.2 Proposed solution methodology

In this subsection, we propose to formulate the stochastic inverse problem as the minimization of a distance (Sec. 2.3-2.5) taking only first-order cylindrical PDFs into account. In the following, we show how this formulation allows us to overcome the aforementioned difficulties.

Computational cost

As described in Section 2.5, the computation of the proposed distances requires the numerical approximation of PDFs and/or integrals, whose dimension is proportional to the order of the cylindrical PDFs that are taken into account. For this reason, the computational cost of the solution method can generally be lowered by formulating the stochastic inverse problem as the minimization of a distance taking only low-order cylindrical PDFs into account.

(In)compatibility of the probabilistic model and the experimental data

In Section 2.2, the potential incompatibility of the probabilistic structural model with the experimental data was studied in the particular case where the non-parametric approach is adopted to build the probabilistic model and the vibration test is undisturbed by experimental noise. Let us now proceed further in this case study.

The probabilistic model was defined to be compatible with the experimental data if the observed TFs belong to the support of the n_{F}-th order cylindrical PDF $\theta^{(n_{\mathrm{F}})}(\cdot|\cdot;\boldsymbol{p})$. Furthermore, this condition was found to be equivalent to requiring that the observed TFs are representable in terms of a triple of reduced matrices, that is to say to requiring the existence of a triple of reduced matrices for which the deterministic reduced matrix model reproduces the observed TF values *concurrently at all discrete frequencies*, i.e.:

$$\exists \boldsymbol{K}, \boldsymbol{D}, \boldsymbol{M} \in \mathrm{M}_{n_{\mathrm{T}}}^{+}(\mathbb{R}) \; : \; \forall \omega_\ell \; : \; \boldsymbol{h}^0(\omega_\ell) = \boldsymbol{h}(\omega_\ell; \boldsymbol{K}, \boldsymbol{D}, \boldsymbol{M}). \tag{2.80}$$

Let us now examine the compatibility of the lower-order cylindrical PDFs with the experimental data in the same way. We define the first-order cylindrical PDFs to be compatible with the experimental data if, for each discrete frequency ω_ℓ, the observed TF value $\boldsymbol{h}^0(\omega_\ell)$ belongs to the support of the first-order cylindrical PDF $\theta^{(1)}(\cdot|\omega_\ell;\boldsymbol{p})$ at that frequency. In the line of Section 2.2, this condition is equivalent to requiring that, *at each discrete frequency ω_ℓ separately*, there exists a triple of reduced matrices for which the deterministic reduced matrix model reproduces the observed TF value at that frequency, i.e.:

$$\forall \omega_\ell \; : \; \exists \boldsymbol{K}, \boldsymbol{D}, \boldsymbol{M} \in \mathrm{M}_{n_{\mathrm{T}}}^{+}(\mathbb{R}) \; : \; \boldsymbol{h}^0(\omega_\ell) = \boldsymbol{h}(\omega_\ell; \boldsymbol{K}, \boldsymbol{D}, \boldsymbol{M}). \tag{2.81}$$

More generally, we define the n-th order cylindrical PDFs to be compatible with the experimental data if, for each n-subset $(\omega_{\ell_1}, \ldots, \omega_{\ell_n})$ of discrete frequencies in $B_{n_{\mathrm{F}}}^n$ (Sec. 2.3.1), the observed TF values $(\boldsymbol{h}^0(\omega_{\ell_1}), \ldots, \boldsymbol{h}^0(\omega_{\ell_n}))$ belong to the support of the n-th order cylindrical PDF $\theta^{(n)}(\cdot|\omega_{\ell_1}, \ldots, \omega_{\ell_n};\boldsymbol{p})$ at those frequencies. This condition is equivalent to requiring that:

$$\forall (\omega_{\ell_1}, \ldots, \omega_{\ell_n}) \in B_{n_{\mathrm{F}}}^n \; : \; \exists \boldsymbol{K}, \boldsymbol{D}, \boldsymbol{M} \in \mathrm{M}_{n_{\mathrm{T}}}^{+}(\mathbb{R}) : \tag{2.82}$$
$$\boldsymbol{h}^0(\omega_{\ell_1}) = \boldsymbol{h}(\omega_{\ell_1}; \boldsymbol{K}, \boldsymbol{D}, \boldsymbol{M}), \; \ldots, \; \boldsymbol{h}^0(\omega_{\ell_n}) = \boldsymbol{h}(\omega_{\ell_n}; \boldsymbol{K}, \boldsymbol{D}, \boldsymbol{M}).$$

The expression (2.82) represents for $n < n_{\mathrm{F}}$ a weaker condition imposed jointly on the probabilistic model and the experimental data than (2.80). In other words, the low-order cylindrical PDFs can be compatible with the experimental data, even when the n_{F}-th order cylindrical PDF is incompatible with the experimental data. This consideration suggests that the risk of encountering incompatibility problems can be reduced by formulating the stochastic inverse problem as the minimization of a distance taking only low-order cylindrical PDFs into account.

Adequacy of the objective function

As discussed in the general introduction, the ways in which a probabilistic structural model can represent epistemic uncertainty are a controversial topic. Nevertheless, in our opinion, it is absolutely necessary to define the intended use of the probabilistic model before embarking on its experimental identification. Among different viable inverse methods, the one which is expected to lead to the identification of a model that is adequate for the intended use can then be selected.

Let this discussion concentrate on the case where the intended use consists in predicting frequency-dependent confidence regions (see Box 2.3). More precisely, we define the aim of the inverse method as identifying the probabilistic model such that, upon using the identified model to forecast a TF of

the real structure, a frequency-dependent confidence region associated with a high probability level for the predicted random TF can adequately be viewed as a region within which the actual TF of the real structure lies.

Let us first consider the case where the vibration test is carried out under noise-free conditions. In view of the above-defined intended predictive use, it seems reasonable to attempt to identify the probabilistic model such that, upon using the identified model to forecast the observed TFs, the observed TF values lie within the confidence bounds for the predicted random TF values. With that goal in mind, we propose to identify the parameters $\boldsymbol{p}$ by minimization of the distance $\mathcal{L}^{(1)}$ defined in (2.31), which only accounts for first-order cylindrical PDFs, i.e.:

$$\hat{\boldsymbol{p}}_{n_{\mathrm{F}}}^{\mathcal{L},1}(\boldsymbol{D}^0) = \arg \min_{\boldsymbol{p}} \frac{-1}{n_{\mathrm{F}}} \sum_{\ell=1}^{n_{\mathrm{F}}} \log \theta^{(1)} \left(\boldsymbol{h}^0(\omega_\ell) \big| \omega_\ell; \boldsymbol{p} \right) . \tag{2.83}$$

When at a fixed frequency ω_ℓ the PDF $\theta^{(1)}(\cdot|\omega_\ell; \boldsymbol{p})$ has a large value at $\boldsymbol{h}^0(\omega_\ell)$, it can reasonably be expected that these observed TF values lie within the confidence bounds for the corresponding predicted random TF values at that frequency. Hence, since the logarithm in expression (2.83) strongly penalizes probabilistic models for which there are frequencies at which $\theta^{(1)}(\boldsymbol{h}^0(\omega_\ell)|\omega_\ell; \boldsymbol{p})$ is small, the inverse method (2.83) can reasonably be expected to lead to the identification of a probabilistic model for which the observed TF values lie within the predicted confidence bounds. When the vibration test is carried out under noisy conditions, we propose, correspondingly, to identify the parameters that minimize either the distance $\mathcal{L}^{(1)}$, defined in (2.40), or the distance $\mathcal{J}^{(1)}$, defined in (2.44).

It should be stressed that the identification of a probabilistic model by the minimization of a distance that only accounts for first-order cylindrical PDFs limits, in our judgement, the predictive capability of the identified model to predictions at separate frequencies. When the intended use of the identified model is to make predictions that rely on a suitably modelled frequency dependence, the use of a distance of this kind is inadequate and higher-order cylindrical PDFs must be accounted for. For example, time-domain predictions are sensitive to the separation between, and the width of, resonance peaks. Such cases are not addressed further in this dissertation.

Box 2.3. Frequency-dependent confidence regions

This box presents a methodology, also used in [Soize and Bjauoui, 2000], for constructing confidence regions for random TFs using the Chebychev inequality.

Let the stochastic process $\{\mathbb{X}(\omega) \mid \omega \in B\}$ defined on $(\mathcal{A}, \mathcal{F}, P)$, indexed by a frequency band B and with values in $\mathbb{C}$ a.s. be a random TF predicted by a probabilistic model. A confidence region associated with a given probability level P_c for the value taken by this random TF at a fixed frequency ω on a logarithmic scale is then defined as a pair of bounds $(dB^-(\omega), dB^+(\omega))$ such that:

$$P\left(dB^-(\omega) < d\mathbb{B}(\omega) < dB^+(\omega)\right) \geq P_c \quad, \tag{2.84}$$

where:

$$d\mathbb{B}(\omega) = \frac{20}{\log 10} \log \left(\frac{|\mathbb{X}(\omega)|}{X^{\mathrm{ref}}} \right) \text{ a.s.} \quad, \tag{2.85}$$

in which X^{ref} is a reference value, equal to 1m/N, 1mHz/N or 1mHz^2/N depending on whether $\mathbb{X}(\omega)$ is a compliance (i.e. a displacement over a force), a mobility (i.e. a velocity over a

force) or an inertance (i.e. an acceleration over a force), respectively. These confidence bounds can be built using the Chebychev equation as follows:

$$dB^+(\omega) = \frac{20}{\log 10} \log \left(\frac{|E\{\mathbb{X}(\omega)\}| + a(\omega)}{X^{\mathrm{ref}}} \right) \quad , \tag{2.86}$$

$$dB^0(\omega) = \frac{20}{\log 10} \log \left(\frac{|E\{\mathbb{X}(\omega)\}|}{X^{\mathrm{ref}}} \right) \quad , \tag{2.87}$$

$$dB^-(\omega) = 2dB^0(\omega) - dB^+(\omega) \quad , \tag{2.88}$$

where:

$$a(\omega)^2 = \frac{E\{|\mathbb{X}(\omega) - E\{\mathbb{X}(\omega)\}|^2\}}{(1 - P_c)}. \tag{2.89}$$

2.6.3 Second-order interpretation of the distances

We employ here Gaussian approximations to examine in more detail the distances accounting only for first-order cylindrical PDFs. With reference to Section 1.4, let the PDFs $\theta^{(1)}(\cdot|\cdot;\boldsymbol{p})$, $\rho^{(1)}$ and $\hat{\psi}_{n_{\mathrm{R}}}^{(1)}(\cdot|\cdot;\boldsymbol{D})$ be such that:

$$\theta^{(1)}(\boldsymbol{h}|\omega;\boldsymbol{p}) = N^{\mathrm{c}} \left(\boldsymbol{h}|\boldsymbol{\mu}^{\mathrm{mod}}(\omega;\boldsymbol{p}), \boldsymbol{C}^{\mathrm{mod}}(\omega;\boldsymbol{p}) \right) \quad , \tag{2.90}$$

$$\rho^{(1)}(\boldsymbol{g}|\omega_\ell;\boldsymbol{h}) = N^{\mathrm{c}} \left(\boldsymbol{g}|\boldsymbol{h}, \boldsymbol{C}^{\mathrm{obs}}(\omega_\ell) \right) \quad , \tag{2.91}$$

$$\hat{\psi}_{n_{\mathrm{R}}}^{(1)}(\boldsymbol{g}|\omega_\ell;\boldsymbol{D}) = N^{\mathrm{c}} \left(\boldsymbol{g}|\boldsymbol{\mu}^{\mathrm{obs}}(\omega_\ell), \boldsymbol{C}^{\mathrm{obs}}(\omega_\ell) \right) \quad , \quad \text{with} \quad \boldsymbol{\mu}^{\mathrm{obs}}(\omega_\ell) = \frac{1}{n_{\mathrm{R}}} \sum_{r=1}^{n_{\mathrm{R}}} \boldsymbol{g}_r^{\mathrm{obs}}(\omega_\ell). \tag{2.92}$$

For a vibration test carried out under noise-free conditions, the expression of the distance $\mathcal{L}^{(1)}$ corresponding to the choice (2.90) reads:

$$\mathcal{L}_{n_{\mathrm{F}}}^{(1)} \left(\boldsymbol{p}; \boldsymbol{D}^0 \right) = \mathcal{L}_0^{(1)} + \mathcal{L}_1^{(1)} \left(\boldsymbol{p}; \boldsymbol{D}^0 \right) + \mathcal{L}_2^{(1)} \left(\boldsymbol{p}; \boldsymbol{D}^0 \right) \quad , \tag{2.93}$$

$$\mathcal{L}_1^{(1)} \left(\boldsymbol{p}; \boldsymbol{D}^0 \right) = \frac{1}{n_{\mathrm{F}}} \sum_{\ell=1}^{n_{\mathrm{F}}} \left(\boldsymbol{C}^{\mathrm{mod}}(\omega_\ell;\boldsymbol{p})^{-1} \left(\boldsymbol{\mu}^{\mathrm{mod}}(\omega_\ell;\boldsymbol{p}) - \boldsymbol{h}^0(\omega_\ell) \right), \overline{\left(\boldsymbol{\mu}^{\mathrm{mod}}(\omega_\ell;\boldsymbol{p}) - \boldsymbol{h}^0(\omega_\ell) \right)} \right) \quad ,$$

$$\mathcal{L}_2^{(1)} \left(\boldsymbol{p}; \boldsymbol{D}^0 \right) = \frac{1}{n_{\mathrm{F}}} \sum_{\ell=1}^{n_{\mathrm{F}}} \log \det \boldsymbol{C}^{\mathrm{mod}}(\omega_\ell;\boldsymbol{p}) \quad ,$$

where $\mathcal{L}_0^{(1)}$ is a constant. The term $\mathcal{L}_1^{(1)}$ is the weighted least-squares distance between the mean of the predicted random TFs and the noise-free observed TFs. The weighting factor is the inverse of the covariance matrix of the predicted random TF values. Hence, it attributes a smaller weight to the predictions that are more sensitive to the uncertainty introduced in the model. The mean and the covariance matrix of the predicted random TF values are primarily influenced respectively by the mean-model parameters $\boldsymbol{p}_0$ and by the dispersion parameters $\boldsymbol{p}_\delta$ (both included in $\boldsymbol{p}$; see Section 1.1). Furthermore, the term $\mathcal{L}_1^{(1)}$ is expected to decrease as the dispersion parameters increase, whereas the term $\mathcal{L}_2^{(1)}$ is expected to increase. Hence, upon minimizing $\mathcal{L}^{(1)}$, the identification of the mean-model parameters essentially consists of a partial minimization of the least-squares distance $\mathcal{L}_1^{(1)}$, while the identified dispersion parameters achieve a balance between the reduction of $\mathcal{L}_1^{(1)}$ and the increment of $\mathcal{L}_2^{(1)}$.

For a vibration test carried out under noisy conditions, it can be verified that the expression of the distance $\mathcal{L}^{(1)}$ corresponding to the choices (2.90) and (2.91) reads:

$$\mathcal{L}^{(1)}_{n_{\mathrm{F}},n_{\mathrm{R}}}(\boldsymbol{p};\boldsymbol{D}) = \mathcal{L}^{(1)}_0 + \mathcal{L}^{(1)}_1(\boldsymbol{p};\boldsymbol{D}) + \mathcal{L}^{(1)}_2(\boldsymbol{p};\boldsymbol{D}) \quad , \tag{2.94}$$

$$\mathcal{L}^{(1)}_1(\boldsymbol{p};\boldsymbol{D}) = \frac{1}{n_{\mathrm{F}}}\sum_{\ell=1}^{n_{\mathrm{F}}}\left(\left(\boldsymbol{C}^{\mathrm{mod}}(\omega_\ell;\boldsymbol{p})+\boldsymbol{C}^{\mathrm{obs}}(\omega_\ell)/n_{\mathrm{R}}\right)^{-1}\left(\boldsymbol{\mu}^{\mathrm{mod}}(\omega_\ell;\boldsymbol{p})-\boldsymbol{\mu}^{\mathrm{obs}}(\omega_\ell)\right),\overline{\left(\boldsymbol{\mu}^{\mathrm{mod}}(\omega_\ell;\boldsymbol{p})-\boldsymbol{\mu}^{\mathrm{obs}}(\omega_\ell)\right)}\right),$$

$$\mathcal{L}^{(1)}_2(\boldsymbol{p};\boldsymbol{D}) = \frac{1}{n_{\mathrm{F}}}\sum_{\ell=1}^{n_{\mathrm{F}}}\log\det\left(\boldsymbol{C}^{\mathrm{mod}}(\omega_\ell;\boldsymbol{p})+\boldsymbol{C}^{\mathrm{obs}}(\omega_\ell)/n_{\mathrm{R}}\right) \quad ,$$

where $\mathcal{L}^{(1)}_0$ is a constant. The term $\mathcal{L}^{(1)}_1$ is the weighted least-squares distance between the mean of the predicted random TFs and the mean of the noisy observed TFs. The weighting factor features, this time, the covariance matrices of the predicted random TF values and of the noisy observed TF values. Hence, it is expected to attribute a smaller weight to the predictions that are more sensitive to the uncertainty introduced in the model, as well as to the measurement results that are more disturbed by noise. Similarly to the previous paragraph, the identified mean-model parameters essentially minimize the least-squares distance, while the identified dispersion parameters achieve a balance between the reduction of $\mathcal{L}^{(1)}_1$ and the increment of $\mathcal{L}^{(1)}_2$. Finally, it should be noted that the expression of the weighting factor in the least-squares distance constitutes a a point of distinction between the two approaches for dealing with the experimental noise, which were introduced in Section 2.3.2. In particular, the inverse methods belonging under the heading "noise filtering" do not have the desirable feature of attributing less weight to data that are more disturbed by noise.

The expression of the distance $\mathcal{J}^{(1)}$ corresponding to the choices (2.90)-(2.92) reads:

$$\mathcal{J}^{(1)}_{n_{\mathrm{F}},n_{\mathrm{R}}}(\boldsymbol{p};\boldsymbol{D}) = \mathcal{L}^{(1)}_1(\boldsymbol{p};\boldsymbol{D}) + \mathcal{J}^{(1)}_2(\boldsymbol{p};\boldsymbol{D}) + \mathcal{J}^{(1)}_3(\boldsymbol{p};\boldsymbol{D}) \quad , \tag{2.95}$$

$$\mathcal{J}^{(1)}_2(\boldsymbol{p};\boldsymbol{D}) = \frac{1}{n_{\mathrm{F}}}\sum_{\ell=1}^{n_{\mathrm{F}}}\log\frac{\det\left(\boldsymbol{C}^{\mathrm{mod}}(\omega_\ell;\boldsymbol{p})+\boldsymbol{C}^{\mathrm{obs}}(\omega_\ell)/n_{\mathrm{R}}\right)}{\det\left(\boldsymbol{C}^{\mathrm{obs}}(\omega_\ell)/n_{\mathrm{R}}\right)} \quad ,$$

$$\mathcal{J}^{(1)}_3(\boldsymbol{p};\boldsymbol{D}) = \frac{1}{n_{\mathrm{F}}}\sum_{\ell=1}^{n_{\mathrm{F}}}\mathrm{tr}\left(\left(\boldsymbol{C}^{\mathrm{mod}}(\omega_\ell;\boldsymbol{p})+\boldsymbol{C}^{\mathrm{obs}}(\omega_\ell)/n_{\mathrm{R}}\right)^{-1}\boldsymbol{C}^{\mathrm{obs}}(\omega_\ell)/n_{\mathrm{R}}-\boldsymbol{I}\right) \quad , \tag{2.96}$$

where the term $\mathcal{L}^{(1)}_1$ is still defined by (2.94). The expression (2.95) is similar to (2.94) and can therefore be interpreted in the same way. The main difference with (2.94) is the presence of the term $\mathcal{J}^{(1)}_3$. This term is expected to have a significant influence only when the magnitude of the fluctuations of the noisy observed TFs is comparable with, or larger than, the magnitude of the fluctuations of the predicted random TFs[17]. It then favours larger dispersion parameters.

---

[17]For a fixed ω_ℓ, let the matrix $\boldsymbol{Z}(\omega_\ell;\boldsymbol{p})$ be defined by:

$$\boldsymbol{Z}(\omega_\ell;\boldsymbol{p}) = \boldsymbol{C}^{\mathrm{mod}}(\omega_\ell;\boldsymbol{p})^{1/2}(\boldsymbol{C}^{\mathrm{obs}}(\omega_\ell)/n_{\mathrm{R}})^{-1}\boldsymbol{C}^{\mathrm{mod}}(\omega_\ell;\boldsymbol{p})^{*/2}. \tag{2.97}$$

Let the n_{M} strictly positive real eigenvalues of $\boldsymbol{Z}(\omega_\ell;\boldsymbol{p})$ be denoted by $\{\lambda_m(\omega_\ell;\boldsymbol{p}) \mid 1 \le m \le n_{\mathrm{M}}\}$. It can be verified that the terms $\mathcal{J}^{(1)}_2$ and $\mathcal{J}^{(1)}_3$ in (2.95) take the following form as a function of these eigenvalues:

$$\mathcal{J}^{(2)}_2(\boldsymbol{p};\boldsymbol{D}) = \frac{1}{n_{\mathrm{F}}}\sum_{\ell=1}^{n_{\mathrm{F}}}\sum_{m=1}^{n_{\mathrm{M}}}\log\left(1+\lambda_m(\omega_\ell;\boldsymbol{p})\right) \quad , \tag{2.98}$$

$$\mathcal{J}^{(2)}_3(\boldsymbol{p};\boldsymbol{D}) = -\frac{1}{n_{\mathrm{F}}}\sum_{\ell=1}^{n_{\mathrm{F}}}\sum_{m=1}^{n_{\mathrm{M}}}\frac{\lambda_m(\omega_\ell;\boldsymbol{p})}{\lambda_m(\omega_\ell;\boldsymbol{p})+1}. \tag{2.99}$$

The eigenvalues of $\boldsymbol{Z}(\omega_\ell;\boldsymbol{p})$ are expected to increase with the dispersion parameters. Furthermore, the calculation of the first-derivatives of (2.98)-(2.99) shows that the sum $\mathcal{J}^{(1)}_2 + \mathcal{J}^{(1)}_3$ is positive and increases monotonically with the eigenvalues $\{\lambda_m(\omega_\ell;\boldsymbol{p}) \mid 1 \le m \le n_{\mathrm{M}}\}$. Hence, the sum $\mathcal{J}^{(1)}_2 + \mathcal{J}^{(1)}_3$ is expected to increase with the dispersion parameters.

2.6.4 *A posteriori* error estimation

After the stochastic inverse problem is solved, two methods can be used to evaluate, *a posteriori*, the identified probabilistic structural model. The first method consists in plotting either the sign-reversed loglikelihood or the relative entropy as a function of the frequency as an *a posteriori* error estimate. A plot of this kind indicates the frequencies at which the separation between the experimental data and the identified model is large. The second method consists in using the identified model to forecast the observed TFs of the real structure. Confidence regions associated with a high probability level for the predicted random TFs can then be plot and compared with either the noise-free observed TFs for an undisturbed vibration test, or with estimates of the noise-free TFs obtained from the noisy observed TFs for a disturbed vibration test (App. C). The identified model is then considered invalid at the frequencies for which the (estimates of the) noise-free observed TFs do not lie within the predicted confidence bounds. These two methods are expected to be equivalent, in that the frequencies at which the distance between the experimental data and the identified model is large are expected to coincide with the frequencies for which the (estimates of the) noise-free observed TFs do not lie within the predicted confidence bounds.

On the basis of *a posteriori* error indications of this kind, it can be decided to adapt the probabilistic model (for instance, by using a more extensive parameterization). Subsequently, the identification procedure can be repeated and it can be evaluated whether the modifications mitigated the discrepancies between the experimental data and the identified model.

2.6.5 Predictive use of the identified probabilistic model

The identified probabilistic structural model can be used to predict the dynamical behaviour of the complete real structure (i.e. not only at points where experimental data are available). For instance, confidence regions associated to a high probability level can be built for predicted random TFs. Upon viewing the latter as confidence bounds within which the actual TFs of the real structure are expected to lie, a characterization of the predictive accuracy is obtained: if the width of the confidence interval is large, the predictive accuracy is small and vice versa.

It should be borne in mind that the predicted confidence regions are not hard bounds in that the actual TFs of the real structure are not guaranteed to lie within the predicted confidence bounds. Whereas it is a simple matter to check to validity of the confidence bounds for the observed TFs, this is not the case for unobserved TFs. An important precondition to obtaining an identified model capable of providing valid confidence bounds for unobserved TFs is, in our impression, the extrapolability of the experimental data. For a simple example, consider the probabilistic modelling of the propagation of ground-borne vibrations in a building. Upon identifying the probabilistic model from experimental data gathered in the basement, the adequacy of the identified model in representing the dynamical behaviour at the ground floor may be questionable. Similarly, when only low-frequency experimental data are used, the adequacy of the identified model in representing the medium-frequency dynamical behaviour may be disputable.

From (2.98)-(2.99), it follows that the influence of the term $\mathcal{J}_3^{(1)}$ is significant only for small eigenvalues of $\boldsymbol{Z}(\omega_\ell; \boldsymbol{p})$, which are expected to occur when the magnitude of the fluctuations of the observed TFs is comparable with, or is larger than, the magnitude of the fluctuations of the predicted random TFs.

Box 2.4. Illustrative example: random oscillator

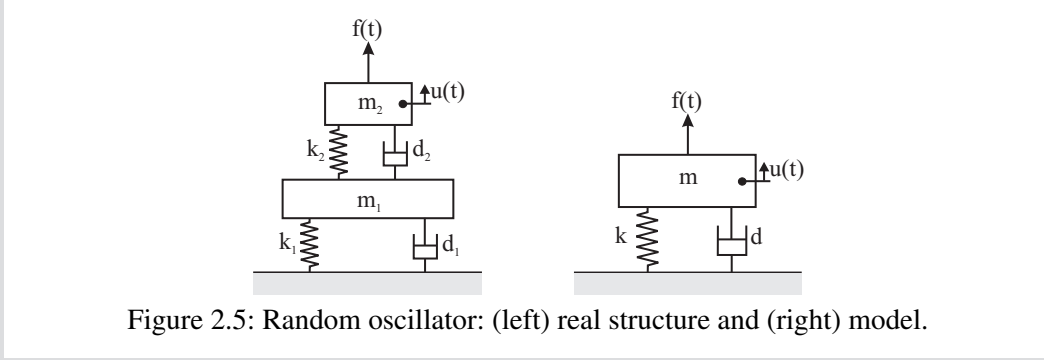This box gives an example of an inverse problem aimed at quantifying epistemic uncertainty.

Figure 2.5: Random oscillator: (left) real structure and (right) model.

Simulated data

Let the real structure be a 2-DOF oscillator (Fig. 2.5), characterized by the eigenfrequencies 30 and 50 Hz. Let a data set $\boldsymbol{D}^0 = \{h^0(\omega_\ell) \mid 1 \le \ell \le n_{\mathrm{F}}\}$ be synthetically generated, which comprises the values taken by the TF from a force applied on the second mass to the displacement of this mass at the discrete frequencies covering the range between 5 and 200 Hz with a step of 5 Hz (hence, $n_{\mathrm{M}} = 1$ and $n_{\mathrm{F}} = 40$).

Construction of the probabilistic model

Let the probabilistic model for the structure be taken as a 1-DOF oscillator with a random stiffness, damping coefficient and mass (Fig. 2.5), modelled by independent gamma random variables $\mathbb{K}(\boldsymbol{p})$, $\mathbb{D}(\boldsymbol{p})$ and $\mathbb{M}(\boldsymbol{p})$ with respective mean values $\underline{k}$, $\underline{d}$ and $\underline{m}$ and dispersion parameters δ_{k}, δ_{d} and δ_{m}. The mean values are chosen equal to $\underline{k} = (2\pi \times 40)^2$ N/m, $\underline{d} = 2 \times 0.02 \times (2\pi \times 40)$ Ns/m and $\underline{m} = 1$ kg (hence, there are no mean-model parameters, i.e. $\boldsymbol{p}_0 = \emptyset$). For the sake of simplicity, it is assumed that $\delta_{\mathrm{k}} = \delta_{\mathrm{d}} = \delta_{\mathrm{m}} = \delta$. Hence, the dispersion level $\boldsymbol{p} = \{\delta\}$ is the only active parameter of the stochastic model.

Stochastic modelling of the vibration test

Let the mapping

$$\gamma_{\mathrm{SDOF}} : \left(\mathbb{R}_0^+\right)^3 \to \mathbb{C}^{n_{\mathrm{F}}} : (k, d, m) \mapsto \gamma_{\mathrm{SDOF}}(k, d, m) = \{h(\omega_\ell; k, d, m) \mid 1 \le \ell \le n_{\mathrm{F}}\} \quad , \tag{2.100}$$

project any set (k, d, m) collecting a deterministic stiffness, damping coefficient and mass onto a corresponding set of deterministic TF values such that, for each discrete frequency ω_ℓ:

$$h(\omega_\ell; k, d, m) = \left(k + i\omega_\ell d - \omega_\ell^2 m\right)^{-1} . \tag{2.101}$$

The predicted random TF values are then obtained by:

$$\{\mathbb{H}(\omega_\ell; \delta) \mid 1 \le \ell \le n_{\mathrm{F}}\} = \gamma_{\mathrm{SDOF}}\big(\mathbb{K}(\delta), \mathbb{D}(\delta), \mathbb{M}(\delta)\big) \text{ a.s.} \quad , \tag{2.102}$$

such that, for each discrete frequency ω_ℓ:

$$\mathbb{H}(\omega_\ell; \delta) = \big(\mathbb{K}(\delta) + i\omega_\ell \mathbb{D}(\delta) - \omega_\ell^2 \mathbb{M}(\delta)\big)^{-1} \text{ a.s.} \tag{2.103}$$

Let $\theta^{(n)}(\cdot | \cdot; \delta)$ denote the n-th order cylindrical PDF of $\{\mathbb{H}(\omega_\ell; \delta) \mid 1 \le \ell \le n_{\mathrm{F}}\}$.

(In)compatibility of the probabilistic model and the data
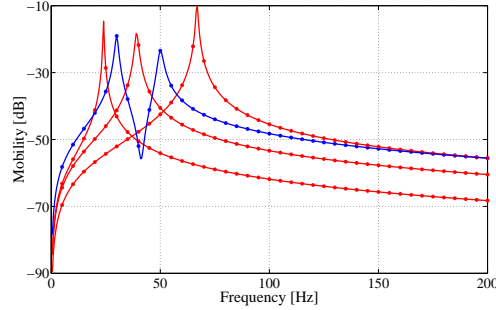
Figure 2.6: Random oscillator: observed TF (blue solid line) and 3 realizations of the random TF for $\delta = 0.5$ (red dashed lines).

Figure 2.6 compares the observed TF with several realizations of the predicted random TF for $\delta = 0.5$. The observed TF and the predicted random TF do not depend on the frequency in the same way. The observed TF belongs to a 2-DOF oscillator and its amplitude attains 2 maxima as a function of the frequency. In contrast, the realizations of the random TF belong to 1-DOF oscillators and their amplitude only has a single maximum. Realizations of the random TF whose amplitude attains 2 maxima do not occur. Consequently, the observed TF does not belong to the support of the probability distribution of $\{\mathbb{H}(\omega_\ell; \delta) \mid 1 \leq \ell \leq n_{\mathrm{F}}\}$, i.e. of the PDF $\theta^{(n_{\mathrm{F}})}(\cdot|\cdot; \delta)$. As a conclusion, the probabilistic model is incompatible with the data.

Let us now examine the compatibility of the lower-order cylindrical PDFs with the data. The first-order cylindrical PDF is compatible with the data since the constraint (2.81) is fulfilled in that, for each discrete frequency, the parameters of the 1-DOF oscillator can be adjusted so as to reproduce the observed TF value at that frequency. However, all higher-order cylindrical PDFs are incompatible with the data. Indeed, for $n > 1$, the three positive real scalar parameters of the 1-DOF oscillator cannot generally be adjusted so as to solve the systems of n complex equations in constraint (2.82).

Frequency-dependent confidence regions
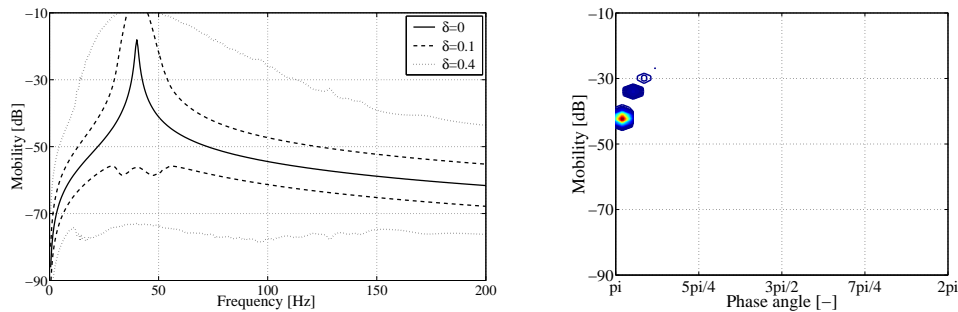
Figure 2.7: Random oscillator: (left) amplitude of the TF predicted by the mean model and 99%-confidence bounds for the random TF for $\delta = 0.1$ and $\delta = 0.4$ and (right) contours of PDF $\theta^{(1)}(\cdot|\omega_\ell; \delta)$ at $\omega_\ell = 50\,\mathrm{Hz}$ for $\delta = 0.1$.

Figure 2.7 shows the frequency-dependent confidence region associated with the probability

level $P_c = 99\%$ for the predicted random TF for the dispersion levels $\delta = 0.1$ and $\delta = 0.4$. The width of the confidence intervals is observed to generally increase with δ. Furthermore, figure 2.7 shows the first-order cylindrical PDF $\theta^{(1)}(\cdot|\omega_\ell; \delta)$ at the frequency $\omega_\ell = 50\,\text{Hz}$ for $\delta = 0.1$. At least 99% of the volume under this PDF is located between the confidence bounds for the predicted random TF value at that frequency (hence, the observed TF value $h^0(\omega_\ell)$ can be expected to lie within the confidence bounds when the PDF $\theta^{(1)}(\cdot|\omega_\ell; \boldsymbol{p})$ has a large value at $h^0(\omega_\ell)$).

The stochastic inverse problem
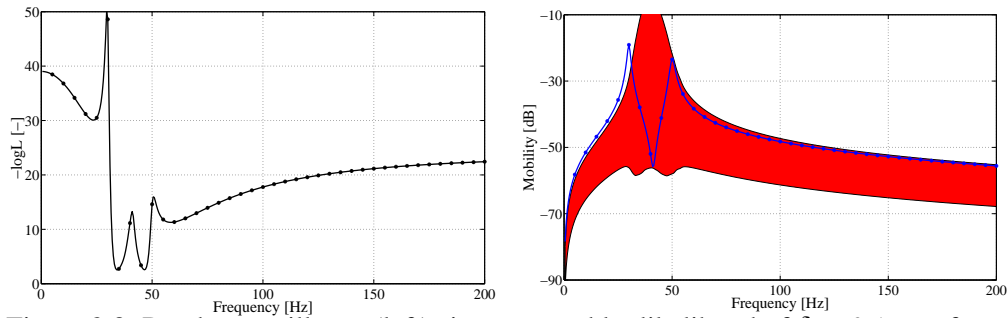
Figure 2.8: Random oscillator: (left) sign-reversed loglikelihood of $\delta = 0.1$ as a function of the frequency and (right) amplitude of the observed TF (blue solid line) and 99%-confidence bounds for the random TF for $\delta = 0.1$ (red patch).

Figure 2.8 shows the sign-reversed loglikelihood of the dispersion level $\delta = 0.1$ as a function of the frequency. Furthermore, figure 2.8 compares the 99%-confidence region for the predicted random TF for $\delta = 0.1$ to the observed TF. The sign-reversed loglikelihood is large at frequencies at which the observed TF value does not lie within the confidence bounds.
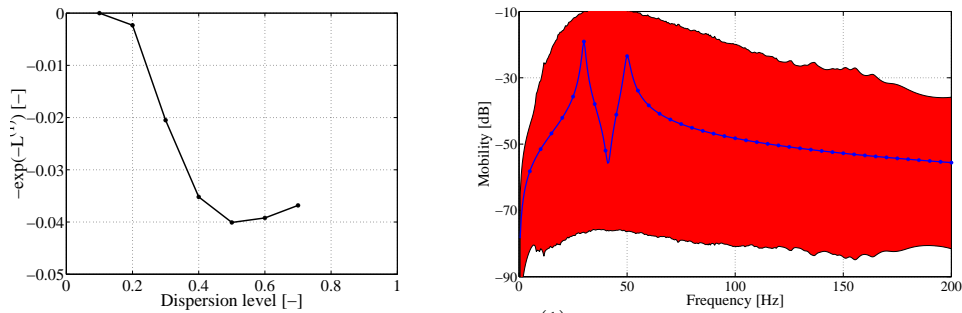
Figure 2.9: Random oscillator: (left) distance $\mathcal{L}_{n_\text{F}}^{(1)}(\delta; \boldsymbol{D}^0)$ as a function of the dispersion level and (right) amplitude of the observed TF (blue solid line) and 99%-confidence bounds for the random TF for $\hat{\delta} = 0.5$ (red patch).

Figure 2.9 shows the distance $\mathcal{L}_{n_\text{F}}^{(1)}(\delta; \boldsymbol{D}^0)$ as a function of the dispersion level δ. The probabilistic model with dispersion level $\hat{\delta} = 0.5$ is identified. Figure 2.9 compares the 99%-confidence region for the predicted random TF for $\hat{\delta} = 0.5$ to the observed TF. The observed TF is seen to lie within the confidence bounds at all frequencies.

2.7 Aleatory uncertainty quantification

This section complements the previous one by proposing a practical methodology for solving stochastic inverse problems aimed at quantifying aleatory uncertainty.

2.7.1 Problem setting

We consider, this time, a *collection of real structures* manufactured according to a fixed design. As discussed in the general introduction, since all manufacturing is subjected to variability, these real structures are expected to be similar but not perfectly identical. Consequently, their dynamical behaviour is expected to exhibit variability.

Let the generic vibration test (Sec. 1.3) be carried out on a subset of real structures out of the entire collection under study, either under noise-free conditions to obtain a data set of the form (1.125)-(1.126), or under noisy conditions to obtain a data set of the form (1.124)-(1.123). Furthermore, let either a non-parametric, or a parametric probabilistic model for the dynamical behaviour of the structure (Sec. 1.1) be built. Let this model be used (Sec. 1.4) to model the vibration test to obtain a stochastic process $\{\mathbb{H}(\omega_\ell; \boldsymbol{p}) \mid 1 \leq \ell \leq n_{\mathrm{F}}\}$. This section then concerns the experimental identification of the parameters $\boldsymbol{p}$ so as to quantify the variability in the dynamical behaviour of the real structures.

With reference to sections 2.1 and 2.2, let us summarize the main difficulties that should be considered when developing methods for solving this stochastic inverse problem:

1. The numerical approximation of high-dimensional PDFs may entail prohibitive computational costs.

2. The probabilistic model may be misspecified and, moreover, incompatible with the data.

2.7.2 Proposed solution methodology

We now examine how the distances introduced in sections 2.3-2.5 can be used to solve the above-stated inverse problem. We first elaborate on the case where the probabilistic structural model is correctly specified and subsequently deal with the case where it is misspecified.

Correctly specified probabilistic model

When the probabilistic model is correctly specified, it is clear that the ultimate aim of the inverse method should be to obtain a "true" value $\boldsymbol{p}^{\mathrm{true}}$ of the parameters, for which the variability in the dynamical behaviour of the real structures is reproduced perfectly. For a vibration test carried out under noise-free conditions, we propose to apply the inverse method (2.34) based on the minimization of the distance $\mathcal{L}^{(n)}$. Upon generalizing the asymptotic results of Section 2.4.1 to distances accounting for cylindrical PDFs of arbitrary order n, this inverse method is seen to be consistent. A "true" value of the parameters can therefore be recovered from the experimental data by increasing the number n_{K} of tested structures to infinity. From the point of view of its large-samples properties, the inverse method (2.38) based on the minimization of the distance $\mathcal{D}^{(n)}$ is less appealing since we were not able to assess its consistency.

The following considerations apply to the choice of the order n. Upon lowering the order n of the cylindrical PDFs that are taken into account, the computational cost is expected to be reduced. However,

an efficiency loss may then occur, in that a larger number n_K of tested structures may be required to achieve estimates of a given accuracy [see, for instance, Lindsay, 1998]. Indeed, upon lowering the order n, less information on the relation between the sought parameters and the stochastic properties of the experimental data is incorporated in the inverse method, which may lead to a consequent loss in the statistical precision of the estimates. As a conclusion, the order n should be chosen so as to achieve a suitable balance between the efficiency and the computational cost.

For a vibration test carried out under noisy conditions, we propose, correspondingly, to apply either the inverse method (2.42), or the inverse method (2.46). These inverse methods may not be consistent. Indeed, as discussed in Section 2.4.2, unless the probabilistic model for the experimental noise (Sec. 1.4) correctly represents the fluctuations of the noisy observed TFs around their noise-free counterparts, the experimental noise may affect the identified parameters, even asymptotically as the number n_R of repetitions of the experiment increases to infinity.

Misspecified probabilistic model

As discussed in Sections 2.1 and 2.2, when the probabilistic model is misspecified, the application of distinct inverse methods is expected to lead to the identification of different models, even asymptotically as the number n_K of tested structures is increased to infinity. Moreover, the adequacy of any inverse method then cannot be judged by evaluating whether it allows to recover a "true" value of the parameters, since such a "true" value does not exist. As in Section 2.6, it is therefore necessary, in our impression, to explicitly define the intended use of the probabilistic model before embarking on its experimental identification. Among different viable inverse methods, the one which is expected to lead to the identification of a model that is adequate for the intended use can then be chosen. The general study and definition of predictive uses of misspecified probabilistic models, which are useful in mechanical engineering, as well as the conception of corresponding inverse methods, is left as an open problem. This section will now focus on discussing particular cases where the distances introduced in the sections 2.3-2.5 can be useful.

In some cases (specifically, when the probabilistic model is misspecified, but, nevertheless, compatible with the dynamical behaviour of the real structures), it may be possible to adapt the stochastic model of the uncertain features (variables, matrices, fields) of the probabilistic model so as to obtain an alternative correctly specified probabilistic model. For instance, instead of using a stochastic model with minimal parameterization, the probability distribution of the uncertain features may be represented by a versatile Karhunen-Loève and/or polynomial chaos expansion (Sec. 1.1). The above-proposed inverse methodology can then be applied to the correctly specified probabilistic model thus obtained.

Besides, in some cases, the parameters p may not only have a mere mathematical meaning as parameters of the probabilistic model, but may themselves also bear a clear physical meaning. For an example, consider a collection of similar real structures whose fields of material properties are heterogeneous and exhibit variability. Let a probabilistic structural model be built by representing these fields of material properties by random fields parameterized by spatial correlation lengths and dispersion levels. It may then be of engineering interest to identify adequate estimates of these parameters, rather than to obtain an adequate comprehensive probabilistic dynamical model. The distances introduced in sections 2.3-2.5 may sometimes be useful in such cases, in particular when the low-order cylindrical PDFs are approximately correctly specified, but the high-order cylindrical PDFs are potentially largely misspecified, or possibly even incompatible with the data. The proposed inverse methods accounting only for low-order cylindrical PDFs are then expected to lead to adequate parameter estimates, even when inverse methods accounting for high-order cylindrical PDFs may lead to unsatisfactory estimates, or may not even be applicable due to incompatibility issues.

2.8 Summary and conclusion

In this chapter, we discussed the numerical difficulties and conceptual problems due to misspecification, which may arise in the inversion of probabilistic structural models. To surmount these difficulties, two versatile methods were proposed for defining and computing the distance between measured TFs and corresponding predicted random TFs, based either on the loglikelihood function, or on the relative entropy. A practical methodology, based on the minimization of a distance of this type, was given for the inversion of probabilistic models aimed at quantifying epistemic uncertainty. The development of a comparable practical methodology for the inversion of probabilistic models aimed at quantifying aleatory uncertainty was initiated.

The following chapters will demonstrate the proposed methodology on examples featuring simulated and real experimental data. First, Chapter 3 presents an example of the identification from simulated data of a non-parametric probabilistic model aimed at quantifying epistemic uncertainty. Then, Chapter 4 describes a civil and environmental engineering case history concerning the identification from real experimental data of a non-parametric probabilistic model aimed at quantifying epistemic uncertainty. Subsequently, Chapter 5 gives an example of the identification from simulated data of a correctly specified parametric probabilistic model aimed at quantifying aleatory uncertainty. Finally, Appendix E presents real experimental data that will be used in future work to further study the identification of dispersion levels and spatial correlation lengths using misspecified parametric probabilistic models.

Part II

Applications

3

Inversion of a probabilistic model of a slender beam

This chapter presents an example of the inversion of a non-parametric probabilistic model aimed at quantifying epistemic uncertainty using simulated data.

3.1 Problem setting
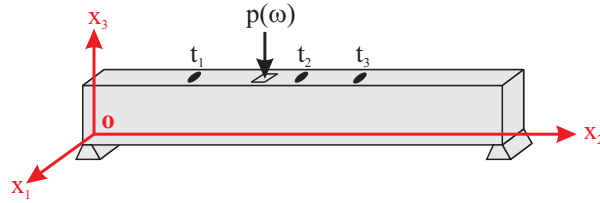
Figure 3.1: Slender beam: schematic representation.

The example concerns the dynamical behaviour of the slender beam shown in Figure 3.1 (hence, a *single* structure is considered). A right-handed Cartesian reference frame (x_1, x_2, x_3) with origin o is defined. The undeformed beam occupies the box-shaped region

$$\Omega = \big\{ -0.5\,\text{m} < x_1 < 0.5\,\text{m},\ 0 < x_2 < 10\,\text{m},\ 0 < x_3 < 1.5\,\text{m} \big\}. \tag{3.1}$$

It is simply supported at $x_2 = 0$ and $x_2 = 10\,\text{m}$. It is constituted of a homogeneous, isotropic, linear elastic material with Young's modulus $E = 33\,\text{GPa}$, Poisson ratio $\nu = 0.3$ and mass density $\rho = 2500\,\text{kg/m}^3$. Its dynamical behaviour is analyzed in the frequency band $B = [0, \omega_{\max}]$, where $\omega_{\max} = 2\pi f_{\max}$ and $f_{\max} = 1000\,\text{Hz}$. Finally, for later use, let t_1, t_2 and t_3 denote the points with coordinates $(0,\ 2.5\,\text{m},\ 0.75\,\text{m})$, $(0,\ 5\,\text{m},\ 0.75\,\text{m})$ and $(0,\ 6.4\,\text{m},\ 0.75\,\text{m})$, respectively.

3.2 Simulated data

A data set is synthetically generated with a three-dimensional (3D) Finite Element (FE) model constituted of $10 \times 100 \times 15$ isoparametric 8-noded brick elements of equal size. Modal damping is assumed with

modal damping ratio $\xi = 0.02$. The beam is loaded by a frequency-dependent pressure $p(\omega)$ uniformly applied on the square portion Γ_p of the top surface centred at $(0.5\,\text{m}, \ 4.2\,\text{m}, \ 0.75\,\text{m})$ and of area ϵ^2 with $\epsilon \ll 1\,\text{m}$. The vertical response is observed at the points t_1, t_2 and t_3. In the following, we will identify the probabilistic model (to be built) using the response at t_2 and t_3. More specifically, we let the data set $D^0 = \{h^0(\omega_\ell) \mid 1 \leq \ell \leq n_F\}$ gather the Transfer Functions (TFs) from the applied pressure field to the vertical response at t_2 and t_3 predicted by the 3D FE model at the discrete frequencies covering the range between 5 and 1000 Hz with a step of 5 Hz (hence, $n_M = 2$ and $n_F = 200$). We will afterwards use the response at t_1 to "validate" the predictive capability of the identified model.

3.3 Probabilistic structural model

In this section, a non-parametric probabilistic model for the dynamical behaviour of the slender beam is built (Algorithm 1 in Section 1.2) and studied.

3.3.1 Deterministic modelling

A one-dimensional (1D) FE model made of 100 2-noded Timoshenko beam elements of equal length is built. At the two edges, the translational Degrees Of Freedom (DOFs) are set to zero, while the rotational DOFs are unconstrained. A reduced matrix model is then created using a reduction basis made of n_T bending eigenmodes, which has the following form (Algorithm 1):

$$[\boldsymbol{K} + i\omega\boldsymbol{D} - \omega^2\boldsymbol{M}]\boldsymbol{q}_{n_T}(\omega) = \boldsymbol{T}_{n_T}^{\mathrm{T}}\boldsymbol{f}_{\mathrm{h}}(\omega), \quad \omega \in B \quad , \tag{3.2}$$

$$\boldsymbol{u}_{\mathrm{h}}(\omega) = \boldsymbol{T}_{n_T}\boldsymbol{q}_{n_T}(\omega) \quad , \tag{3.3}$$

where $\boldsymbol{K}, \boldsymbol{D}, \boldsymbol{M} \in \mathrm{M}_{n_T}^+(\mathbb{R})$, the reduced stiffness, damping and mass matrices are diagonal. Their j-th diagonal entries are given by $K_{jj} = (w_j^{1D})^2$, $D_{jj} = 2\xi(w_j^{1D})$ and $M_{jj} = 1$, respectively, where w_j^{1D} is the j-th angular eigenfrequency of the 1D FE model.

(a) TF at t_2.
(b) TF at t_3.
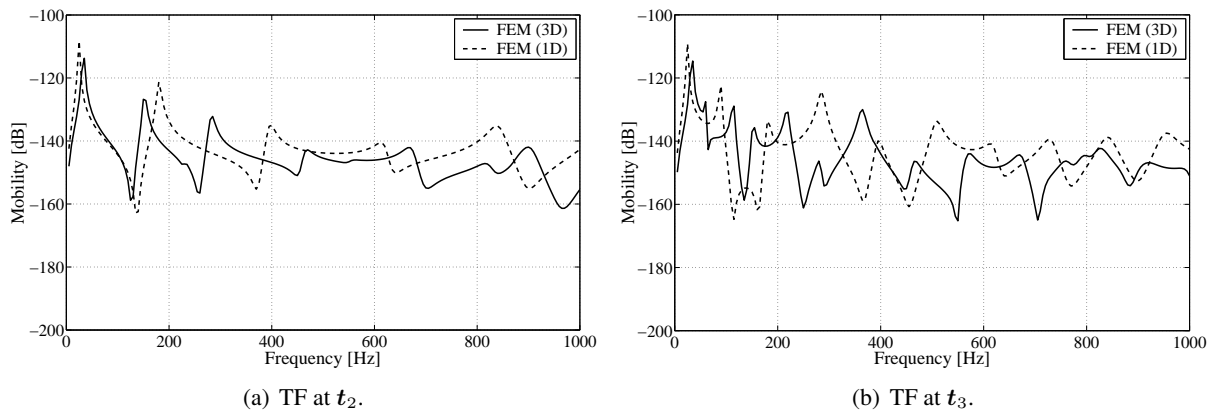
Figure 3.2: Slender beam: amplitude of the TFs predicted by the 3D FE model and the 1D FE model at (a) t_2 and (b) t_3.

Figure 3.2 shows that the TFs at t_2 and t_3 predicted by the 3D FE model and the 1D FE model are in reasonable agreement at frequencies lower than about 100 Hz, and exhibit significant differences at higher frequencies.

3.3.2 Probabilistic modelling

A non-parametric probabilistic model is built of the form (1.96)-(1.97), i.e.:

$$[\mathbb{K}(\boldsymbol{p}) + i\omega\mathbb{D}(\boldsymbol{p}) - \omega^2\mathbb{M}(\boldsymbol{p})]\mathbb{Q}_{n_\text{T}}(\omega;\boldsymbol{p}) = \boldsymbol{T}_{n_\text{T}}^\text{T}\boldsymbol{f}_\text{h}(\omega) \text{ a.s.}, \quad \omega \in B \quad , \tag{3.4}$$

$$\mathbb{U}_\text{h}(\omega;\boldsymbol{p}) = \boldsymbol{T}_{n_\text{T}}\mathbb{Q}_{n_\text{T}}(\omega;\boldsymbol{p}) \text{ a.s.} \tag{3.5}$$

with $\mathbb{K}(\boldsymbol{p})$, $\mathbb{D}(\boldsymbol{p})$ and $\mathbb{M}(\boldsymbol{p})$ denoting the random reduced stiffness, damping and mass matrix, respectively, parameterized by $\boldsymbol{p}$.

The mean values of the random reduced matrices are chosen equal to their deterministic counterparts in model (3.2)-(3.3), i.e.:

$$E\{\mathbb{K}(\boldsymbol{p})\} = \boldsymbol{K} , \quad E\{\mathbb{D}(\boldsymbol{p})\} = \boldsymbol{D} , \quad E\{\mathbb{M}(\boldsymbol{p})\} = \boldsymbol{M}. \tag{3.6}$$

Hence, there are no mean-model parameters, i.e. $\boldsymbol{p}_0 = \emptyset$, and the random matrices $\mathbb{K}(\boldsymbol{p})$, $\mathbb{D}(\boldsymbol{p})$ and $\mathbb{M}(\boldsymbol{p})$ are parameterized solely by their respective dispersion parameters δ_K, δ_D and δ_M. For the sake of simplicity, it is assumed that $\delta_\text{K} = \delta_\text{D} = \delta_\text{M} = \delta$, so that $\boldsymbol{p} = \{\delta\}$ is the only active parameter of the probabilistic model.

3.3.3 Computations with the probabilistic model

As already mentioned, the FE method is used for the discretization of the space. The Monte Carlo Simulation (MCS) method is applied to discretize the random dimension. The computations are performed in Matlab using the Structural Dynamics Toolbox [Balmès and Leclère, 2006].

3.3.4 Random matrix eigenvalue problem

(a) (b)
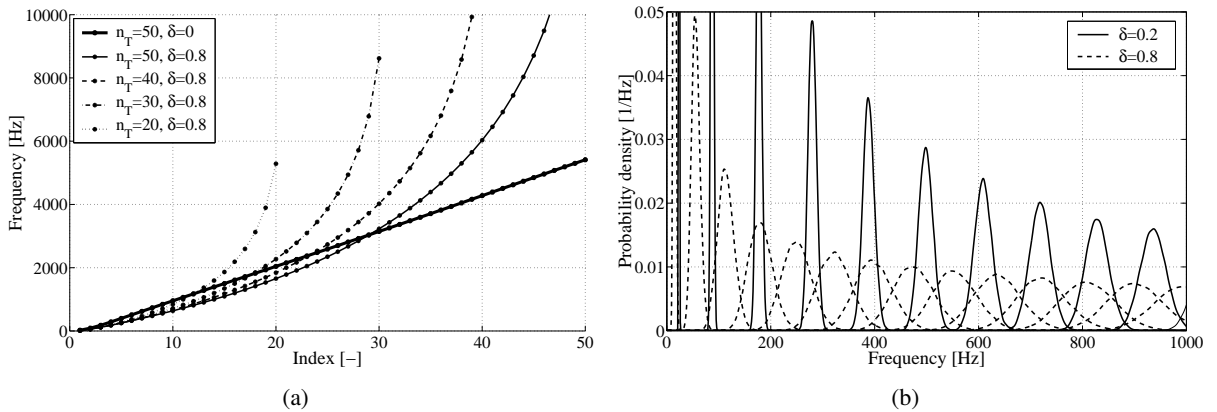
Figure 3.3: Slender beam: (a) PDFs of the random eigenfrequencies between 0 and 1000 Hz for $\delta = 0.2$ and $\delta = 0.8$ and (b) 50 lowest deterministic eigenfrequencies of the mean model, and mean of the random eigenfrequencies for δ=0.8 and $n_\text{T} = 20$, $n_\text{T} = 30$, $n_\text{T} = 40$ and $n_\text{T} = 50$.

Before studying in the next subsection the stochastic properties of the random TFs predicted by the probabilistic model (3.4)-(3.5), this subsection analyzes the random matrix eigenvalue problem (app. B) defined by the random reduced stiffness and mass matrices $\mathbb{K}(\boldsymbol{p})$ and $\mathbb{M}(\boldsymbol{p})$. Since the stochastic properties

of the predicted random TFs are strongly related to the properties of the random eigenfrequencies and eigenmodes associated to these random matrices, the analysis of the latter provides useful insight on the former. The random eigenfrequencies are now studied for frequencies lower than $1.5 \times f_{\max} = 1500\,\text{Hz}$.

First, the stochastic properties of the eigenfrequencies as a function of the reduction basis dimension n_T are studied. Figure 3.3(a) shows the 50 lowest deterministic eigenfrequencies of the mean model, and the mean value (computed using $n_S = 10000$ Monte Carlo simulations) of the random eigenfrequencies for δ=0.8 and $n_T = 20,\ 30,\ 40$ and 50. Since the eigenfrequencies are non-linear functions of the stiffness and mass matrices, their mean value differs from the deterministic eigenfrequencies. For a fixed n_T, the mean values of the low eigenfrequencies (approximately the lowest $n_T/2$) are observed to be smaller than the deterministic values, while the mean values of the high eigenfrequencies are observed to be larger. For the eigenfrequencies lower than 1000 Hz, reasonable convergence is obtained for $n_T = 50$. In the remainder of this chapter, all computations are performed with $n_T = 50$ eigenmodes.

Figure 3.3(b) shows the Probability Density Functions (PDFs) (computed using $n_S = 10000$ Monte Carlo simulations) of the random eigenfrequencies for $\delta = 0.2$ and $\delta = 0.8$ in the frequency range up to 1000 Hz. For $\delta = 0.2$, the dispersion of the random eigenfrequencies is small compared to the eigenfrequency separation and the PDFs do not overlap. For $\delta = 0.8$, the dispersion of the random eigenfrequencies is large compared to the eigenfrequency separation and the PDFs do overlap except for the 3 lowest eigenfrequencies. Furthermore, these random eigenfrequencies are observed to decrease as δ increases.

3.3.5 Predicted random TFs
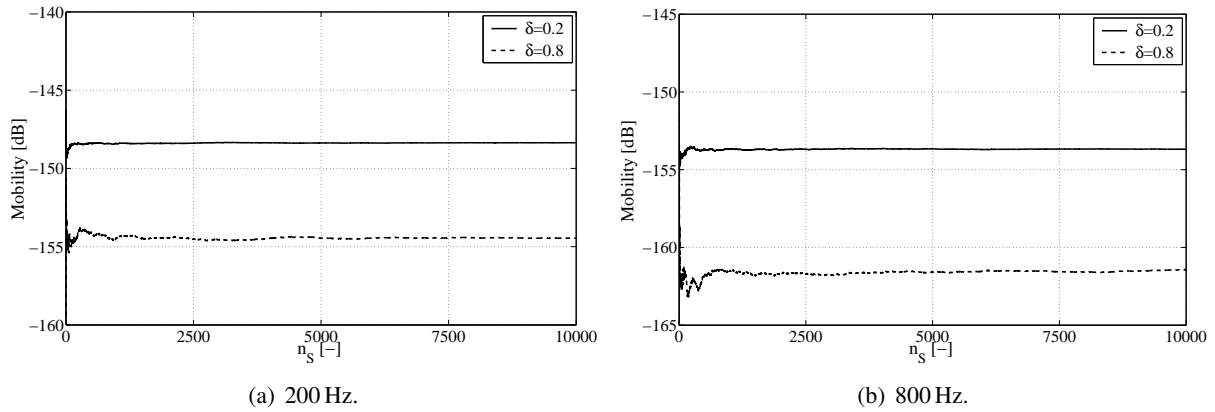
(a) 200 Hz. (b) 800 Hz.

Figure 3.4: Slender beam: statistical mean of the realizations of the predicted random TF at t_2 for $\delta = 0.2$ and $\delta = 0.8$ at frequencies (a) 200 Hz and (b) 800 Hz.

Figure 3.4 shows, as a function of the number n_S of Monte Carlo simulations, the statistical mean of the realizations of the predicted random TF at t_2 for the dispersion levels $\delta = 0.2$ and $\delta = 0.8$ at the frequencies 200 Hz and 800 Hz. The larger δ and the higher the frequency, the larger the required number n_S becomes. Fully converged results are clearly obtained for $n_S = 10000$. All results to follow have been obtained using $n_S = 10000$ Monte Carlo simulations.

Figure 3.5 shows the 99%-confidence regions (Box 2.3 of Section 2.6) for the predicted random TF at t_2 and t_3 for $\delta = 0.2$ and $\delta = 0.8$. Their width is observed to increase with δ and also with the frequency, which stresses that the predictions become more sensitive to uncertainties as the frequency increases.
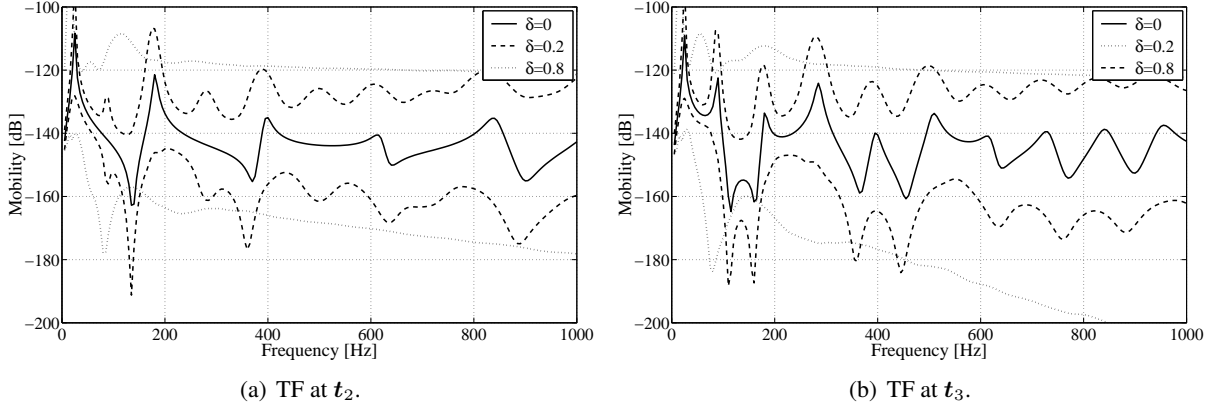
(a) TF at t_2.

(b) TF at t_3.

Figure 3.5: Slender beam: amplitude of the TF predicted by the mean model, and 99%-confidence regions for the random TF for $\delta = 0.2$ and $\delta = 0.8$ at (a) t_2 and (b) t_3.

At low frequencies below approximately 200 Hz, the frequencies of the resonance peaks are observed to decrease when δ increases. On the other hand, at frequencies above 200 Hz, the confidence bounds for $\delta = 0.2$ show resonance peaks while the confidence bounds for $\delta = 0.8$ do not. Indeed, for $\delta = 0.2$, the dispersion of the random eigenfrequencies is small compared to the eigenfrequency separation resulting in resonances randomly occurring in distinct frequency ranges. In contrast, for $\delta = 0.8$, the dispersion is large compared to the separation, so that resonances randomly occur at all frequencies.

3.4 Stochastic inverse problem

The methodology proposed in Section 2.6 is now applied to invert the probabilistic model.

3.4.1 Identification of the probabilistic model
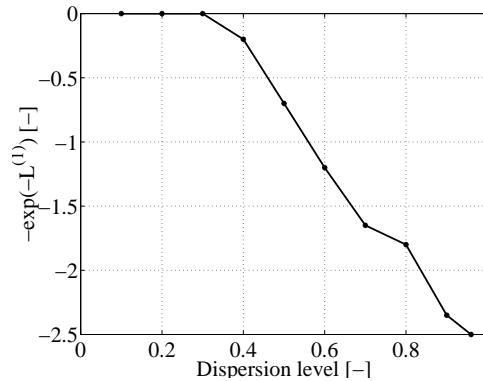
Figure 3.6: Slender beam: distance $\mathcal{L}_{n_F}^{(1)}(\delta; \boldsymbol{D}^0)$ as a function of δ.

The suitable dispersion level is identified by minimizing the distance $\mathcal{L}^{(1)}$, defined in (2.31). Figure 3.6 shows that the probabilistic model with the largest admissible dispersion level $\hat{\delta} = 0.96$ (with reference to inequality (1.46)) is optimal in the sense of the distance $\mathcal{L}_{n_F}^{(1)}(\delta; \boldsymbol{D}^0)$.

3.4.2 *A posteriori* error estimation

Figure 3.7 shows the sign-reversed loglikelihood of $\hat{\delta} = 0.96$ as a function of the frequency. Figures 3.8 and 3.9 compare the 99%-confidence regions for the identified predicted random TFs to the observed TFs at t_2 and t_3. The sign-reversed loglikelihood is seen to be large at frequencies for which the observed TFs do not lie within, or nearly lie within, the confidence bounds. At low frequencies below 200 Hz, the agreement of the identified model with the data is unsatisfactory. Due to the decrease of the low random eigenfrequencies with δ, the low-frequency resonances of the random TFs are located at lower frequencies than those of the observed TFs.

3.4.3 Adaptation of the probabilistic model

To mitigate the discrepancy at the low frequencies, the probabilistic model is adapted. The non-parametric probabilistic model used in the following has the same form (3.4)-(3.5), but, this time, the mean values of the random reduced stiffness and damping matrices are defined by:

$$E\left\{\mathbb{K}(\boldsymbol{p})\right\} = \boldsymbol{K}(w_1, w_2, w_3)\,, \quad E\left\{\mathbb{D}(\boldsymbol{p})\right\} = \boldsymbol{D}(w_1, w_2, w_3)\quad, \tag{3.7}$$

with:

$$K_{jj}(w_1, w_2, w_3) = w_j^2\,, \qquad D_{jj}(w_1, w_2, w_3) = 2\xi w_j \quad (j = 1, 2, 3)\quad,$$
$$K_{jj}(w_1, w_2, w_3) = (w_j^{\mathrm{1D}})^2\,, \quad D_{jj}(w_1, w_2, w_3) = 2\xi w_j^{\mathrm{1D}} \quad (4 \leq j \leq n_{\mathrm{T}}).$$

The three lowest angular eigenfrequencies w_1, w_2 and w_3 are now used as mean-model parameters. The mean value of the random reduced mass matrix is still defined by (3.6). The three dispersion parameters are again chosen equal: $\boldsymbol{p}_\delta = \{\delta\}$, such that now $\boldsymbol{p} = \{w_1, w_2, w_3, \delta\}$.

3.4.4 Identification of the adapted probabilitic model

The distance $\mathcal{L}_{n_{\mathrm{F}}}^{(1)}(\boldsymbol{p}; \boldsymbol{D}^0)$ is minimized by the parameters $\hat{w}_1/2\pi = 46.67\,\mathrm{Hz}$, $\hat{w}_2/2\pi = 172.63\,\mathrm{Hz}$, $\hat{w}_3/2\pi = 230.00\,\mathrm{Hz}$ and $\hat{\delta} = 0.67$ (obtained using the simulated annealing algorithm).

3.4.5 *A posteriori* error estimation

Figure 3.10 shows the sign-reversed loglikelihood of $\hat{w}_1/2\pi = 46.67\,\mathrm{Hz}$, $\hat{w}_2/2\pi = 172.63\,\mathrm{Hz}$, $\hat{w}_3/2\pi = 230.00\,\mathrm{Hz}$ and $\hat{\delta} = 0.67$ as a function of the frequency. Figures 3.11 and 3.12 compare the 99%-confidence regions for the identified predicted random TFs to the observed TFs at t_2 and t_3. Compared to Figure 3.7, the sign-reversed loglikelihood has been reduced at the low frequencies. The observed TFs are seen to lie within the confidence bounds at all frequencies. The introduction of the mean-model parameters has allowed to compensate for the decrease of the lowest random eigenfrequencies.

3.4.6 Predictive use of the identified probabilistic model

To "validate" the predictive capability of the identified probabilistic model, Figure 3.13 compares the 99%-confidence region for the random TF predicted by the identified probabilistic model at the point t_1 to the corresponding TF predicted by the 3D FE model. The latter TF is seen to lie within the confidence bounds at all frequencies. This result suggests that the identified model can be used to predict the dynamical behaviour of the complete slender beam, and not only at points where data are available.
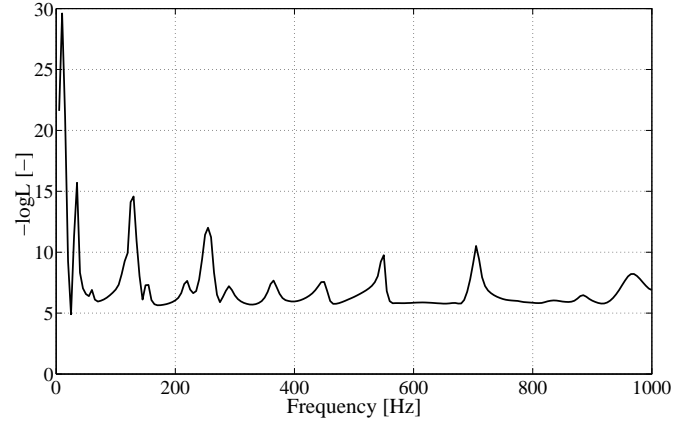
Figure 3.7: Slender beam: sign-reversed loglikelihood of $\hat{\delta} = 0.96$ as a function of the frequency.
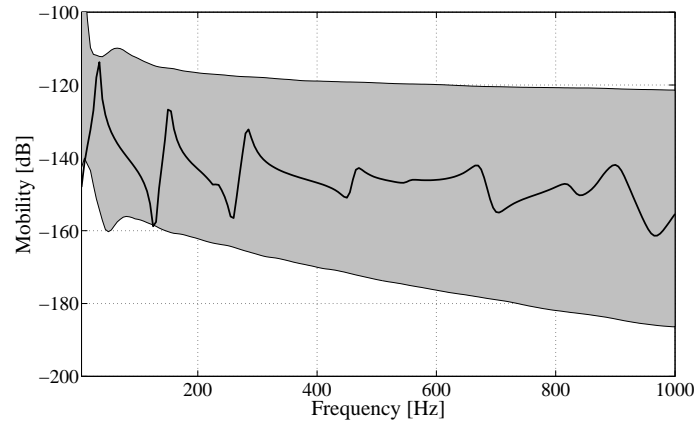

Figure 3.8: Slender beam: amplitude of the observed TF (solid line) and 99%-confidence bounds for the random TF identified in Section 3.4.1 (grey patch) at t_2.
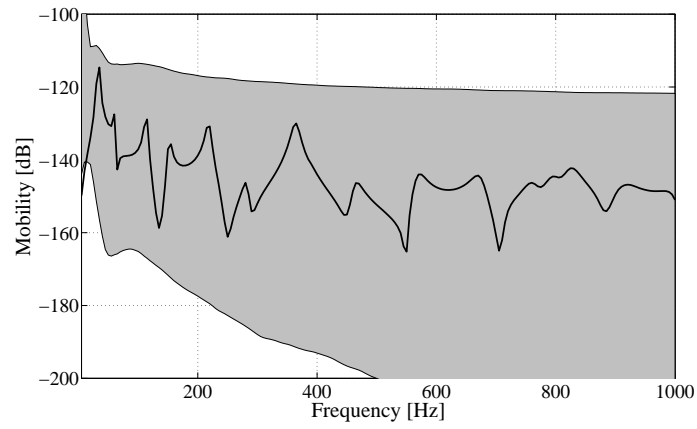

Figure 3.9: Slender beam: amplitude of the observed TF (solid line) and 99%-confidence bounds for the random TF identified in Section 3.4.1 (grey patch) at t_3.
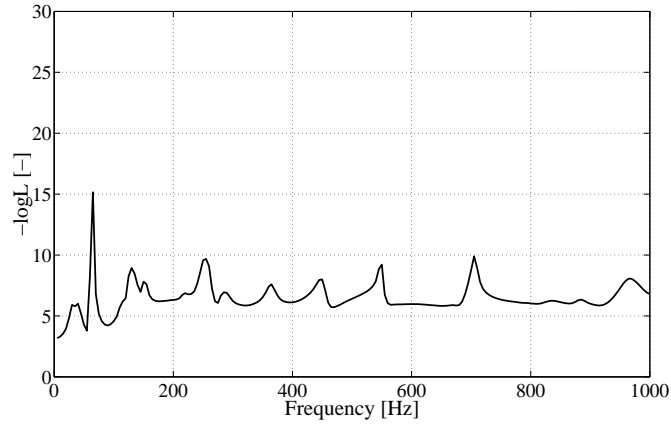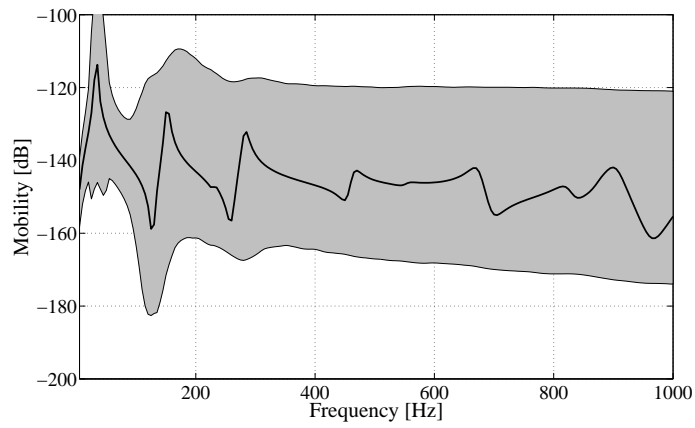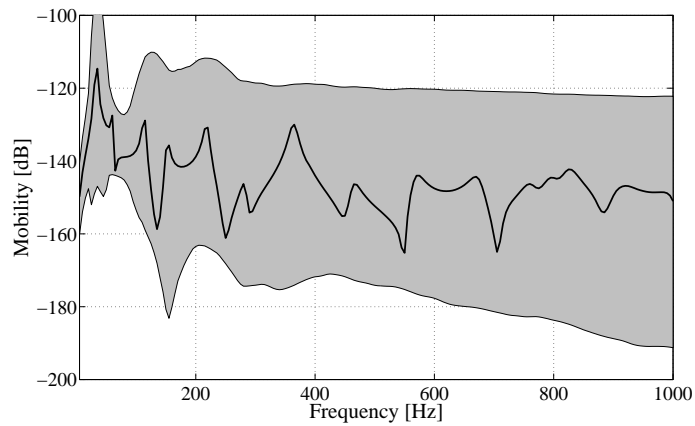
Figure 3.10: Slender beam: sign-reversed loglikelihood of $\hat{w}_1/2\pi = 46.67\,\text{Hz}$, $\hat{w}_2/2\pi = 172.63\,\text{Hz}$, $\hat{w}_3/2\pi = 230.00\,\text{Hz}$ and $\hat{\delta} = 0.67$ as a function of the frequency.

Figure 3.11: Slender beam: amplitude of the observed TF (solid line) and 99%-confidence bounds for the random TF identified in Section 3.4.4 (grey patch) at t_2.

Figure 3.12: Slender beam: amplitude of the observed TF (solid line) and 99%-confidence bounds for the random TF identified in Section 3.4.4 (grey patch) at t_3.
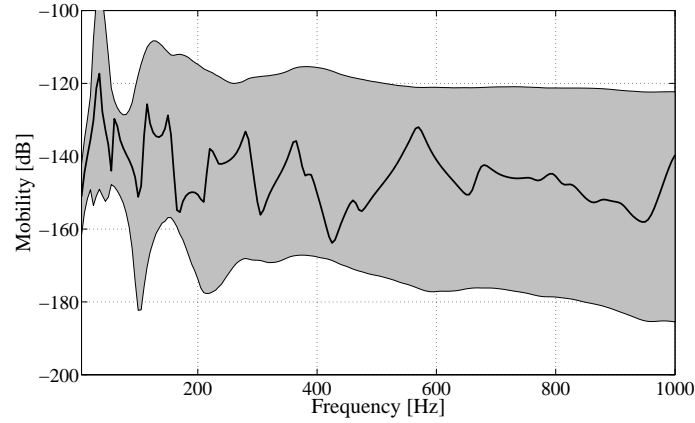
Figure 3.13: Slender beam: amplitude of the TF predicted by the 3D FE model (solid line) and 99%-confidence bounds for the random TF identified in Section 3.4.4 (grey patch) at t_1.

3.5 Summary and conclusion

In this chapter, an illustrative example was presented of the inversion of a non-parametric probabilistic model using simulated data. The inverse method based on the minimization of the distance $\mathcal{L}^{(1)}$ was successfully applied to identify a model that is adequate to predict frequency-dependent confidence regions.

The example highlighted that it may sometimes be useful to include mean-model parameters in non-parametric probabilistic models with minimal parameterization. Indeed, the low-frequency random eigen-frequencies of probabilistic models of this kind were found to decrease as the dispersion level increases. If a large dispersion level is required, the introduction of mean-model parameters allows to compensate for this decrease. The mean-model parameters must clearly be identified together with the dispersion parameters.

In the example, the simplifying assumption was made that the dispersion levels of the stiffness, damping and mass matrix are identical. A natural direction for future work consists in relaxing this assumption.

4

Inversion of a probabilistic model for ground-borne vibrations in buildings

This chapter presents a civil and environmental engineering case history involving the inversion of a non-parametric probabilistic model aimed at quantifying epistemic uncertainty from real experimental data.
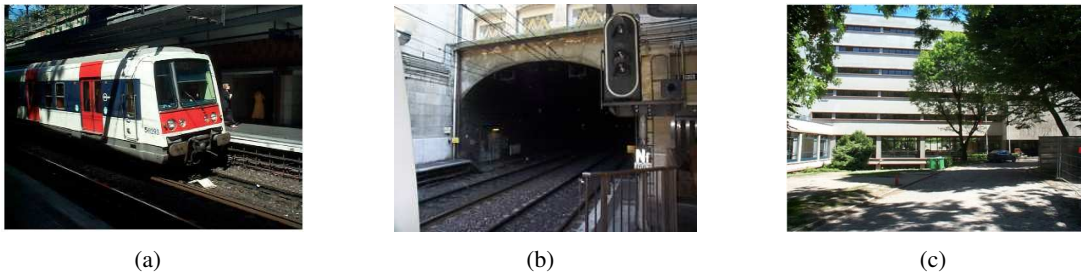
4.1   Problem setting

(a)   (b)   (c)

Figure 4.1: Ground-borne vibrations in the Maison du Mexique: (a) train at the station Gentilly, (b) tunnel at the station Gentilly and (c) side view of the Maison du Mexique.

The case history concerns the transmission of vibrations from the underground-railway tunnel of the RER B line of RATP to the Maison du Mexique building at the Cité Universitaire site in Paris in France (Fig. 4.1) (hence, a *single* structure is considered). The tunnel is a masonry cut-and-cover tunnel at a shallow depth of about 9.3 m below the free surface of the soil embedded in sand layers. Two classic ballast tracks are running in the tunnel. The rails are supported by grooved rubber pads and are resting on mono-block concrete sleepers. A Spectral Analysis of Surface Waves (SASW) test (app. D) was performed to determine the thickness and the dynamical characteristics of the shallow soil layers [Pyl and Degrande, 2002]. This test demonstrated the presence of a thin layer with a thickness of approximately 1.4 m and a shear wave velocity of 115 m/s, a stiffer layer with a thickness of 3.0 m and a shear wave velocity of 220 m/s on top of a halfspace with a shear wave velocity of 315 m/s. The Maison du Mexique is a six-storey reinforced-concrete frame structure. It has two sets of eight columns such that the floor spans are approximately 6.2 m. The floor-to-ceiling height is approximately 2.85 m.
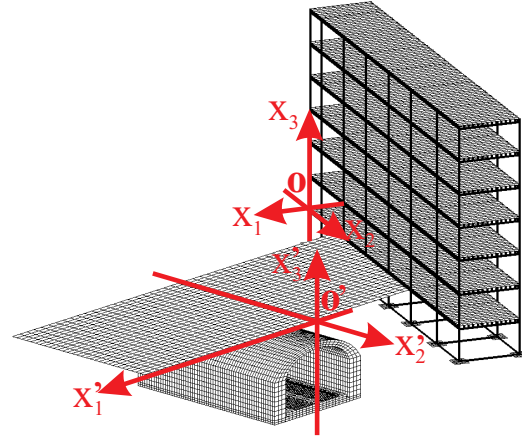
Figure 4.2: Ground-borne vibrations in the Maison du Mexique: schematic overview.

For the tunnel, a right-handed Cartesian frame of reference (i'_1, i'_2, i'_3) is defined with the origin o' at the free surface of the soil (Fig. 4.2). For the building, a right-handed Cartesian frame of reference (i_1, i_2, i_3) is defined with the origin o in the left corner at the ground floor (Fig. 4.2). The origin of the reference frame of the building has coordinates $(x'_1 = -23.5\,\text{m}, \ x_2 = -24.3\,\text{m}, \ x_3 = 0)$ in the reference frame of the tunnel. The angle between i_2 and i'_2 is $25°$.

4.2 Real experimental data
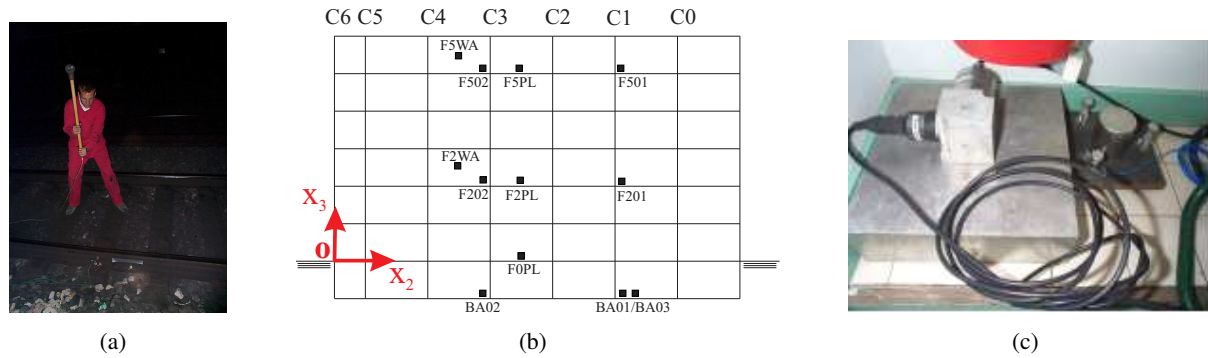
Figure 4.3: Ground-borne vibrations in the Maison du Mexique: (a) impact hammer, (b) measurement locations and (c) accelerometers at the position F501.

In the frame of the European CONVURT project (the CONtrol of Vibrations from Underground Railway Traffic), *in situ* measurements were performed of the dynamical response in the Maison du Mexique due to excitations applied on the rails in the tunnel. Vibrations were generated by an impact of an instrumented hammer with a mass of 5.3 kg and a soft tip on the rail head at the point with coordinates $(x'_1 = -2.5\,\text{m}, \ x'_2 = 0, \ x'_3 = -8.2\,\text{m})$, and recorded by accelerometers placed at different locations in the Maison du Mexique (Fig. 4.3). We will consider here the vertical response at the locations BA01, BA03, F0PL and F201 (Fig. 4.3(b) and Table 4.1).
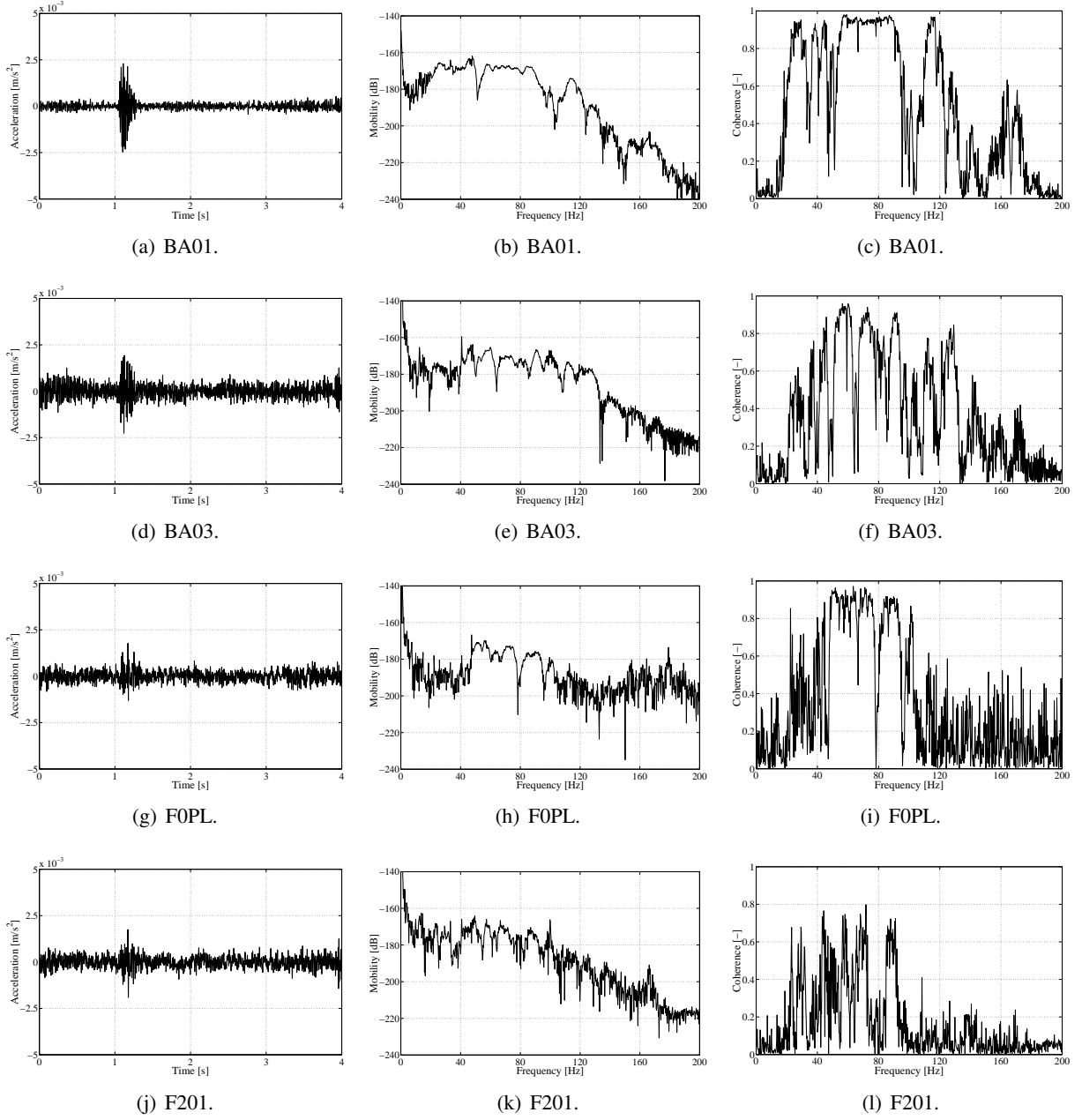
Figure 4.4: Ground-borne vibrations in the Maison du Mexique: (a, d, g, j) time history of the measured acceleration during the sixth event, (b, e, h, k) amplitude of the estimated noise-free TF and (c, f, i, l) coherence function between the applied force and the measured response at BA01, BA03, F0PL and F201.

Label	Location	Coordinates $(x_1,\ x_2,\ x_3)$
BA01	in the basement next to column C1	$(-0.5\,\mathrm{m},\ 26.5\,\mathrm{m},\ -3.6\,\mathrm{m})$
BA03	in the basement at 1 m from column C1	$(-1.5\,\mathrm{m},\ 26.5\,\mathrm{m},\ -3.6\,\mathrm{m})$
F0PL	at the ground floor between columns C2 and C3	$(-2.9\,\mathrm{m},\ 18.2\,\mathrm{m},\ 0)$
F201	at the second floor right next to column C1	$(-0.5\,\mathrm{m},\ 26.5\,\mathrm{m},\ 6.8\,\mathrm{m})$

Table 4.1: Ground-borne vibrations in the Maison du Mexique: measurement locations.

A total of $n_\mathrm{R} = 25$ events was recorded. The A/D conversion was performed at a rate of 1000 Hz. A total of 4096 data points was recorded for each event (hence, the frequency-domain resolution is 0.2441 Hz). Estimates of the noise-free Transfer Functions (TFs) from the force applied on the rail head to the vertical velocity in the building have been deduced from the noisy experimental data using the $H1$-estimation method (App. C). The coherence function between the measured applied force and the measured responses has also been estimated (App. C). Figure 4.4 shows the time history of the response measured during the sixth event, the estimated noise-free TF and the coherence function at BA01, BA03, F0PL and F201. Due to experimental noise, low coherence values, indicating low data quality, are observed at frequencies below 20 Hz and at frequencies above 100 Hz. The coherence decreases with the distance to the impact point.

In the following, we will identify the probabilistic model (to be built) using the TFs at BA01 and F0PL. More specifically, we let the data set $\boldsymbol{D} = \{\boldsymbol{g}_1^{\mathrm{obs}}(\omega_\ell),\ldots,\boldsymbol{g}_{n_\mathrm{R}}^{\mathrm{obs}}(\omega_\ell) \mid 1 \leq \ell \leq n_\mathrm{F}\}$ gather the observed TFs from the applied force to the response at BA01 and F0PL at the discrete frequencies covering the range between 20 and 100 Hz with a step of 0.2441 Hz (hence, $n_\mathrm{M} = 2$ and $n_\mathrm{F} = 327$). We will afterwards use the vertical response at the measurement locations BA03 and F201 to "validate" the predictive capability of the identified model.

4.3 Probabilistic structural model

In this section, a non-parametric probabilistic model for the groundborne vibrations in the Maison du Mexique is built (Algorithm 1 of Section 1.2) and studied.

4.3.1 Deterministic modelling

In the frame of the CONVURT project, a deterministic model was built for the transmission of vibrations from the underground-railway tunnel of the RER B line to the Maison du Mexique at the Cité Universitaire site [Arnst, 2003, Chebli et al., 2007, Clouteau et al., 2005, Degrande et al., 2006]. Assuming that the dynamic interaction of the track, the tunnel and the soil is only weakly coupled to the dynamic interaction of the soil and the building, the transmission of the vibrations is modelled in two steps.

First, a model for the dynamical interaction of the track, the tunnel and the soil is used to compute the wave field radiated into the soil due to forces applied on the rails in the tunnel. The dynamic track-tunnel-soil interaction model is based on the periodic coupled Finite Element-Boundary Element (FE-BE) formulation proposed by Clouteau et al. [2005], Degrande et al. [2006].

Subsequently, a model for the dynamic interaction of the soil and the building is used to compute the structural vibration induced by this incident wave field. The dynamic soil-building interaction model uses a classical coupled FE-BE formulation [see, for instance, Aubry and Clouteau, 1992, Clouteau and Aubry, 2003] in conjunction with the Craig-Bampton substructuring method [Craig and Bampton,
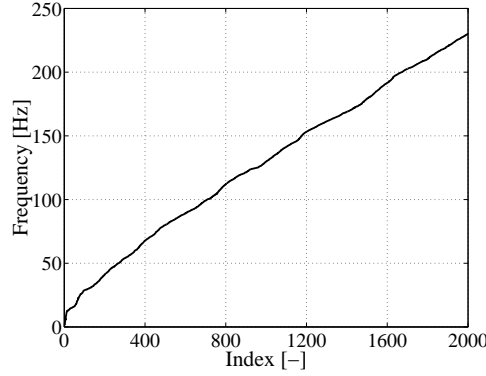
Figure 4.5: Ground-borne vibrations in the Maison du Mexique: lowest 2000 eigenfrequencies of the building model.

1968], and is set up as follows. The FE model of the Maison du Mexique is limited to the main structural parts. Only the columns, beams and floors of the reinforced-concrete frame structure are included in the model. Two-noded beam elements are used for the columns and the beams. Four-noded quadrilateral plate elements are used for the floor slabs. The FE model has 64308 Degrees Of Freedom (DOFs). The foundation is modelled by 16 rigid foundation plates (one for each column), which constitute the interface between the soil and the building. The displacements of the foundation are decomposed on a basis of interface modes chosen equal to the 96 rigid-body modes of the 16 plates. The basis of static transmissions into the building of the interface modes is extended with fixed-interface eigenmodes of the building. Figure 4.5 shows the 2000 lowest eigenfrequencies. Figure 4.6 shows the 2nd, 35th and 535th eigenmodes. In the frequency range between 0 and 12 Hz, global eigenmodes of longitudinal bending (1-4th), transverse bending (1-3th) and torsion (1-3th) are found. From 12 Hz to approximately 17 Hz, a high density of local first-order plate bending modes is obtained, as well as some higher-order global modes. From approximately 28 Hz, a high density of local higher-order plate bending modes is found with some high-order global modes. The 2000th eigenfrequency is 230.13 Hz.

A reduced matrix model for the groundborne vibrations in the Maison du Mexique is built using a reduction basis made of the 96 constraint modes and of n_T fixed-interface eigenmodes, which has the following form [Arnst, 2003, Arnst et al., 2006]:

$$[\boldsymbol{K} + i\omega\boldsymbol{D} - \omega^2\boldsymbol{M} + \boldsymbol{K}_S(\omega)]\boldsymbol{q}_{n_T}(\omega) = \boldsymbol{f}_S(\omega)\,, \quad \omega \in B \quad , \tag{4.1}$$

$$\boldsymbol{u}_h(\omega) = \boldsymbol{T}_{n_T}\boldsymbol{q}_{n_T}(\omega). \tag{4.2}$$

The matrices $\boldsymbol{K}$ and $\boldsymbol{D}$ are the positive semi-definite reduced stiffness and damping matrices and $\boldsymbol{M}$ is the positive definite reduced mass matrix of the building. For a fixed circular frequency ω, the matrix $\boldsymbol{K}_S(\omega)$ is the dynamic soil impedance matrix, $\boldsymbol{f}_S(\omega)$ is the vector of the generalized forces (the virtual work on the interface modes generated by the tractions induced by the incident wave field on a fixed foundation), $\boldsymbol{q}_{n_T}(\omega)$ is the vector of the generalized coordinates and $\boldsymbol{u}_h(\omega)$ collects the FE DOFs of the building. The rectangular matrix $\boldsymbol{T}_{n_T}$ is the transformation matrix of the reduction basis.

Predicted deterministic TFs

The predicted deterministic TFs are obtained in two steps. First, the dynamic track-tunnel-soil interaction model is used to compute the wave field radiated by the tunnel into the soil due to the application

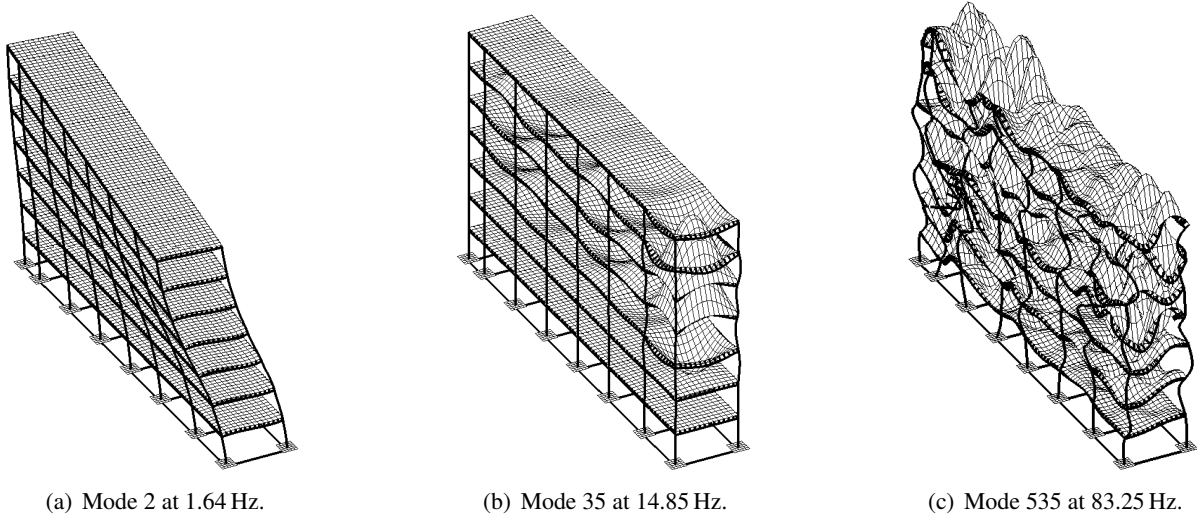(a) Mode 2 at 1.64 Hz. (b) Mode 35 at 14.85 Hz. (c) Mode 535 at 83.25 Hz.

Figure 4.6: Ground-borne vibrations in the Maison du Mexique: (a) first-order global torsion and transverse-bending mode, (b) first-order local plate bending mode and (c) higher-order local plate bending mode.

of a unitary vertical excitation on the rail head at the point with coordinates ($x_1' = -2.5$ m, $x_2' = 0$, $x_3' = -8.2$ m). Subsequently, the model (4.4)-(4.5) is used to compute the building response due to this incident wave field.

Figure 4.7(a) shows the amplitude of the vertical component of the incident wave field at the point with coordinates ($x_1 = -0.5$ m, $x_2 = 26.5$ m, $x_3 = -4$ m) located in the soil directly under the foundation plate under the column C1 (that is located right next to the position BA01). Figure 4.7(b) shows the 9th entry of the vector $\boldsymbol{f}_S(\omega)$ of the generalized forces in (4.4)-(4.5), which is the virtual work on the pumping mode of the foundation plate under the column C1 generated by the tractions induced by the incident wave field on a fixed foundation. At frequencies between about 20 and 30 Hz, an energy loss of the incident wave field is observed, which results in a consequent drop in the virtual work. Figure 4.8 compares the estimated noise-free TFs to the predicted TFs (computed using $n_T = 1500$ eigenmodes) at BA01 and F0PL. At the frequencies for which the coherence function is large (Fig. 4.4), i.e. for which the experimental data are not too distorted by noise, the predicted TFs are generally in reasonable agreement with the estimated noise-free TFs. At BA01, the model is not in good agreement with the data at frequencies between about 20 and 30 Hz. The energy loss in the computed incident wave field results in a drop of the amplitude of the predicted building response, which does not occur in the measured response.

Harmonic response of the tunnel, the soil and the building

Figure 4.9 shows the harmonic response of the tunnel, the soil and the building at the frequencies 15 Hz and 60 Hz due to a vertical excitation on the rail head at the point with coordinates ($x_1' = -2.5$ m, $x_2' = 0$, $x_3' = -8.2$ m). At low-frequencies, the building response is mainly governed by global low-order bending and torsion and by first-order local plate bending of the slabs. At higher frequencies, the building response is mainly governed by local plate bending of the slabs and also by global higher-order bending and torsion.
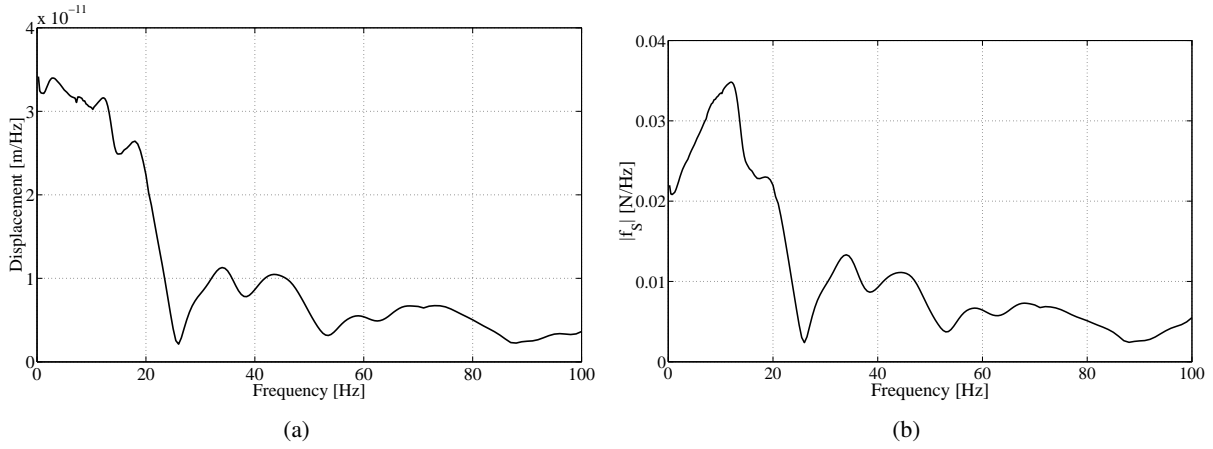
(a)

(b)

Figure 4.7: Ground-borne vibrations in the Maison du Mexique: (a) amplitude of the incident wave field at point $(x_1 = -0.5\,\text{m}, \ x_2 = 26.5\,\text{m}, \ x_3 = -4\,\text{m})$ and (b) amplitude of the 9th entry of the vector $\boldsymbol{f}_\text{S}(\omega)$.
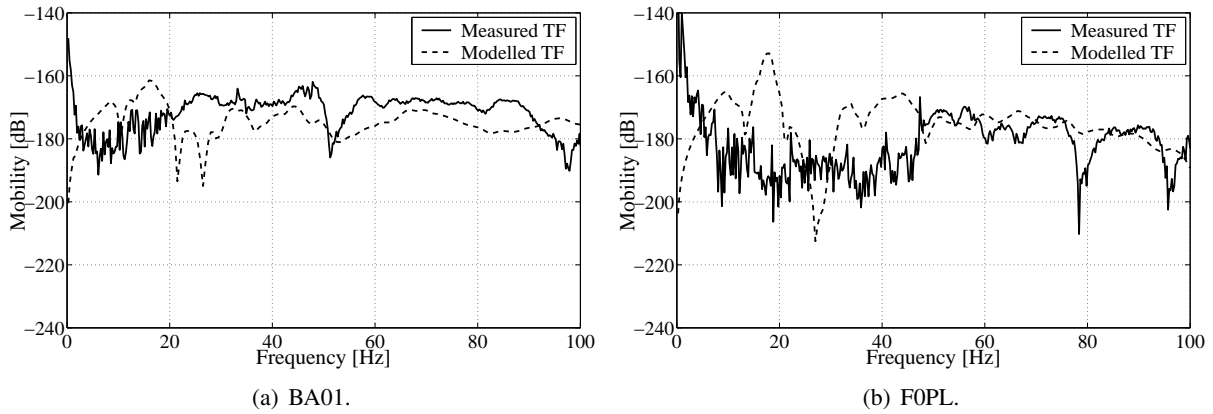

(a) BA01.

(b) F0PL.

Figure 4.8: Ground-borne vibrations in the Maison du Mexique: amplitude of the TF predicted by the deterministic model (dashed line) and the estimated noise-free TF (solid line) at (a) BA01 and (b) F0PL.

Transient response of the tunnel, the soil and the building

Figures 4.10 and 4.11 show the transient response of the tunnel, the soil and the building due to a hammer impact on the rail head in the point with coordinates $(x'_1 = -2.5\,\text{m}, \ x'_2 = 0, \ x'_3 = -8.2\,\text{m})$. The impact force is modelled in the time domain by means of a very narrow Gaussian-shaped function

$$f(t) = -\exp\left(-\frac{(t-t_0)^2}{T^2}\right) \quad , \tag{4.3}$$

where the parameters are chosen equal to t_0=0.1 s and T=0.0025 s. Figure 4.10 shows three snapshots of the displacements of the tunnel and the soil. After the impact, a fast wavefront of vertical upward displacements is seen to propagate away from the tunnel, immediately followed by a strong wavefront of vertical downward displacements. The fast wavefront is made up of body waves that are generated by the bottom plate of the tunnel and propagate essentially in the fast soil halfspace. The strong wavefront is the fundamental surface wave (the generalized Rayleigh wave) of the soil layering. Figure 4.11 shows six

103

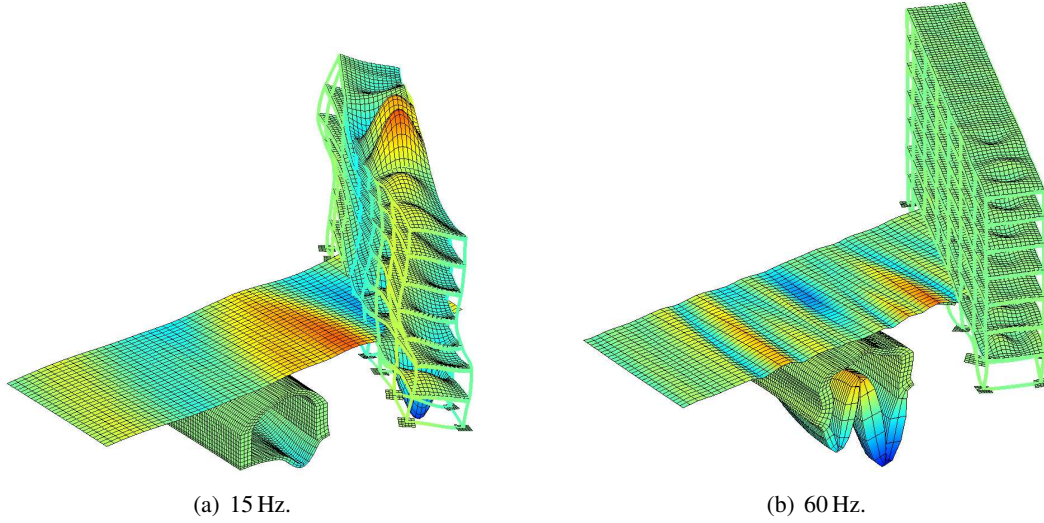(a) 15 Hz.   (b) 60 Hz.

Figure 4.9: Ground-borne vibrations in the Maison du Mexique: harmonic response at (a) 15 Hz and (b) 60 Hz (the colour is proportional to the vertical displacement; the colour scale is 10 times more sensitive for the soil).

snapshots of the displacements of the soil and the building. Both global bending and torsion eigenmodes of the whole building and local plate bending eigenmodes are observed to be excited by the incident wave field.

4.3.2 Probabilistic modelling

A non-parametric probabilistic model, associated to the deterministic model (4.4)-(4.5), is built:

$$[\mathbb{K}(\boldsymbol{p}) + i\omega\mathbb{D}(\boldsymbol{p}) - \omega^2\mathbb{M}(\boldsymbol{p}) + \boldsymbol{K}_{\mathrm{S}}(\omega)]\mathbb{Q}_{n_{\mathrm{T}}}(\omega;\boldsymbol{p}) = \boldsymbol{f}_{\mathrm{S}}(\omega) \text{ a.s.,} \quad \omega \in B \quad , \tag{4.4}$$

$$\mathbb{U}_{\mathrm{h}}(\omega;\boldsymbol{p}) = \boldsymbol{T}_{n_{\mathrm{T}}}\mathbb{Q}_{n_{\mathrm{T}}}(\omega;\boldsymbol{p}) \text{ a.s.} \tag{4.5}$$

The reduced stiffness, damping and mass matrices of the building are modelled by the random matrices $\mathbb{K}(\boldsymbol{p})$, $\mathbb{D}(\boldsymbol{p})$ and $\mathbb{M}(\boldsymbol{p})$, respectively, parameterized by $\boldsymbol{p}$. The dynamic soil impedance matrix and the vector of the generalized forces are kept deterministic.

The mean values of the random reduced matrices are chosen equal to their deterministic counterparts in model (4.4)-(4.5), i.e.:

$$E\{\mathbb{K}(\boldsymbol{p})\} = \boldsymbol{K} , \quad E\{\mathbb{D}(\boldsymbol{p})\} = \boldsymbol{D} , \quad E\{\mathbb{M}(\boldsymbol{p})\} = \boldsymbol{M}. \tag{4.6}$$

Hence, there are no mean-model parameters, i.e. $\boldsymbol{p}_0 = \emptyset$, and the random matrices $\mathbb{K}(\boldsymbol{p})$, $\mathbb{D}(\boldsymbol{p})$ and $\mathbb{M}(\boldsymbol{p})$ are parameterized solely by their respective dispersion parameters δ_{K}, δ_{D} and δ_{M}. For the sake of simplicity, it is assumed that $\delta_{\mathrm{K}} = \delta_{\mathrm{D}} = \delta_{\mathrm{M}} = \delta$, such that $\boldsymbol{p} = \{\delta\}$ is the only active parameter of the probabilistic model.

4.3.3 Computations with the probabilistic model

As already mentioned, a coupled FE-BE formulation is used for the spatial discretization. The FE computations are performed in Matlab using the Structural Dynamics Toolbox [Balmès and Leclère, 2006].
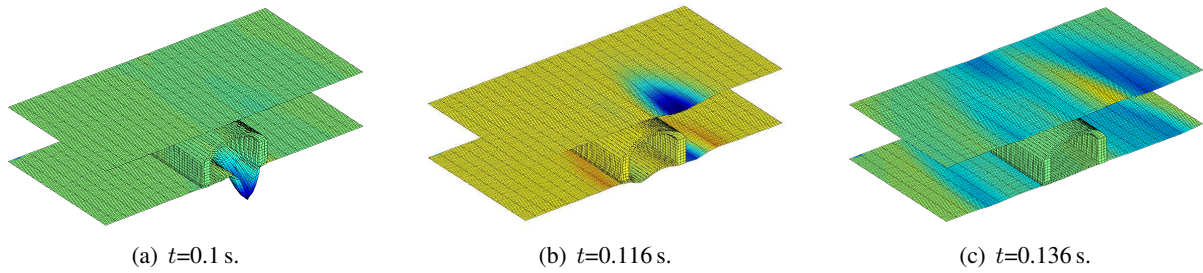
(a) t=0.1 s. (b) t=0.116 s. (c) t=0.136 s.

Figure 4.10: Ground-borne vibrations in the Maison du Mexique: transient response at times (a) t=0.1 s (moment of impact), (b) t=0.116 s and (c) t=0.136 s (the colour is proportional to the vertical displacement; the colour scale is 10 times more sensitive for the soil).
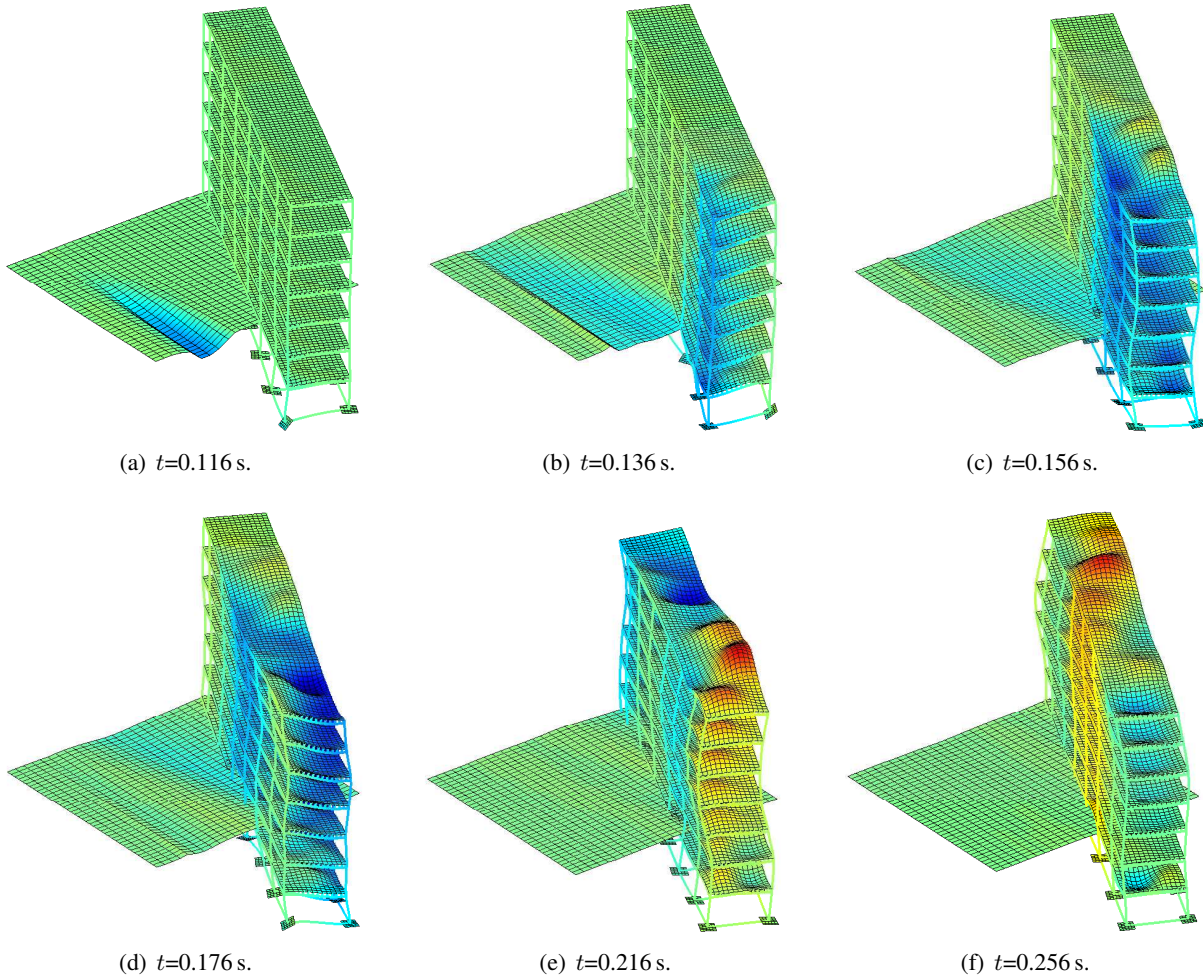

(a) t=0.116 s. (b) t=0.136 s. (c) t=0.156 s.

(d) t=0.176 s. (e) t=0.216 s. (f) t=0.256 s.

Figure 4.11: Ground-borne vibrations in the Maison du Mexique: transient response at times (a) t=0.116 s, (b) t=0.116 s, (c) t=0.136 s, (d) t=0.156 s, (e) t=0.216 s and (f) t=0.256 s (the colour is proportional to the vertical displacement).

The BE computations are performed using the program MISS3D [Clouteau, 2005]. The Monte Carlo Simulation (MCS) method is applied to discretize the random dimension.

4.3.4 Random matrix eigenvalue problem

Let the reduced stiffness and mass matrices of the deterministic model (4.1)-(4.2) be block-decomposed, separating the generalized coordinates related to the fixed-interface eigenmodes from those associated to the static-transmission modes:

$$
\boldsymbol{K} = \begin{bmatrix} \boldsymbol{K}_0 & \boldsymbol{0} \\ \boldsymbol{0} & \boldsymbol{K}_\Sigma \end{bmatrix} \;, \quad \boldsymbol{M} = \begin{bmatrix} \boldsymbol{M}_0 & \boldsymbol{M}_c \\ \boldsymbol{M}_c^T & \boldsymbol{M}_\Sigma \end{bmatrix}. \tag{4.7}
$$

In this block-decomposition, the square matrices $\boldsymbol{K}_0, \boldsymbol{M}_0 \in \mathrm{M}_{n_T}^+(\mathbb{R})$ are the projection of the FE stiffness and mass matrices of the building onto the n_T fixed-interface eigenmodes, while the square matrices $\boldsymbol{K}_\Sigma \in \mathrm{M}_{96}^{+0}(\mathbb{R})$ and $\boldsymbol{M}_\Sigma \in \mathrm{M}_{96}^+(\mathbb{R})$ are their projection onto the 96 static-transmission modes. The rectangular mass coupling matrix $\boldsymbol{M}_c$ is in $\mathrm{M}_{n_T \times 96}(\mathbb{R})$. Let $\mathbb{K}_0(\delta)$ and $\mathbb{M}_0(\delta)$ then be random reduced stiffness and mass matrices such that:

$$
\mathbb{K}_0(\delta) = \boldsymbol{L}_K^T \mathbb{N}_K(\delta) \boldsymbol{L}_K \text{ a.s. }, \quad \mathbb{M}_0(\delta) = \boldsymbol{L}_M^T \mathbb{N}_M(\delta) \boldsymbol{L}_M \text{ a.s. } , \tag{4.8}
$$

where $\mathbb{N}_K(\delta)$ and $\mathbb{N}_M(\delta)$ are normalized random matrices in the set SG^+, defined in Section 1.1, and $\boldsymbol{L}_K$ and $\boldsymbol{L}_M$ are the Cholesky factors of $\boldsymbol{K}_0$ and $\boldsymbol{M}_0$, respectively.
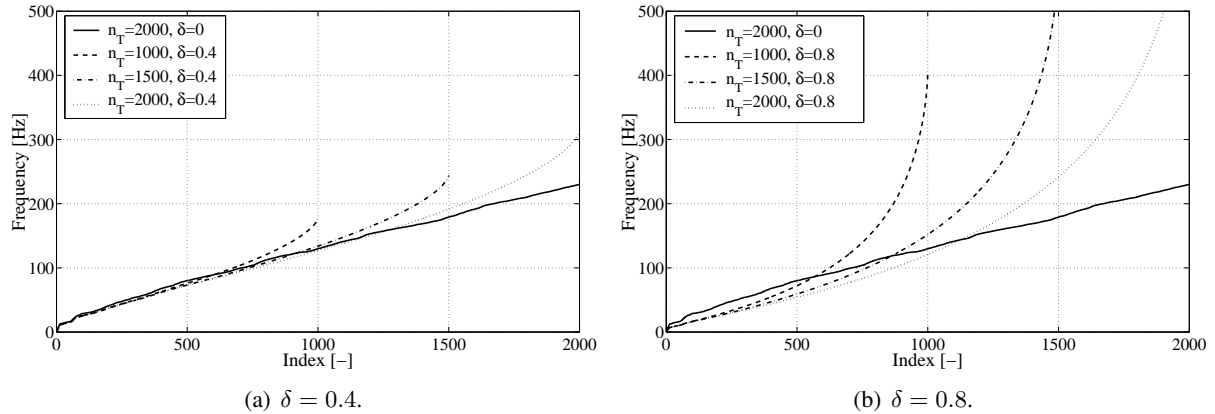

Figure 4.12: Ground-borne vibrations in the Maison du Mexique: 2000 lowest deterministic eigenfrequencies of the mean model, and mean of the random eigenfrequencies for (a) δ=0.4 and (b) δ=0.8 for $n_T = 1000$, $n_T = 1500$ and $n_T = 2000$.

The random matrix eigenvalue problem (App. B) defined by $\mathbb{K}_0(\delta)$ and $\mathbb{M}_0(\delta)$ is now analyzed. First, the stochastic properties of the eigenfrequencies as a function of the dispersion level δ and the number n_T of eigenmodes are studied. Figure 4.12 shows the mean value (computed using $n_S = 400$ Monte Carlo simulations) of the random eigenfrequencies for $\delta = 0.4$ and $\delta = 0.8$ for n_T=1000, 1500 and 2000. Like in Section 3.3, for fixed δ and n_T, the mean values of the low random eigenfrequencies (approximately the lowest $n_T/2$) are observed to be smaller than the deterministic values, while the mean values of the high random eigenfrequencies (approximately the highest $n_T/2$) are observed to be larger. The difference between the mean of the random eigenfrequencies and the deterministic eigenfrequencies is seen to

(a) Eigenmode 4.

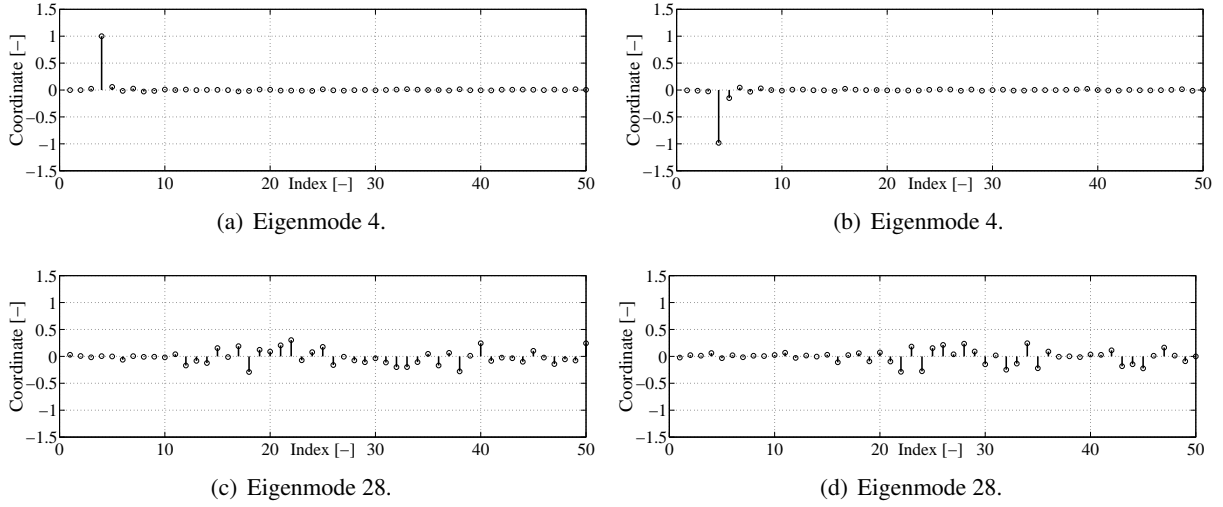(b) Eigenmode 4.

(c) Eigenmode 28.

(d) Eigenmode 28.

Figure 4.13: Ground-borne vibrations in the Maison du Mexique: entries 1 to 50 of two realizations of the (a, b) 4th and the (c, d) 28th random eigenvector for $\delta = 0.8$.

increase with δ. For the eigenfrequencies lower than 100 Hz, reasonable convergence is obtained for $n_T = 1500$. In the following, all computations are performed with $n_T = 1500$ eigenmodes.

Figure 4.13 shows the entries 1 to 50 of two realizations of the 4th (global second-order bending of the whole building) and the 28th (local first-order plate bending) random eigenvector for $\delta = 0.8$. With reference to equation (B.4), it is seen that, at low frequencies, where global bending and torsion modes of the whole building are found and the eigenfrequency separation is relatively large, the global eigenmodes are only slightly modified by perturbations of the mass and stiffness. At higher frequencies, where densely packed clusters of local plate bending eigenmodes are found, perturbations of the mass and stiffness significantly modify the local eigenmodes.

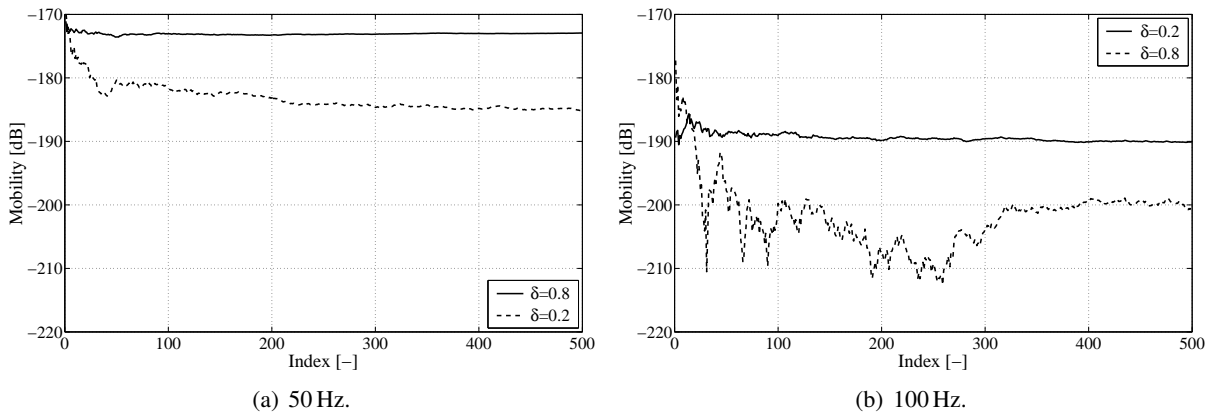### 4.3.5 Predicted random TFs

(a) 50 Hz.

(b) 100 Hz.

Figure 4.14: Ground-borne vibrations in the Maison du Mexique: statistical mean of the realizations of the predicted random TF at F0PL for $\delta = 0.2$ and $\delta = 0.8$ at frequencies (a) 50 Hz and (b) 100 Hz.

The predicted random TFs are obtained in two steps. First, the (still deterministic) dynamic track-tunnel-soil interaction model is used to compute the wave field radiated by the tunnel into the soil due to the application of a unitary vertical excitation on the rail head at the point with coordinates ($x'_1 = -2.5\,\text{m}$, $x'_2 = 0$, $x'_3 = -8.2\,\text{m}$). Subsequently, the model (4.4)-(4.5) is used to compute the random building response due to this incident wave field.

Figure 4.14 shows, as a function of the number n_S of Monte Carlo simulations, the statistical mean of the realizations of the predicted random TF at F0PL for the dispersion levels $\delta = 0.2$ and $\delta = 0.8$ at the frequencies 50 Hz and 100 Hz. Reasonably converged results are obtained for $n_\text{S} = 400$, and this value is used for all subsequent computations.
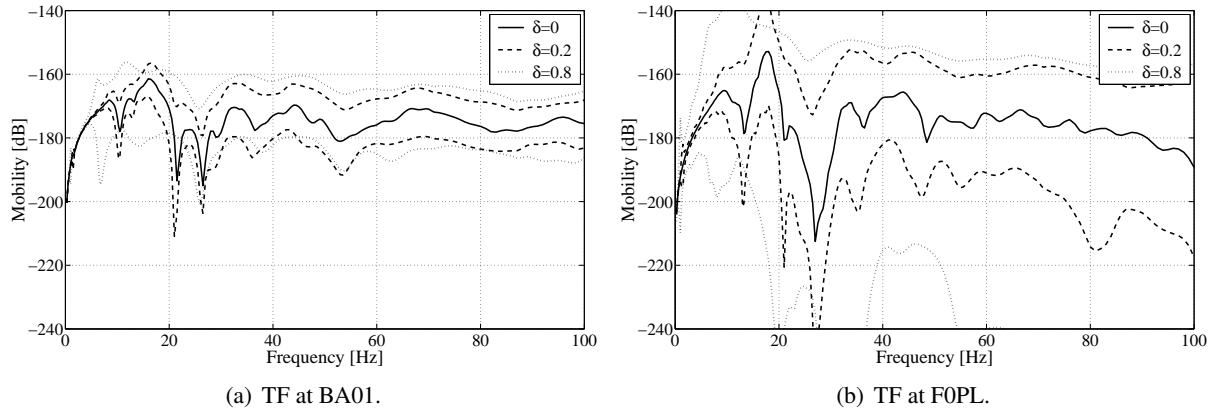

(a) TF at BA01. (b) TF at F0PL.

Figure 4.15: Ground-borne vibrations in the Maison du Mexique: amplitude of the TF predicted by the mean model, and 99%-confidence regions for the random TF for $\delta = 0.2$ and $\delta = 0.8$ at (a) BA01 and (b) F0PL.

Figure 4.15 shows the 99%-confidence regions (Box 2.3 in Section 2.6) for the predicted random TFs at BA01 and F0PL for $\delta = 0.2$ and $\delta = 0.8$. Their width is observed to increase with δ and also with the frequency, highlighting that the predictions become more sensitive to uncertainties as the frequency increases. At the floor slabs of the building, where the response is governed by local plate bending modes, the confidence regions are very wide, even for small values of δ. The sensitivity of the local eigenmodes to uncertainties in the mass and stiffness results in a large sensitivity of the medium-frequency response to uncertainties.

4.4 Stochastic inverse problem

The methodology proposed in Section 2.6 is now applied to invert the probabilistic model.

4.4.1 Identification of the probabilistic model

Figure 4.16 shows the distances $\mathcal{L}^{(1)}_{n_\text{F},n_\text{R}}(\delta; \boldsymbol{D})$ and $\mathcal{J}^{(1)}_{n_\text{F},n_\text{R}}(\delta; \boldsymbol{D})$, defined in (2.40) and (2.44), as a function of the dispersion level δ (these distances have been computed using a probabilistic for the experimental noise, built as proposed in Section 1.4). The probabilistic structural model with the dispersion level $\hat{\delta} = 0.8$ is seen to be optimal for both distances.
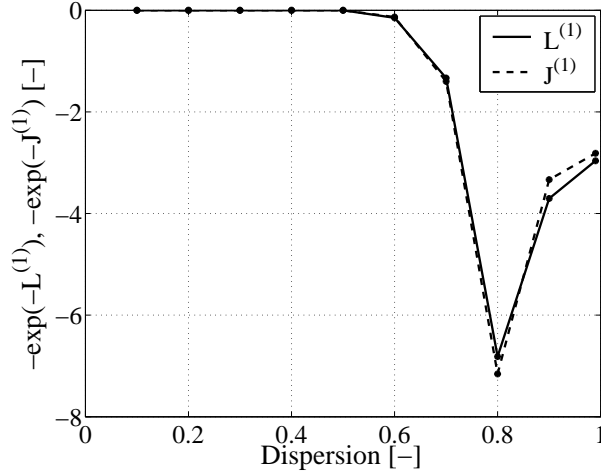
Figure 4.16: Ground-borne vibrations in the Maison du Mexique: distances $\mathcal{L}_{n_{\mathrm{F}},n_{\mathrm{R}}}^{(1)}(\delta;\boldsymbol{D})$ and $\mathcal{J}_{n_{\mathrm{F}},n_{\mathrm{R}}}^{(1)}(\delta;\boldsymbol{D})$ as a function of δ.

4.4.2 *A posteriori* error estimation

Figure 4.17 shows the sign-reversed loglikelihood of, and the relative entropy for, $\hat{\delta} = 0.8$ as a function of the frequency. Figures 4.18 and 4.19 compare the 99%-confidence region for the identified predicted random TF to the estimate of the noise-free TF at BA01 and F0PL. At the frequencies for which the coherence function is large (Fig. 4.4), the sign-reversed loglikelihood and the relative entropy are large whenever the estimates of the noise-free TFs do not lie within, or nearly lie within, the confidence bounds. At frequencies between about 20 and 30 Hz, the agreement of the identified model with the data is unsatisfactory at BA01. This discrepancy is clearly due to the aforementioned energy loss in the computed incident wave field (Sec. 4.3.1). For this reason, it does not seem appropriate to attempt to mitigate this discrepancy by endowing the probabilistic model with mean-model parameters. Instead, a first possible step that could be taken is to modify the dynamic track-tunnel-soil interaction model so as to bring the computed incident wave field into agreement with the experimental data. Another possibility is to introduce uncertainty in the incident wave field, or, equivalently, in the vector of the generalized forces in (4.4)-(4.5). Such adaptations are not addressed in this thesis and are left as a direction for future work.

4.4.3 Predictive use of the identified probabilistic model

Even though the identification of the probabilistic model was not fully successful, the predictive capability of the identified model is now examined. Figure 4.20 compares the 99%-confidence region for the random TF predicted by the identified probabilistic model to the estimate of the noise-free TF at BA03 and F201. At the frequencies for which the coherence function is large (Fig. 4.4), the estimate of the noise-free TF is seen to lie within the confidence bounds, excepting a very small discrepancy at BA03 at about 90 Hz. It should be noted that the results for F201 are not very conclusive since the measured response at F201 is very noisy.
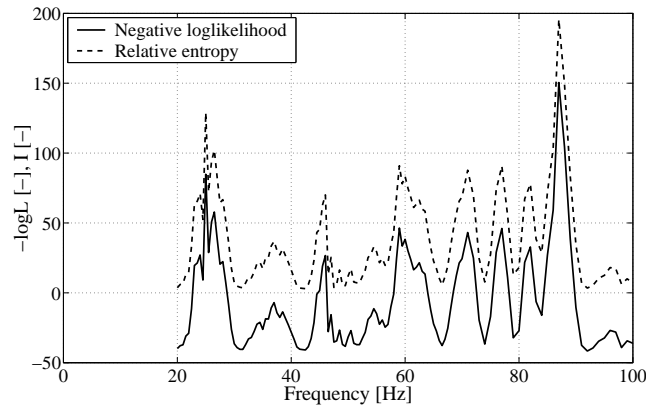
Figure 4.17: Ground-borne vibrations in the Maison du Mexique: sign-reversed loglikelihood (solid line) and relative entropy (dashed line) of $\hat{\delta} = 0.8$ as a function of the frequency.

Figure 4.18: Ground-borne vibrations in the Maison du Mexique: amplitude of the estimated noise-free TF (solid line) and 99%-confidence bounds for the identified random TF (grey patch) at BA01.

Figure 4.19: Ground-borne vibrations in the Maison du Mexique: amplitude of the estimated noise-free TF (solid line) and 99%-confidence bounds for the identified random TF (grey patch) at BA01.
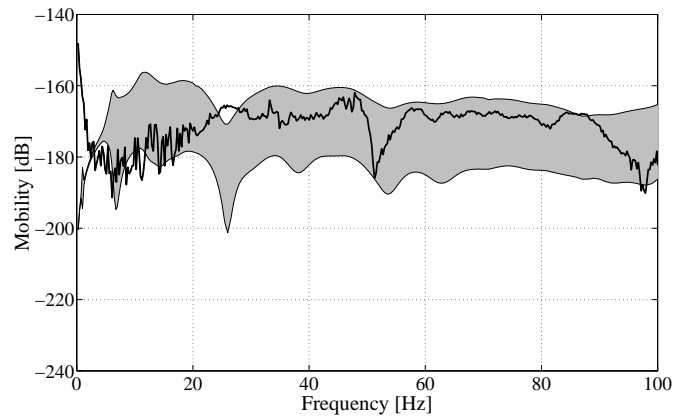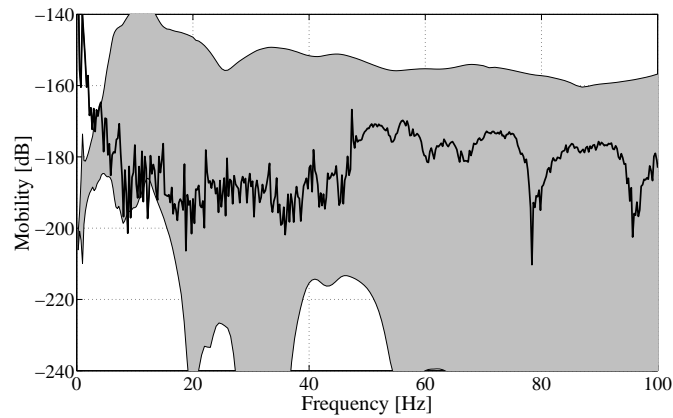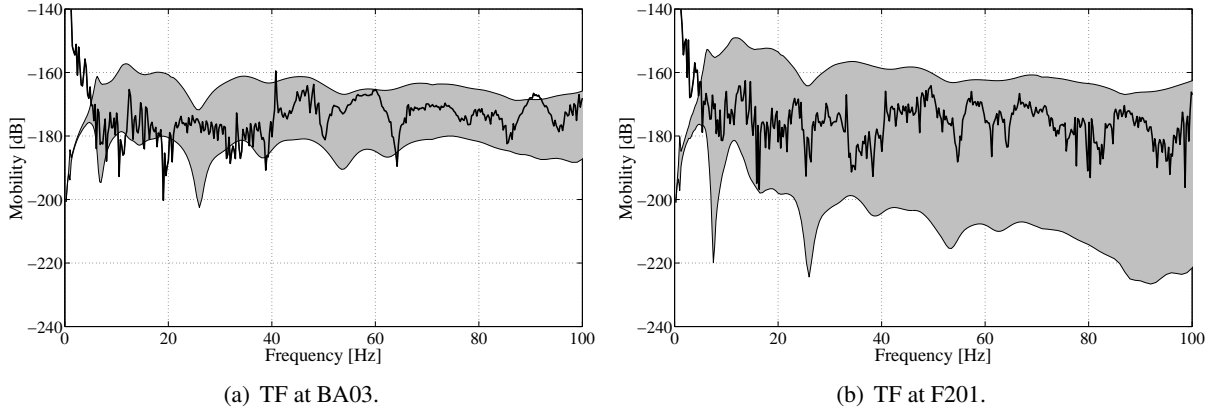
(a) TF at BA03.

(b) TF at F201.

Figure 4.20: Ground-borne vibrations in the Maison du Mexique: amplitude of the estimated noise-free TF (solid line) and 99%-confidence bounds for the identified random TF (grey patch) at (a) BA03 and (b) F201.

4.5   Summary and conclusion

In this chapter, a civil and environmental engineering case history was presented, which involved the inversion of a non-parametric probabilistic model using real experimental data. The inverse methods based on the minimization of the distances $\mathcal{L}^{(1)}$ and $\mathcal{J}^{(1)}$ were found to lead to similar results in that, in this particular example, the same dispersion level was found to be optimal in the sense of the two distances. The application of the inversion procedure was not fully successful. In the basement, where the magnitude of the predicted dynamical response depends strongly on the computed incident wave field, the fit of the identified model to the experimental data was found to be unsatisfactory at certain frequencies. On the slabs, where the dynamical response is made up of densely packed clusters of local plate bending eigenmodes and is therefore very sensitive to uncertainties, the identified model leads to very wide confidence regions, within which the actual TFs of the coupled track-tunnel-soil-building system can be expected to lie.

In the case history, the soil impedance matrix was kept deterministic. The probabilistic modelling of the impedance matrix [Cottereau, 2007] is a natural direction for future work. Furthermore, in the frame of the CONVURT project, the dynamic track-tunnel-soil interaction model has recently been coupled to a source model, which allows to compute the moving loads applied on the rail heads in the tunnel due to passing trains. Moreover, the dynamic soil-building interaction model has been coupled to a vibroacoustic model, which allows to compute the reradiated noise in the building induced by the structural vibration [Gupta et al., 2006]. A second direction for future work is to quantify the uncertainty in the predictions of this model.

5

Inversion of a probabilistic model of heterogeneous bars

This chapter presents an example of the inversion of a parametric probabilistic model aimed at quantifying aleatory uncertainty using simulated data.
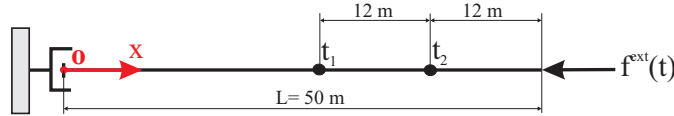
5.1 Problem setting

Figure 5.1: Heterogeneous bars: schematic representation.

Let us consider a *collection* of similar, but not perfectly identical, bars of equal length $L = 50$ m and of equal and position-invariant cross-sectional area $A = 1 \, \mathrm{m}^2$ (fig. 5.1). Let all bars be constituted of a heterogeneous, locally isotropic, linear, visco-elastic material with equal and homogeneous mass density $\rho = 2500 \, \mathrm{kg/m}^3$ and viscosity modulus $\zeta = 2 \times 10^8 \, \mathrm{Pa\,s}$. Let the field giving the Young's modulus as a function of the position be heterogeneous and exhibit statistical variability. Finally, let the mean Young's modulus field be homogeneous and equal to $\underline{E} = 27 \times 10^9$ Pa. The example concerns the experimental identification of a spatial correlation length and a dispersion level characterizing the variability in the Young's modulus field.

In the following, we will propose a methodology that uses the dispersive characteristics of mechanical waves travelling through heterogeneous specimens to infer the spatial correlation length and the dispersion level. More specifically, to obtain an experimental data set, a subset of bars out of the entire collection will be loaded by a broadband time-limited concentrated axial load $t \mapsto f^{\mathrm{ext}}(t)$ at the right end point ($x = 50$ m), while being supported by a damper with impedance $\mu = \rho\sqrt{\underline{E}/\rho}$ at the left end point ($x = 0$), so as to absorb outgoing waves. The axial response will be measured at two points $\boldsymbol{t}_1(x = x_{\boldsymbol{t}_1} = 26 \, \mathrm{m})$ and $\boldsymbol{t}_2(x = x_{\boldsymbol{t}_2} = 38 \, \mathrm{m})$ (fig. 5.1). For each tested specimen, the time-dependent observed responses will be transformed to a frequency-dependent phase velocity using Nazarian's method (App. D). Upon building a parametric probabilistic structural model to predict the frequency-dependent phase velocities as a function of the spatial correlation length and the dispersion

113

level to be identified, the inverse problem will be formulated as an optimization problem following the methodology proposed in Section 2.7.

It should be noted that the present problem is elaborated with future extensions in mind. In particular, the application of the methodology to the identification of random field models for elastic material properties of heterogeneous soils is envisaged. Considering that it is presently difficult to adequately model the amplitude decay with the propagation distance due to the material damping of the soil (insofar as we can judge it, the construction of adequate models for the material damping of soils is still a largely open problem), it seems useful to base the identification only on the dispersive characteristics of the observed waves and not on the amplitude characteristics. Furthermore, a time-domain algorithm will be used in the following to numerically simulate the wave propagation, which counts among its advantages the applicability to very large computational domains, including large soil deposits (App. E).

5.2 Probabilistic structural model

A time-domain parametric probabilistic model (App. A) for the dynamical behaviour of the heterogeneous bars is now built and studied.

5.2.1 Deterministic modelling

This subsection first gives the deterministic equations governing the time-domain dynamical behaviour. Subsequently, the variational formulation of these equations is presented.

Deterministic strong formulation

Let $[0, T]$ be the time interval of analysis, where $T \in \mathbb{R}_0^+$. Let the Young's modulus field be modelled by the strictly positive and essentially bounded function $x \mapsto E(x)$. The deterministic strong formulation of the Boundary Value Problem (BVP) then consists in finding the position- and time-dependent response field $(x; t) \mapsto u(x; t)$ such that:

$$\frac{\partial}{\partial x} \left(E \frac{\partial u}{\partial x} \right) + \zeta \frac{\partial^3 u}{\partial x^2 \partial t} = \rho \frac{\partial^2 u}{\partial t^2} \qquad \text{in }]0, L[\times]0, T[\quad , \qquad (5.1)$$

with the boundary conditions:

$$E \frac{\partial u}{\partial x} = \mu \frac{\partial u}{\partial t} \qquad \text{at } x = 0 \text{ for } t \in]0, T[\quad , \qquad (5.2)$$

$$AE \frac{\partial u}{\partial x} = f^{\text{ext}} \qquad \text{at } x = L \text{ for } t \in]0, T[\quad , \qquad (5.3)$$

and the initial conditions:

$$u(x; 0) = 0 \qquad \text{in }]0, L[\quad , \qquad (5.4)$$

$$\frac{\partial u}{\partial t}(x; 0) = 0 \qquad \text{in }]0, L[. \qquad (5.5)$$

Deterministic variational formulation

Let $V = \{v \in H^1(]0, L[, \mathbb{R})\}$. The deterministic variational formulation of the BVP consists in finding the sufficiently regular (App. A) position- and time-dependent response field $t \mapsto u(x; t)$ with values in V such that $\forall v \in V$:

$$k\left(u(t), v\right) + d\left(u'(t), v\right) + m\left(\frac{du'}{dt}(t), v\right) = f(t; v), \quad \text{a.e. } t \in [0, T] \quad, \tag{5.6}$$

fulfilling the initial conditions (5.4)-(5.5). The stiffness, damping and mass forms are bilinear forms defined by:

$$k(v_1, v_2) = \int_0^L E \frac{\partial v_1}{\partial x} \frac{\partial v_2}{\partial x} dx \quad, \tag{5.7}$$

$$d(v_1, v_2) = \int_0^L \zeta \frac{\partial w_1}{\partial x} \frac{\partial w_2}{\partial x} dx + \mu v_1(0) v_2(0) \quad, \tag{5.8}$$

$$m(v_1, v_2) = \int_0^L \rho v_1 v_2 dx. \tag{5.9}$$

The linear form representing the external force is defined by:

$$f(v; t) = f^{\text{ext}}(t) v(L). \tag{5.10}$$

When $t \mapsto f^{\text{ext}}(t)$ is square-integrable, it can be shown [Dautray and Lions, 1987, ch. 18 sec. 5] that the variational formulation (5.4)-(5.5)-(5.6) is mathematically well-posed.

5.2.2 Probabilistic modelling

A time-domain parametric probabilistic model is now built by modelling the Young's modulus field in the variational formulation (5.4)-(5.5)-(5.6) by a random field.

Stochastic model for the random Young's modulus field

We follow Soize's principle of construction, which was outlined in Section 1.1, and model the Young's modulus field by the random field $\{\mathbb{E}(x; L_{\mathbb{G}}; \delta) \mid x \in]0, L[\}$ indexed by $]0, L[$ and with values in $\mathbb{R}_0^+$ a.s. such that:

$$\left(\forall x \in]0, L[: \mathbb{E}(x; L_{\mathbb{G}}; \delta) = \underline{E} \, N\left(\mathbb{G}(x; L_{\mathbb{G}}); \delta\right)\right) \text{ a.s.} \quad, \tag{5.11}$$

where $L_{\mathbb{G}}$ is the spatial correlation length of the stochastic germ and δ is the dispersion level. The stochastic germ $\{\mathbb{G}(x; L_{\mathbb{G}}) \mid x \in [0, L]\}$ is the restriction to $[0, L]$ of a sample-continuous, Gaussian, zero mean, unit variance, stationary random field $\{\mathbb{G}(x; L_{\mathbb{G}}) \mid x \in \mathbb{R}\}$ with values in $\mathbb{R}$ a.s. and with power spectral density function $k \mapsto S_{\mathbb{G}}(k; L_{\mathbb{G}})$ such that:

$$S_{\mathbb{G}}(k; L_{\mathbb{G}}) = \frac{L_{\mathbb{G}}}{\pi} \Delta\left(\frac{k L_{\mathbb{G}}}{\pi}\right) \quad, \tag{5.12}$$

where $\Delta(\cdot)$ is the triangle function, defined in (1.77). The function $N(\cdot; \delta) : \mathbb{R} \to \mathbb{R}_0^+$ is the transformation function defined in Box 1.4 of Section 1.2 and is such that, for each $x \in [0, L]$, $N(\mathbb{G}(x; L_{\mathbb{G}}); \delta)$ is a gamma random variable with unit mean and standard deviation δ.

Parametric probabilistic model

The parametric probabilistic model then consists in finding the sufficiently regular (App. A) second-order stochastic process $\{\mathbb{U}(t; L_{\mathbb{G}}, \delta) \mid t \in [0, T]\}$ indexed by $[0, T]$ and with values in V such that:

$$\left(\mathbb{K}\big(\mathbb{U}(t; L_{\mathbb{G}}, \delta), v; L_{\mathbb{G}}, \delta\big) + d\big(\mathbb{U}'(t; L_{\mathbb{G}}, \delta), v\big) + m\left(\frac{d\mathbb{U}'}{dt}(t; L_{\mathbb{G}}, \delta), v\right) = f(t; v), \text{a.e. } t \in [0, T], \forall v \in V\right) \text{ a.s.,} \tag{5.13}$$

fulfilling the initial conditions, i.e.:

$$\mathbb{U}(0; L_{\mathbb{G}}, \delta) = 0 \text{ a.s.}, \quad \mathbb{U}'(0; L_{\mathbb{G}}, \delta) = 0 \text{ a.s.} \tag{5.14}$$

The random stiffness form is defined by:

$$\mathbb{K}(v_1, v_2; L_{\mathbb{G}}, \delta) = \int_0^L \mathbb{E}(x; L_{\mathbb{G}}, \delta)\frac{\partial v_1}{\partial x}(x)\frac{\partial v_2}{\partial x}(x)dx \text{ a.s.} \tag{5.15}$$

When $t \mapsto f^{\text{ext}}(t)$ is square-integrable and the dispersion level δ fulfils the inequality (1.46), it can be shown (App. A) that the stochastic variational formulation (5.13)-(5.14) is mathematically well-posed.

5.2.3 Predicted random dispersion curves

The transformation of the predicted random time-dependent bar response into a random frequency-dependent phase velocity is now presented. Let the concentrated load $t \mapsto f^{\text{ext}}(t)$ be a Gaussian-shaped function

$$f^{\text{ext}}(t) = -\exp\left(-\frac{(t - t_0)^2}{\alpha^2}\right). \tag{5.16}$$

Let the stochastic process $\{\mathbb{V}(t; L_{\mathbb{G}}, \delta) = \mathbb{U}'(t; L_{\mathbb{G}}, \delta) \mid t \in [0, T]\}$ be the induced random time-dependent axial velocity predicted by the probabilistic model (5.13)-(5.14) (we work with the axial velocity, rather than with the axial displacement, to avoid leakage errors of the Discrete Fourier Transform (DFT) in the following). The random axial velocity at the aforedefined points t_1 and t_2 is sampled in the time domain to obtain the stochastic processes

$$\{\mathbb{V}(x_{t_1}; j\Delta t; L_{\mathbb{G}}, \delta) \mid 1 \le j \le n_{\text{T}}\}, \quad \{\mathbb{V}(x_{t_2}; j\Delta t; L_{\mathbb{G}}, \delta) \mid 1 \le j \le n_{\text{T}}\}, \tag{5.17}$$

where $\{j\Delta t \mid 1 \le j \le n_{\text{T}}\}$ is the set of n_{T} discrete time instants, such that $1/\Delta t = T/n_{\text{T}}$ is the sampling frequency. The random time-sampled axial velocities thus obtained are subsequently transformed into the frequency domain by means of the DFT to obtain the stochastic processes

$$\{\mathbb{V}(x_{t_1}; \omega_\ell; L_{\mathbb{G}}, \delta) \mid 1 \le \ell \le n_{\text{F}}\}, \quad \{\mathbb{V}(x_{t_2}; \omega_\ell; L_{\mathbb{G}}, \delta) \mid 1 \le \ell \le n_{\text{F}}\}, \tag{5.18}$$

where $\{\omega_\ell \mid 1 \le \ell \le n_{\text{F}}\}$ is the set of $n_{\text{F}} = n_{\text{T}}/2$ discrete circular frequencies, such that $\omega_\ell = 2\pi(\ell - 1)/T$. Nazarian's method (App. D) is then followed to obtain a stochastic process

$$\{\mathbb{C}(\omega_\ell; L_{\mathbb{G}}, \delta) \mid 1 \le \ell \le n_{\text{F}}\}, \tag{5.19}$$

which gathers, for each discrete frequency ω_ℓ, a random phase velocity $\mathbb{C}(\omega_\ell; L_{\mathbb{G}}, \delta)$ defined by:

$$\mathbb{C}(\omega_\ell; L_{\mathbb{G}}, \delta) = \frac{\omega_\ell \Delta L}{\phi(\omega_\ell; L_{\mathbb{G}}, \delta)} \text{ a.s.}, \tag{5.20}$$

where $\Delta L = x_{\boldsymbol{t}_2} - x_{\boldsymbol{t}_1}$ is the receiver spacing and $\oint(\omega_\ell; L_{\mathbb{G}}, \delta)$ is the random unwrapped phase shift between the two receivers:

$$\oint(\omega_\ell; L_{\mathbb{G}}, \delta) = \tan^{-1}\left(\frac{\Re\big(\mathbb{V}(x_{\boldsymbol{t}_2}; \omega_\ell; L_{\mathbb{G}}, \delta)/\mathbb{V}(x_{\boldsymbol{t}_1}; \omega_\ell; L_{\mathbb{G}}, \delta)\big)}{\Im\big(\mathbb{V}(x_{\boldsymbol{t}_2}; \omega_\ell; L_{\mathbb{G}}, \delta)/\mathbb{V}(x_{\boldsymbol{t}_1}; \omega_\ell; L_{\mathbb{G}}, \delta)\big)}\right) \text{ a.s.} \tag{5.21}$$

It should be noted that the wave field propagating in a heterogeneous bar can generally be expected to be constituted of multiple forward and backward propagating waves reflected upon, and transmitted through, the heterogeneities. Hence, the velocity obtained in (5.20) does not correspond to a single time-harmonic wave and must therefore be considered as an apparent phase velocity reflecting contributions of several waves.

Finally, the n-th order cylindrical PDF of the stochastic process (5.19) is denoted by:

$$\theta^{(n)}(\cdot|\omega_{\ell_1}, \ldots, \omega_{\ell_n}; L_{\mathbb{G}}, \delta) : \mathbb{R}^n \to \mathbb{R}^+ \quad, \tag{5.22}$$

and is defined as the joint PDF of the n random variables $\{\mathbb{C}(\omega_{\ell_1}; L_{\mathbb{G}}, \delta), \ldots, \mathbb{C}(\omega_{\ell_n}; L_{\mathbb{G}}, \delta)\}$.

5.2.4 Computations with the probabilistic model

The hp-version of the Finite Element (FE) method, more specifically the spectral element method [see, for instance, Komatitsch, 1997, Maday and Patera, 1989, Schwab, 1999], is used to discretize the space. The Newmark time integration algorithm in its central difference version [see, for instance, Géradin and Rixen, 1992, Hughes, 1987] is used to discretize time. The Monte Carlo Simulation (MCS) method is applied to discretize the random dimension. The Young's modulus random field is simulated using the spectral representation method (Box 1.5 of Section 1.2). The computations are performed in Matlab. The computer code was created from scratch by Ta [2006] in the frame of a master's thesis project.

The spectral element method involves meshing the bar using 2-noded elements of equal length h. On each element, the displacement field is approximated on a basis of (Gauss-Lobatto-based) polynomial shape functions of degree p. Convergence is achieved by diminishing h and increasing p. We apply the spectral element method in order to avoid numerical dispersion, which is the effect whereby the discretized model fails to propagate the mechanical waves at the correct speed, resulting in phase leads or lags in the FE approximation. The numerical dispersion is closely related to the so-called pollution of FE solutions, which refers to the effect whereby, upon keeping the number of elements per wavelength constant, the space discretization error increases rapidly with the wavenumber. Several studies in the literature [Ainsworth, 2004, Ihlenburg and Babuška, 1995, 1997, Oden et al., 2005, Thompson and Pinsky, 1994] showed that, by increasing p, higher-order elements control the pollution and dispersion error well.

5.2.5 Numerical illustration

The probabilistic model (5.13)-(5.14) is now used to investigate the dependence of the stochastic properties of the random phase velocities on the parameters $L_{\mathbb{G}}$ and δ of the random Young's modulus field. The parameters of the force (5.16) are chosen equal to $t_0 = 0.05\,\text{s}$ and $\alpha = 6 \times 10^{-4}\,\text{s}$. The parameters of the time-domain sampling in (5.17) are chosen equal to $\Delta t = 1/4096\,\text{s}$ and $n_{\text{T}} = 2048$. Hence, the frequency-domain resolution is $2.001\,\text{Hz}$ and the Nyquist frequency is $2048\,\text{Hz}$. The parameters of the FE discretization are set to $h = 0.5\,\text{m}$ and $p = 10$.

Figure 5.2 shows the time history and the frequency content of the force. The signal energy is seen to be negligible at frequencies above the Nyquist frequency. Most of the signal energy is distributed over the frequency band between 0 and $1500\,\text{Hz}$.
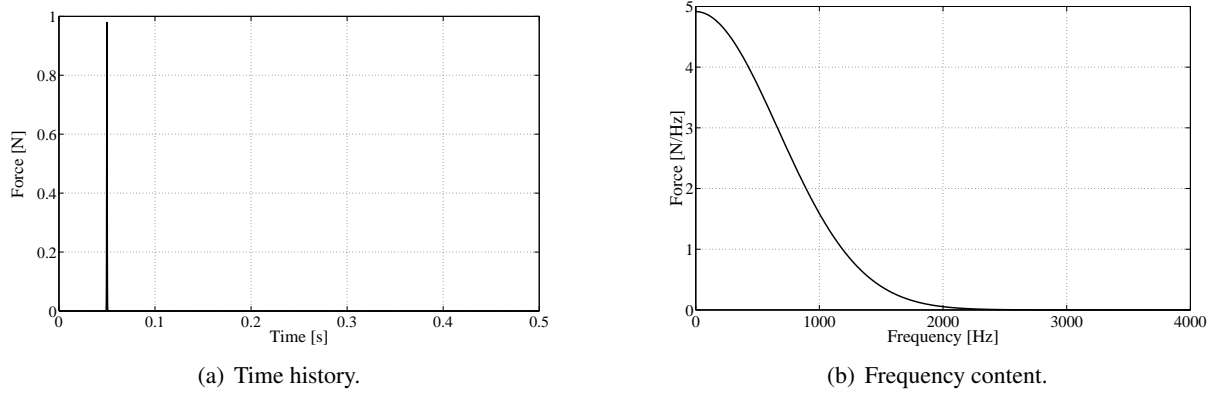
(a) Time history.

(b) Frequency content.

Figure 5.2: Heterogeneous bars: (a) time history and (b) frequency content of the external loading.
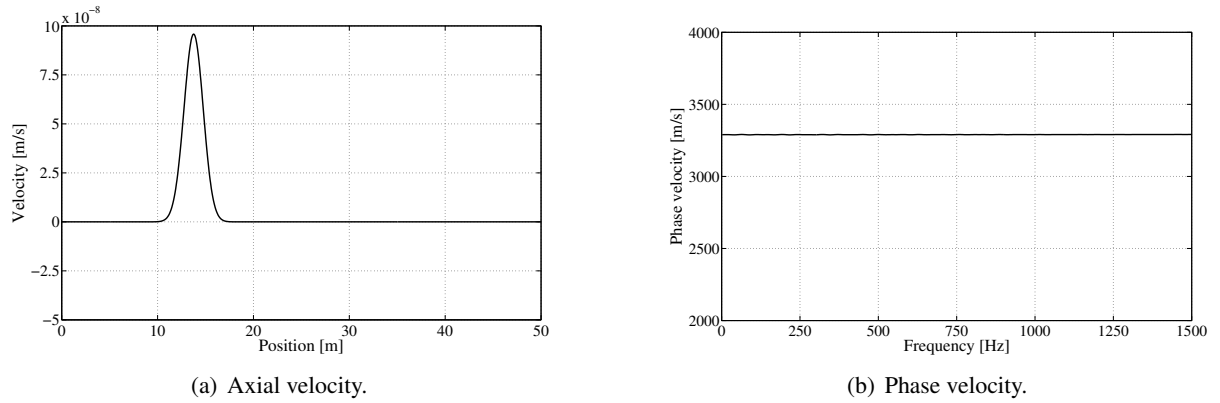

(a) Axial velocity.

(b) Phase velocity.

Figure 5.3: Heterogeneous bars: (a) axial velocity at the time instant $t = 0.061$ s and (b) phase velocity for a homogeneous bar with Young's modulus $\underline{E}$.

Let us first consider a homogeneous bar with Young's modulus $\underline{E}$. Figure 5.3(a) shows the axial velocity then obtained as a function of the position at the time instant $t = 0.061$ s. The wave field is seen to comprise a single pulse, which propagates from the left end point to the right end point. Figure 5.3(b) shows the phase velocity as a function of the frequency, obtained by transforming the axial velocities at the locations t_1 and t_2 following the methodology outlined in Section 5.2.3. The phase velocity is observed to be independent of the frequency. As expected, it is equal to the compression wave velocity $c_P = \sqrt{\underline{E}/\rho} = 3286$ m/s.

Let us subsequently consider random heterogeneous bars. Figure 5.4 shows the power spectral density function $k \mapsto S_{\mathbb{G}}(k; L_{\mathbb{G}})$ of the random field $\{\mathbb{G}(x; L_{\mathbb{G}}) \mid x \in \mathbb{R}\}$ for $L_{\mathbb{G}} = 1$ m and $L_{\mathbb{G}} = 5$ m. For $L_{\mathbb{G}} = 1$ m, the power of $\{\mathbb{G}(x; L_{\mathbb{G}}) \mid x \in \mathbb{R}\}$ is seen to be distributed over harmonics with wavelength larger than 2 m (with wavenumber smaller than $\pi/L_{\mathbb{G}}$). In contrast, for $L_{\mathbb{G}} = 5$ m, the power is observed to be distributed over a narrower range of harmonics with wavelength, this time, larger than 10 m.

Figure 5.5 shows several sample paths of the random Young's modulus field $\{\mathbb{E}(x; L_{\mathbb{G}}; \delta) \mid x \in]0, L[\}$ for $L_{\mathbb{G}} = 1$ m and $\delta = 0.1$, $L_{\mathbb{G}} = 1$ m and $\delta = 0.2$ and $L_{\mathbb{G}} = 5$ m and $\delta = 0.2$. The magnitude of the fluctuations is seen to increase with δ. Furthermore, the sample paths for $L_{\mathbb{G}} = 1$ m are observed to have a higher wavenumber content than those for $L_{\mathbb{G}} = 5$ m in that they oscillate more rapidly as a function of the position.
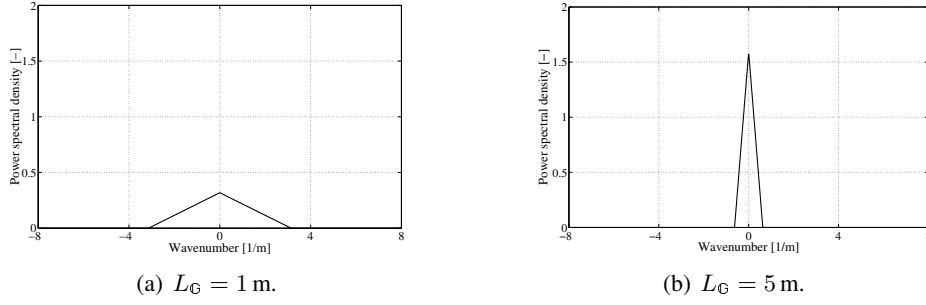
(a) $L_{\mathbb{G}} = 1$ m.

(b) $L_{\mathbb{G}} = 5$ m.

Figure 5.4: Heterogeneous bars: power spectral density function $k \mapsto S_{\mathbb{G}}(k; L_{\mathbb{G}})$ for (a) $L_{\mathbb{G}} = 1$ m and (b) $L_{\mathbb{G}} = 5$ m.

(a) $L_{\mathbb{G}} = 1$ m and $\delta = 0.1$.

(b) $L_{\mathbb{G}} = 1$ m and $\delta = 0.2$.
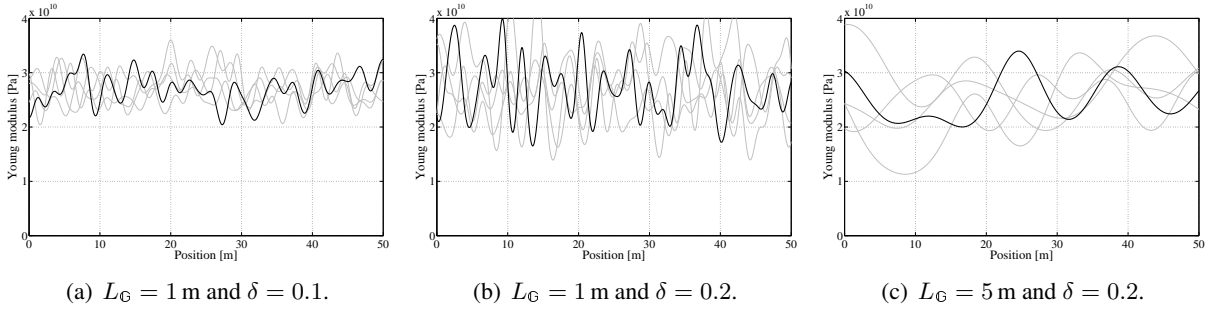
(c) $L_{\mathbb{G}} = 5$ m and $\delta = 0.2$.

Figure 5.5: Heterogeneous bars: five sample paths of the random Young's modulus field $\{\mathbb{E}(x; L_{\mathbb{G}}; \delta) \mid x \in]0, L[\}$ (thick solid line and thin grey lines) for (a) $L_{\mathbb{G}} = 1$ m and $\delta = 0.1$, (b) $L_{\mathbb{G}} = 1$ m and $\delta = 0.2$ and (c) $L_{\mathbb{G}} = 5$ m and $\delta = 0.2$.

(a) $L_{\mathbb{G}} = 1$ m and $\delta = 0.1$.

(b) $L_{\mathbb{G}} = 1$ m and $\delta = 0.2$.
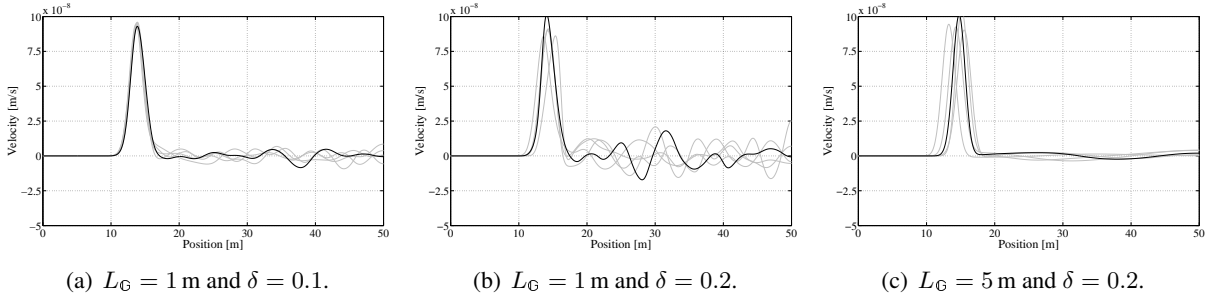
(c) $L_{\mathbb{G}} = 5$ m and $\delta = 0.2$.

Figure 5.6: Heterogeneous bars: five realizations of the random axial velocity at the time instant $t = 0.061$ s (thick solid line and thin grey lines) for (a) $L_{\mathbb{G}} = 1$ m and $\delta = 0.1$, (b) $L_{\mathbb{G}} = 1$ m and $\delta = 0.2$ and (c) $L_{\mathbb{G}} = 5$ m and $\delta = 0.2$.

(a) $L_{\mathbb{G}} = 1$ m and $\delta = 0.1$.

(b) $L_{\mathbb{G}} = 1$ m and $\delta = 0.2$.

(c) $L_{\mathbb{G}} = 5$ m and $\delta = 0.2$.

Figure 5.7: Heterogeneous bars: five sample paths of the random phase velocity $\{\mathbb{C}(\omega_\ell; L_{\mathbb{G}}, \delta) \mid 1 \leq \ell \leq n_{\mathrm{F}}\}$ (thick solid line and thin grey lines) for (a) $L_{\mathbb{G}} = 1$ m and $\delta = 0.1$, (b) $L_{\mathbb{G}} = 1$ m and $\delta = 0.2$ and (c) $L_{\mathbb{G}} = 5$ m and $\delta = 0.2$.

Figure 5.6 shows several realizations of the random axial velocity as a function of the position at $t = 0.061\,\mathrm{s}$ for $L_{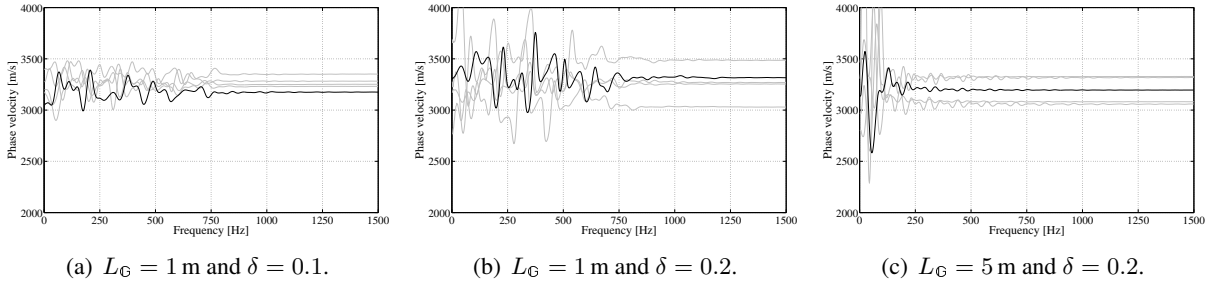\mathbb{G}} = 1\,\mathrm{m}$ and $\delta = 0.1$, $L_{\mathbb{G}} = 1\,\mathrm{m}$ and $\delta = 0.2$ and $L_{\mathbb{G}} = 5\,\mathrm{m}$ and $\delta = 0.2$. As opposed to the result shown in figure 5.3 for a homogeneous bar, the main pulse is, this time, accompanied by several minor waves reflected upon, and transmitted through, the heterogeneities. The magnitude of the minor waves is seen to increase with δ. Furthermore, the minor waves are observed to have a higher wavenumber content for $L_{\mathbb{G}} = 1\,\mathrm{m}$ than for $L_{\mathbb{G}} = 5\,\mathrm{m}$.

Figure 5.7 shows several sample paths of the random phase velocity $\{\mathbb{C}(\omega_\ell; L_{\mathbb{G}}, \delta) \mid 1 \leq \ell \leq n_{\mathrm{F}}\}$ for $L_{\mathbb{G}} = 1\,\mathrm{m}$ and $\delta = 0.1$, $L_{\mathbb{G}} = 1\,\mathrm{m}$ and $\delta = 0.2$ and $L_{\mathbb{G}} = 5\,\mathrm{m}$ and $\delta = 0.2$. As opposed to the frequency-independent phase velocity obtained for the homogeneous bar, the material heterogeneity is seen to induce dispersion phenomena. *At a fixed frequency*, the magnitude of the fluctuations of the random phase velocity is observed to increase with δ. *As a function of the frequency*, the behaviour of the sample paths of the random phase velocity is observed to be governed essentially by $L_{\mathbb{G}}$. For $L_{\mathbb{G}} = 1\,\mathrm{m}$, the phase velocity oscillates heavily as a function of the frequency in the frequency range below about $750\,\mathrm{Hz}$ and is quite straight at higher frequencies. In contrast, for $L_{\mathbb{G}} = 5\,\mathrm{m}$, the oscillations only occur in the frequency range below about below about $200\,\mathrm{Hz}$. These results highlight that the behaviour of the phase velocity depends on the relative scale of, on the one hand, the wavelengths of the harmonics that make up the propagating wave field and, on the other hand, the wavelengths of the harmonics that make up the Young's modulus field. When the former are of the order of the latter, the propagating waves interact strongly with the heterogeneities (back- and forward scattering) and the consequent phase velocity oscillates heavily as a function of the frequency. In contrast, when the former are smaller than the latter, the propagating waves behave, locally, as if they were propagating through a homogeneous medium (forward scattering). The phase velocity is then approximately equal to the average of the local compression wave velocity between the two receivers.

5.3   Simulated data

A data set is synthetically generated using the probabilistic model (5.13)-(5.14). The methodology of Section 5.2.3 is followed, using the computational parameters of Section 5.2.5, to generate n_{K} sample paths of the random phase velocity $\{\mathbb{C}(\omega_\ell; L_{\mathbb{G}}, \delta) \mid 1 \leq \ell \leq n_{\mathrm{F}}\}$ for the spatial correlation length $L_{\mathbb{G}}^{\mathrm{true}} = 2\,\mathrm{m}$ and the dispersion level $\delta^{\mathrm{true}} = 0.2$. These sample paths are gathered in the generic data set

$$\boldsymbol{D}^0 = \{c_k^0(\omega_\ell) \mid 1 \leq \ell \leq n_{\mathrm{F}} \, , \, 1 \leq k \leq n_{\mathrm{K}}\} \quad , \tag{5.23}$$

where $c_k^0(\omega_\ell)$ is the phase velocity for the k-th sample path at the discrete frequency ω_ℓ.

5.4   Stochastic inverse problem

Having set up a probabilistic model and a data set, our objective in this section is to invert the probabilistic model so as to identify a spatial correlation length and a dispersion level characterizing the variability in the data-generating random Young's modulus field.

5.4.1 Proposed inverse methods

Following Section 2.3, we define two distances $\mathcal{L}^{(1)}$ and $\mathcal{L}^{(2)}$, which respectively account for the first- and the second-order cylindrical PDF of the predicted random phase velocity:

$$\mathcal{L}^{(1)}_{n_{\mathrm{F}},n_{\mathrm{K}}}\left(L_{\mathbb{G}},\delta;\boldsymbol{D}^0\right) = -\frac{1}{n_{\mathrm{F}}}\sum_{\ell=1}^{n_{\mathrm{F}}}\frac{1}{n_{\mathrm{K}}}\sum_{k=1}^{n_{\mathrm{K}}}\log\theta^{(1)}\left(c_k^0(\omega_\ell)\big|\omega_\ell;L_{\mathbb{G}},\delta\right) \quad, \tag{5.24}$$

$$\mathcal{L}^{(2)}_{n_{\mathrm{F}},n_{\mathrm{K}}}\left(L_{\mathbb{G}},\delta;\boldsymbol{D}^0\right) = -\frac{2}{n_{\mathrm{F}}(n_{\mathrm{F}}-1)}\sum_{\substack{(\omega_{\ell_1},\omega_{\ell_2})\\\omega_{\ell_1}\neq\omega_{\ell_2}}}\frac{1}{n_{\mathrm{K}}}\sum_{k=1}^{n_{\mathrm{K}}}\log\theta^{(2)}\left(c_k^0(\omega_{\ell_1}),c_k^0(\omega_{\ell_2})\big|\omega_{\ell_1},\omega_{\ell_2};L_{\mathbb{G}},\delta\right). \tag{5.25}$$

With the help of $\mathcal{L}^{(1)}$ and $\mathcal{L}^{(2)}$, the unknown parameters can be estimated from the data by:

$$\left(\hat{L}_{\mathbb{G}}^{(1)},\hat{\delta}^{(1)}\right) = \arg\min_{L_{\mathbb{G}},\delta}\mathcal{L}^{(1)}_{n_{\mathrm{F}},n_{\mathrm{K}}}\left(L_{\mathbb{G}},\delta;\boldsymbol{D}^0\right) \quad, \tag{5.26}$$

$$\left(\hat{L}_{\mathbb{G}}^{(2)},\hat{\delta}^{(2)}\right) = \arg\min_{L_{\mathbb{G}},\delta}\mathcal{L}^{(2)}_{n_{\mathrm{F}},n_{\mathrm{K}}}\left(L_{\mathbb{G}},\delta;\boldsymbol{D}^0\right). \tag{5.27}$$

With reference to Section 2.1, it is clear that the probabilistic model under study is correctly specified. Indeed, upon setting its parameters equal to the "true" spatial correlation length $L_{\mathbb{G}}^{\mathrm{true}}$ and dispersion level δ^{true}, the data-generating probability distribution is perfectly reproduced. With reference to sections 2.4 and 2.7, both inverse methods (5.26) and (5.27) are expected to be consistent, such that the parameter estimates are expected to converge to $L_{\mathbb{G}}^{\mathrm{true}}$ and δ^{true} as the number n_{K} of tested specimens is increased. Finally, with reference to Section 2.7, the inverse method (5.26) is expected to be less efficient than (5.27), such that a larger number n_{K} of tested specimens is expected to be required by the former to achieve estimates of a given accuracy. Indeed, as opposed to the distance $\mathcal{L}^{(1)}$, the distance $\mathcal{L}^{(2)}$ is sensitive to the frequency-dependence of the phase velocity, which was shown in Section 5.2.5 to bear much information on the spatial correlation length, and the inverse method (5.27) is consequently expected to have a higher statistical precision.

5.4.2 Numerical illustration

Figure 5.8 shows the distances $\mathcal{L}^{(1)}_{n_{\mathrm{F}},n_{\mathrm{K}}}\left(L_{\mathbb{G}},\delta;\boldsymbol{D}^0\right)$ and $\mathcal{L}^{(2)}_{n_{\mathrm{F}},n_{\mathrm{K}}}\left(L_{\mathbb{G}},\delta;\boldsymbol{D}^0\right)$ as a function of $L_{\mathbb{G}}$ and δ for data sets comprising $n_{\mathrm{K}}=5$, $n_{\mathrm{K}}=20$ and $n_{\mathrm{K}}=40$ samples (computed using the computational parameters of Section 5.2.5 and using $n_{\mathrm{S}}=250$ Monte Carlo simulations for the numerical estimation of the cylindrical PDFs of the random phase velocity). For $n_{\mathrm{K}}=40$, the "true" parameters $L_{\mathbb{G}}^{\mathrm{true}}=2\,\mathrm{m}$ and $\delta^{\mathrm{true}}=0.2$ are seen to be optimal in the sense of both distances, highlighting that both inverse methods allow recovering the "true" values from the data by increasing the number n_{K} of tested specimens (consistency). For $n_{\mathrm{K}}=5$ and $n_{\mathrm{K}}=20$, the distance $\mathcal{L}^{(1)}_{n_{\mathrm{F}},n_{\mathrm{K}}}\left(L_{\mathbb{G}},\delta;\boldsymbol{D}^0\right)$ has multiple local minima that do not coincide with $L_{\mathbb{G}}^{\mathrm{true}}$ and δ^{true}, whereas the distance $\mathcal{L}^{(2)}_{n_{\mathrm{F}},n_{\mathrm{K}}}\left(L_{\mathbb{G}},\delta;\boldsymbol{D}^0\right)$ shows a global minimum at $L_{\mathbb{G}}^{\mathrm{true}}$ and δ^{true}, highlighting that the inverse method (5.27) requires less samples than (5.26) to recover the "true" values from the data (greater efficiency of (5.27) compared to (5.26)).

5.4.3 Spatial correlation length of the random Young's modulus field

Considering that our aim is to identify a spatial correlation length and a dispersion level characterizing the variability in the data-generating random Young's modulus field, the estimates (5.26) and (5.27) are not entirely satisfactory results of the identifcation procedure since $L_{\mathbb{G}}$ is the spatial correlation length
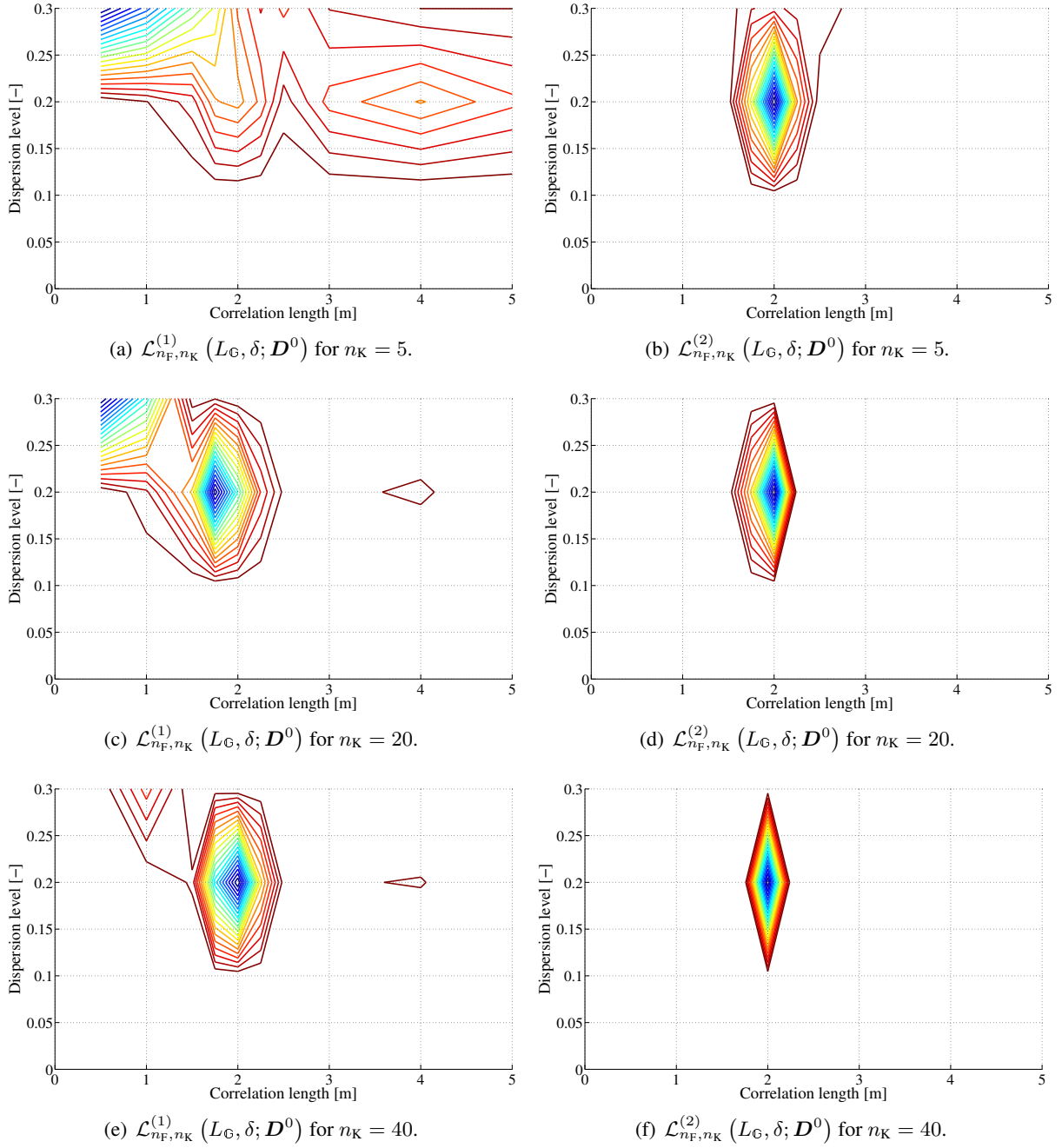
121

(a) $\mathcal{L}^{(1)}_{n_F,n_K}\left(L_\mathbb{G},\delta;\boldsymbol{D}^0\right)$ for $n_K = 5$.

(b) $\mathcal{L}^{(2)}_{n_F,n_K}\left(L_\mathbb{G},\delta;\boldsymbol{D}^0\right)$ for $n_K = 5$.

(c) $\mathcal{L}^{(1)}_{n_F,n_K}\left(L_\mathbb{G},\delta;\boldsymbol{D}^0\right)$ for $n_K = 20$.

(d) $\mathcal{L}^{(2)}_{n_F,n_K}\left(L_\mathbb{G},\delta;\boldsymbol{D}^0\right)$ for $n_K = 20$.

(e) $\mathcal{L}^{(1)}_{n_F,n_K}\left(L_\mathbb{G},\delta;\boldsymbol{D}^0\right)$ for $n_K = 40$.

(f) $\mathcal{L}^{(2)}_{n_F,n_K}\left(L_\mathbb{G},\delta;\boldsymbol{D}^0\right)$ for $n_K = 40$.

Figure 5.8: Heterogeneous bars: contours of the distances (a, c, e) $\mathcal{L}^{(1)}_{n_F,n_K}\left(L_\mathbb{G},\delta;\boldsymbol{D}^0\right)$ and (b, d, f) $\mathcal{L}^{(2)}_{n_F,n_K}\left(L_\mathbb{G},\delta;\boldsymbol{D}^0\right)$ as a function of $L_\mathbb{G}$ and δ for data sets comprising $n_K = 5$, $n_K = 20$ and $n_K = 40$ samples.

of the stochastic germ and not of the random Young's modulus field. To circumvent this difficulty, we introduce an alternative stationary random Young's modulus field $\{\mathbb{E}(x; L_\mathbb{G}, \delta) \mid x \in \mathbb{R}\}$, indexed, this time, by $\mathbb{R}$, such that:

$$\left(\forall x \in \mathbb{R} \; : \; \mathbb{E}(x; L_\mathbb{G}; \delta) = \underline{E}\, N\big(\mathbb{G}(x; L_\mathbb{G}); \delta\big) \right) \text{ a.s.} \quad , \tag{5.28}$$

where the random field $\{\mathbb{G}(x; L_\mathbb{G}) \mid x \in \mathbb{R}\}$ and the transformation function $N(\cdot; \delta) : \mathbb{R} \to \mathbb{R}_0^+$ were defined in Section 5.2.2. The spatial correlation length $L_\mathbb{E}(L_\mathbb{G}, \delta)$ characterizing the random Young's modulus field is then defined by:

$$L_\mathbb{E}(L_\mathbb{G}, \delta) = \frac{\int_{\mathbb{R}_0^+} |R_\mathbb{E}(\eta; L_\mathbb{G}, \delta)| \, d\eta}{R_\mathbb{E}(0; L_\mathbb{G}, \delta)} \quad , \tag{5.29}$$

where the autocorrelation function $\eta \mapsto R_\mathbb{E}(\eta; L_\mathbb{G}, \delta)$ is such that:

$$R_\mathbb{E}(\eta; L_\mathbb{G}, \delta) = E\left\{ \Big(\underline{E} N\big(\mathbb{G}(x; L_\mathbb{G})\big) - \underline{E} \Big) \Big(\underline{E} N\big(\mathbb{G}(x+\eta; L_\mathbb{G}); \delta\big) - \underline{E} \Big) \right\} \quad , \tag{5.30}$$

in which $E\{\cdot\}$ denotes the mathematical expectation. For $n = 1$ or $n = 2$, the values $L_\mathbb{E}(\hat{L}_\mathbb{G}^{(n)}, \hat{\delta}^{(n)})$ and $\hat{\delta}^{(n)}$ are taken as the result of the identification procedure. For the above-given numerical illustration, a Monte Carlo simulation with $n_\mathrm{S} = 10000$ samples yields $L_\mathbb{E}(\hat{L}_\mathbb{G}^{(n)}, \hat{\delta}^{(n)}) = 2.18\,\mathrm{m}$ for $\hat{L}_\mathbb{G}^{(n)} = 2\,\mathrm{m}$ and $\hat{\delta}^{(n)} = 0.2$.

5.5 Summary and conclusion

In this chapter, a methodology was proposed for the experimental identification of spatial correlation lengths and dispersion levels characterizing the variability in heterogeneous fields of material properties of structures using the dispersive characteristics of mechanical waves travelling through specimens. It was successfully applied on an example featuring a correctly specified probabilistic structural model and simulated data.

The main direction for future work is to apply the proposed methodology to examples featuring mis-specified probabilistic structural models. A data set can, for instance, be synthetically generated by the means of the probabilistic model (5.13)-(5.14) using, however, a different power spectral density function than the one proposed in (5.12), or, a different transformation function than the one defined in Box 1.4. It seems interesting to investigate under which conditions accurate estimates of the spatial correlation length and the dispersion level of the data-generating random field are obtained in the presence of model misspecification. Once the effect of model misspecification is understood well, it can be envisaged to apply the methodology to real experimental data (for which, as discussed in Section 2.2, a probabilistic structural model with minimal parameterization is likely to be misspecified).

A second direction for future work is to further investigate the dependence of the dispersive characteristics of the propagating wave field on the features of the material heterogeneity. A way to improve understanding of their dependence on the wavenumber content of the field of elastic moduli may be to apply Floquet theory to compute the dispersion curves for periodic heterogeneous bars [as in Ainsworth, 2004, Ihlenburg and Babuška, 1995, 1997, Thompson and Pinsky, 1994].

A third direction for future work is to study the efficiency of the proposed inverse method from the theoretical point of view (for correctly specified probabilistic models). It seems interesting to derive expressions for the asymptotic covariances of the estimators associated to the proposed estimation rules [as

in Lindsay, 1998]. Such expressions are expected to involve the Fisher information matrix, defined in Box 2.1 of Section 2.1, of the cylindrical PDFs that are taken into account.

In the example, a one-dimensional structure was considered and the heterogeneous material was assumed to be locally isotropic. A natural direction for future work consists in relaxing these assumptions to extend the methodology to three-dimensional structures and heterogeneous anisotropic materials.

Conclusions and recommendations for future research

This chapter presents general conclusions (Sec. 1) and directions for future research (Sec. 2).

1 General conclusions

This section summarizes the presented work and evaluates the main interests and drawbacks of the items that were introduced or used in this dissertation.

Probabilistic structural models with minimal parameterization

Throughout the dissertation, we worked with probabilistic structural models with minimal parameterization. Their first interest is that, by construction, they fulfil the essential mathematical and physical properties of probabilistic structural models. Their second advantage is that, since they usually exhibit only a small set of parameters, their experimental identification can generally be formulated as a mathematically well-posed inverse problem that is numerically solvable with a reasonable computational effort. Their main drawback is that they are expected to be misspecified in practice (Secs. 2.2 and 2.7).

Measured frequency-domain TFs as experimental data

We used measured frequency-domain Transfer Functions (TFs) as experimental data. The main advantages are the possibility to select data in a specific frequency range of interest and the relatively easy characterization of the distortion of the data due to experimental noise (Sec. 1.4 and App. C). However, the use of experimental data of this kind may be problematic when the dynamical behaviour of the structure(s) under study is non-linear.

Formulation of stochastic inverse problems as minimization problems

We showed that the classical methods of estimation from the theory of mathematical statistics are not well-adapted to the identification of probabilistic structural models with minimal parameterization from measured frequency-domain TFs (Sec. 2.2). In particular, we showed that computational difficulties, and conceptual problems due to model misspecification, may hinder the application of the classical methods. These difficulties motivated us to formulate the inversion of probabilistic models alternatively as the minimization, with respect to the unknown parameters to be identified, of an objective function that

measures the distance between the experimental data and the probabilistic model. Two principles of construction for the definition of such distances were proposed, based either upon the loglikelihood function, or the relative entropy (Sec. 2.3). We discussed how the use of distances accounting only for low-order cylindrical Probability Density Functions (PDFs) allows to circumvent the aforementioned computational difficulties and conceptual problems due to model misspecification (Secs. 2.6 and 2.7).

As already mentioned in Section 2.3.3, the proposed inverse methods are not new, but apply existing concepts from the general theory of mathematical statistics. Their originality lies in the application of these general concepts to particular problems in computational mechanics.

Quantification of either epistemic, or aleatory uncertainty

We distinguished between stochastic inverse problems aimed at quantifying either epistemic, or aleatory uncertainty. First, the identification of probabilistic structural models aimed at quantifying the epistemic uncertainty in the predicted dynamical behaviour of a single structure under study was focused upon:

1. Concentrating on the case where the intended use of the probabilistic model is to predict frequency-dependent confidence regions, a fairly comprehensive inverse methodology was proposed, involving the minimization of a distance taking only first-order cylindrical PDFs into account (Sec. 2.6).

2. This inverse methodology was demonstrated on the inversion of non-parametric probabilistic models using simulated and real experimental data (Chs. 3 and 4).

Subsequently, the identification of probabilistic structural models aimed at quantifying the variability in the dynamical behaviour of a collection of structures was considered. We focused in particular on the identification of spatial correlation lengths and dispersion levels characterizing the variability in heterogeneous fields of elastic material properties of structures:

1. Parametric probabilistic models with minimal parameterization for the time- and frequency-domain dynamical behaviour of structures were set up (Sec. 1.1 and App. A), and their main mathematical properties were demonstrated (App. A).

2. An inverse methodology was proposed for the inversion of probabilistic models of this kind using the dispersive characteristics of mechanical waves travelling through sample structures, i.e. using only the phases of the measured frequency-domain TFs, and not the amplitudes (Sec. 2.7 and Ch. 5). The main benefit of taking only the phases into account is that the material damping of the structures need not necessarily be modelled.

3. The inverse methodology was demonstrated on an example featuring a correctly specified parametric probabilistic model and simulated data (Ch. 5).

4. Real experimental data were gathered (App. E).

2 Recommendations for future research

Several directions for future research are now suggested.

Acquisition of practical engineering experience

The inverse methodology proposed for the identification of probabilistic models aimed at quantifying the epistemic uncertainty in the predicted dynamical behaviour of structures was developed to a fairly complete set of theoretical and numerical tools. In our judgement, its further refinement would benefit mostly from the acquisition of practical experience in its application to real engineering case histories. Once a large amount of practical experience is collated, it seems especially challenging to define how stochastic inverse methods of this kind can be incorporated in industrial design and decision processes.

Inversion of the spatial correlation and dispersion of fields of elastic soil properties

The inverse methodology proposed for the identification of spatial correlation lengths and dispersion levels using the dispersive characteristics of mechanical waves seems to us very promising. Within the framework of the PhD. thesis of Quang Anh Ta (2006-...) at Ecole Centrale Paris in France, this methodology is currently being researched and further developed, particularized to the identification of the spatial correlation and dispersion of fields of elastic soil properties. As mentioned in Chapter 5 and Appendix E, a very important aspect to be further studied is the effect of model misspecification. The application of the methodology to the real experimental data presented in Appendix E is envisaged.

Formulation of alternative objective functions

We mention here the possibility to define alternative objective functions by replacing the logarithm in the distances based upon the loglikelihood function by an alernative function, or, analogously, by substituting a different functional aimed at measuring the separation between PDFs [see, for instance, Csiszár, 1967] for the relative entropy.

Future work may also consider the definition of objective functions using, instead of frequency-domain experimental data, time-domain data, thus opening the way to consider structures whose dynamical behaviour is non-linear.

Model selection in stochastic inverse problems

An active topic of discussion in the computational mechanics community is the choice between either the non-parametric, or the parametric approach to build probabilistic models of structures. An interesting trail to follow may be to cast this choice as a model selection problem [see, for instance, Burnham and Anderson, 2003]. In practice, both a non-parametric and a parametric probabilistic model for the structure(s) under study can be set up, and that probabilistic model can subsequently be chosen, which allows to minimize the distance (in the sense of a suitable objective function) to the experimental data. In the line of the numerical methods proposed in Section 2.5, it may be worth noting that model selection problems of this kind can be solved numerically using the Metropolis-Hastings algorithm in its reversible jump version [see, for instance, Green, 1995].

Regularization of stochastic inverse problems

The inverse methods proposed in this dissertation are not limited in application to the identification of probabilistic models with minimal parameterization. Indeed, they can equally be applied to cases in which the probabilistic model depends on a large number of parameters, for instance the coefficients of a polynomial chaos expansion [as in Desceliers et al., 2006]. However, an important aspect to be further studied is that the stochastic inverse problems then obtained may be mathematically ill-posed. The uniqueness property may in particular be problematic, in that a large subspace of the parameter space may solve the optimization problem. An interesting direction for future research is therefore the regularization of stochastic inverse problems. A first possibility is to augment the objective function to be minimized with Tikhonov regularization terms [Tikhonov and Arsenin, 1977]. A second possibility is to include *a priori* information on the sought parameters using the Bayesian paradigm [Tarantola, 2005].

Further development of efficient parallel numerical solvers

Although this aspect has perhaps not yet been stressed sufficiently, it is clear that the inverse methods proposed in this dissertation require substantial computational efforts. Considering the rapidly increasing availability of (massively-)parallel computing platforms, an important direction for future work is therefore the further development of efficient procedures for solving probabilistic direct problems, as well as optimization problems, on multiprocessor machines.

A

Construction of time-domain parametric probabilistic models

In Chapter 1, the construction of non-parametric and parametric probabilistic models with minimal parameterization for the frequency-domain dynamical behaviour of structures was described. Our goal in this appendix is to present the construction of parametric probabilistic models with minimal parameterization for the time-domain dynamical behaviour of structures.

In the following, we first give the deterministic equations governing the time-domain dynamical behaviour of structures (Sec. A.1). Subsequently, we describe the construction of time-domain parametric probabilistic structural models with minimal parameterization (Sec. A.2). Finally, the main mathematical properties of the probabilistic model thus obtained are demonstrated (Secs. A.3-A.7).

A.1 Deterministic structural model

This section first gives the deterministic equations governing the time-domain dynamical behaviour of structures. Subsequently, the variational formulation of these equations is presented.

Deterministic strong formulation

Let us consider the model problem outlined in Section 1.1. Let $[0, T]$ be the time interval of analysis, where $T \in \mathbb{R}_0^+$. Let the mass density be modelled by the deterministic field $\boldsymbol{x} \mapsto \rho(\boldsymbol{x})$ (see footnote 3). Let the elasticity tensor and the viscosity tensor of the structure be modelled by the deterministic fields $\boldsymbol{x} \mapsto \boldsymbol{C}^{\mathrm{e}}(\boldsymbol{x})$ and $\boldsymbol{x} \mapsto \boldsymbol{C}^{\mathrm{v}}(\boldsymbol{x})$ belonging to the function space $\mathrm{T}_4^+(\Omega)$ (see footnote 4).

Let the applied external body and surface force fields be modelled by the respective position- and time-dependent functions $(\boldsymbol{x}; t) \mapsto \boldsymbol{f}_{\mathrm{v}}(\boldsymbol{x}; t)$ and $(\boldsymbol{x}; t) \mapsto \boldsymbol{f}_{\mathrm{s}}(\boldsymbol{x}; t)$. Let $\boldsymbol{x} \mapsto \boldsymbol{u}^0(\boldsymbol{x})$ and $\boldsymbol{x} \mapsto \boldsymbol{u}^1(\boldsymbol{x})$ denote the prescribed initial displacement and velocity field.

The deterministic strong formulation of the BVP then consists in finding the position- and time-dependent

Appendix A. Construction of time-domain parametric probabilistic models

response field $(\boldsymbol{x}; t) \mapsto \boldsymbol{u}(\boldsymbol{x}; t)$ such that:

$$\mathbf{Div}_{\boldsymbol{x}}\boldsymbol{\sigma}(\boldsymbol{u}) + \boldsymbol{f}_{\mathrm{v}} = \rho\frac{\partial^2 \boldsymbol{u}}{\partial t^2} \qquad \text{in } \Omega\times]0, T[\quad, \tag{A.1}$$

$$\boldsymbol{\epsilon}(\boldsymbol{u}) = \frac{1}{2}\left(\mathbf{D}_{\boldsymbol{x}}\boldsymbol{u} + \mathbf{D}_{\boldsymbol{x}}\boldsymbol{u}^{\mathrm{T}}\right) \qquad \text{in } \Omega\times]0, T[\quad, \tag{A.2}$$

$$\boldsymbol{\sigma}(\boldsymbol{u}) = \boldsymbol{C}^{\mathrm{e}}\left(\boldsymbol{\epsilon}(\boldsymbol{u})\right) + \boldsymbol{C}^{\mathrm{v}}\left(\frac{\partial\boldsymbol{\epsilon}(\boldsymbol{u})}{\partial t}\right) \qquad \text{in } \Omega\times]0, T[\quad, \tag{A.3}$$

with the boundary conditions:

$$\boldsymbol{u} = \boldsymbol{0} \qquad \text{on } \Gamma_{\mathrm{u}}\times]0, T[\quad, \tag{A.4}$$

$$\boldsymbol{\sigma}(\boldsymbol{u})(\boldsymbol{n}) = \boldsymbol{f}_{\mathrm{s}} \qquad \text{on } \Gamma_{\sigma}\times]0, T[\quad, \tag{A.5}$$

and the initial conditions:

$$\boldsymbol{u}(\boldsymbol{x}; 0) = \boldsymbol{u}^0(\boldsymbol{x}) \qquad \text{in } \Omega \quad, \tag{A.6}$$

$$\frac{\partial\boldsymbol{u}}{\partial t}(\boldsymbol{x}; 0) = \boldsymbol{u}^1(\boldsymbol{x}) \qquad \text{in } \Omega \quad, \tag{A.7}$$

in which $\boldsymbol{\epsilon}(\boldsymbol{u})$ and $\boldsymbol{\sigma}(\boldsymbol{u})$ denote the linearized strain and stress tensor.

Deterministic functional spaces

Let us introduce the following function spaces of position-dependent response fields:

$$H_0 = \left\{\boldsymbol{v} \in \left(L^2(\Omega, \mathbb{R})\right)^3 \mid \boldsymbol{v} = \boldsymbol{0} \text{ on } \Gamma_{\mathrm{u}}\right\} \quad, \tag{A.8}$$

$$V_0 = \left\{\boldsymbol{v} \in \left(H^1(\Omega, \mathbb{R})\right)^3 \mid \boldsymbol{v} = \boldsymbol{0} \text{ on } \Gamma_{\mathrm{u}}\right\}. \tag{A.9}$$

They are Hilbert spaces for the following respective norms:

$$||\boldsymbol{v}||_H^2 = \int_{\Omega}(\boldsymbol{v}, \boldsymbol{v})\, d\Omega\,, \quad ||\boldsymbol{v}||_V^2 = \int_{\Omega}(\boldsymbol{v}, \boldsymbol{v})\, d\Omega + \int_{\Omega}\mathrm{tr}\left(\mathbf{D}_{\boldsymbol{x}}\boldsymbol{v}\mathbf{D}_{\boldsymbol{x}}\boldsymbol{v}\right)d\Omega. \tag{A.10}$$

Deterministic variational formulation

We proceed to elaborate the weak formulation of the BVP. First, we introduce the admissible function space $W(]0, T[, V_0)$ of the problem comprising the sufficiently regular[18] deterministic position- and time-dependent response fields of the structure. The deterministic variational formulation of the BVP consists in finding the position- and time-dependent response field

$$\boldsymbol{u} \in W(]0, T[, V_0) \quad, \tag{A.12}$$

---

[18]The admissible function space is chosen [Dautray and Lions, 1987, ch. 18 sec. 5] equal to the space

$$W(]0, T[, V_0) = \left\{t \mapsto \boldsymbol{v}(t) \;\middle|\; \boldsymbol{v} \in L^2(]0, T[, V_0)\,, \boldsymbol{v}' = \frac{d\boldsymbol{v}}{dt} \in L^2(]0, T[, V_0)\,, \frac{d\boldsymbol{v}'}{dt} \in L^2(]0, T[, V_0')\right\}. \tag{A.11}$$

such that $\forall \boldsymbol{v} \in V_0$:

$$k\left(\boldsymbol{u}(t), \boldsymbol{v}\right) + d\left(\boldsymbol{u}'(t), \boldsymbol{v}\right) + m\left(\frac{d\boldsymbol{u}'}{dt}(t), \boldsymbol{v}\right) = f(t; \boldsymbol{v}) , \quad \text{a.e. } t \in [0, T] \quad , \tag{A.13}$$

and the initial conditions (A.6)-(A.7) are fulfilled. The stiffness, damping and mass forms[19] are bilinear forms defined by:

$$k\left(\boldsymbol{v}_1, \boldsymbol{v}_2\right) = \int_\Omega \text{tr}\left(\boldsymbol{C}^{\text{e}}\left(\boldsymbol{\epsilon}(\boldsymbol{v}_1)\right) \boldsymbol{\epsilon}(\boldsymbol{v}_2)\right) d\Omega \quad , \tag{A.14}$$

$$d\left(\boldsymbol{v}_1, \boldsymbol{v}_2\right) = \int_\Omega \text{tr}\left(\boldsymbol{C}^{\text{v}}\left(\boldsymbol{\epsilon}(\boldsymbol{v}_1)\right) \boldsymbol{\epsilon}(\boldsymbol{v}_2)\right) d\Omega \quad , \tag{A.15}$$

$$m\left(\boldsymbol{v}_1, \boldsymbol{v}_2\right) = \int_\Omega \rho\left(\boldsymbol{v}_1, \boldsymbol{v}_2\right) d\Omega. \tag{A.16}$$

The form representing the external loading is a linear form defined by:

$$f(t; \boldsymbol{v}) = \int_\Omega \left(\boldsymbol{f}_{\text{v}}(\boldsymbol{x}; t), \boldsymbol{v}(\boldsymbol{x})\right) d\Omega + \int_{\Gamma_\sigma} \left(\boldsymbol{f}_{\text{s}}(\boldsymbol{x}; t), \boldsymbol{v}(\boldsymbol{x})\right) dS. \tag{A.17}$$

For sufficiently regular[20] functions $\boldsymbol{f}_{\text{v}}$, $\boldsymbol{f}_{\text{s}}$, $\boldsymbol{u}^0$ and $\boldsymbol{u}^1$, it can be shown [Dautray and Lions, 1987, ch. 18 sec. 5] that the variational formulation (A.6)-(A.7)-(A.13) is mathematically well-posed and, furhermore, that the displacement field $\boldsymbol{u}$ and the velocity field $\boldsymbol{u}'$ are continuous functions of the time:

$$\boldsymbol{u} \in \mathcal{C}^0([0, T], V_0) , \quad \boldsymbol{u}' \in \mathcal{C}^0([0, T], H_0). \tag{A.19}$$

For later reference, let γ_{P} denote the mapping that, for given data $\{\boldsymbol{C}^{\text{v}}, \rho, \boldsymbol{f}_{\text{v}}, \boldsymbol{f}_{\text{s}}, \boldsymbol{u}^0, \boldsymbol{u}^1\}$, maps the tensor field $\boldsymbol{x} \mapsto \boldsymbol{C}^{\text{e}}(\boldsymbol{x})$ onto the unique corresponding weak solution $\boldsymbol{u}$ of (A.6)-(A.7)-(A.13):

$$\gamma_{\text{P}} : \text{T}_4^+(\Omega) \to W\left(]0, T[, V_0\right) : \boldsymbol{C}^{\text{e}} \mapsto \gamma_{\text{P}}\left(\boldsymbol{C}^{\text{e}}\right) = \boldsymbol{u}. \tag{A.20}$$

A.2 Parametric probabilistic model

We now present the construction of a time-domain parametric probabilistic model with minimal parameterization by modelling the elasticity tensor field in the variational formulation (A.6)-(A.7)-(A.13) by the random tensor field $\{\mathbb{C}^{\text{e}}(\boldsymbol{x}; \boldsymbol{p}) \mid \boldsymbol{x} \in \Omega\}$ defined on the probability measure space $(\mathcal{A}, \mathcal{F}, P)$, which was introduced in Section 1.1.

The parametric probabilistic model then consists in finding the random response field $\mathbb{U}(\boldsymbol{p})$ defined on $(\mathcal{A}, \mathcal{F}, P)$ with values in $W(]0, T[, V_0)$ a.s. such that[21]:

$$\left(\mathbb{K}\left(\mathbb{U}(t; \boldsymbol{p}), \boldsymbol{v}; \boldsymbol{p}\right) + d\left(\mathbb{U}'(t; \boldsymbol{p}), \boldsymbol{v}\right) + m\left(\frac{d\mathbb{U}'}{dt}(t; \boldsymbol{p}), \boldsymbol{v}\right) = f(t; \boldsymbol{v}) , \text{ a.e. } t \in [0, T] , \forall \boldsymbol{v} \in V_0\right) \text{ a.s.,} \tag{A.21}$$

---

[19]The stiffness and damping forms are symmetric, positive definite and continuous on $V_0 \times V_0$, whereas the mass form is symmetric, positive definite and continuous on $H_0 \times H_0$.

[20]The position- and time-dependent force fields $\boldsymbol{f}_{\text{v}}$ and $\boldsymbol{f}_{\text{s}}$ and the position-dependent initial displacement and velocity fields $\boldsymbol{u}^0$ and $\boldsymbol{u}^1$ are taken [Dautray and Lions, 1987, ch. 18 sec. 5] in the following functional spaces:

$$\boldsymbol{f}_{\text{v}} \in L^2\left(]0, T[, \left(L^2(\Omega, \mathbb{R})\right)^3\right) , \quad \boldsymbol{f}_{\text{s}} \in L^2\left(]0, T[, \left(L^2(\Gamma_\sigma, \mathbb{R})\right)^3\right) , \quad \boldsymbol{u}^0 \in V_0 , \quad \boldsymbol{u}^1 \in H_0. \tag{A.18}$$

and the initial conditions are fulfilled:

$$\mathbb{U}(0; \boldsymbol{p}) = \boldsymbol{u}^0 \text{ a.s. }, \quad \mathbb{U}'(0; \boldsymbol{p}) = \boldsymbol{u}^1 \text{ a.s.} \tag{A.22}$$

The random stiffness form is defined by:

$$\mathbb{K}\left(\boldsymbol{v}_1, \boldsymbol{v}_2; \boldsymbol{p}\right) = \int_\Omega \operatorname{tr}\big(\mathbb{C}^{\mathrm{e}}(\boldsymbol{p})\left(\boldsymbol{\epsilon}(\boldsymbol{v}_1)\right)\boldsymbol{\epsilon}(\boldsymbol{v}_2)\big)d\Omega \text{ a.s.} \tag{A.23}$$

It can be shown (see Section A.4) that there exists a unique random response field $\mathbb{U}(\boldsymbol{p})$ with values in $W(]0, T[, V_0)$ a.s., which solves (A.21)-(A.22).

In view of the property (A.19), the realizations of $\mathbb{U}(\boldsymbol{p})$ and $\mathbb{U}'(\boldsymbol{p})$ are a.s. continuous functions of the time, which allows [see, for instance, Krée and Soize, 1986, ch. 10] to collect the position-dependent random displacement and velocity fields obtained at all the time instants in $[0, T]$ in the stochastic processes

$$\{\mathbb{U}(t; \boldsymbol{p}) \mid t \in [0, T]\}, \quad \{\mathbb{U}'(t; \boldsymbol{p}) \mid t \in [0, T]\} \quad, \tag{A.24}$$

defined on $(\mathcal{A}, \mathcal{F}, P)$, indexed by $[0, T]$ and with values in V_0 and H_0 a.s. If the dispersion parameter δ (included in the parameter set $\boldsymbol{p}$) of the random tensor field fulfils the inequality (1.46), it can be shown (Sec. A.7) that:

$$\forall t \in [0, T] : E\left\{||\mathbb{U}(t; \boldsymbol{p})||_V^2\right\} < +\infty, \quad E\left\{||\mathbb{U}'(t; \boldsymbol{p})||_H^2\right\} < +\infty. \tag{A.25}$$

The stochastic processes (A.24) then are of the second order. This mathematical property ensures that the theoretical properties and computational tools for second-order random variables are applicable.

For later reference, we note that the equations (A.21)-(A.22) propagate the uncertainty introduced in the elasticity tensor field *through the deterministic model* to the dynamical response field. This consideration is highlighted by writing the equations (A.21)-(A.22) in the following equivalent form (see also footnote 14):

$$\mathbb{U}(\boldsymbol{p}) = \gamma_{\mathrm{P}}\big(\mathbb{C}^{\mathrm{e}}(\boldsymbol{p})\big) \text{ a.s.} \quad, \tag{A.26}$$

where the mapping γ_{P} was defined in (A.20).

A.3 Definitions and notations for the proofs

The remaining sections of this appendix demonstrate the existence, uniqueness and square-integrability of the random solution of the time-domain parametric probabilistic model (A.21)-(A.22). Our objective in the present section is to introduce some definitions and notations for later use. We note that, in the remainder of this appendix, we make use of the theory of functional analysis and of the theory of measure and integration. For comprehensive accounts of these theories, we refer the reader, for instance, to [Billingsley, 1995, Brezis, 1999, Da Prato and Zabczyk, 1992, Dautray and Lions, 1987, Dudley, 2002, Krée and Soize, 1986, Ledoux and Talagrand, 1991, Reed and Simon, 1980, Royden, 1988].

---

[21]Since the equations (A.21)-(A.22) are written in the almost sure sense with respect to the random coordinate, the solution $\mathbb{U}(\boldsymbol{p})$ is such that, for almost all $a \in \mathcal{A}$, the realization $\mathbb{U}(a; \boldsymbol{p})$ solves the deterministic variational formulation (A.6)-(A.7)-(A.13) wherein the elasticity tensor field is chosen equal to the sample path $\mathbb{C}^{\mathrm{e}}(a; \boldsymbol{p})$ of the random elasticity tensor field. In order to ensure the well-posedness of that deterministic variational formulation, we apply the theory of the random variables in functional spaces (see box 3.1) and require the random response field $\mathbb{U}(\boldsymbol{p})$ to have values in $W(]0, T[, V_0)$ a.s.

Let us now introduce several functional spaces, norms and distances. First, the space $\mathcal{C}^0(\overline{\Omega}, \mathbb{R})$ of continuous functions from $\overline{\Omega}$ into $\mathbb{R}$ is introduced (we recall from Section 1.1 that $\overline{\Omega} = \Omega \cup \partial\Omega$ is the closure of the open domain Ω occupied by the structure at static equilibrium), endowed with the norm

$$||\boldsymbol{v}||_{\mathcal{C}^0(\mathbb{R})} = \sup_{\boldsymbol{x} \in \overline{\Omega}} ||\boldsymbol{v}(\boldsymbol{x})||. \qquad (A.27)$$

Then, the space $\mathrm{T}_4^+(\Omega)$ of admissible fourth-rank tensor fields is equipped with the following distance (since this space is not a vector space, we cannot introduce a norm):

$$d_T(\boldsymbol{C}_1, \boldsymbol{C}_2) = \sup_{k,\ell} \left(\text{ess.} \sup_{\boldsymbol{x} \in \Omega} \left| [\widehat{\boldsymbol{C}}_1(\boldsymbol{x}) - \widehat{\boldsymbol{C}}_2(\boldsymbol{x})]_{k\ell} \right| \right) \quad, \qquad (A.28)$$

where the notation $\widehat{\cdot}$ refers to the second-rank tensor representation for fourth-rank tensors, which was defined in Section 1.1.

Subsequently, the spaces $\mathcal{C}^0([0,T], H_0)$ and $\mathcal{C}^0([0,T], V_0)$ of continuous functions from $[0,T]$ into H_0 and V_0 are endowed, respectively, with the following norms:

$$||\boldsymbol{v}||_{\mathcal{C}^0(H_0)} = \sup_{t \in [0,T]} ||\boldsymbol{v}(t)||_H \ , \quad ||\boldsymbol{v}||_{\mathcal{C}^0(V_0)} = \sup_{t \in [0,T]} ||\boldsymbol{v}(t)||_V. \qquad (A.29)$$

Finally, the Hilbert space $L^2(]0,T[, V_0)$ of square-integrable functions from $]0,T[$ into V_0 is introduced and endowed with the norm

$$||\boldsymbol{v}||_{L^2(V_0)}^2 = \int_0^T ||\boldsymbol{v}(t)||_V^2 \, dt. \qquad (A.30)$$

Let $S = \{\mathcal{C}^0(\overline{\Omega}, \mathbb{R}), \ \mathrm{T}_4^+(\Omega), \ \mathcal{C}^0([0,T], H_0), \ \mathcal{C}^0([0,T], V_0), \ L^2(]0,T[, V_0), H_0, \ V_0\}$. For any pair $X, Y \in S$ of function spaces, any mapping from X into Y will simply be called *continuous* if it is continuous with respect to the topologies induced by the above-chosen norms. Moreover, each function space $X \in S$ is equipped with a Borel σ-algebra $\mathscr{B}(X)$ generated by the open sets induced by the above-chosen norm on X. Any random variable defined on $(\mathcal{A}, \mathcal{F}, P)$ with values in X a.s. will simply be called *Borel measurable* if it is measurable from $(\mathcal{A}, \mathcal{F})$ into $(X, \mathscr{B}(X))$.

A.4 Proof: existence and uniqueness of the random solution

This section demonstrates the existence and the uniqueness of the solution $\mathbb{U}(\boldsymbol{p})$ of the time-domain parametric probabilistic model (A.21)-(A.22). In this section, unlike elsewhere in this appendix, the distinction is made between random variables and their a.s. equivalence class.

Let us first show the existence of a solution. In particular, let us show that, for a given random elasticity tensor field $\{\mathbb{C}^e(\boldsymbol{x}; \boldsymbol{p}) \mid \boldsymbol{x} \in \Omega\}$, at least one random variable $\mathbb{U}_0(\boldsymbol{p})$ defined on $(\mathcal{A}, \mathcal{F}, P)$ with values in $W(]0,T[, V_0)$ a.s. can be constructed, which solves the equations (A.21)-(A.22).

Let $\mathbb{C}^e(\boldsymbol{p})$ denote the random variable defined on $(\mathcal{A}, \mathcal{F}, P)$ with values in the function space $\mathrm{T}_4^+(\Omega)$ a.s. defined by the sample paths of $\{\mathbb{C}^e(\boldsymbol{x}; \boldsymbol{p}) \mid \boldsymbol{x} \in \Omega\}$ (see also box 1.3). Let $\mathbb{C}_0^e(\boldsymbol{p})$ be a random variable defined on $(\mathcal{A}, \mathcal{F}, P)$ which is a.s. equal to $\mathbb{C}^e(\boldsymbol{p})$ and whose image is entirely included in $\mathrm{T}_4^+(\Omega)$ (and not only "almost surely"). Upon composing the mapping

$$\mathbb{C}_0^e(\boldsymbol{p}) : \mathcal{A} \to \mathrm{T}_4^+(\Omega) : a \mapsto \mathbb{C}_0^e(a; \boldsymbol{p}) \qquad (A.31)$$

with the mapping γ_P, which was defined in (A.20), we construct a random response field

$$\mathbb{U}_0(\boldsymbol{p}) : \mathcal{A} \to W(]0, T[, V_0) : a \mapsto \mathbb{U}_0(a; \boldsymbol{p}) = \gamma_P\big(\mathbb{C}_0^e(a; \boldsymbol{p})\big). \tag{A.32}$$

Since $\mathbb{C}_0^e(\boldsymbol{p})$ is a.s. equal to $\mathbb{C}^e(\boldsymbol{p})$, we have:

$$P\left(\Big\{a \in \mathcal{A} \ : \ \mathbb{C}_0^e(a; \boldsymbol{p}) = \mathbb{C}^e(a; \boldsymbol{p})\Big\}\right) = 1. \tag{A.33}$$

Since the deterministic variational formulation is mathematically well-posed, the mapping γ_P is many-to-one such that:

$$P\left(\Big\{a \in \mathcal{A} \ : \ \mathbb{U}_0^e(a; \boldsymbol{p}) = \gamma_P\big(\mathbb{C}^e(a; \boldsymbol{p})\big)\Big\}\right) = 1. \tag{A.34}$$

As a conclusion, the constructed random response field $\mathbb{U}_0^e(a; \boldsymbol{p})$ solves equation (A.26), or, equivalently, equations (A.21)-(A.22) (existence).

Since the equations (A.21)-(A.22) are written in the "almost sure" sense, they are not solved by a unique random variable. Let us now show that, for a given random elasticity tensor field $\{\mathbb{C}^e(\boldsymbol{x}; \boldsymbol{p}) \mid \boldsymbol{x} \in \Omega\}$, the equations (A.21)-(A.22) are solved by a unique a.s. equivalence class $\mathbb{U}(\boldsymbol{p})$ of random variables.

Let $\mathbb{U}_1(\boldsymbol{p})$ and $\mathbb{U}_2(\boldsymbol{p})$ be two random variables defined on $(\mathcal{A}, \mathcal{F}, P)$ with values in $W(]0, T[, V_0)$ a.s., which solve (A.21)-(A.22) and let $F_1, F_2 \in \mathcal{F}$ be the following events:

$$F_1 = \Big\{a \in \mathcal{A} \ : \ \mathbb{U}_1(a; \boldsymbol{p}) \neq \gamma_P\big(\mathbb{C}^e(a; \boldsymbol{p})\big)\Big\}, \quad F_2 = \Big\{a \in \mathcal{A} \ : \ \mathbb{U}_2(a; \boldsymbol{p}) \neq \gamma_P\big(\mathbb{C}^e(a; \boldsymbol{p})\big)\Big\}. \tag{A.35}$$

Since $\mathbb{U}_1(\boldsymbol{p})$ and $\mathbb{U}_2(\boldsymbol{p})$ solve (A.21)-(A.22), $P(F_1) = P(F_2) = 0$. Since the mapping γ_P is many-to-one, we have:

$$0 \leq P\Big(\big\{a \in \mathcal{A} \ , \ \mathbb{U}_1(\boldsymbol{p}) \neq \mathbb{U}_2(\boldsymbol{p})\big\}\Big) \leq P(F_1) + P(F_2) = 0 \tag{A.36}$$

such that $\mathbb{U}_1(\boldsymbol{p}) = \mathbb{U}_2(\boldsymbol{p})$ a.s. (uniqueness).

A.5   Proof: continuity of the deterministic variational formulation

As a first step towards proving the square-integrability of the random solution of the time-domain parametric probabilistic model (A.21)-(A.22), this section presents and proves continuity properties verified by the weak solution of the deterministic variational formulation (A.6)-(A.7)-(A.13) with respect to perturbations of the elasticity tensor field. The proof is based upon a comparable demonstration given in [Dautray and Lions, 1987, ch. 18 sec. 4] concerning, however, initial-boundary value problems of the first order in time.

Theorem. *Let $\boldsymbol{u}_1$ be the solution of (A.6)-(A.7)-(A.13) for the data $\{\boldsymbol{C}_1^e, \boldsymbol{C}^v, \rho, \boldsymbol{f}_s, \boldsymbol{f}_v, \boldsymbol{u}^0, \boldsymbol{u}^1\}$ and let $\boldsymbol{u}_2$ be the solution corresponding to $\{\boldsymbol{C}_2^e, \boldsymbol{C}^v, \rho, \boldsymbol{f}_s, \boldsymbol{f}_v, \boldsymbol{u}^0, \boldsymbol{u}^1\}$. Then, there exists a monotonically increasing function $\varphi : \mathbb{R}^+ \to \mathbb{R}^+$ such that:*

$$\|\boldsymbol{u}_1 - \boldsymbol{u}_2\|_{\mathcal{C}^0(V_0)} \ \leq \ \varphi\big(d_T(\boldsymbol{C}_1^e, \boldsymbol{C}_2^e)\big) \|\boldsymbol{u}_1\|_{L^2(V_0)}^2 \quad, \tag{A.37}$$

$$\|\boldsymbol{u}_1' - \boldsymbol{u}_2'\|_{\mathcal{C}^0(H_0)} \ \leq \ \varphi\big(d_T(\boldsymbol{C}_1^e, \boldsymbol{C}_2^e)\big) \|\boldsymbol{u}_1\|_{L^2(V_0)}^2 \quad, \tag{A.38}$$

provided that $d_T(\boldsymbol{C}_1^e, \boldsymbol{C}_2^e)$ is sufficiently small (the exact constraint is defined in the following).

Corollary. *The variational formulation (A.6)-(A.7)-(A.13) is continuous at all elasticity tensor fields $\boldsymbol{C}_1^e$, that is to say, $\boldsymbol{u}_2$ and $\boldsymbol{u}_2'$ converge to $\boldsymbol{u}_1$ and $\boldsymbol{u}_1'$ whenever $\boldsymbol{C}_2^e$ converges to $\boldsymbol{C}_1^e$:*

$$\lim_{d_T(\boldsymbol{C}_1^e, \boldsymbol{C}_2^e) \to 0} \|\boldsymbol{u}_1 - \boldsymbol{u}_2\|_{\mathcal{C}^0(V_0)} = 0 \ , \quad \lim_{d_T(\boldsymbol{C}_1^e, \boldsymbol{C}_2^e) \to 0} \|\boldsymbol{u}_1' - \boldsymbol{u}_2'\|_{\mathcal{C}^0(H_0)} = 0. \tag{A.39}$$

Proof. In this proof, we make use of the second-rank tensor representation for fourth-rank tensors, which was introduced in Section 1.1.4. Let k_1 and k_2 be the stiffness forms corresponding to the elasticity tensor fields $\boldsymbol{x} \rightarrow \boldsymbol{C}_1^{\text{e}}(\boldsymbol{x})$ and $\boldsymbol{x} \rightarrow \boldsymbol{C}_2^{\text{e}}(\boldsymbol{x})$:

$$k_1(\boldsymbol{v}_1, \boldsymbol{v}_2) = \int_\Omega \text{tr}\big(\boldsymbol{C}_1^{\text{e}}\left(\boldsymbol{\epsilon}(\boldsymbol{v}_1)\right)\boldsymbol{\epsilon}(\boldsymbol{v}_2)\big)d\Omega = \int_\Omega \left(\widehat{\boldsymbol{C}}_1^{\text{e}}\widehat{\boldsymbol{\epsilon}}(\boldsymbol{v}_1), \widehat{\boldsymbol{\epsilon}}(\boldsymbol{v}_2)\right)d\Omega \quad , \tag{A.40}$$

$$k_2(\boldsymbol{v}_1, \boldsymbol{v}_2) = \int_\Omega \text{tr}\big(\boldsymbol{C}_2^{\text{e}}\left(\boldsymbol{\epsilon}(\boldsymbol{v}_1)\right)\boldsymbol{\epsilon}(\boldsymbol{v}_2)\big)d\Omega = \int_\Omega \left(\widehat{\boldsymbol{C}}_2^{\text{e}}\widehat{\boldsymbol{\epsilon}}(\boldsymbol{v}_1), \widehat{\boldsymbol{\epsilon}}(\boldsymbol{v}_2)\right)d\Omega. \tag{A.41}$$

The stiffness form k_1, the damping form d and the mass form m are positive definite. Let $c_{k1}, c_d, c_m \in \mathbb{R}_0^+$ be positive constants such that:

$$k_1(\boldsymbol{v}, \boldsymbol{v}) \geq c_{k1} \left\|\boldsymbol{v}\right\|_V^2 \;, \quad d(\boldsymbol{v}, \boldsymbol{v}) \geq c_d \left\|\boldsymbol{v}\right\|_V^2 \;, \quad m(\boldsymbol{v}, \boldsymbol{v}) \geq c_m \left\|\boldsymbol{v}\right\|_H^2 \;. \tag{A.42}$$

The stiffness forms k_1 and k_2 verify:

$$\begin{aligned}
\left|k_1(\boldsymbol{v}_1, \boldsymbol{v}_2) - k_2(\boldsymbol{v}_1, \boldsymbol{v}_2)\right| &= \left|\int_\Omega \left(\left(\widehat{\boldsymbol{C}}_1^{\text{e}} - \widehat{\boldsymbol{C}}_2^{\text{e}}\right)\widehat{\boldsymbol{\epsilon}}(\boldsymbol{v}_1), \widehat{\boldsymbol{\epsilon}}(\boldsymbol{v}_2)\right)d\Omega\right| \\
&\leq \sum_{k,\ell} \int_\Omega \left|\left(\widehat{\boldsymbol{C}}_1^{\text{e}}(\boldsymbol{x}) - \widehat{\boldsymbol{C}}_2^{\text{e}}(\boldsymbol{x})]_{k\ell}\right)[\widehat{\boldsymbol{\epsilon}}(\boldsymbol{v}_1)]_\ell[\widehat{\boldsymbol{\epsilon}}(\boldsymbol{v}_2)]_k\right|d\Omega \\
&\leq \sup_{k,\ell}\left(\text{ess.}\sup_{\boldsymbol{x} \in \Omega}\left|[\widehat{\boldsymbol{C}}_1^{\text{e}}(\boldsymbol{x}) - \widehat{\boldsymbol{C}}_2^{\text{e}}(\boldsymbol{x})]_{k\ell}\right|\right)\sum_{k,\ell}\int_\Omega \left|[\widehat{\boldsymbol{\epsilon}}(\boldsymbol{v}_1)]_\ell[\widehat{\boldsymbol{\epsilon}}(\boldsymbol{v}_2)]_k\right|d\Omega \\
&= d_T(\boldsymbol{C}_1^{\text{e}}, \boldsymbol{C}_2^{\text{e}})\sum_{k,\ell}\int_\Omega \left|[\widehat{\boldsymbol{\epsilon}}(\boldsymbol{v}_1)]_\ell[\widehat{\boldsymbol{\epsilon}}(\boldsymbol{v}_2)]_k\right|d\Omega.
\end{aligned} \tag{A.43}$$

The Hölder inequality is applied on (A.43):

$$\left|k_1(\boldsymbol{v}_1, \boldsymbol{v}_2) - k_2(\boldsymbol{v}_1, \boldsymbol{v}_2)\right| \leq d_T(\boldsymbol{C}_1^{\text{e}}, \boldsymbol{C}_2^{\text{e}})\sum_{k,\ell}\sqrt{\int_\Omega ([\widehat{\boldsymbol{\epsilon}}(\boldsymbol{v}_1)]_\ell)^2\,d\Omega}\sqrt{\int_\Omega ([\widehat{\boldsymbol{\epsilon}}(\boldsymbol{v}_2)]_k)^2\,d\Omega}. \tag{A.44}$$

Hence, there exists a positive constant $\alpha \in \mathbb{R}_0^+$ such that:

$$\left|k_1(\boldsymbol{v}_1, \boldsymbol{v}_2) - k_2(\boldsymbol{v}_1, \boldsymbol{v}_2)\right| \leq \alpha\,d_T(\boldsymbol{C}_1^{\text{e}}, \boldsymbol{C}_2^{\text{e}})\left\|\boldsymbol{v}_1\right\|_V\left\|\boldsymbol{v}_2\right\|_V. \tag{A.45}$$

The stiffness form k_2 verifies:

$$\begin{aligned}
k_2(\boldsymbol{v}, \boldsymbol{v}) &= \int_\Omega \left(\widehat{\boldsymbol{C}}_2^{\text{e}}\widehat{\boldsymbol{\epsilon}}(\boldsymbol{v}), \widehat{\boldsymbol{\epsilon}}(\boldsymbol{v})\right)d\Omega \\
&= k_1(\boldsymbol{v}, \boldsymbol{v}) + \int_\Omega \left(\left(\widehat{\boldsymbol{C}}_2^{\text{e}} - \widehat{\boldsymbol{C}}_1^{\text{e}}\right)\widehat{\boldsymbol{\epsilon}}(\boldsymbol{v}), \widehat{\boldsymbol{\epsilon}}(\boldsymbol{v})\right)d\Omega \\
&\geq c_{k1}\left\|\boldsymbol{v}\right\|_V^2 - \alpha d_T(\boldsymbol{C}_1^{\text{e}}, \boldsymbol{C}_2^{\text{e}})\left\|\boldsymbol{v}\right\|_V^2 \\
&= \left(c_{k1} - \alpha\,d_T(\boldsymbol{C}_1^{\text{e}}, \boldsymbol{C}_2^{\text{e}})\right)\left\|\boldsymbol{v}\right\|_V^2.
\end{aligned} \tag{A.46}$$

In the following, the distance $d_T(\boldsymbol{C}_1^{\text{e}}, \boldsymbol{C}_2^{\text{e}})$ is required to be sufficiently small such that:

$$c_{k1} - \alpha\,d_T(\boldsymbol{C}_1^{\text{e}}, \boldsymbol{C}_2^{\text{e}}) > 0. \tag{A.47}$$

The solution $\boldsymbol{u}_1$ fulfils the weak equilibrium

$$k_1\left(\boldsymbol{u}_1(t), \boldsymbol{v}\right) + d\left(\boldsymbol{u}_1'(t), \boldsymbol{v}\right) + m\left(\frac{d\boldsymbol{u}_1'}{dt}(t), \boldsymbol{v}\right) = f(t; \boldsymbol{v})\;, \quad \text{a.e. } t \in [0, T]\;, \quad \forall \boldsymbol{v} \in V_0 \quad , \tag{A.48}$$

and the initial conditions $\boldsymbol{u}_1(0) = \boldsymbol{u}^0$ and $\boldsymbol{u}_1'(0) = \boldsymbol{u}^1$. The solution $\boldsymbol{u}_2$ solves, in contrast, the weak equilibrium

$$k_2\left(\boldsymbol{u}_2(t), \boldsymbol{v}\right) + d\left(\boldsymbol{u}_2'(t), \boldsymbol{v}\right) + m\left(\frac{d\boldsymbol{u}_2'}{dt}(t), \boldsymbol{v}\right) = f(t; \boldsymbol{v})\;, \quad \text{a.e. } t \in [0, T]\;, \quad \forall \boldsymbol{v} \in V_0 \quad , \tag{A.49}$$

and fulfils the same initial conditions $\boldsymbol{u}_2(0) = \boldsymbol{u}^0$ and $\boldsymbol{u}_2'(0) = \boldsymbol{u}^1$. Let $\boldsymbol{w} = \boldsymbol{u}_2 - \boldsymbol{u}_1$. From (A.48)-(A.49), it follows that $\boldsymbol{w}$ verifies:

$$k_2\left(\boldsymbol{w}(t), \boldsymbol{v}\right) + d\left(\boldsymbol{w}'(t), \boldsymbol{v}\right) + m\left(\frac{d\boldsymbol{w}'}{dt}(t), \boldsymbol{v}\right) = k_1\left(\boldsymbol{u}_1(t), \boldsymbol{v}\right) - k_2\left(\boldsymbol{u}_1(t), \boldsymbol{v}\right)\;, \quad \text{a.e. } t \in [0, T]\;, \quad \forall \boldsymbol{v} \in V_0 \quad , \tag{A.50}$$

with

$$\boldsymbol{w}(0) = \boldsymbol{0} \,, \quad \boldsymbol{w}'(0) = \boldsymbol{0}. \tag{A.51}$$

Upon choosing $\boldsymbol{v} = \boldsymbol{w}'(t)$ and using the symmetry properties of the forms k_2 and m, (A.50) is rewritten as:

$$\frac{1}{2}\frac{d}{dt}\{k_2(\boldsymbol{w}(t), \boldsymbol{w}(t)) + m(\boldsymbol{w}'(t), \boldsymbol{w}'(t))\} + d(\boldsymbol{w}'(t), \boldsymbol{w}'(t)) = k_1(\boldsymbol{u}_1(t), \boldsymbol{w}'(t)) - k_2(\boldsymbol{u}_1(t), \boldsymbol{w}'(t)) \,, \quad \text{a.e. } t \in [0, T]. \tag{A.52}$$

Integrating the two members of (A.52) with respect to the time over $]0, t[$ with $0 < t < T$ and taking into account (A.51), the following "energy equation" is obtained:

$$\frac{1}{2}\{k_2(\boldsymbol{w}(t), \boldsymbol{w}(t)) + m(\boldsymbol{w}'(t), \boldsymbol{w}'(t))\} + \int_0^t d(\boldsymbol{w}'(\tau), \boldsymbol{w}'(\tau))d\tau \tag{A.53}$$

$$= \int_0^t \left(k_1(\boldsymbol{u}_1(\tau), \boldsymbol{w}'(\tau)) - k_2(\boldsymbol{u}_1(\tau), \boldsymbol{w}'(\tau))\right)d\tau.$$

Since the forms k_2, m and d are positive definite, it is deduced from (A.53) that:

$$k_2(\boldsymbol{w}(t), \boldsymbol{w}(t)) \le 2 \int_0^t \left|k_1(\boldsymbol{u}_1(\tau), \boldsymbol{w}'(\tau)) - k_2(\boldsymbol{u}_1(\tau), \boldsymbol{w}'(\tau))\right|d\tau \quad, \tag{A.54}$$

$$m(\boldsymbol{w}'(t), \boldsymbol{w}'(t)) \le 2 \int_0^t \left|k_1(\boldsymbol{u}_1(\tau), \boldsymbol{w}'(\tau)) - k_2(\boldsymbol{u}_1(\tau), \boldsymbol{w}'(\tau))\right|d\tau \quad, \tag{A.55}$$

$$\int_0^t d(\boldsymbol{w}'(\tau), \boldsymbol{w}'(\tau))d\tau \le \int_0^t \left|k_1(\boldsymbol{u}_1(\tau), \boldsymbol{w}'(\tau)) - k_2(\boldsymbol{u}_1(\tau), \boldsymbol{w}'(\tau))\right|d\tau. \tag{A.56}$$

Upon using the inequalities (A.42), (A.45) and (A.46), (A.54)-(A.55)-(A.56) yield:

$$(c_{k1} - \alpha\, d_T(\boldsymbol{C}_1^{\text{e}}, \boldsymbol{C}_2^{\text{e}})) \left\|\boldsymbol{w}(t)\right\|_V^2 \le 2\alpha\, d_T(\boldsymbol{C}_1^{\text{e}}, \boldsymbol{C}_2^{\text{e}}) \int_0^t \left\|\boldsymbol{u}_1(\tau)\right\|_V \left\|\boldsymbol{w}'(\tau)\right\|_V d\tau \quad, \tag{A.57}$$

$$c_m \left\|\boldsymbol{w}'(t)\right\|_H^2 \le 2\alpha\, d_T(\boldsymbol{C}_1^{\text{e}}, \boldsymbol{C}_2^{\text{e}}) \int_0^t \left\|\boldsymbol{u}_1(\tau)\right\|_V \left\|\boldsymbol{w}'(\tau)\right\|_V d\tau \quad, \tag{A.58}$$

$$c_d \int_0^t \left\|\boldsymbol{w}'(\tau)\right\|_V^2 d\tau \le \alpha\, d_T(\boldsymbol{C}_1^{\text{e}}, \boldsymbol{C}_2^{\text{e}}) \int_0^t \left\|\boldsymbol{u}_1(\tau)\right\|_V \left\|\boldsymbol{w}'(\tau)\right\|_V d\tau. \tag{A.59}$$

For two functions $a, b \in L^2(]0, t[, \mathbb{R})$, we have:

$$\int_0^t a(\tau)b(\tau)d\tau \le \frac{1}{2}\int_0^t \left(a(\tau)\right)^2 d\tau + \frac{1}{2}\int_0^t \left(b(\tau)\right)^2 d\tau. \tag{A.60}$$

Inequality (A.60) is applied on (A.59) with

$$a(\tau) = \frac{\alpha\, d_T(\boldsymbol{C}_1^{\text{e}}, \boldsymbol{C}_2^{\text{e}})}{\sqrt{c_d}} \left\|\boldsymbol{u}_1(\tau)\right\|_V \,, \quad b(\tau) = \sqrt{c_d} \left\|\boldsymbol{w}'(\tau)\right\|_V \quad, \tag{A.61}$$

to obtain:

$$\int_0^t \left\|\boldsymbol{w}'(\tau)\right\|_V^2 d\tau \le \frac{(\alpha\, d_T(\boldsymbol{C}_1^{\text{e}}, \boldsymbol{C}_2^{\text{e}}))^2}{c_d^2} \int_0^T \left\|\boldsymbol{u}_1(\tau)\right\|_V^2 d\tau. \tag{A.62}$$

Finally, inequality (A.60) is applied on (A.57) and (A.58) with

$$a(\tau) = \alpha\, d_T(\boldsymbol{C}_1^{\text{e}}, \boldsymbol{C}_2^{\text{e}}) \left\|\boldsymbol{u}_1(\tau)\right\|_V \,, \quad b(\tau) = \left\|\boldsymbol{w}'(\tau)\right\|_V \quad, \tag{A.63}$$

to obtain, using (A.62):

$$\left\|\boldsymbol{w}(t)\right\|_V^2 \le \frac{(\alpha\, d_T(\boldsymbol{C}_1^{\text{e}}, \boldsymbol{C}_2^{\text{e}}))^2}{(c_{k1} - \alpha\, d_T(\boldsymbol{C}_1^{\text{e}}, \boldsymbol{C}_2^{\text{e}}))} \left(1 + \frac{1}{c_d^2}\right) \int_0^T \left\|\boldsymbol{u}_1(\tau)\right\|_V^2 d\tau \quad, \tag{A.64}$$

$$\left\|\boldsymbol{w}'(t)\right\|_H^2 \le \frac{(\alpha\, d_T(\boldsymbol{C}_1^{\text{e}}, \boldsymbol{C}_2^{\text{e}}))^2}{c_m} \left(1 + \frac{1}{c_d^2}\right) \int_0^T \left\|\boldsymbol{u}_1(\tau)\right\|_V^2 d\tau. \tag{A.65}$$

The theorem follows from inequalities (A.64) and (A.65). $\qquad\qquad\square$

A.6 Proof: measurability of the random solution

As a second step towards proving the square-integrability of the random solution of the time-domain parametric probabilistic model (A.21)-(A.22), this section studies the measurability properties of this random solution. From the point of view of the measurability, the construction of the time-domain parametric probabilistic model involves the following steps:

- First, 21 mutually independent stochastic germs of the form (1.78) are chosen in the set $\mathcal{E}_{\mathbb{G}}$, defined in Section 1.1. In view of the sample-continuity of the random fields in $\mathcal{E}_{\mathbb{G}}$, each stochastic germ defines a random variable on $(\mathcal{A}, \mathcal{F}, P)$ with values in the function space $\mathcal{C}^0(\overline{\Omega}, \mathbb{R})$ a.s. It can be shown [see Krée and Soize, 1986, ch. 10 sec. 4]) that this random variable is Borel measurable.

- Then, these 21 stochastic germs are gathered in a set of the form (1.82) and transformed through the continuous mappings defined by (1.80) and (1.86) to obtain the random elasticity tensor field $\mathbb{C}^{\mathrm{e}}(\boldsymbol{p})$ defined on $(\mathcal{A}, \mathcal{F}, P)$ with values in $\mathrm{T}_4^+(\Omega)$ a.s.

- Subsequently, $\mathbb{C}^{\mathrm{e}}(\boldsymbol{p})$ is transformed through the continuous (Sec. A.5) mapping γ_{P} to define the random position- and time-dependent displacement and velocity fields $\mathbb{U}(\boldsymbol{p})$ and $\mathbb{U}'(\boldsymbol{p})$ on $(\mathcal{A}, \mathcal{F}, P)$ with values in $\mathcal{C}^0([0, T], V_0)$ and $\mathcal{C}^0([0, T], H_0)$ a.s., respectively.

- Finally, $\mathbb{U}(\boldsymbol{p})$ and $\mathbb{U}'(\boldsymbol{p})$ can be transformed through a continuous mapping of the form $\delta_t : \boldsymbol{v} \mapsto \boldsymbol{v}(t)$ to obtain the random variables $\mathbb{U}(t; \boldsymbol{p})$ and $\mathbb{U}'(t; \boldsymbol{p})$ on $(\mathcal{A}, \mathcal{F}, P)$ with values in V_0 and H_0 a.s., which are the random position-dependent displacement and velocity fields at a time instant $t \in [0, T]$ of interest. It is noted that the sample-continuity of the response field with respect to the time is essential to ensure the continuity of δ_t.

Since the composition of a measurable mapping with a continuous (hence, measurable) mapping is also a measurable mapping, all aforementioned random variables are Borel measurable. The Borel measurability is an important mathematical property in view of the later study of the integrability properties of the response field. As an example, let $P_{\mathbb{U}(t)}(\cdot; \boldsymbol{p})$ denote the probability measure induced by $\mathbb{U}(t; \boldsymbol{p})$ on the measurable space $(V_0, \mathscr{B}(V_0))$. Then, the norm

$$E\left\{\left|\left|(\mathbb{U}(t; \boldsymbol{p}))\right|\right|_V^2\right\} = \int_{V_0} \left|\left|(\boldsymbol{v})\right|\right|_V^2 P_{\mathbb{U}(t)}(d\boldsymbol{v}; \boldsymbol{p}) \tag{A.66}$$

is well-defined as the Lebesgue integral of the measurable mapping $||\cdot||_V^2$ from the measured space $(V_0, \mathscr{B}(V_0), P_{\mathbb{U}(t)}(\cdot; \boldsymbol{p}))$ into $(\mathbb{R}, \mathscr{B}(\mathbb{R}))$, where $\mathscr{B}(\mathbb{R})$ denotes the Borel σ-algebra on $\mathbb{R}$.

A.7 Proof: square-integrability of the random solution

Having established in the previous section the Borel measurability of the random solution of the time-domain parametric probabilistic model (A.21)-(A.22), this section demonstrates the square-integrabililty of this solution. In particular, it is proved that, if the dispersion parameter δ in $\boldsymbol{p}$ fulfils the inequality (1.46), then the inequalities (A.25) are fulfilled. The proof is based upon comparable demonstrations given in [Soize, 2000, 2001] for time- and frequency-domain non-parametric probabilistic models and in [Soize, 2006] for elastostatic parametric probabilistic models.

Appendix A. Construction of time-domain parametric probabilistic models

Proof. In this proof, we make use of the second-rank tensor representation for fourth-rank tensors, which was introduced in Section 1.1. For the sake of the simplicity of the notations, the dependence on $\boldsymbol{p}$ is suppressed everywhere and, moreover, the initial displacement and velocity fields are assumed vanishing (the generalization poses no theoretical difficulty):

$$\mathbb{U}(0) = \mathbf{0} \text{ a.s. }, \quad \mathbb{U}'(0) = \mathbf{0} \text{ a.s.} \tag{A.67}$$

Let $\underline{k}$ be the stiffness form corresponding to the mean elasticity tensor field $\boldsymbol{x} \to \underline{\boldsymbol{C}}^{\text{e}}(\boldsymbol{x})$:

$$\underline{k}(\boldsymbol{v}_1, \boldsymbol{v}_2) = \int_\Omega \text{tr}\big(\underline{\boldsymbol{C}}^{\text{e}}\,(\boldsymbol{\epsilon}(\boldsymbol{v}_1))\,\boldsymbol{\epsilon}(\boldsymbol{v}_2)\big)d\Omega = \int_\Omega \big(\underline{\widehat{\boldsymbol{C}}}^{\text{e}}\widehat{\boldsymbol{\epsilon}}(\boldsymbol{v}_1), \widehat{\boldsymbol{\epsilon}}(\boldsymbol{v}_2)\big)\,d\Omega. \tag{A.68}$$

The stiffness form $\underline{k}$, the damping form d and the mass form m are positive definite. Let $c_k, c_d, c_m \in \mathbb{R}_0^+$ be positive constants such that:

$$\underline{k}(\boldsymbol{v}, \boldsymbol{v}) \geq c_k \,||\boldsymbol{v}||_V^2 \ , \quad d(\boldsymbol{v}, \boldsymbol{v}) \geq c_d \,||\boldsymbol{v}||_V^2 \ , \quad m(\boldsymbol{v}, \boldsymbol{v}) \geq c_m \,||\boldsymbol{v}||_H^2 \ . \tag{A.69}$$

In view of (A.18), the form f representing the external loading fulfils:

$$f(t; \boldsymbol{v}) \leq ||\boldsymbol{f}(t)||_{V'} \,||\boldsymbol{v}||_V \ , \quad \text{a.e. } t \in [0, T] \quad , \tag{A.70}$$

where the force vector $\boldsymbol{f}(t)$ is such that $\langle \boldsymbol{f}(t), \boldsymbol{v}\rangle = f(t; \boldsymbol{v})$ and $||\cdot||_{V'}$ is the norm on V_0' defined by:

$$||\boldsymbol{g}||_{V'} = \sup_{\boldsymbol{v} \in V_0, \boldsymbol{v} \neq 0} \frac{|\langle \boldsymbol{g}, \boldsymbol{v}\rangle|}{||\boldsymbol{v}||_V}. \tag{A.71}$$

In view of (A.18), we have:

$$\boldsymbol{f} \in L^2(]0, T[, V_0'). \tag{A.72}$$

With reference to (1.86), the stiffness form $\underline{k}$ verifies:

$$\underline{k}(\boldsymbol{v}, \boldsymbol{v}) = \int_\Omega \big(\underline{\boldsymbol{L}_C}\widehat{\boldsymbol{\epsilon}}(\boldsymbol{v}), \underline{\boldsymbol{L}_C}\widehat{\boldsymbol{\epsilon}}(\boldsymbol{v})\big)\,d\Omega \tag{A.73}$$

$$= \int_\Omega \big(\mathbb{N}^{-1}\sqrt{\mathbb{N}}\underline{\boldsymbol{L}_C}\widehat{\boldsymbol{\epsilon}}(\boldsymbol{v}), \sqrt{\mathbb{N}}\underline{\boldsymbol{L}_C}\widehat{\boldsymbol{\epsilon}}(\boldsymbol{v})\big)\,d\Omega$$

$$\leq \int_\Omega ||\mathbb{N}^{-1}||\,\Big|\Big|\sqrt{\mathbb{N}}\underline{\boldsymbol{L}_C}\widehat{\boldsymbol{\epsilon}}(\boldsymbol{v})\Big|\Big|^2\,d\Omega$$

$$\leq \sup_{\boldsymbol{x} \in \overline{\Omega}}\big(||\mathbb{N}(\boldsymbol{x})^{-1}||\big)\int_\Omega \big(\sqrt{\mathbb{N}}\underline{\boldsymbol{L}_C}\widehat{\boldsymbol{\epsilon}}(\boldsymbol{v}), \sqrt{\mathbb{N}}\underline{\boldsymbol{L}_C}\widehat{\boldsymbol{\epsilon}}(\boldsymbol{v})\big)\,d\Omega$$

$$= \sup_{\boldsymbol{x} \in \overline{\Omega}}\big(||\mathbb{N}(\boldsymbol{x})^{-1}||\big)\int_\Omega \big(\underline{\boldsymbol{L}_C}^{\text{T}}\mathbb{N}\underline{\boldsymbol{L}_C}\widehat{\boldsymbol{\epsilon}}(\boldsymbol{v}), \widehat{\boldsymbol{\epsilon}}(\boldsymbol{v})\big)\,d\Omega$$

$$= \sup_{\boldsymbol{x} \in \overline{\Omega}}\big(||\mathbb{N}(\boldsymbol{x})^{-1}||\big)\,\mathbb{K}(\boldsymbol{v}, \boldsymbol{v}).$$

Upon choosing $\boldsymbol{v} = \mathbb{U}'(t)$, (A.21) reads:

$$\left(\mathbb{K}\big(\mathbb{U}(t), \mathbb{U}'(t)\big) + d\big(\mathbb{U}'(t), \mathbb{U}'(t)\big) + m\left(\frac{d\mathbb{U}'}{dt}(t), \mathbb{U}'(t)\right) = f\big(t; \mathbb{U}'(t)\big) , \quad \text{a.e. } t \in [0, T]\right) \text{ a.s.} \tag{A.74}$$

Upon using the symmetry properties of the forms $\mathbb{K}$ and m, (A.74) is rewritten as:

$$\left(\frac{1}{2}\frac{d}{dt}\big\{\mathbb{K}\big(\mathbb{U}(t), \mathbb{U}(t)\big) + m\big(\mathbb{U}'(t), \mathbb{U}'(t)\big)\big\} + d\big(\mathbb{U}'(t), \mathbb{U}'(t)\big) = f\big(t; \mathbb{U}'(t)\big) , \quad \text{a.e. } t \in [0, T]\right) \text{ a.s.} \tag{A.75}$$

Integrating the two members of (A.75) with respect to the time over $]0, t[$ with $0 < t < T$ and taking into account (A.67), the following "energy equation" is obtained:

$$\frac{1}{2}\big\{\mathbb{K}\big(\mathbb{U}(t), \mathbb{U}(t)\big) + m\big(\mathbb{U}'(t), \mathbb{U}'(t)\big)\big\} + \int_0^t d\big(\mathbb{U}'(\tau), \mathbb{U}'(\tau)\big)d\tau = \int_0^t f\big(\tau; \mathbb{U}'(\tau)\big)d\tau \text{ a.s.} \tag{A.76}$$

Since the forms $\mathbb{K}$, m and d are a.s. positive definite, it is deduced from (A.76) that:

$$\mathbb{K}\big(\mathbb{U}(t), \mathbb{U}(t)\big) \leq 2\int_0^t \big|f\big(\tau; \mathbb{U}'(\tau)\big)\big|\,d\tau \text{ a.s.} \quad , \tag{A.77}$$

$$m\big(\mathbb{U}'(t), \mathbb{U}'(t)\big) \leq 2\int_0^t \big|f\big(\tau; \mathbb{U}'(\tau)\big)\big|\,d\tau \text{ a.s.} \quad , \tag{A.78}$$

$$\int_0^t d\big(\mathbb{U}'(\tau), \mathbb{U}'(\tau)\big)d\tau \leq \int_0^t \big|f\big(\tau; \mathbb{U}'(\tau)\big)\big|\,d\tau \text{ a.s.} \tag{A.79}$$

Upon using the inequalities (A.69), (A.70) and (A.73), it follows that:

$$c_k \left|\left|\mathbb{U}(t)\right|\right|_V^2 \leq 2 \int_0^t \left|\left|\boldsymbol{f}(\tau)\right|\right|_{V'} \sup_{\boldsymbol{x} \in \overline{\Omega}} \left(\left|\left|\mathbb{N}(\boldsymbol{x})^{-1}\right|\right|\right) \left|\left|\mathbb{U}'(\tau)\right|\right|_V d\tau \text{ a.s. } , \tag{A.80}$$

$$c_m \left|\left|\mathbb{U}'(t)\right|\right|_H^2 \leq 2 \int_0^t \left|\left|\boldsymbol{f}(\tau)\right|\right|_{V'} \left|\left|\mathbb{U}'(\tau)\right|\right|_V d\tau \text{ a.s. } , \tag{A.81}$$

$$c_d \int_0^t \left|\left|\mathbb{U}'(\tau)\right|\right|_V^2 d\tau \leq \int_0^t \left|\left|\boldsymbol{f}(\tau)\right|\right|_{V'} \left|\left|\mathbb{U}'(\tau)\right|\right|_V d\tau \text{ a.s.} \tag{A.82}$$

Upon taking the mathematical expectation, inequalities (A.80)-(A.81)-(A.82) yield:

$$c_k E\left\{\left|\left|\mathbb{U}(t)\right|\right|_V^2\right\} \leq 2 \int_0^t \left|\left|\boldsymbol{f}(\tau)\right|\right|_{V'} E\left\{\sup_{\boldsymbol{x} \in \overline{\Omega}} \left(\left|\left|\mathbb{N}(\boldsymbol{x})^{-1}\right|\right|\right) \left|\left|\mathbb{U}'(\tau)\right|\right|_V\right\} d\tau , \tag{A.83}$$

$$c_m E\left\{\left|\left|\mathbb{U}'(t)\right|\right|_H^2\right\} \leq 2 \int_0^t \left|\left|\boldsymbol{f}(\tau)\right|\right|_{V'} E\left\{\left|\left|\mathbb{U}'(\tau)\right|\right|_V\right\} d\tau , \tag{A.84}$$

$$c_d \int_0^t E\left\{\left|\left|\mathbb{U}'(\tau)\right|\right|_V^2\right\} d\tau \leq \int_0^t \left|\left|\boldsymbol{f}(\tau)\right|\right|_{V'} E\left\{\left|\left|\mathbb{U}'(\tau)\right|\right|_V\right\} d\tau. \tag{A.85}$$

Upon applying the Hölder inequality, (A.83)-(A.84)-(A.85) yield:

$$c_k E\left\{\left|\left|\mathbb{U}(t)\right|\right|_V^2\right\} \leq 2 \int_0^t \left|\left|\boldsymbol{f}(\tau)\right|\right|_{V'} \sqrt{E\left\{\left(\sup_{\boldsymbol{x} \in \overline{\Omega}} \left|\left|\mathbb{N}(\boldsymbol{x})^{-1}\right|\right|\right)^2\right\}} \sqrt{E\left\{\left|\left|\mathbb{U}'(\tau)\right|\right|_V^2\right\}} d\tau , \tag{A.86}$$

$$c_m E\left\{\left|\left|\mathbb{U}'(t)\right|\right|_H^2\right\} \leq 2 \int_0^t \left|\left|\boldsymbol{f}(\tau)\right|\right|_{V'} \sqrt{E\left\{\left|\left|\mathbb{U}'(\tau)\right|\right|_V^2\right\}} d\tau , \tag{A.87}$$

$$c_d \int_0^t E\left\{\left|\left|\mathbb{U}'(\tau)\right|\right|_V^2\right\} d\tau \leq \int_0^t \left|\left|\boldsymbol{f}(\tau)\right|\right|_{V'} \sqrt{E\left\{\left|\left|\mathbb{U}'(\tau)\right|\right|_V^2\right\}} d\tau. \tag{A.88}$$

Inequality (A.60) is applied on (A.88) with:

$$a(\tau) = \frac{1}{\sqrt{c_d}} \left|\left|\boldsymbol{f}(\tau)\right|\right|_{V'} , \quad b(\tau) = \sqrt{c_d} \sqrt{E\left\{\left|\left|\mathbb{U}'(\tau)\right|\right|_V^2\right\}} , \tag{A.89}$$

to obtain:

$$\int_0^t E\left\{\left|\left|\mathbb{U}'(\tau)\right|\right|_V^2\right\} d\tau \leq \frac{1}{c_d^2} \int_0^T \left|\left|\boldsymbol{f}(\tau)\right|\right|_{V'}^2 d\tau. \tag{A.90}$$

Finally, inequality (A.60) is applied on (A.86)-(A.87) respectively with:

$$a(\tau) = \frac{\sqrt{E\left\{\left(\sup_{\boldsymbol{x} \in \overline{\Omega}} \left|\left|\mathbb{N}(\boldsymbol{x})^{-1}\right|\right|\right)^2\right\}}}{\sqrt{c_k}} \left|\left|\boldsymbol{f}(\tau)\right|\right|_{V'} , \qquad b(\tau) = \sqrt{c_k} \sqrt{E\left\{\left|\left|\mathbb{U}'(\tau)\right|\right|_V^2\right\}} , \tag{A.91}$$

$$a(\tau) = \frac{1}{\sqrt{c_m}} \left|\left|\boldsymbol{f}(\tau)\right|\right|_{V'} , \qquad b(\tau) = \sqrt{c_m} \sqrt{E\left\{\left|\left|\mathbb{U}'(\tau)\right|\right|_V^2\right\}} , \tag{A.92}$$

to obtain, using (A.90):

$$E\left\{\left|\left|\mathbb{U}(t)\right|\right|_V^2\right\} \leq \left(\frac{E\left\{\left(\sup_{\boldsymbol{x} \in \overline{\Omega}} \left|\left|\mathbb{N}(\boldsymbol{x})^{-1}\right|\right|\right)^2\right\}}{c_k^2} + \frac{1}{c_d^2}\right) \int_0^T \left|\left|\boldsymbol{f}(\tau)\right|\right|_{V'}^2 d\tau , \tag{A.93}$$

$$E\left\{\left|\left|\mathbb{U}'(t)\right|\right|_H^2\right\} \leq \left(\frac{1}{c_m^2} + \frac{1}{c_d^2}\right) \int_0^T \left|\left|\boldsymbol{f}(\tau)\right|\right|_{V'}^2 d\tau. \tag{A.94}$$

The inequalities (A.25) follow from the inequalities (A.93)-(A.94) using (A.72) and the property (1.85). $\square$

Appendix A. Construction of time-domain parametric probabilistic models

B

Random matrix eigenvalue problem

In the frame of the non-parametric probabilistic modelling of the dynamical behaviour of structures in Chapter 1, a stochastic model with minimal parameterization for random reduced structural matrices was presented. In this appendix, a random matrix eigenvalue problem is formulated using random structural matrices of this kind. We note that considerable effort has already been expended in the literature to the study of random matrix eigenvalue problems [see, for instance, Adhikari, 2007, Collins and Thomson, 1969, Ghosh et al., 2005, Rahman, 2006].

Let us consider the model problem outlined in Section 1.1. Let $\boldsymbol{K}$ and $\boldsymbol{M}$ be the reduced stiffness and mass matrices obtained by the projection of corresponding stiffness and mass forms onto a reduction basis $\{\boldsymbol{\varphi}_k \mid 1 \leq k \leq n_\mathrm{T}\}$. Let $\mathbb{K}$ and $\mathbb{M}$ be corresponding random reduced stiffness and mass matrices such that:

$$\mathbb{K} = \boldsymbol{L}_\mathrm{K}^\mathrm{T}\mathbb{N}_\mathrm{K}\boldsymbol{L}_\mathrm{K} \text{ a.s.}, \quad \mathbb{M} = \boldsymbol{L}_\mathrm{M}^\mathrm{T}\mathbb{N}_\mathrm{M}\boldsymbol{L}_\mathrm{M} \text{ a.s.} \quad , \tag{B.1}$$

where $\mathbb{N}_\mathrm{K}$ and $\mathbb{N}_\mathrm{M}$ are normalized random matrices in the set SG^+, which was defined in Section 1.1, and $\boldsymbol{L}_\mathrm{K}$ and $\boldsymbol{L}_\mathrm{M}$ are the Cholesky factors of $\boldsymbol{K}$ and $\boldsymbol{M}$, respectively. Since $\mathbb{N}_\mathrm{K}$ and $\mathbb{N}_\mathrm{M}$ are normalized matrices, we have:

$$E\{\mathbb{K}\} = \boldsymbol{K} , \quad E\{\mathbb{M}\} = \boldsymbol{M}. \tag{B.2}$$

The random matrices $\mathbb{K}$ and $\mathbb{M}$ define the following random matrix eigenvalue problem:

$$\mathbb{K}\mathbb{Q}_k = \mathbb{W}_k^2\mathbb{M}\mathbb{Q}_k \text{ a.s.} \quad , \tag{B.3}$$

where the collection $\{\mathbb{Q}_k \mid 1 \leq k \leq n_\mathrm{T}\}$ gathers the random eigenvectors and $\{\mathbb{W}_k \mid 1 \leq k \leq n_\mathrm{T}\}$ collects the random circular eigenfrequencies. Each random eigenvector $\mathbb{Q}_k$ defines a corresponding random vector Φ_k with values in the space spanned by the reduction basis such that:

$$\Phi_k = \sum_{\alpha=1}^{n_\mathrm{T}} [\mathbb{Q}_k]_\alpha \boldsymbol{\varphi}_\alpha \text{ a.s.} \tag{B.4}$$

Since the eigenfrequencies are non-linear functions of the reduced matrices, the mean values of the random eigenfrequencies generally differ from the eigenfrequencies of the mean matrices $\boldsymbol{K}$ and $\boldsymbol{M}$. The lowest, and the highest, random eigenfrequencies are generally smaller, and larger, than the corresponding eigenfrequencies of the mean matrices. This can be understood from the Rayleigh quotient. For a fixed $a \in \mathcal{A}$, the realizations $\{\mathbb{W}_k(a) \mid 1 \leq k \leq n_\mathrm{T}\}$ associated to the realizations $\mathbb{K}(a)$ and $\mathbb{M}(a)$ can be obtained by the sequential minimization of the Rayleigh quotient [see, for instance, Géradin and Rixen, 1992]:

$$\mathbb{W}_k^2(a) = \arg \min_{\boldsymbol{x} \in \mathcal{W}_k(a)} \frac{(\mathbb{K}(a)\boldsymbol{x}, \boldsymbol{x})}{(\mathbb{M}(a)\boldsymbol{x}, \boldsymbol{x})} \quad , \tag{B.5}$$

where $\mathcal{W}_k(a)$ is the subspace of $\mathbb{R}^{n_{\mathrm{T}}}$ orthogonal to the eigenvectors with lower eigenfrequencies. The sequential minimization first finds the vectors $\boldsymbol{x}$ combining a smaller elastic energy $(\mathbb{K}(a)\boldsymbol{x}, \boldsymbol{x}) < (\boldsymbol{K}\boldsymbol{x}, \boldsymbol{x})$ with a larger kinetic energy $(\mathbb{M}(a)\boldsymbol{x}, \boldsymbol{x}) > (\boldsymbol{M}\boldsymbol{x}, \boldsymbol{x})$ such that the lowest random eigenfrequencies (and their mean values) are generally smaller than the corresponding eigenfrequencies of $\boldsymbol{K}$ and $\boldsymbol{M}$. In contrast, at the end of the sequential minimization process, the space $\mathcal{W}_k(a)$ spans vectors $\boldsymbol{x}$ with $(\mathbb{K}(a)\boldsymbol{x}, \boldsymbol{x}) > (\boldsymbol{K}\boldsymbol{x}, \boldsymbol{x})$ and $(\mathbb{M}(a)\boldsymbol{x}, \boldsymbol{x}) < (\boldsymbol{M}\boldsymbol{x}, \boldsymbol{x})$ such that the highest random eigenfrequencies (and their mean values) are generally larger the corresponding eigenfrequencies of $\boldsymbol{K}$ and $\boldsymbol{M}$.

C

Signal processing methods for transfer function measurements

This appendix, which presents known material, describes the signal processing methods for the measurement of Transfer Functions (TFs), which are applied in this dissertation. We refer the reader to [Bendat and Piersol, 1986, Pintelon and Schoukens, 2001] for a more complete account of the theory of signal processing.

C.1 Problem setting

Let us consider a general problem where a vibration test is carried out on a single structure under noisy conditions. Let a broadband time-limited excitation (for instance, a hammer impact) be applied on the structure under study at a fixed point and let the induced mechanical motion be measured at another fixed point (located at a sufficiently large distance from the applied loading) along a fixed direction. Let this experiment be repeated n_R times. The time-sampled data thus obtained are subsequently transformed into the frequency domain by means of the Discrete Fourier Transform (DFT) to obtain:

$$\{f_r(\omega_\ell) \in \mathbb{C} \mid 1 \leq \ell \leq n_\mathrm{F} , \ 1 \leq r \leq n_\mathrm{R}\} \quad , \tag{C.1}$$

$$\{y_r(\omega_\ell) \in \mathbb{C} \mid 1 \leq \ell \leq n_\mathrm{F} , \ 1 \leq r \leq n_\mathrm{R}\} \quad , \tag{C.2}$$

where $\{\omega_\ell \mid 1 \leq \ell \leq n_\mathrm{F}\}$ is the set of n_F discrete frequencies.

C.2 Random signal processing

The observed data (C.1)-(C.2) obtained for the n_R repetitions of the experiment are expected to exhibit variability due to the experimental noise. In the framework of random signal processing, the fundamental modelling assumption is made that the fluctuations can be described in a stochastic framework, and, in particular, that the observed data values can adequately be viewed as independent and identically-distributed (iid) realizations of a data-generating stochastic process. Let the measured applied forces and responses (C.1)-(C.2) be n_R iid realizations of two stochastic processes $\{\tilde{\mathbb{F}}(\omega_\ell) \mid 1 \leq \ell \leq n_\mathrm{F}\}$ and $\{\tilde{\mathbb{Y}}(\omega_\ell) \mid 1 \leq \ell \leq n_\mathrm{F}\}$ indexed by the discrete frequencies $\{\omega_\ell \mid 1 \leq \ell \leq n_\mathrm{F}\}$ and with values

in $\mathbb{C}$ a.s. These random signals are processed as follows. For a fixed frequency ω_ℓ, the energy cross-spectral density $S_{\mathrm{yf}}(\omega_\ell) \in \mathbb{C}$ is defined by:

$$S_{\mathrm{yf}}(\omega_\ell) = E\left\{\tilde{\mathbb{Y}}(\omega_\ell)\overline{\tilde{\mathbb{F}}}(\omega_\ell)\right\}. \tag{C.3}$$

The energy autospectral densities $S_{\mathrm{ff}}(\omega_\ell) \in \mathbb{R}^+$ and $S_{\mathrm{yy}}(\omega_\ell) \in \mathbb{R}^+$ are defined by:

$$S_{\mathrm{ff}}(\omega_\ell) = E\left\{\tilde{\mathbb{F}}(\omega_\ell)\overline{\tilde{\mathbb{F}}}(\omega_\ell)\right\}, \quad S_{\mathrm{yy}}(\omega_\ell) = E\left\{\tilde{\mathbb{Y}}(\omega_\ell)\overline{\tilde{\mathbb{Y}}}(\omega_\ell)\right\}. \tag{C.4}$$

If $\tilde{\mathbb{Y}}(\omega_\ell)$ can be predicted by a linear relation from $\tilde{\mathbb{F}}(\omega_\ell)$, i.e. if $\tilde{\mathbb{Y}}(\omega_\ell) = h(\omega_\ell)\tilde{\mathbb{F}}(\omega_\ell)$ a.s., then:

$$S_{\mathrm{yy}}(\omega_\ell) = |h(\omega_\ell)|^2 S_{\mathrm{ff}}(\omega_\ell), \quad S_{\mathrm{yf}}(\omega_\ell) = h(\omega_\ell)S_{\mathrm{ff}}(\omega_\ell). \tag{C.5}$$

Finally, the coherence $\gamma^2(\omega_\ell)$ of $\tilde{\mathbb{F}}(\omega_\ell)$ and $\tilde{\mathbb{Y}}(\omega_\ell)$ is defined by:

$$\gamma^2(\omega_\ell) = \frac{|S_{\mathrm{yf}}(\omega_\ell)|^2}{S_{\mathrm{ff}}(\omega_\ell)S_{\mathrm{yy}}(\omega_\ell)}. \tag{C.6}$$

Due to the Hölder inequality, we have:

$$\left|E\left\{\tilde{\mathbb{Y}}(\omega_\ell)\overline{\tilde{\mathbb{F}}}(\omega_\ell)\right\}\right| \leq E\left\{\left|\tilde{\mathbb{Y}}(\omega_\ell)\overline{\tilde{\mathbb{F}}}(\omega_\ell)\right|\right\} \leq \sqrt{E\left\{\left|\tilde{\mathbb{Y}}(\omega_\ell)\right|^2\right\}}\sqrt{E\left\{\left|\tilde{\mathbb{F}}(\omega_\ell)\right|^2\right\}}. \tag{C.7}$$

Hence, for each ω_ℓ, $\gamma^2(\omega_\ell)$ satisfies $0 \leq \gamma^2(\omega_\ell) \leq 1$. If $\tilde{\mathbb{Y}}(\omega_\ell)$ can be predicted by a linear relationship from $\tilde{\mathbb{F}}(\omega_\ell)$, then $\gamma^2(\omega_\ell) = 1$.

C.3 Discrete signal processing and estimation

Since the stochastic processes $\{\tilde{\mathbb{F}}(\omega_\ell) \mid 1 \leq \ell \leq n_{\mathrm{F}}\}$ and $\{\tilde{\mathbb{Y}}(\omega_\ell) \mid 1 \leq \ell \leq n_{\mathrm{F}}\}$ are usually unknown in practice, the signal processing methods described in the previous subsection are not of direct practical use. However, it will now be shown that very useful estimation methods can be defined on the basis of the above-introduced concepts.

For a fixed frequency ω_ℓ, let the vectors $\boldsymbol{f}(\omega_\ell)$ and $\boldsymbol{y}(\omega_\ell)$ collect the n_{R} measured forces and responses such that:

$$\boldsymbol{f}(\omega_\ell) = \left(f_1(\omega_\ell), \ldots, f_{n_{\mathrm{R}}}(\omega_\ell)\right), \quad \boldsymbol{y}(\omega_\ell) = \left(y_1(\omega_\ell), \ldots, y_{n_{\mathrm{R}}}(\omega_\ell)\right). \tag{C.8}$$

With reference to (C.5) and (C.6), we define the following estimates of the TF from the applied force to the induced response (sometimes called the H1-estimate) and of the coherence:

$$\hat{h}_{n_{\mathrm{R}}}\left(\boldsymbol{f}(\omega_\ell), \boldsymbol{y}(\omega_\ell)\right) = \frac{\frac{1}{n_{\mathrm{R}}}\sum_{r=1}^{n_{\mathrm{R}}} y_r(\omega_\ell)\overline{f}_r(\omega_\ell)}{\frac{1}{n_{\mathrm{R}}}\sum_{r=1}^{n_{\mathrm{R}}} |f_r(\omega_\ell)|^2}, \tag{C.9}$$

$$\hat{\gamma}^2_{n_{\mathrm{R}}}\left(\boldsymbol{f}(\omega_\ell), \boldsymbol{y}(\omega_\ell)\right) = \frac{\left|\frac{1}{n_{\mathrm{R}}}\sum_{r=1}^{n_{\mathrm{R}}} y_r(\omega_\ell)\overline{f}_r(\omega_\ell)\right|^2}{\left(\frac{1}{n_{\mathrm{R}}}\sum_{r=1}^{n_{\mathrm{R}}} |f_r(\omega_\ell)|^2\right)\left(\frac{1}{n_{\mathrm{R}}}\sum_{r=1}^{n_{\mathrm{R}}} |y_r(\omega_\ell)|^2\right)}. \tag{C.10}$$

C.4   Asymptotic properties of the estimators

In order to establish the usefulness of the estimates (C.9)-(C.10), we place ourselves again in the framework of random signal analysis and postulate that, for each ω_ℓ, the random variables $\tilde{\mathbb{F}}(\omega_\ell)$ and $\tilde{\mathbb{Y}}(\omega_\ell)$ have the following generic form:

$$\tilde{\mathbb{F}}(\omega_\ell) = \tilde{\mathbb{F}}^0(\omega_\ell) + \tilde{\mathbb{E}}_f(\omega_\ell) \text{ a.s.} \quad , \tag{C.11}$$

$$\tilde{\mathbb{Y}}(\omega_\ell) = \tilde{\mathbb{Y}}^0(\omega_\ell) + \tilde{\mathbb{E}}_y(\omega_\ell) \text{ a.s. with } \tilde{\mathbb{Y}}^0(\omega_\ell) = h^0(\omega_\ell)\tilde{\mathbb{F}}^0(\omega_\ell) \text{ a.s.} \tag{C.12}$$

To improve the readability, the equations (C.11)-(C.12) are represented by a block diagram:
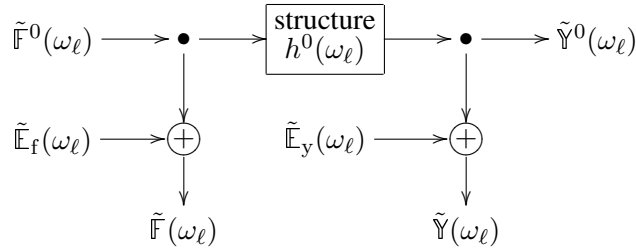
The random variable $\tilde{\mathbb{F}}^0(\omega_\ell)$ represents the inherent variability of the loading (for instance, the excitation generated by a hand held hammer is inherently different for each repetition). The random variable $\tilde{\mathbb{Y}}^0(\omega_\ell)$ represents the consequent variability of the induced structural response. The function $h^0 : \mathbb{R} \to \mathbb{C} : \omega \mapsto h^0(\omega)$ is the noise-free TF of the structure. The random variables $\tilde{\mathbb{E}}_f(\omega_\ell)$ and $\tilde{\mathbb{E}}_y(\omega_\ell)$ represent the experimental noise disturbing the measurement of the force and the response, respectively. They are assumed to satisfy:

$$E\left\{\tilde{\mathbb{E}}_f(\omega_\ell)\right\} = 0 \,, \qquad\qquad E\left\{\tilde{\mathbb{E}}_y(\omega_\ell)\right\} = 0 \quad , \tag{C.13}$$

$$E\left\{\left|\tilde{\mathbb{E}}_f(\omega_\ell)\right|^2\right\} = \sigma_f^2(\omega_\ell) \,, \qquad\qquad E\left\{\left|\tilde{\mathbb{E}}_y(\omega_\ell)\right|^2\right\} = \sigma_y^2(\omega_\ell) \quad , \tag{C.14}$$

$$E\left\{\tilde{\mathbb{E}}_f(\omega_\ell)\tilde{\mathbb{E}}_y(\omega_\ell)\right\} = 0 \,, \qquad\qquad E\left\{\tilde{\mathbb{E}}_f(\omega_\ell)\overline{\tilde{\mathbb{E}}}_y(\omega_\ell)\right\} = 0. \tag{C.15}$$

Finally, $\tilde{\mathbb{E}}_f(\omega_\ell)$ and $\tilde{\mathbb{E}}_y(\omega_\ell)$ are assumed to be independent of $\tilde{\mathbb{F}}^0(\omega_\ell)$ and $\tilde{\mathbb{Y}}^0(\omega_\ell)$. Let the vectors

$$\mathbb{F}(\omega_\ell) = \left(\mathbb{F}_1(\omega_\ell),\ldots,\mathbb{F}_{n_R}(\omega_\ell)\right) \,, \quad \mathbb{Y}(\omega_\ell) = \left(\mathbb{Y}_1(\omega_\ell),\ldots,\mathbb{Y}_{n_R}(\omega_\ell)\right) \tag{C.16}$$

collect n_R independent copies of $\tilde{\mathbb{F}}(\omega_\ell)$ and $\tilde{\mathbb{Y}}(\omega_\ell)$. The estimators related to the estimates (C.9)-(C.10) then read as:

$$\hat{h}_{n_R}\left(\mathbb{F}(\omega_\ell),\mathbb{Y}(\omega_\ell)\right) = \frac{\frac{1}{n_R}\sum_{r=1}^{n_R}\mathbb{Y}_r(\omega_\ell)\overline{\mathbb{F}}_r(\omega_\ell)}{\frac{1}{n_R}\sum_{r=1}^{n_R}|\mathbb{F}_r(\omega_\ell)|^2} \text{ a.s.} \quad , \tag{C.17}$$

$$\hat{\gamma}_{n_R}^2\left(\mathbb{F}(\omega_\ell),\mathbb{Y}(\omega_\ell)\right) = \frac{\left|\frac{1}{n_R}\sum_{r=1}^{n_R}\mathbb{Y}_r(\omega_\ell)\overline{\mathbb{F}}_r(\omega_\ell)\right|^2}{\left(\frac{1}{n_R}\sum_{r=1}^{n_R}|\mathbb{F}_r(\omega_\ell)|^2\right)\left(\frac{1}{n_R}\sum_{r=1}^{n_R}|\mathbb{Y}_r(\omega_\ell)|^2\right)} \text{ a.s.} \tag{C.18}$$

The usefulness of the estimates (C.9)-(C.10) is found in the asymptotic properties of the estimators (C.17)-(C.18). Upon applying the Strong Law of Large Numbers (SLLN) and, subsequently, accounting for the

aforementioned hypotheses, we have:

$$\lim_{n_{\mathrm{R}} \to +\infty} \hat{h}_{n_{\mathrm{R}}} \left(\mathbb{F}(\omega_\ell), \mathbb{Y}(\omega_\ell) \right) = \frac{E\left\{ \mathbb{Y}(\omega_\ell)\overline{\mathbb{F}}(\omega_\ell) \right\}}{E\left\{ |\mathbb{F}(\omega_\ell)|^2 \right\}} = \frac{h^0(\omega_\ell)}{1 + \frac{\sigma_{\mathrm{f}}^2(\omega_\ell)}{E\left\{ |\mathbb{F}^0(\omega_\ell)|^2 \right\}}} \text{ a.s.} \quad , \tag{C.19}$$

$$\lim_{n_{\mathrm{R}} \to +\infty} \hat{\gamma}_{n_{\mathrm{R}}}^2 \left(\mathbb{F}(\omega_\ell), \mathbb{Y}(\omega_\ell) \right) = \frac{\left| E\left\{ \mathbb{Y}(\omega_\ell)\overline{\mathbb{F}}(\omega_\ell) \right\} \right|^2}{E\left\{ |\mathbb{F}(\omega_\ell)|^2 \right\} E\left\{ |\mathbb{Y}(\omega_\ell)|^2 \right\}} \text{ a.s.} \tag{C.20}$$

$$= \frac{1}{\left(1 + \frac{\sigma_{\mathrm{f}}^2(\omega_\ell)}{E\left\{ |\mathbb{F}^0(\omega_\ell)|^2 \right\}} \right) \left(1 + \frac{\sigma_{\mathrm{y}}^2(\omega_\ell)}{E\left\{ |\mathbb{Y}^0(\omega_\ell)|^2 \right\}} \right)}.$$

Expression (C.19) means that the estimator (C.17) converges a.s. to the value $h^0(\omega_\ell)$ taken by the noise-free TF of the structure at the frequency ω_ℓ if there is no input measurement noise, i.e. $\tilde{\mathbb{E}}_{\mathrm{f}}(\omega_\ell) = 0$ a.s. As a conclusion, under all aforementioned hypotheses, the H1-estimation method allows recovering the noise-free TF of the structure from noisy experimental data provided that the input noise is negligible.

Expression (C.20) means that the (converged estimate of the) coherence is an indication of the disturbance of the measured applied forces and responses due to noise: small coherence values indicate a significant contamination of the data due to noise. We note that, in practice, small coherence values may also arise due to leakage errors of the DFT or non-linearities in the dynamical behaviour of the tested structure [see Pintelon and Schoukens, 2001, ch. 2 sec. 6].

D

SASW inverse method

This appendix, which presents known material, describes the Spectral Analysis of Surface Waves (SASW) inverse method, which was introduced by Al-Hunaidi [1993], Heisey et al. [1982], Nazarian and Stokoe II [1986], Sanchez-Salinero et al. [1987]. This method uses the dispersive characteristics of surface waves to infer a profile of the shear modulus of a soil as a function of the depth from (nondestructive and nonintrusive) *in situ* wave propagation measurements. We note that, in the remainder of this appendix, we use elements of the theory of the wave propagation in elastic media. For a detailed account of this theory, we refer the reader, for instance, to [Achenbach, 1984, Aki and Richards, 1980, Bedford and Drumheller, 1994, Ewing et al., 1957, Pilant, 1979, Viktorov, 1967].

D.1   *In situ* testing
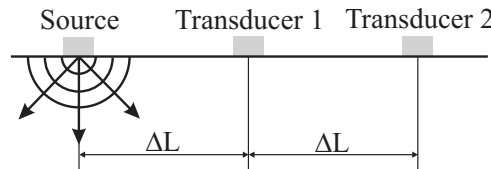
Figure D.1: SASW inverse method: setup of a typical *in situ* test.

In a typical *in situ* SASW test, a time-limited broadband excitation is applied on the free soil surface to generate transient mechanical waves, including surface waves, which are recorded by two transducers placed in line with the loading at fixed separations ΔL (Fig. D.1). The excitation is most commonly generated using an impact hammer, a falling-weight device or a hydraulic shaker. The most often used transducers are accelerometers and geophones. The experiment is usually repeated several times.

D.2   Discrete signal processing and estimation

The data set obtained from a typical SASW test consists of a time-dependent applied force and of time-dependent responses measured at 2 locations for n_R repetitions of the experiment. Accordingly, let $f_r(t)$, $y_{r1}(t)$ and $y_{r2}(t)$ denote the measured applied force and the response at the 2 sensors, respectively, for

the r-th repetition. The time-sampled data are transformed into the frequency domain by means of the Discrete Fourier Transform (DFT) to obtain:

$$\{f_1(\omega_\ell), \ldots, f_{n_R}(\omega_\ell) \mid 1 \leq \ell \leq n_F\} \quad, \tag{D.1}$$

$$\{y_{1m}(\omega_\ell), \ldots, y_{n_R m}(\omega_\ell) \mid 1 \leq \ell \leq n_F \,,\, 1 \leq m \leq 2\} \quad, \tag{D.2}$$

where $\{\omega_\ell \mid 1 \leq \ell \leq n_F\}$ is the set of n_F discrete frequencies. These experimental data are processed following a three-step procedure. First, the Transfer Function (TF) from the response in the first transducer to the response in the second transducer is estimated (App. C) by:

$$\hat{h}(\omega_\ell) = \frac{\frac{1}{n_R}\sum_{r=1}^{n_R} y_{r2}(\omega_\ell)\overline{y}_{r1}(\omega_\ell)}{\frac{1}{n_R}\sum_{r=1}^{n_R} |y_{r1}(\omega_\ell)|^2}. \tag{D.3}$$

The coherence function between the responses in the two tranducers is estimated (App. C) by:

$$\hat{\gamma}^2(\omega_\ell) = \frac{\left|\frac{1}{n_R}\sum_{r=1}^{n_R} y_{r2}(\omega_\ell)\overline{y}_{r1}(\omega_\ell)\right|^2}{\left(\frac{1}{n_R}\sum_{r=1}^{n_R} |y_{r1}(\omega_\ell)|^2\right)\left(\frac{1}{n_R}\sum_{r=1}^{n_R} |y_{r2}(\omega_\ell)|^2\right)}. \tag{D.4}$$

Then, it is assumed, *a priori*, that (i) the soil response at the receivers is dominated by the fundamental surface wave (the generalized Rayleigh wave) of the soil layering and (ii) the wavefront curvature is large compared to the wavelength permitting a plane wave approximation. Under these assumptions, the phase velocity of the fundamental surface wave at the frequency ω_ℓ is estimated by:

$$\hat{c}(\omega_\ell) = \frac{\omega_\ell \Delta L}{\hat{\theta}(\omega_\ell)} \quad, \tag{D.5}$$

where $\hat{\theta}(\omega_\ell)$ is the unwrapped phase of $\hat{h}(\omega_\ell)$, that is to say the phase shift between the two receivers at the frequency ω_ℓ without artificial 2π-phase jumps [Poggiagliolmi et al., 1982]:

$$\hat{\theta}(\omega_\ell) = \tan^{-1}\left(\frac{\Re\left(\hat{h}(\omega_\ell)\right)}{\Im\left(\hat{h}(\omega_\ell)\right)}\right). \tag{D.6}$$

Finally, several filter criteria are applied to ensure, *a posteriori*, that the aforementioned assumptions are valid. More specifically, the phase velocity $\hat{c}(\omega_\ell)$ at the frequency ω_ℓ is withdrawn only if:

$$\hat{\gamma}^2(\omega_\ell) \geq \gamma^{\min} \quad, \tag{D.7}$$

$$\frac{\Delta L}{\hat{\lambda}(\omega_\ell)} \geq x^{\min} \quad, \tag{D.8}$$

$$\frac{\Delta L}{\hat{\lambda}(\omega_\ell)} \leq x^{\max} \quad, \tag{D.9}$$

$$\omega^{\min} \leq \omega_\ell \leq \omega^{\max} \quad, \tag{D.10}$$

where $\hat{\lambda}(\omega_\ell) = 2\pi\hat{c}(\omega_\ell)/\omega_\ell$ is the estimated frequency-dependent wavelength. The criterion (D.7) imposes a threshold value on the coherence function to limit the influence of (incoherent) noise (app C). We note that a frequently used parameter value is $\gamma^{\min} = 0.95$ [see, for instance, Pyl and Degrande, 2002, Schevenels et al., 2006].

Following Chen et al. [2004], Gucunski and Woods [1992], Tokimatsu et al. [1992], let us interpret the expressions (D.8)-(D.9) as criteria imposed on ΔL. The aim of (D.8)-(D.9) is to isolate a wavelength-dependent subregion of the free soil surface where the wavefield is dominated by the fundamental surface wave and the curvature of the wavefront is sufficiently large. In the complementary part of the free surface, body waves and higher order surface wave modes contribute to the response, or the curvature of the wavefront is too small. We note that frequently used parameter values are $x^{\min} = 1$ and $x^{\max} = 3$ [see, for instance, Pyl and Degrande, 2002, Schevenels et al., 2006].

In view of the criteria (D.8)-(D.9), short receiver spacings commonly lead to high-frequency results, whereas long receiver spacings are required to obtain low-frequency results. From this point of view, it can be useful to repeat the test for different values of ΔL so as to obtain results covering the entire frequency band of interest.

Surface waves with shorter wavelengths are attenuated more rapidly with the distance from the applied loading by the material damping (see, for instance, [Aki and Richards, 1980, Pilant, 1979] for attenuation models, or, [Lai et al., 2002, Rix et al., 2000] for the experimental identification of attenuation curves). In view of the energy loss of the source-generated surface waves with distance, a second purpose of (D.9) is to ensure a sufficiently high signal-to-noise ratio at both receivers (in this sense, the results rejected by (D.9) may coincide with those already eliminated by (D.7)).

The surface waves may sometimes be scattered by lateral variations of the mechanical soil properties, underground obstacles or cavities and artificial variations such as foundations [see, for instance, Gucunski et al., 1996, Keilis-Borok et al., 1989]. These scattered waves are source-dependent and are therefore not eliminated by (D.7). A third purpose of the criterion (D.9) is to limit the influence of wave scattering on the experimental phase velocities.

Finally, the criterion (D.10) allows eliminating the spurious results that persist after the application of criteria (D.7)-(D.9) (engineering judgement).

D.3 Experimental dispersion curve inversion

The SASW inverse method is based upon the consideration that generalized Rayleigh waves with longer wavelengths (usually at lower frequencies) penetrate deeper into the soil such that their phase velocity is affected by the soil properties over a greater depth. For this reason, the frequency-dependent phase velocity of the fundamental surface wave is an image of the variation of the soil properties with the depth and, inversely, can be used to infer the soil properties.

The SASW inverse method follows a three-step procedure. First, the soil is modelled as a stack of horizontal layers overlying a halfspace, constituted of homogeneous, linear elastic, isotropic materials. The parameters necessary to define this model are the layer thicknesses and the shear wave velocities, Poisson ratios and mass densities of the layers and the halfspace. To simplify the inversion process, reasonable values are usually assigned to the Poisson ratios and mass densities such that the layer thicknesses and shear wave velocities are the only active parameters that must be determined. Subsequently, the soil model thus obtained is used to compute the theoretical dispersion curve of the plane fundamental surface wave travelling through the layered soil medium, that is to say its phase velocity as a function of the frequency. Finally, the suitable layer thicknesses and shear wave velocities are obtained by minimizing the distance between the experimental and the theoretical phase velocities. This least-squares distance is most commonly used.

Appendix D. SASW inverse method

E

In situ measurements at a site in Lincent

This appendix presents the results of an experimental study of the spatial variability in the dynamical behaviour of the soil at a site in Lincent (Belgium). In the following, we first describe the experimental setup (Sec. E.1). Subsequently, we present and study the experimental results (Sec. E.2). Finally, a first glance at the probabilistic modelling of the dynamical soil behaviour at this site is given (Sec. E.3).

E.1   Experimental setup

Figure E.1: Site of Lincent: overview of the measurement site (picture taken on November 3, 2005).

The measurement site is located in Lincent (Belgium) next to the high-speed railway track Brussels-Liège (Fig. E.1). Several measurement campaigns had already been performed at this site. In preparation of the construction of the railway track, borings and Cone Penetration Tests (CPT) had been carried out [Karl, 2005]. In the frame of the STWW-project "Traffic-induced vibrations in buildings", Seismic Cone Penetration Tests (SCPT) and Spectral Analysis of Surface Waves tests (SASW) (App. D) had been performed by K.U.Leuven and R.U.Gent [Karl, 2005, Pyl and Degrande, 2001, Schevenels et al.,

2006]. The borings [Karl, 2005] revealed the presence of a silt top layer with a thickness of about 1.2 m, followed by a fine sand layer reaching to a depth of 3.2 m. Below the shallow layers, a sequence of very stiff layers of arenite and clay was found. The SASW tests [Pyl and Degrande, 2001, Schevenels et al., 2006] indicated the presence of a shallow layer with a thickness of about 3 m and a shear wave velocity of 150 m/s over a halfspace with a shear wave velocity of about 260 m/s.

Figure E.2: Site of Lincent: experimental setup.

The present measurements were carried out on February 14, 2006 by Mattias Schevenels and Geert Lombaert (K.U.Leuven) and Reza Taherzadeh, Quang Anh Ta, Régis Cottereau and Maarten Arnst (Ecole Centrale Paris). Vibrations were generated by the impact of an instrumented hammer with a mass of 5.3 kg and a soft tip on a small concrete foundation (Figs. E.2 and E.3), which had been cast in situ on January 23, 2006. The side length, height and mass of the square concrete foundation are 0.5 m, 0.2 m and 125 kg, respectively. The vibrations were measured by 12 accelerometers placed in the free field and by 3 accelerometers mounted on the top surface of the foundation (Figs. E.2 and E.3). Uniaxial accelerometers were used and only the vertical component of the acceleration was measured.

Measurements were performed for a total of 6 different setups of the free-field accelerometers. To define those setups, a right-handed Cartesian frame of reference (i_1, i_2, i_3) is defined with the origin o located at the centre of the concrete foundation (Fig. E.4). Six straight lines A, B, C, D, E and F are defined, which cross o and form angles $0°$, $18°$, $36°$, $54°$, $72°$ and $90°$, respectively, with the x_1-axis (hence, line F coincides with the x_2-axis). Furthermore, 8 concentric circles are introduced with centre o and radii 3, 4, 6, 8, 12, 16, 24 and 32 m. The 6 setups are labelled 3-6, 4-8, 6-12, 8-16, 12-24 and 16-32 and accommodate the 12 free-field accelerometers at the first-quadrant (i.e. $x_1 > 0$ and $x_2 > 0$) crossings of the lines with the circles with radii 3 and 6 m, 4 and 8 m, 6 and 12 m, 8 and 16 m, 12 and 24 m and 16 and 32 m, respectively. Hence, for each setup, two accelerometers are located on each measurement line in such a way that the distance between the foundation centre and the nearest receiver is equal to the distance between the two receivers. In the remaining of the appendix, only the free-field response is considered.

For each setup, a total of 40 events was recorded. The A/D conversion was performed at a rate of 1000 Hz. A total of 2048 data points was recorded for each event (hence, the frequency-domain resolution equals 0.4882 Hz).

(a)　　　　　　　　　　　　　　　　(b)

(c)　　　　　　　　(d)　　　　　　　　(e)

Figure E.3: Site of Lincent: (a) concrete foundation, (b) instrumented hammer, (c) accelerometer mounted on the foundation and (d, e) accelerometers in the free field.
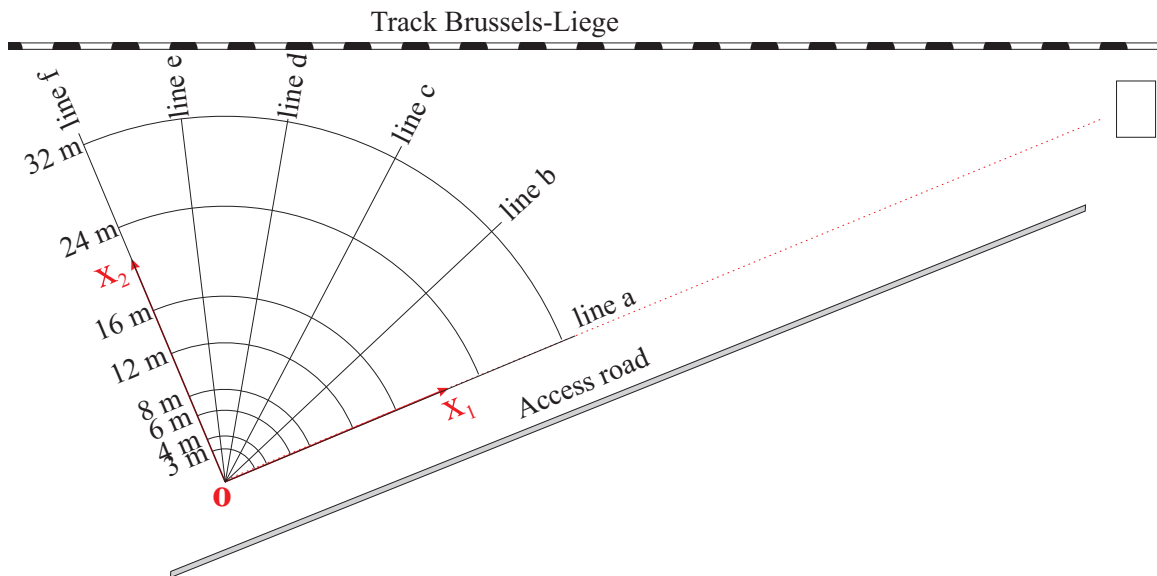
Figure E.4: Site of Lincent: schematic representation of the measurement site.

E.2 Experimental data

The experimental results are now presented. For the sake of brevity, only a small selection of the results is shown here, sufficient to deduce the main conclusions of the experimental study. We refer the reader to [Arnst et al., 2006] for a more complete overview of the measurement results.

E.2.1 Excitation

(a) Time history.

(b) Frequency content.
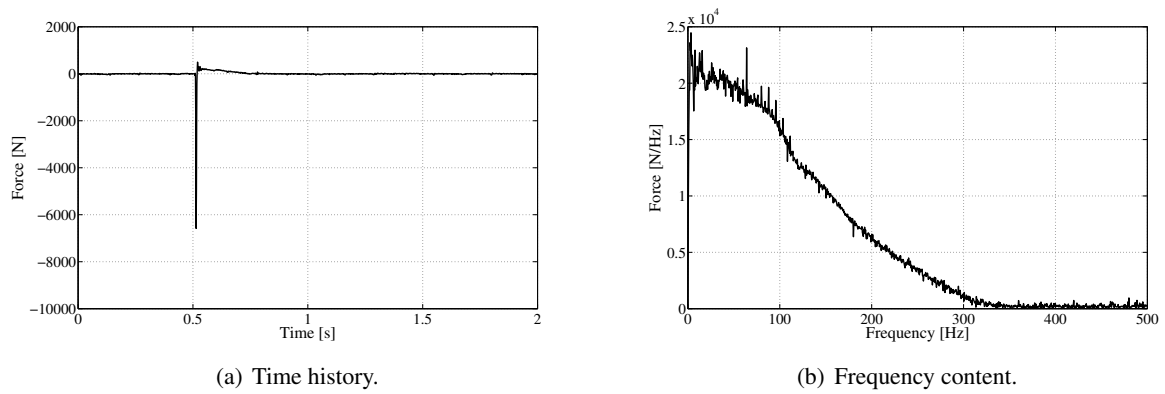
Figure E.5: Site of Lincent: (a) time history and (b) frequency content of the applied force, measured during the first event of setup $3 - 6$.

Figure E.5 shows the time history and frequency content of the applied force, measured during the first event of setup $3 - 6$. The impulsive force has a peak value of about $6\,kN$. The signal energy is seen to be distributed over the frequency band between 0 and about $300\,Hz$.

E.2.2 Free-field accelerations
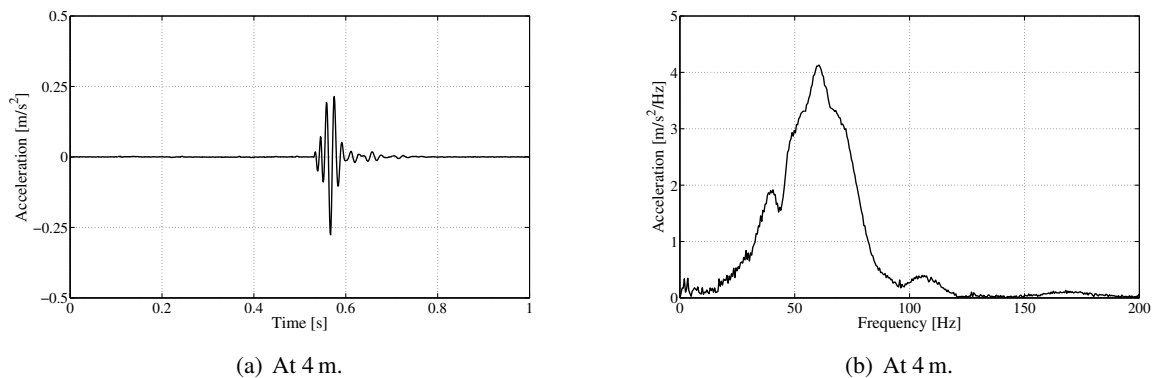
(a) At 4 m.

(b) At 4 m.

Figure E.6: Site of Lincent: (a, c, e, g) time history and (b, d, f, h) frequency content of the free-field accelerations on line A at 4, 8, 16 and 32 m, measured during the first event of the setups.
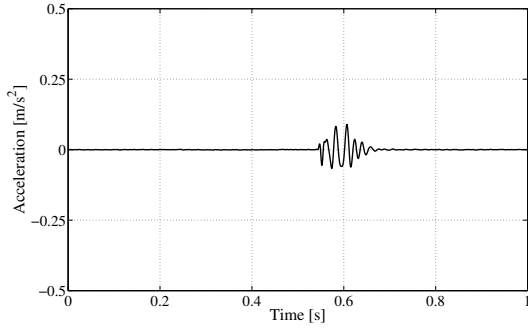
(c) At 8 m (setup 4-8).
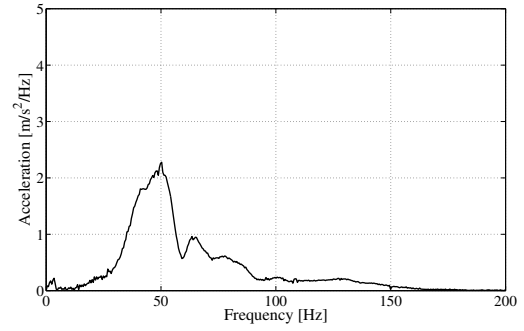
(d) At 8 m (setup 4-8).
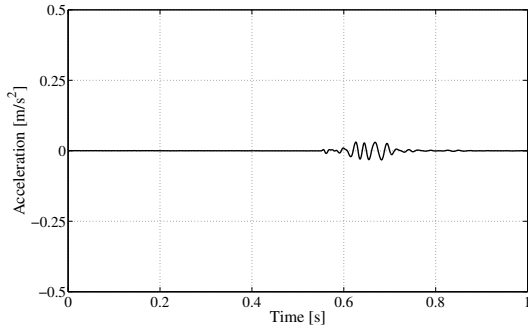
(e) At 16 m (setup 16-32).
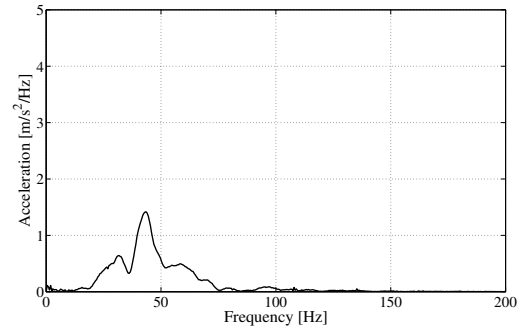
(f) At 16 m (setup 16-32).
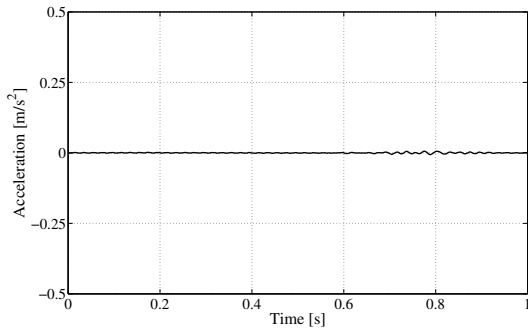
(g) At 32 m.
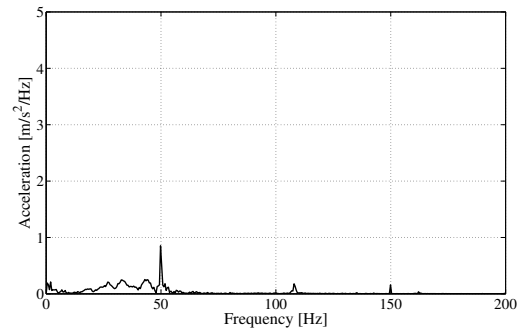
(h) At 32 m.

Figure E.6: Site of Lincent: (a, c, e, g) time history and (b, d, f, h) frequency content of the free-field accelerations on line A at 4, 8, 16 and 32 m, measured during the first event of the setups (cont.).

Figure E.6 shows the time history and frequency content of the free-field accelerations on line A at 4, 8, 16 and 32 m, measured during the first event of the setups. The amplitude of the measured accelerations is observed to decrease with the distance from the applied force, due to the geometrical spreading and the material damping. In the vicinity of the concrete foundation, the signal energy is distributed over a broad range of frequencies up to 120 Hz. In contrast, at great distance from the applied loading (at 24 or 32 m), the high frequencies have been attenuated by the material damping and the signal energy is distributed over a narrower range of frequencies up to approximately 60 Hz.

E.2.3 Coherence functions

(a) At 4 m.

(b) At 8 m (setup 4-8).

(c) At 16 m (setup 8-16).

(d) At 32 m.
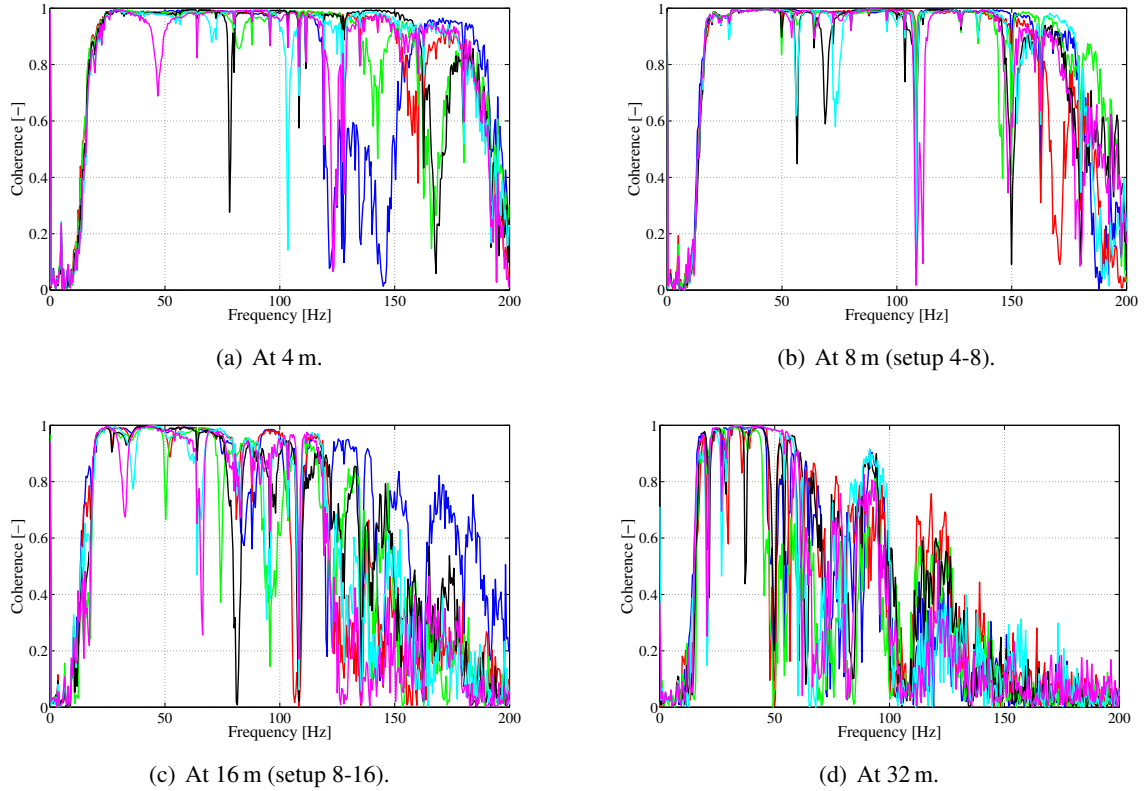
Figure E.7: Site of Lincent: coherence functions between the measured applied forces and the free-field accelerations at (a) 4 m, (b) 8 m, (c) 16 m and (d) 32 m on line A (blue), B (red), C (green), D (black), E (cyan) and F (magenta).

Figure E.7 shows the coherence functions (App. C) between the measured applied forces and free-field accelerations at 4, 8, 16 and 32 m. At low frequencies below 20 Hz, the impact hammer does not allow transferring sufficient energy into the soil, such that the source-generated wave field does not surpass the ambient noise and low coherence values are observed. In the vicinity of the foundation, the measured forces and responses are generally coherent between about 20 and 100 Hz. At great distance from the applied loading, the high-frequency source-generated wave field has been attenuated by the material damping and the measured forces and responses are reasonably coherent only between about 20 and 50 Hz.

E.2.4 Free-field transfer functions

Figure E.8 shows the estimates of the noise-free Transfer Functions (TFs) from the force applied on the foundation to the vertical velocity in the free field at 4, 8, 16 and 32 m, deduced from the noisy experimental data using the H1-estimation method (App. C). The results show a considerable spatial variability between the measurement lines (up to a factor of about 3).

(a) At 4 m.

(b) At 8 m (setup 4-8).

(c) At 16 m (setup 16-32).

(d) At 32 m.
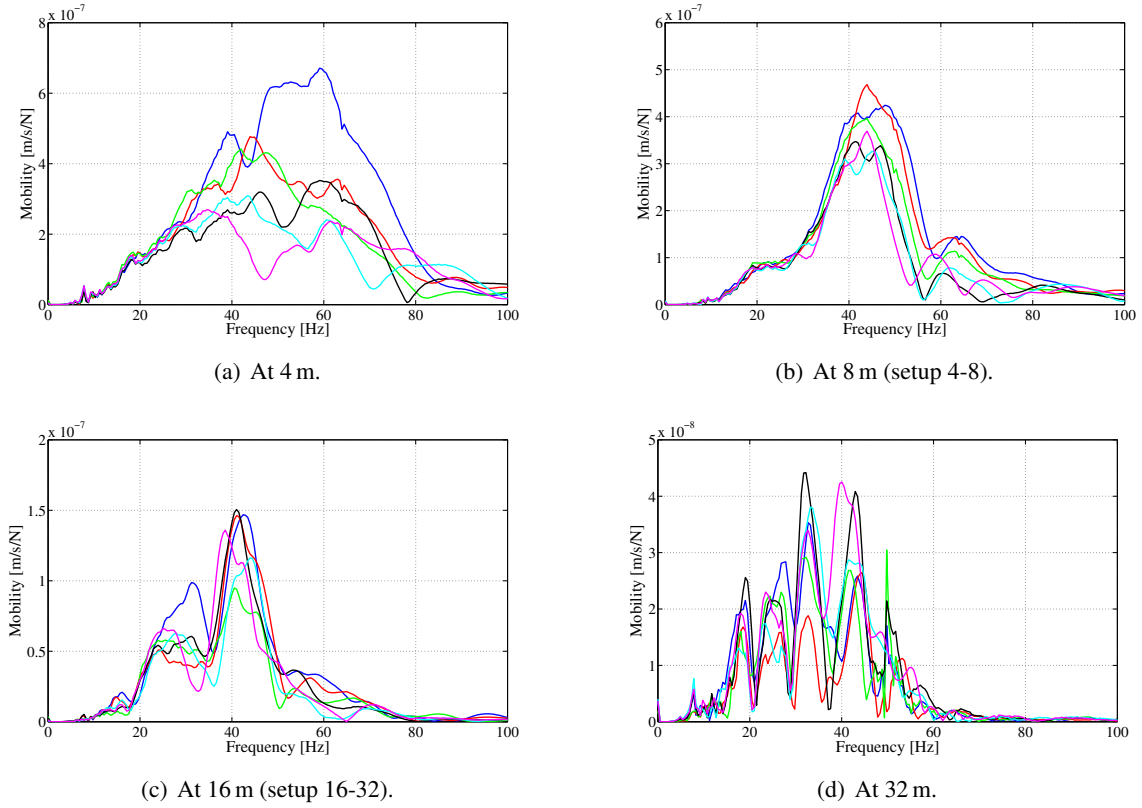
Figure E.8: Site of Lincent: amplitude of the estimated noise-free TFs at (a) 4 m, (b) 8 m, (c) 16 m and (d) 32 m on line A (blue), B (red), C (green), D (black), E (cyan) and F (magenta).

E.2.5 Experimental dispersion curves

Nazarian's method (App. D) has been applied to deduce experimental dispersion curves from the experimental data. The parameters of the filter criteria (D.7)-(D.9) have been chosen equal to $\gamma^{\min} = 0.98$, $x^{\min} = 1$ and $x^{\max} = 3$. Figure E.9 shows the thus obtained experimental dispersion curves for the pairs of receivers located at 4 and 8 m and at 16 and 32 m. Due to the filter criteria (D.8)-(D.9), the long receiver spacing 16 m is observed to lead to estimated phase velocities at low frequencies, whereas the short receiver spacing 4 m yields estimated phase velocities at higher frequencies.

At 20 Hz, a phase velocity in the order of 150 m/s is obtained, while, at 80 Hz, a phase velocity of about 100 m/s is revealed. Upon attributing these phase velocities to the fundamental surface wave (the generalized Rayleigh wave) of the soil layering, whose penetration depth is approximately one wavelength, the obtained experimental phase velocities correspond to penetration depths between about 7.5 and 1.25 m. Hence, according to the aforementioned boring and SASW results, they belong to waves travelling essentially in the shallow silt/sand layers. Only at the lowest frequencies, they penetrate (but not profoundly) into the deep stiff arenite/clay layers.

The low-frequency phase velocities obtained for the receiver spacing 16 m show only very small differences between the measurement lines. The higher-frequency phase velocities obtained for the receiver spacing 4 m show more considerable fluctuations (up to about 20%).
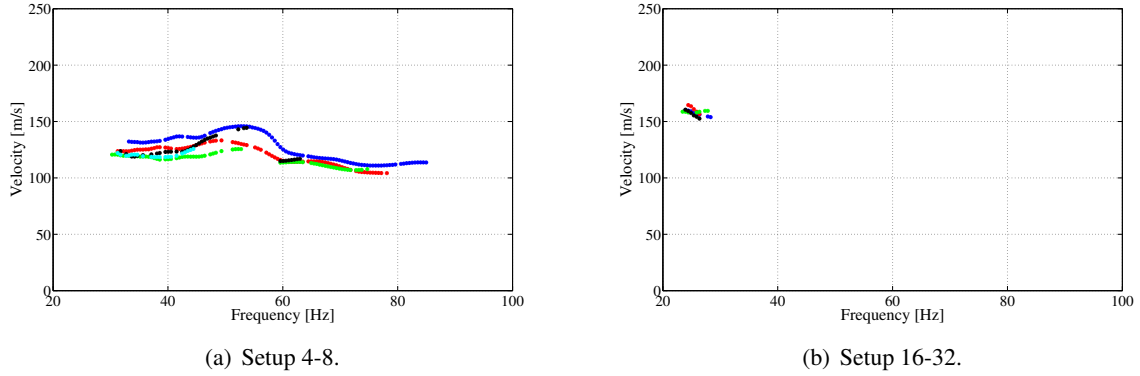
(a) Setup 4-8.

(b) Setup 16-32.

Figure E.9: Site of Lincent: experimental dispersion curve for the pair of receivers located (a) at 4 and 8 m and (b) at 16 and 32 m on line A (blue), B (red), C (green), D (black), E (cyan) and F (magenta).

E.3 Probabilistic modelling of the dynamical soil behaviour

This section presents first results of ongoing research on building and inverting a probabilistic model for the dynamical soil behaviour at the site of Lincent.

E.3.1 Parametric probabilistic model

A time-domain parametric probabilistic model (App. A) has been set up for the dynamical soil behaviour. The undeformed soil is represented as a halfspace occupying the domain $\{\boldsymbol{x} \in \mathbb{R}^3 \mid x_3 < 0\}$. It is modelled as a linear, locally isotropic, elastic solid material, whose fields of elastic moduli are represented by random fields.

E.3.2 Computations with the probabilistic model

The hp-version of the Finite Element (FE) method, more specifically the spectral element method [see, for instance, Komatitsch, 1997, Maday and Patera, 1989, Schwab, 1999], is used to discretize the space. A box-shaped region

$$\Omega = \left\{ -\frac{L_1}{3} < x_1 < \frac{2L_1}{3} \;,\quad -\frac{L_2}{3} < x_2 < \frac{2L_2}{3} \;,\quad -L_3 < x_3 < 0 \right\} \tag{E.1}$$

is meshed using 8-noded elements of equal size $h \times h \times h$. On each element, the displacement field is approximated on a basis of three-dimensional shape functions, constructed by taking tensor products of one-dimensional (Gauss-Lobatto-based) polynomial shape functions of degree p. The computational domain Ω is surrounded by Perfectly Matched Layers (PMLs) [Bérenger, 1994, Festa and Vilotte, 2005] on all sides, except for the free soil surface, to absorb outgoing waves. The Newmark time integration algorithm in its central difference version [see, for instance, Géradin and Rixen, 1992, Hughes, 1987] is used to discretize time. Let $\{j\Delta t \mid 1 \leq j \leq n_\mathrm{T}\}$ be the set of n_T discrete time instants, such that Δt is the time step. The Monte Carlo Simulation (MCS) method is applied to discretize the random dimension. The random fields of elastic moduli are simulated using the spectral representation method (Box 1.5 of Section 1.2).

The pre- and post-processing are performed in Matlab using the Structural Dynamics Toolbox [Balmès and Leclère, 2006]. For each Monte Carlo trial, the FE computations and the time integration are performed using the program SPEC [Festa and Vilotte, 2005], developed by the team of prof. Vilotte at the Institut de Physique du Globe de Paris in France. This program was implemented in Fortran and uses the Message Passing Interface (MPI) to allow execution on parallel platforms.

E.3.3 Numerical illustration

Let the computational domain Ω have here the dimensions $L_1 = L_2 = 24\,\text{m}$ and $L_3 = 12\,\text{m}$, and be subdivided in two domains

$$\Omega_1 = \{-8\,\text{m} < x_1 < 16\,\text{m}\,, \quad -8\,\text{m} < x_2 < 16\,\text{m}\,, \quad -3\,\text{m} < x_3 < 0\}\quad, \tag{E.2}$$

$$\Omega_2 = \{-8\,\text{m} < x_1 < 16\,\text{m}\,, \quad -8\,\text{m} < x_2 < 16\,\text{m}\,, \quad -12\,\text{m} < x_3 < -3\,\text{m}\}\quad, \tag{E.3}$$

which represent the shallow silt/sand layers and the deep stiff arenite/clay layers at the site of Lincent. Results are presented for two different computations. In both computations, the soil occupying the domain Ω_2 is modelled as a homogeneous material with a shear wave velocity of 260 m/s, a compression wave velocity of 1000 m/s and a mass density of 1800 kg/m^3. In the first computation (Fig. E.10), the soil occupying the domain Ω_1 is modelled as a homogeneous material with a shear wave velocity of 110 m/s, a compression wave velocity of 280 m/s and a mass density of 1800 kg/m^3. In the second computation (Fig. E.12), it is modelled as a heterogeneous material with a homogeneous Lamé coefficient $\lambda = 121.680\,\text{MPa}$ and a homogeneous mass density of 1800 kg/m^3, but with a heterogeneous shear modulus field, equal to one sample path of the random shear modulus field $\{\mu(\boldsymbol{x}; L_{\mathbb{G}1}, L_{\mathbb{G}2}, L_{\mathbb{G}3}; \delta) \mid \boldsymbol{x} \in \Omega_1\}$, defined by:

$$\Big(\forall \boldsymbol{x} \in \Omega_1 \;:\; \mu(x; L_{\mathbb{G}1}, L_{\mathbb{G}2}, L_{\mathbb{G}3}; \delta) = \underline{\mu}\, N\big(\mathbb{G}(\boldsymbol{x}; L_{\mathbb{G}1}, L_{\mathbb{G}2}, L_{\mathbb{G}3}); \delta\big)\Big)\ \text{a.s.}\quad, \tag{E.4}$$

where $\underline{\mu} = 21.780\,\text{MPa}$ is the mean shear modulus (such that the mean shear and compression wave velocities are 110 m/s and 280 m/s), the random field $\{\mathbb{G}(\boldsymbol{x}; L_{\mathbb{G}1}, L_{\mathbb{G}2}, L_{\mathbb{G}3}) \mid \boldsymbol{x} \in \Omega_1\}$ is a stochastic germ in the set $\mathcal{E}_{\mathbb{G}}$ defined in Section 1.1, and the function $N(\cdot; \delta) : \mathbb{R} \to \mathbb{R}_0^+$ is the transformation function defined in Box 1.4 of Section 1.2. The spatial correlation lengths of the stochastic germ and the dispersion level are chosen equal to $L_{\mathbb{G}1} = L_{\mathbb{G}2} = L_{\mathbb{G}3} = 2\,\text{m}$ and $\delta = 0.6$.

The soil is loaded by a time-dependent pressure $p^{\text{ext}}(t)$ uniformly applied on the square portion Γ of the free soil surface centred at $\boldsymbol{o}$ and of area ϵ^2 with $\epsilon \ll 1\,\text{m}$. The pressure is modelled in the time domain by means of a very narrow Gaussian-shaped function

$$p^{\text{ext}}(t) = -\exp\left(-\frac{(t-t_0)^2}{T^2}\right)\quad, \tag{E.5}$$

where the parameters are chosen equal to $t_0 = 0.05\,\text{s}$ and $T = 0.0064\,\text{s}$, such that most of the signal energy is distributed over the frequency band between 0 and 150 Hz.

The parameters of the FE discretization are set to $h = 0.5\,\text{m}$ and $p = 6$, such that the heterogeneous shear modulus field and the propagating mechanical wave field are represented accurately. The FE model has about 11×10^6 FE Degrees Of Freedom (DOFs). The parameters of the time-domain sampling are chosen equal to $\Delta t = 1.5 \times 10^{-5}\,\text{s}$ and $n_{\text{T}} = 30000$, such that the Courant stability condition is fulfilled. The computation with the program SPEC of a discretized problem of this kind on 15 Itanium 2 type processors using about 50 Gb RAM takes about 50 hours.
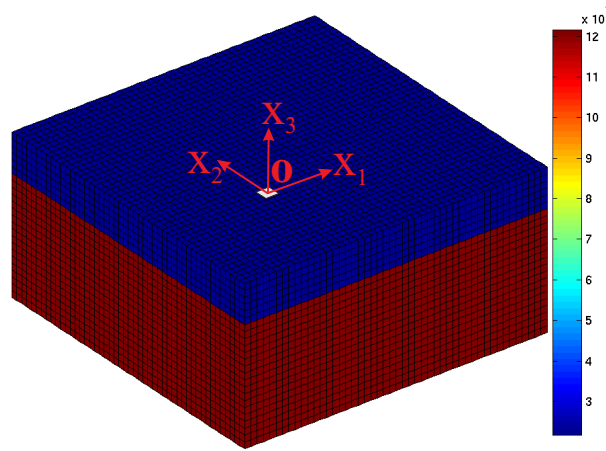
Figure E.10: Site of Lincent: FE mesh for the homogeneous-layer-over-halfspace model (the colour is proportional to the soil shear modulus)
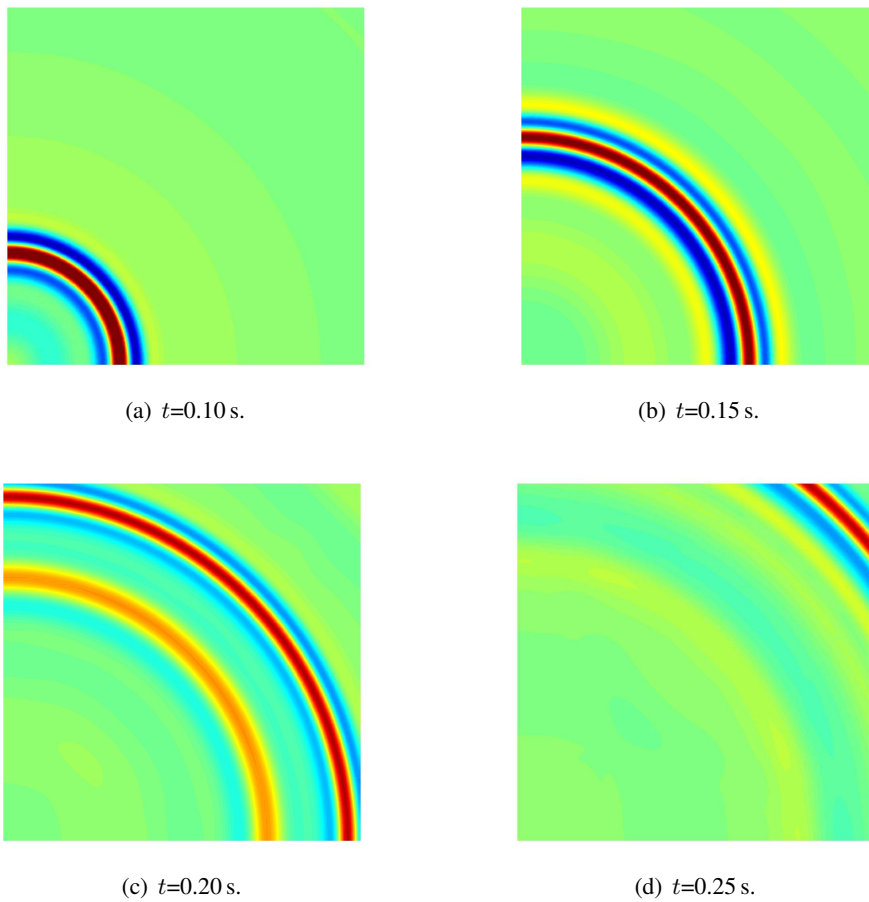

(a) t=0.10 s.

(b) t=0.15 s.

(c) t=0.20 s.

(d) t=0.25 s.

Figure E.11: Site of Lincent: transient response at the free soil surface of the homogeneous-layer-over-halfspace model at times (a) t=0.10 s, (b) t=0.15 s, (c) t=0.20 s and (d) t=0.25 s (the colour is proportional to the vertical acceleration).
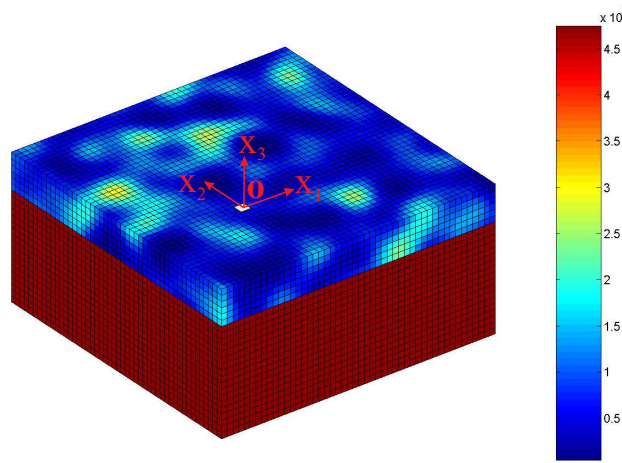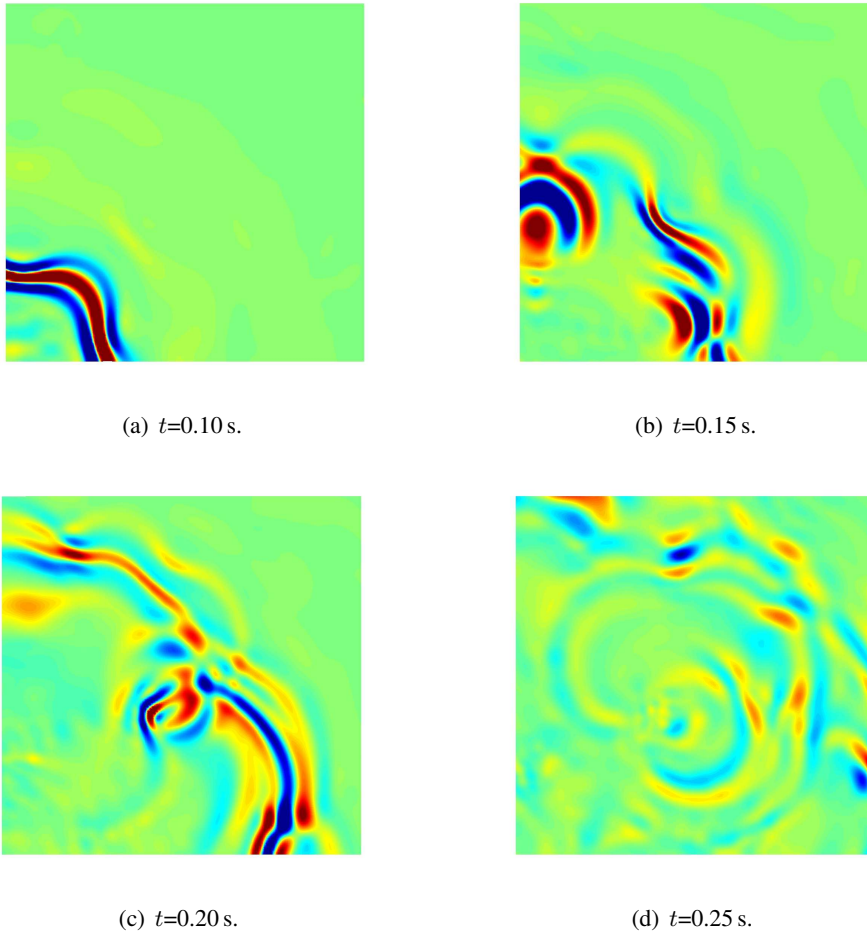
Figure E.12: Site of Lincent: FE mesh for the heterogeneous-layer-over-halfspace model (the colour is proportional to the soil shear modulus).

(a) t=0.10 s.

(b) t=0.15 s.

(c) t=0.20 s.

(d) t=0.25 s.

Figure E.13: Site of Lincent: transient response at the free soil surface of the heterogeneous-layer-over-halfspace model at times (a) t=0.10 s, (b) t=0.15 s, (c) t=0.20 s and (d) t=0.25 s (the colour is proportional to the vertical acceleration).

Figure E.11 shows four snapshots of the transient first-quadrant free-field response for the homogeneous-layer-over-halfspace model. The mechanical wave field is observed to be axisymmetric. A strong wave, being the fundamental surface wave (the generalized Rayleigh wave) of the soil layering, is seen to propagate away from the loading point. It is followed by several slightly faster waves of smaller magnitude, being higher-order surface-wave modes that are propagating in the layer, but evanescent in the halfspace.

Figure E.13 shows four snapshots of the transient first-quadrant free-field response for the heterogeneous-layer-over-halfspace model. The mechanical wave field is observed to be very complex, and no longer axisymmetric. It is made up of multiple waves transmitted through, and reflected upon, the shallow heterogeneities.

E.4   Summary and conclusion

In this appendix, an experimental study was presented of the spatial variability in the dynamic soil behaviour at a site in Lincent. A considerable spatial variability was found in the free-field response. In the frequency band of analysis between 20 and 100 Hz, the amplitude of the free-field mobilities shows variations up to a factor of about 3 between the measurement lines. At the lowest frequencies, the experimental dispersion curves are subjected to little variability, whereas, at higher frequencies, they show considerable fluctuations. These results indicate the need to incorporate spatial variability into the fields of material properties of predictive mathematical-mechanical models for the dynamical behaviour of soils.

Future work may focus on the stochastic inverse problem involving the identification of spatial correlation lengths and dispersion levels characterizing the variability in the fields of mechanical properties of the soil. The methodology proposed in Chapter 5 can, for instance, be applied to invert the probabilistic model of Section E.3 from the experimental dispersion curves of Section E.2.5. Two main difficulties should be addressed in future work. First, as already mentioned in Chapter 5, the effect of model misspecification should be investigated. Second, to lower the required computational effort, it seems interesting to investigate under which conditions approximations from statistical physics can be applied to solve the probabilistic direct problem, such as the First-Order Smoothing Approximation (FOSA) of the Dyson equation or the ladder approximation of the Bethe-Salpeter equation [as in Lombaert and Clouteau, 2006, Turner and Anugonda, 2001].

List of publications

Journal Papers

M. Arnst, D. Clouteau, and M. Bonnet. Identification of non-parametric probabilistic models from measured frequency transfer functions. *Computer Methods in Applied Mechanics and Engineering*, 2007. Submitted for publication.

H. Chebli, R. Othman, D. Clouteau, M. Arnst and G. Degrande. 3D periodic BE-FE model for various transportation structures interacting with soil. *Computers and Geotechnics*, 2007. Accepted for publication.

G. Degrande, D. Clouteau, R. Othman, M. Arnst, H. Chebli, R. Klein, P. Chatterjee and B. Janssens. A numerical model for ground-borne vibrations from underground railway traffic based on a periodic finite element-boundary element formulation. *Journal of Sound and Vibration*, 293(3-5):645–666, 2006.

M. Arnst, D. Clouteau, H. Chebli, R. Othman and G. Degrande. A non-parametric probabilistic model for ground-borne vibrations in buildings. *Probabilistic Engineering Mechanics*, 21(1):18–34, 2006.

D. Clouteau, M. Arnst, T.M. Al-Hussaini and G. Degrande. Freefield vibrations due to dynamic loading on a tunnel embedded in a stratified medium. *Journal of Sound and Vibration*, 283(1-2):173–199, 2005.

Conference Proceedings

M. Arnst, Q.A. Ta, D. Clouteau and M. Bonnet. Identification of random field models for elastic moduli from spectral analysis of compression wave experiments. In *ISMA2006 International Conference on Noise and Vibration Engineering*, Leuven, Belgium, 2006.

M. Arnst, D. Clouteau and M. Bonnet. Identification of non-parametric structural dynamics models from measured transfer functions. In *WCCM2006 World Congress on Computational Mechanics*, Los Angeles, United States, 2006.

M. Arnst, D. Clouteau and M. Bonnet. Identification of probabilistic structural dynamics models: application to Soize's non-parametric model. In *Eurodyn2005 6th International Conference on Structural Dynamics*, Paris, France, 2005.

M. Arnst, D. Clouteau, M. Bonnet and G. Degrande. Identification de modèles probabilistes non paramétriques. In *Actes du Septième Colloque National en Calcul des Structures*, Giens, France, 2005.

M. Arnst, H. Chebli, R. Othman, D. Clouteau, and G. Degrande. A non-parametric, probabilistic model for ground-borne structural vibration due to excitations in a tunnel. In *ISMA2004 International Conference on Noise and Vibration Engineering*, Leuven, Belgium, 2004.

D. Clouteau, R. Othman, M. Arnst, H. Chebli, G. Degrande, R. Klein, P. Chatterjee and B. Janssens. A numerical model for ground-borne vibrations from underground railway traffic based on a periodic fe-be formulation. In *IWRN8 Eight International Workshop on Railway Noise*, Buxton, United Kingdom, 2004.

M. Arnst, H. Chebli, R. Othman, D. Clouteau and G. Degrande. Uncertainty quantification of a prediction model for ground-borne vibrations in buildings. In *ICSV11 International Congress on Sound and Vibration*, St-Petersburg, Russia, 2004.

Bibliography

M. Abramowitz and I. A. Stegun. *Handbook of Mathematical Functions with Formulas, Graphs, and Mathematical Tables*. Dover, 1964. 32, 36

J.D. Achenbach. *Wave Propagation in Elastic Solids*. Elsevier Science, 1984. 147

S. Adhikari. Random matrix eigenvalue problems in structural dynamics. *International Journal for Numerical Methods in Engineering*, 69:562–591, 2007. 141

AIAA. *Guide for the Verification and Validation of Computational Fluid Dynamics Simulations*. American Institute of Aeronautics and Astronautics, 1998. 4

M. Ainsworth. Discrete dispersion relation for hp-version finite element approximation at high wave number. *SIAM Journal on Numerical Analysis*, 42:553–575, 2004. 117, 123

K. Aki and P.G. Richards. *Quantitative Seismology: Theory and Methods*, volume 1. W.H. Freeman and Company, 1980. 147, 149

M.O. Al-Hunaidi. Insights on the SASW nondestructive testing method. *Canadian Journal of Civil Engineering*, 20:940–950, 1993. 147

S. Andrieux. Problèmes inverses. Lecture Notes, École Polytechnique, France, 2005. 2

M. Arnst. Three-dimensional modelling of free field and structural vibration due to harmonic and transient loading in a tunnel. Master's thesis, Department of Civil Engineering K.U.Leuven and Ecole Centrale Paris, Belgium, 2003. 5, 100, 101

M. Arnst, D. Clouteau, H. Chebli, R. Othman, and G. Degrande. A nonparametric probabilistic model for ground-borne vibrations in buildings. *Probabilistic Engineering Mechanics*, 21:18–34, 2006. 6, 101

M. Arnst, Q.A. Ta, R. Taherzadeh, R. Cottereau, M. Schevenels, G. Lombaert, D. Clouteau, M. Bonnet, and G. Degrande. Measurements at a site in Lincent: transfer functions, dispersion curves and seismograms. Technical report, Ecole Centrale Paris, France, 2006. 154

D. Aubry and D. Clouteau. A subdomain approach to dynamic soil-structure interaction. In V. Davidovici and R. Clough, editors, *Recent Advances in Earthquake Engineering and Structural Dynamics*, pages 251–272. OUEST Editions/AFPS, Nantes, 1992. 100

I. Babuška and T. Strouboulis. *The Finite Element Method and its Reliability*. Oxford University Press, 2001. 35

Bibliography

I. Babuška, R. Tempone, and G.E. Zouraris. Solving elliptic boundary value problems with uncertain coefficients by the finite element method: the stochastic formulation. *Computer Methods in Applied Mechanics and Engineering*, 194:1251–1294, 2005. 34

R.R. Bahadur. On Fisher's bound for asymptotic variances. *Annals of Mathematical Statistics*, 35: 1545–1552, 1964. 53

E. Balmès. High modal density, curve veering, localization: a different perspective on the structural response. *Journal of Sound and Vibration*, 161:358–363, 1993. 16

E. Balmès and J.-M. Leclère. *Structural Dynamics Toolbox and FEMLink*. SDTools, 2006. 19, 20, 89, 104, 159

I.V. Basawa and B.L.S. Prakasa Rao. Asymptotic inference for stochastic processes. *Stochastic Processes and their Applications*, 10:221–254, 1980. 50

A. Basu and B.G. Lindsay. Minimum disparity estimation for continuous models: efficiency, distributions and robustness. *Annals of the Instititue of Statistical Mathematics*, 46:683–705, 1994. 10

R.T. Bayes. An essay toward solving a problem in the doctrine of chances. *Philosophical Transactions of the Royal Society of London*, 53:370–418, 1763. 3, 9, 10, 51

J.L. Beck and L.S. Katafygiotis. Updating models and their uncertainties I: Bayesian statistical framework. *Journal of Engineering Mechanics*, 124:455–461, 1998. 10

A. Bedford and D.S. Drumheller. *Introduction to Elastic Wave Propagation*. John Wiley and Sons, 1994. 147

J.S. Bendat and A.G. Piersol. *Random Data: Analysis and Measurement Procedures*. John Wiley and Sons, 1986. 143

R. Beran. Minimum Hellinger distance estimates for parametric models. *The Annals of Statistics*, 5: 445–463, 1977. 10

J.P. Bérenger. A perfectly matched layer for the absorption of electromagnetic waves. *Journal of Computational Physics*, 114:185–200, 1994. 158

R.H. Berk. Limiting behaviour of posterior distributions when the model is incorrect. *The Annals of Mathematical Statistics*, 37:51–58, 1966. 55

R.H. Berk. Consistency a posteriori. *The Annals of Mathematical Statistics*, 41:894–906, 1970. 55

D. Bernoulli. Diiudicatio maxime probabilis plurium observationem discrepantium atque verisimillima inductio inde formanda. *Acta Academiae Scientiarum Imperialis Petropolitanae*, 1:3–23, 1778. 9

J. Besag. Spatial interaction and the statistical analysis of lattice systems. *Journal of the Royal Statistical Society B*, 36:192–236, 1974. 63

J. Besag. Statistical analysis of non-lattice data. *The Statistician*, 24:179–195, 1975. 63

P. Billingsley. *Probability and Measure*. John Wiley and Sons, 1995. d, 30, 132

A. Bobillot. *Méthodes de réduction pour le recalage - Application au cas d'Ariane 5*. PhD thesis, École Centrale Paris, France, 2002. 2

M. Bonnet. *Problèmes inverses*. Lecture Notes of Master Recherche DSSC, École Centrale Paris, France, 2006. 2

M. Bonnet and A. Frangi. *Analyse des solides déformables par la méthode des éléments finis*. Éditions de l'École Polytechnique, 2006. 34

H. Brezis. *Analyse fonctionnelle: Théorie et applications*. Dunod, 1999. d, 132

O. Bunke and X. Milhaud. Asymptotic behavior of Bayes estimates under possibly incorrect models. *The Annals of Statistics*, 26:617–644, 1998. 55, 66

K.P. Burnham and D. Anderson. *Model Selection and Multi-Model Inference*. Springer, 2003. 127

E. Capiez-Lernout. *Dynamique des structures tournantes à symétrie cyclique en présence d'incertitudes aléatoires. Application au désaccordage des roues aubagées*. PhD thesis, Université de Marne-La-Vallée, France, 2004. 7, 10

G. Casella and R.L. Berger. *Statistical Inference*. Duxbury Press, 2001. 9, 49

P. Chatterjee, G. Degrande, S. Jacobs, J. Charlier, P. Bouvet, and D. Brassenx. Experimental results of free field and structural vibrations due to underground railway traffic. In *Proceedings of the 10th International Congress on Sound and Vibration*, Stockholm, Sweden, 2003. 6

H. Chebli, R. Othman, D. Clouteau, M. Arnst, G. Degrande, and P. Chatterjee. 3d periodic fe-be model for various transportation structures interacting with soil. *Computers and Geotechniques*, 2007. Accepted for publication. 5, 100

C. Chen, D. Duhamel, and C. Soize. Probabilistic approach for model and data uncertainties and its experimental identification in structural dynamics: Case of composite sandwich panels. *Journal of Sound and Vibration*, 294:64–81, 2006. 10

L. Chen, J. Zhu, X. Yan, and C. Song. On arrangement of source and receivers in SASW testing. *Soil Dynamics and Earthquake Engineering*, 24:389–396, 2004. 149

L.A. Chernov. *Wave Propagation in a Random Medium*. Dover Publications, 1968. 10

P.G. Ciarlet. *The Finite Element Method for Elliptic Problems. North Holland*. North Holland, 1978. 34

P.G. Ciarlet. *Introduction à l'analyse numérique matricielle et à l'optimisation*. Dunod, 2000. 22

D. Clouteau. *MISS Manuel Scientifique*. École Centrale Paris, France, 6.4 edition, 2005. 106

D. Clouteau and D. Aubry. A subdomain approach to dynamic soil-structure interaction. In W.S. Hall and G. Oliveto, editors, *Boundary Element Methods for Soil-Structure Interaction*, pages 61–125. Springer, 2003. 100

D. Clouteau, M. Arnst, T.M. Al Hussaini, and G. Degrande. Free field vibrations due to dynamic loadings on a tunnel embedded in a stratified medium. *Journal of Sound and Vibration*, 283:173–199, 2005. 5, 100

J. Collins and W. Thomson. The eigenvalue problem for structural systems with statistical properties. *AIAA Journal*, 7:642–648, 1969. 141

D. Colton and R. Kress. *Inverse Acoustic and Electromagnetic Scattering Theory*. Springer, 1992. 2

Bibliography

R. Cottereau. *Probabilistic models of impedance matrices. Application to dynamic soil-structure interaction.* PhD thesis, École Centrale Paris, France, 2007. 111

D.R. Cox and N. Reid. A note on pseudolikelihood constructed from marginal densities. *Biometrika*, 91: 729–737, 2004. 63

R.R. Craig and M.C.C. Bampton. Coupling of substructures for dynamic analysis. *AIAA Journal*, 6: 1313–1319, 1968. 100

H. Cramér. *Mathematical Methods of Statistics*. Princeton University Press, 1946. 9, 10, 49, 53

I. Csiszár. Information type measures of difference of probability distributions and indirect observations. *Studia Scientiarum Mathematicarum Hungarica*, 2:299–318, 1967. 51, 127

G. Da Prato and J. Zabczyk. *Stochastic equations in infinite dimensions*. Cambridge University Press, 1992. d, 29, 132

R. Dautray and J.L. Lions. *Analyse mathématique et calcul numérique pour les sciences et les techniques*. Masson, 1987. d, 17, 19, 115, 130, 131, 132, 134

M.K. Deb, I. Babuška, and J.T. Oden. Solution of stochastic partial differential equations using galerkin finite element techniques. *Computer Methods in Applied Mechanics and Engineering*, 190:6359–6372, 2001. 34

G. Degrande, D. Clouteau, R. Othman, M. Arnst, H. Chebli, R. Klein, P. Chatterjee, and B. Janssens. A numerical model for ground-borne vibrations from underground railway traffic based on a periodic finite element - boundary element formulation. *Journal of Sound and Vibration*, 2006. Special Issue: Proceedings of the 8th International Workshop on Railway Noise. Accepted for publication. 5, 100

L. Demkowicz, W. Rachowicz, and P. Devloo. A fully automatic hp-adaptivity. *Journal of Scientific Computing*, 17:127–155, 2002. 35

A. Deraemaeker. *Sur la maîtrise des modèles en dynamique des structures à partir de résultats d'essais*. PhD thesis, École Normale Supérieure de Cachan, France, 2001. 2

C. Desceliers, R. Ghanem, and C. Soize. Maximum likelihood estimation of stochastic chaos representations from experimental data. *International Journal for Numerical Methods in Engineering*, 66: 978–1001, 2006. 9, 20, 27, 128

C. Desceliers, C. Soize, and R.G. Ghanem. Identification of chaos representations of elastic properties of random media using experimental vibration tests. *Computational Mechanics*, 2006. In Press. 10

R.M. Dudley. The sizes of compact subsets of Hilbert space and continuity of Gaussian processes. *Journal of Funcional Analysis*, 1:290–330, 1967. 28, 31

R.M. Dudley. *Real Analysis and Probability*. Cambridge University Press, 2002. d, 49, 65, 132

R.M. Dudley. Mathematical statistics. Lecture Notes Massachusetts Institute of Technology, USA, 2005. 49

G. Duvaut and J.L. Lions. *Les inéquations en mécanique et en physique*. Dunod, 1972. 18, 44

W.M. Ewing, W.S. Jardetzky, and F. Press. *Elastic waves in layered media*. McGraw Hill, 1957. 147

T.S. Ferguson. *A Course in Large Sample Theory*. Chapman & Hall, 1996. 49

G. Festa and J.-P. Vilotte. The newmark scheme as a velocity-stress time staggering: An efficient PML for spectral element simulations of elastodynamics. *Geophysical Journal International*, 161:789–812, 2005. 158, 159

R.A. Fisher. On an absolute criterion for fitting frequency curves. *Messenger of Mathematics*, 41:155–160, 1912. 10, 51

R.A. Fisher. On the mathematical foundations of theoretical statistics. *Philosophical Transactions of the Royal Society A*, 222:309–368, 1922. 53

G. Floquet. Sur les équations différentielles linéaires à coefficients périodiques. *Annales Scientifiques de l'École Normale Supérieure Série 2*, 12:9–46, 1883. 123

D.B. Fogel. *Evolutionary Computation : Towards a New Philosophy of Machine Intelligence*. IEEE Computer Society Press, 1995. 71

M.J. Friswell and J.E. Mottershead. *Finite element model updating in structural dynamics*. Kluwer, 1995. 2

D. Gamerman. *Markov Chain Monte Carlo: Stochastic Simulation for Bayesian Inference*. Chapmann & Hall/CRC, 1997. 71

C.F. Gauss. *Theoria motus corporum coelestium in sectionibus conicis solem ambientium*. Perthes and Besser, 1809. 9

M. Géradin and D. Rixen. *Mechanical Vibrations : Theory and Applications to Structural Dynamics*. John Wiley & Sons, 1992. 117, 141, 158

R. Ghanem and P. Spanos. *Stochastic Finite Elements:A Spectral Approach*. Springer, 1991. 4, 8, 9, 20, 27, 34

R.G. Ghanem and A. Doostan. On the construction and analysis of stochastic models: Characterization and propagation of the errors associated with limited data. *Journal of Computational Physics*, 217: 63–81, 2006. 10

D. Ghosh, R. Ghanem, and J. Red-Horse. Analysis of eigenvalues and modal interaction of stochastic systems. *AIAA Journal*, 43:2196–2201, 2005. 141

P. Gibert. Low and medium frequencies in highly heterogeneous structures. *Comptes Rendus de l'Académie des Sciences, Série II*, 295:951–954, 1982. 16

D.E. Goldberg. *Genetic Algorithms in Search, Optimization and Machine Learning*. Addison-Wesley Professional, 1989. 71

G.C. Goodwin, M. Gevers, and B. Ninness. Quantifying the error in estimated transfer functions with application to model order selection. *IEEE Transactions on Automatic Control*, 37:913–928, 1992. 10

P.J. Green. Reversible jump Markov Chain Monte Carlo computation and Bayesian model determination. *Biometrika*, 82:711–732, 1995. 127

N. Gucunski and R.D. Woods. Numerical simulation of the SASW test. *Soil Dynamics and Earthquake Engineering*, 11:213–227, 1992. 149

N. Gucunski, V. Ganji, and M.H. Maher. Effects of obstacles on Rayleigh wave dispersion obtained from the SASW test. *Soil Dynamics and Earthquake Engineering*, 15:223–231, 1996. 149

Bibliography

S. Gupta, P. Fiala, M.F.M. Hussein, H. Chebli, G. Degrande, F. Augusztinovicz, H.E.M. Hunt, and D. Clouteau. A numerical model for ground-borne vibrations and re-radiated noise in buildings from underground railways. In P. Sas and M. De Munck, editors, *Proceedings of ISMA2006 International Conference on Noise and Vibration Engineering*, pages 1741–1756, Belgium, 2006. 111

J. Hadamard. *Lectures on Cauchy's problem in Linear Partial Differential Equations*. Yale University Press, 1923. 2

L.P. Hansen. Large sample properties of generalized method of moments estimators. *Econometrica*, 50: 1029–1054, 1982. 10, 63

W.K. Hastings. Monte Carlo sampling methods using Markov Chains and their applications. *Biometrika*, 57:97–109, 1970. 71

J.S. Heisey, K.H. Stokoe II, and A.H. Meyer. Moduli of pavement systems from spectral analysis of surface waves. *Transportation Research Record*, 852:22–31, 1982. 147

F.M. Hemez. Uncertainty quantification and the verification and validation of computational models. In D.J. Inman, C.R. Farrar, V. Lopes Jr., and V. Steffen Jr., editors, *Damage Prognosis for Aerospace, Civil and Mechanical Systems*, pages 201–220. John Wiley & Sons Ltd., 2004. 4

W. Heylen, S. Lammens, and P. Sas. *Modal Analysis Theory and Testing*. KUL Press, 1997. 40

P.J. Huber. The behavior of maximum likelihood estimates under nonstandard conditions. In *Proceedings of the Fifth Berkeley Symposium on Mathematical Statistics and Probability*, pages 221–233, Berkeley, USA, 1967. University of California Press. 10, 54, 63, 65

P.J. Huber. *Robust Statistics*. Wiley-Interscience, 1981. 10, 63

T.J.R. Hughes. *The Finite Element Method - Linear Static and Dynamic Finite Element Analysis*. Prentice Hall, 1987. 34, 117, 158

R.A. Ibrahim. Structural dynamics with parameter uncertainties. *ASME Applied Mechanics Reviews*, 40: 309–328, 1987. 4, 8

F. Ihlenburg and I. Babuška. Finite element solution of the Helmholtz equation with high wave number part I: The h-version of the FEM. *Computers & Mathematics with Applications*, 30:9–37, 1995. 117, 123

F. Ihlenburg and I. Babuška. Finite element solution of the Helmholtz equation with high wave number part II: The $h - p$ version of the FEM. *SIAM Journal on Numerical Analysis*, 34:315–358, 1997. 117, 123

D.J. Inman. *Engineering vibration*. Prentice-Hall, 1994. 40

B. Iooss. Seismic reflection traveltimes in two-dimensional statistically anisotropic random media. *Geophysical Journal International*, 135:999–1010, 1998. 10

E.T. Jaynes. Information theory and statistical mechanics. *Physical Review*, 106:620–630, 1957. 9, 21, 22

E.T. Jaynes. *Probability theory: The Logic of Science*. Cambridge University Press, 2003. 4, 9, 21, 22

J.N. Kapur and H.K. Kesavan. *Entropy optimisation principles with applications*. Academic Press, San Diego, 1992. 49

L. Karl. *Dynamic soil properties out of SCPT and bender element tests with emphasis on material damping*. PhD thesis, Laboratory of Soil Mechanics, R.U.Gent, Belgium, 2005. 151, 152

V.I. Keilis-Borok, A.L. Levshin, T.B. Yanovskaya, A.V. Lander, B.G. Bukchin, M.P. Barmin, and L.I. Ratnikova. *Seismic surface waves in laterally inhomogeneous earth*. Kluwer Academic Publishers, 1989. 149

J.B. Keller. Inverse problems. *The Americal Mathematical Monthly*, 83:107–118, 1976. 1

A. Keziou. *Utilisation des Divergences entre Mesures en Statistique Inférentielle*. PhD thesis, Université Paris 6, France, 2003. 10

S. Kirkpatrick, C.D. Gelatt, and M.P. Vecchi. Optimization by simulated annealing. *Science*, 220:671–680, 1983. 71

A. Kirsch. *An Introduction to th Mathematical Theory of Inverse Problems*. Springer, 1996. 2

D. Komatitsch. *Méthodes spectrales et éléments spectraux pour l'équation de l'élastodynamique 2D et 3D en milieu hétérogène*. PhD thesis, Institut de Physique du Globe de Paris, France, 1997. 117, 158

Y.A. Kravtsov, A. Kasilar, S.A. Shapiro, S. Buske, and T. Müller. Estimating statistical parameters of an elastic random medium from traveltime fluctuations of refracted waves. *Waves in Random and Complex Media*, 15:43–60, 2005. 10

P. Krée and C. Soize. *Mathematics of Random Phenomena: Random Vibrations of Mechanical Structures*. D. Reidel Publishing Company, 1986. d, 29, 30, 31, 132, 137

S. Kullback. *Information Theory and Statistics*. Dover Publications, 1968. 9, 49, 51, 52

C.G. Lai, G.J. Rix, S. Foti, and V. Roma. Simultaneous measurement and inversion of surface wave dispersion and attenuation curves. *Soil Dynamics and Earthquake Engineering.*, 22:923–930, 2002. 149

E. Laporte and P. Le Tallec. *Numerical Methods in Sensitivity Analysis and Shape Optimization*. Birkhäuser, 2002. 22

L. Le Cam. *Asymptotic Methods in Statistical Decision Theory*. Springer, 1986. 49

P. Le Tallec. *Introduction à la dynamique des structures*. Éditions Ellipses, 2000. 19

M. Ledoux and M. Talagrand. *Probability in Banach spaces*. Springer, 1991. d, 29, 31, 132

E.L. Lehmann and G. Casella. *Theory of Point Estimation*. Springer, 1998. 9, 49

Y.K. Lin and G.Q. Cai. *Probabilistic Structural Dynamics*. McGraw-Hill, 1995. d, 4, 8, 31

B.G. Lindsay. Composite likelihood methods. In N.U. Prabhu, editor, *Statistical Inference from Stochastic Processes*, pages 221–239. Americal Mathematical Society, 1998. 63, 82, 124

L. Ljung. *System Identification: Theory for the User*. Prentice Hall PTR, 1987. 10

L. Ljung. Some results on identifying linear systems using frequency domain data. In *Proceedings of the 32nd IEEE Conference on Decision and Control*, pages 3534–3538, San Antonio, USA, 1993. 10

G. Lombaert and D. Clouteau. Resonant multiple wave scattering in the seismic response of a city. *Waves in Random and Complex Media*, 16:205–230, 2006. 162

Bibliography

R.H. Lyon. *Statistical Energy Analysis of Dynamical Systems: Theory and Applications*. The MIT Press, 1975. 16

Y. Maday and T. Patera. Spectral-element methods for the incompressible navier-stokes equation. In A.K. Noor, editor, *State-of-the-art Surveys in Computational Mechanics*, pages 71–143. ASME, 1989. 117, 158

C.S. Manohar and R.A. Ibrahim. Progress in structural dynamics with stochastic parameter variations 1987-1998. *ASME Applied Mechanics Reviews*, 52:177–197, 1999. 8

K.G. McConnell. *Vibration Testing: Theory and Practice*. John Wiley and Sons, 1995. 40

J. Mercer. Functions of positive and negative type and their connection with the theory of integral equations. *Philosophical Transactions of the Royal Society A*, 209:415–446, 1909. 27

N. Metropolis, A.W. Rosenbluth, M.N. Rosenbluth, A.H. Teller, and E. Teller. Equations of state calculations by fast computing machines. *The Journal of Chemical Physics*, 21:1087–1092, 1953. 71

K. Mosegaard and A. Tarantola. Probabilistic approach to inverse problems. In W.H.K. Lee, P. Jennings, H. Kanamori, and C. Kisslinger, editors, *International Handbook of Earthquake & Engineering Seismology*, volume A, pages 237–265. Academic Press, 2002. 50

S. Nazarian and K.H. Stokoe II. Use of surface waves in pavement evaluation. *Transportation Research Record*, 1070:132–144, 1986. 147

D.J. Nott and T. Ryden. Pairwise likelihood methods for inference in image models. *Biometrika*, 86: 661–676, 1999. 63

J.T. Oden and J.N. Reddy. *An Introduction to the Mathematical Theory of Finite Elements*. John Wiley, 1976. 34

J.T. Oden, S. Prudhomme, and L. Demkowicz. A posteriori error estimation for acoustic wave propagation problems. *Archives of Computational Mechanics and Engineering*, 12:343–389, 2005. 117

A. O'Hagan and J. Forster. *Kendall's Advanced Theory of Statistics, Volume 2B: Bayesian Inference*. Arnold Hodder, 2004. 9, 49

T. O'Hagan. Dicing with the unknown. *Significance*, 1:132–133, 2004. 3, 4

R. Ohayon and C. Soize. *Structural Acoustics and Vibration*. Academic Press, 1998. 16, 19

E. Parzen. On estimation of probability density function and mode. *Annals of Mathematical Statistics*, 33:1065–1076, 1962. 71

K. Pearson. Contributions to the mathematical theory of evolution. *Philosophical Transactions of the Royal Society A*, 185:71–110, 1894. 10, 50

B. Picinbono. *Random Signals and Systems*. Prentice-Hall, 1993. 46

W. L. Pilant. *Elastic Waves in the Earth*. Elsevier Scientific Publishing Company, 1979. 147, 149

R. Pintelon and J. Schoukens. *System Identification: a Frequency Domain Approach*. Wiley-IEEE Press, 2001. 11, 40, 46, 143, 146

V.I. Piterbarg. *Asymptotic Methods in the Theory of Gaussian Processes and Fields, Translations of Mathematical Monographs vol. 148*. American Mathematical Society, 1996. 31, 32

E. Poggiagliolmi, A.J. Berkhout, and M.M. Boone. Phase unwrapping, possibilities and limitations. *Geophysical Prospecting*, 30:281–291, 1982. 148

F. Poirion and C. Soize. Simulation numérique de champs vectoriels stochastiques gaussiens homogènes et non-homogènes. *La Recherche Aérospatiale*, 1:41–61, 1989. 38, 39

K. Popper. *The Logic of Scientific Discovery*. Hutchinson & Co., 1959. 5

B. Puig. *Modélisation et simulation de processus stochastiques non-Gaussiens*. PhD thesis, Université Pierre et Marie Curie - Paris VI, France, 2003. 38

L. Pyl and G. Degrande. Determination of the dynamic soil characteristics with the SASW method at a site in Lincent. Technical report, Department of Civil Engineering, K.U.Leuven, Belgium, 2001. 151, 152

L. Pyl and G. Degrande. Determination of the dynamic soil characteristics with the SASW method at the site of Cité Universitaire in Paris. Technical report, Department of Civil Engineering, K.U.Leuven, Belgium, 2002. 97, 148, 149

S. Rahman. A solution of the random eigenvalue problem by a dimensional decomposition method. *International Journal for Numerical Methods in Engineering*, 67:1318–1340, 2006. 141

M. Reed and B. Simon. *Methods of Modern Mathematical Analysis*. Academic Press, 1980. d, 132

W. Reinelt, A. Garulli, and L. Ljung. Comparing different approaches to model error modelling in robust identification. *Automatica*, 38:787–803, 2002. 10

G.J. Rix, C.G. Lai, and W.S. Spang. In situ measurement of damping ratio using surface waves. *Journal of Geotechnical and Geoenvironmental Engineering*, 126:472–480, 2000. 149

C.P. Robert and G. Casella. *Monte Carlo Statistical Methods*. Springer, 2005. 21, 37, 71

M. Rosenblatt. Remarks on some nonparametric estimates of a density function. *Annals of Mathematical Statistics*, 27:832–837, 1956. 71

H. Royden. *Real Analysis*. Prentice Hall, 1988. d, 132

R.Y. Rubinstein. *Simulation and the Monte Carlo Method*. Wiley-Interscience, 1981. 21

I. Sanchez-Salinero, J.M. Roesset, K.-Y. Shao, K.H. Stokoe II, and G.J. Rix. Analytical evaluation of variables affecting surface wave testing of pavements. *Transportation Research Record*, 1136:86–95, 1987. 147

A. Sarkar and R. Ghanem. Mid-Frequency structural dynamics with parameter uncertainty. *Computer Methods in Applied Mechanics and Engineering*, 191:5499–5513, 2002. 19

E. Savin. Midfrequency vibrations of a complex structure: experiments and comparison with numerical simulations. *AIAA Journal*, 40:1876–1884, 2002. 16

M. Schevenels, G. Lombaert, G. Degrande, and M. Arnst. Measurement and numerical prediction of the soil's transfer function at a site in Lincent. Technical report, Department of Civil Engineering, K.U.Leuven, Belgium, 2006. 148, 149, 151, 152

Bibliography

G.I. Schueller. Computational stochastic mechanics - recent advances. *Computers and Structures*, 79: 2225–2234, 2001. 8

G.I. Schueller, L.A. Bergman, C.G. Bucher, G. Dasgupta, G. Deotdatis, R.G. Ghanem, M. Grigoriu, M. Hoshiya, E.A. Johnson, N.A. Naess, H.J. Pradlwarter, M. Shinozuka, K. Sobszyck, P.D. Spanos, B.F. Spencer, A. Sutoh, T. Takada, W.V. Wedig, S.F. Wojtkiewicz, I. Yoshida, B.A. Zeldin, and R. Zhang. A state-of-the-art report on computational stochastic mechanics. *Probabilistic Engineering Mechanics*, 12:197–321, 1997. 8

Ch. Schwab. *p- and hp- Finite Element Methods*. Oxford University Press, 1999. 35, 117, 158

D.W. Scott. *Multivariate Density Estimation: Theory, Practice, and Visualization*. Wiley-Interscience, 1992. 71

C. Shannon. A mathematical theory of communications. *Bell Systems Technical Journal*, 27:379–423, 1948. 9, 21

M. Shinozuka and C.-M. Jan. Digital simulation of random processes and its applications. *Journal of Sound and Vibration*, 25:111–128, 1972. 38

C. Soize. *Méthodes mathématiques en analyse du signal*. Masson, 1993. d, 31

C. Soize. Reduced models in the medium frequency range for general dissipative structural-dynamics systems. *European Journal of Mechanics, A:Solids*, 17:657–685, 1998a. 19

C. Soize. A non-parametric model of random uncertainties for reduced matrix models in structural dynamics. *Probabilistic Engineering Mechanics*, 15:277–294, 2000. iii, 8, 9, 15, 20, 23, 31, 36, 137

C. Soize. Maximum entropy approach for modeling random uncertainties in transient elastodynamics. *Journal of the Acoustical Society of America*, 109:1979–1996, 2001. iii, 8, 9, 15, 20, 21, 23, 31, 33, 36, 137

C. Soize. Random matrix theory for modeling uncertainties in computational mechanics. *Computer Methods in Applied Mechanics and Engineering*, 194:1333–1366, 2005a. 10

C. Soize. A comprehensive overview of non-parametric probabilistic approach of random uncertainties for predictive models in structural dynamics. *Journal of Sound and Vibration*, 288:623–652, 2005b. 10

C. Soize. Non-Gaussian positive-definite matrix-valued random fields for elliptic stochastic partial differential operators. *Computer Methods in Applied Mechanics and Engineering*, 195:26–64, 2006. iii, iv, 4, 9, 10, 12, 15, 27, 28, 30, 31, 32, 36, 115, 137

C. Soize and K. Bjauoui. Estimation of fuzzy structure parameters for continuous junctions. *Journal of the Acoustical Society of America*, 107:2011–2020, 2000. 74

C. Soize and R. Ghanem. Physical systems with random uncertainties: chaos representations with arbitrary probability measure. *SIAM Journal on Scientific Computing*, 26:395–410, 2004. 9, 20, 27

H. Strasser. Consistency of maximum likelihood and Bayes estimates. *The Annals of Statistics*, 9:1107–1113, 1981. 10, 53

A. Stuart, K. Ord, and S. Arnold. *Kendall's Advanced Theory of Statistics, Volume 2A: Classical Inference and the Linear Model*. Arnold Hodder, 1999. 9, 49

174

Q.A. Ta. Étude de la propagation d'ondes dans des barres hétérogènes et aléatoires par la méthode des éléments spectraux. Master's thesis, École Centrale Paris, France, 2006. 117

A. Tarantola. *Inverse Problem Theory and Methods for Model Parameter Estimation*. SIAM, 2005. 2, 3, 50, 128

A. Tarantola. Popper, Bayes and the inverse problem. *Nature Physics*, 2:492–494, 2006. 5

A. Tarantola. Mapping of probabilities: Theory for the interpretation of uncertain physical measurements. In preparation, 2008. 3, 50

A. Teughels. *Inverse Modelling of Civil Engineering Structures based on Operational Model Data*. PhD thesis, KULeuven, Belgium, 2003. 2

L.L. Thompson and P.M. Pinsky. Complex wavenumber Fourier analysis of the p-version finite element method. *Computational Mechanics*, 13:255–275, 1994. 117, 123

A.N. Tikhonov and V.Y. Arsenin. *Solutions of ill-posed problems*. Winston and Sons, 1977. 3, 128

K. Tokimatsu, S. Tamura, and H. Kokima. Effects of multiple modes on Rayleigh wave dispersion characteristics. *Journal of Geotechnical Engineering*, 118:1529–1543, 1992. 149

J.A. Turner and P. Anugonda. Scattering of elastic waves in heterogeneous media with local isotropy. *Journal of the Acoustical Society of America*, 109:1787–1795, 2001. 162

F. E. Udwadia. Some results on maximum entropy distributions for parameters known to lie in finite intervals. *SIAM Review*, 31:103–109, 1989. 22

I.A. Viktorov. *Rayleigh and Lamb waves: physical theory and applications*. Plenum Press, 1967. 147

A. Wald. Note on the consistency of the maximum likelihood estimate. *Annals of Mathematical Statistics*, 20:595–601, 1949. 10, 53

N. Wiener. The homogeneous chaos. *Americal Journal of Mathematics*, 60:897–936, 1938. 9, 20, 27

D. Williams. *Probability with Martingales*. Cambridge University Press, 1991. 49

K.-V. Yuen and L.S. Katafygiotis. Bayesian modal updating using complete input and incomplete response noisy measurements. *Journal of Engineering Mechanics*, 128:340–350, 2002. 10

O.C. Zienkiewicz and R.L. Taylor. *The Finite Element Method, volume 1 : the basis*. Butterworth-Heinemann, 2000a. 34

O.C. Zienkiewicz and R.L. Taylor. *The Finite Element Method, volume 2 : solid mechanics*. Butterworth-Heinemann, 2000b. 34

Résumé

L'objectif de la thèse est de développer une méthodologie d'identification expérimentale de modèles probabilistes qui prédisent le comportement dynamique de structures. Nous focalisons en particulier sur l'inversion de modèles probabilistes à paramétrage minimal, introduits par Soize, à partir de fonctions de transfert expérimentales. Nous montrons d'abord que les méthodes classiques d'estimation de la théorie des statistiques mathématiques, telle que la méthode du maximum de vraisemblance, ne sont pas bien adaptées pour aborder ce problème. En particulier, nous montrons que des difficultés numériques, ainsi que des problèmes conceptuels dus au risque d'une mauvaise spécification des modèles, peuvent entraver l'application des méthodes classiques. Ces difficultés nous motivent à formuler l'inversion de modèles probabilistes alternativement comme la minimisation, par rapport aux paramètres recherchés, d'une fonction objectif, mesurant une distance entre les données expérimentales et le modèle probabiliste. Nous proposons deux principes de construction pour la définition de telles distances, basé soit sur la fonction de logvraisemblance, soit l'entropie relative. Nous montrons comment la limitation de ces distances aux lois marginales d'ordre bas permet de surmonter les difficultés mentionnées plus haut. La méthodologie est appliquée à des exemples avec des données simulées et à un problème en ingénierie civile et environnementale avec des mesures réelles.

Mots-clés: modélisation probabiliste, inversion, identification, quantification d'incertitudes, champ stochastique

Abstract

The aim of this thesis is to develop a methodology for the experimental identification of probabilistic models for the dynamical behaviour of structures. The inversion of probabilistic structural models with minimal parameterization, introduced by Soize, from measured transfer functions is in particular considered. It is first shown that the classical methods of estimation from the theory of mathematical statistics, such as the method of maximum likelihood, are not well-adapted to formulate and solve this inverse problem. In particular, numerical difficulties and conceptual problems due to model misspecification are shown to prohibit the application of the classical methods. The inversion of probabilistic structural models is then formulated alternatively as the minimization, with respect to the parameters to be identified, of an objective function measuring a distance between the experimental data and the probabilistic model. Two principles of construction for the definition of this distance are proposed, based on either the log-likelihood function, or the relative entropy. The limitation of the distance to low-order marginal laws is demonstrated to allow to circumvent the aforementioned difficulties. The methodology is applied to examples featuring simulated data and to a civil and environmental engineering case history featuring real experimental data.

Keywords: probabilistic modelling, inversion, identification, uncertainty quantification, random field